Study on the role of nuclear Cofilin1

Dissertation

zur

Erlangung der Doktorgrades (Dr. rer. nat.)

der

Mathematisch-Naturwissenschaftlichen Fakultät

der

Rheinischen Friedrich-Wilhelms-Universität Bonn

vorgelegt von

Nina Roy

aus

Bocholt

Bonn, im Mai 2015

Angefertigt mit Genehmigung der Mathematischen-Naturwissenschaftlichen Fakultät
der Rheinischen Friedrich-Wilhelms-Universität Bonn.

1. Gutachter: Prof. Dr. Walter Witke

2. Gutachter: Prof. Dr. Frank Bradke

Tag der Promotion: _____

Erscheinungsjahr: _____

EIDESSTATTLICHE ERKLÄRUNG

Hiermit versichere ich, dass die vorliegende Arbeit selbständig und ohne Benutzung anderer als der angegebenen Quellen und Hilfsmittel angefertigt wurde.

Bonn, 15.Mai 2015

_____

Nina Roy

Danksagung

Ein besonderer Dank gilt meinem Doktorvater Prof. Dr. Walter Witke für die Überlassung des sehr interessanten Themas, die vielen wertvollen Ratschläge und dass seine Tür immer offen stand. Aber vor allem möchte ich mich für seine Geduld und seinen Humor bedanken. Weiterhin möchte ich ihm für die Begutachtung dieser Arbeit und die freundliche Aufnahme in seine Arbeitsgruppe danken.

Herrn Prof. Dr. Frank Bradke danke ich für die Übernahme des Koreferats sowie Herrn PD. Dr. Gregor Kirfel und Herrn Prof. Dr. Valentin Stein für ihre Teilnahme an der Prüfungskommission als fachnaher und fachangrenzender Gutachter.

Besonders herzlich möchte ich mich bei meiner Betreuerin Dr. Christine Gurniak bedanken, die sich stetig Zeit für meine Fragen und anregende Diskussionen nahm. Insbesondere möchte ich mich für ihre Mühen, sich durch meine Texte zu kämpfen, und für ihre konstruktiven Anmerkungen bedanken.

Herzlich gedankt sei allen, die zum Gelingen dieser Arbeit beigetragen haben. Einige Personen möchte ich dabei ganz besonders hervorheben.

Ein großer Dank gilt Gabriele Matern, ohne die die Histologie in dieser Form nicht möglich gewesen wäre.

Des Weiteren möchte ich mich bei Christian Liemersdorf bedanken, der mir endlose Stunden beim Erstellen von Schemata geholfen hat.

Weiterhin möchte ich allen jetzigen und ehemaligen Mitarbeitern der AG Witke für die ihre ständige Hilfsbereitschaft, die vielen guten Ratschläge, die aufmunternden Worte und das freundschaftliche Arbeitsklima danken. Besonders bedanken möchte ich mich bei Dr. Pietro Pilo Boyl, Melanie Jokwitz, Gerda Hertig, Steffi Stöcker, Stefan Klein, Susi und Gertrud Dienst.

Ganz besonders bedanken möchte ich mich bei Kathrin Bläsius, Andree Salz, Christian Liemersdorf und „Häubsche“ Hecker für die Filmabende, die Yogastunden, die Umarmungen, den „Bachelor- Gesangstag“, die stetige Hilfe und Unterstützung, das Määh, den unendlichen Schokoladen- und Eiskonsum, das Zuhören und das gemeinsame Weinen und Lachen und den allgemeinen Wahnsinn.

Mein größter Dank gilt meinen Eltern und meinem Bruder, die immer für mich da waren und jeden einzelnen Schritt mit mir gemeinsam gegangen sind. Ich möchte besonders meiner Mutter danken, die immer für mich stark geblieben ist. Meinem Vater, der immer eine Umarmung für mich hatte. Meinem Bruder, der mir in den letzten neun Jahren nicht nur ein großer Bruder sondern auch ein Vater war. Ich danke euch, dass ihr mich seit ich denken kann in allem unterstützt habt, stets das Beste für mich wollt und an mich geglaubt habt. Aber vor allem danke ich Euch, weil ihr immer an meiner Seite gestanden habt.

Summary

Cofilin1, an actin depolymerizing factor, is a member of the ADF/Cofilin family. The ADF/Cofilin family members carry a conserved nuclear translocation signal (NTS) comprising the core amino acid sequence KKRKK. *In vitro* studies showed wt-Cofilin1 in the cytoplasm and the nucleus, whereas Cofilin1 NTS mutants were restricted to the cytoplasm. In this thesis the physiological consequences of a mutation of the NTS to KTRTK were studied with the help of a mouse line. Even though Cofilin2, ADF and Cofilin1 share similar biochemical properties, they differ in regulation and expression pattern and are not functionally identical.

Cofilin1$^{KTRTK/KTRTK}$ mutants were not born but viable until the time of birth. Homozygous KTRTK-Cofilin1 mutants showed an exencephalic phenotype, a cranial neural tube closure defect, apparent at embryonic day 10 (E10). Massive malformations of brain structures, seemingly a defect in the midbrain and diencephalon development, resulting in characteristics of an everted brain were observed. *In vitro* neurons displayed increased branching activity and astrocytes indicated a delay in maturation. Analysis of mouse embryonic fibroblasts (Mefs) derived from Cofilin1$^{KTRTK/KTRTK}$ embryos revealed distinct disturbances in the progression of the G2/M phase of the cell cycle, significantly reduced proliferation rates and morphological differences in the form of multinucleate cells and increase in cell size as well. FACS analyses observed changes in G- and F-actin ratios in Cofilin1$^{KTRTK/KTRTK}$ mutant cells. This could be responsible for cytokinesis and growth defects in Mefs and aberrant brain development. Actin assays showed reduced depolymerizing activity of KTRTK-Cofilin1, confirming that KTRTK-Cofilin1 was not fully functional. Protein level analysis revealed the decrease of KTRTK-Cofilin1 during embryonic development. Decrease did not result from transcriptional modifications, changed protein stability or altered solubility. Microarray data showed alterations in gene expression of extracellular matrix proteins and actin isoforms for instance. Acquired data indicates that the subcellular location of Cofilin1 is essential for maintenance of the cell homeostasis. Nucleo-cytoplasmic shuffling of actin, makes Cofilin1 a critical regulator of transcriptional activity.

Multiple proof experiments lead to the solid conclusion that Cofilin1 is connected to disparate and highly complex events for embryonic development, morphogenesis and cellular functionality.

Table of content

Abbreviation

°C	Degrees Celsius
µg	Microgram
µm	Micrometer
A.bidest	Aqua bidestillata
ABP	Actin-binding proteins
ADF	Actin depolymerizing factor
ADP	Adenosine diphosphate
Amp	Ampicillin
AP	Alkaline phosphatase
approx.	Approximately
APS	Ammonium persulfate
Arp	Actin-related protein
ATP	Adenosine triphosphate
Beta-Gal	Beta- galactosidase
Bp	Base pair
BSA	Bovine serum albumin
Ca	Calcium
CFDA SE	Carboxyfluorescein diacetate, succinimidyl ester
Cfl	Cofilin
Cfl1	Cofilin1
Cfl2	Cofilin2
DAB	3,3'-Diaminobenzidine
DAPI	4',6-diamidino-2-phenylindole
DEPC	Diethylpyrocarbonate
DMEM	Dulbecco's modified Eagle's medium
DMF	N,N- Dimethylformamide
DMSO	Dimethyl sulfoxide
DNA	Deoxyribonucleic acid
dNTP	Deoxynucleotide triphosphate
E.coli	Escherichia coli
e.g.	exempli gratia = for example
ECL	Enhanced chemiluminescence
EDTA	Ethylenediaminetetraacetic acid
EGF	Epidermal growth factor
EGTA	Ethylene glycol tetraacetic acid
Elix	Distilled water
et al.	et alii = and others
EtBr	Ethidiumbromide
EtOH	Ethanol
Ex	Embryonic day x

FA	Formaldehyde
FACS	Fluorescence activated cell sorter
F-actin	Filamentous actin
FCS	Fetal calf serum
Fig	Figure
Flow-Cyt	Flow cytometry
FRET	Fluorescence resonance energy transfer
g	Gram
G418	Geneticin
GA	Glutaraldehyde
G-actin	Globular actin, monomeric actin
GAPDH	Glyceraldehyde 3-phosphate dehydrogenase
GFAP	*Glial fibrillary acidic protein*
GFP	Green fluorescent protein
GST	Glutathione *S*-transferase
H_20	Chemical formula for water
HEPES	Hydroxyethyl-piperazinyl-ethanesulfonic
Het	Heterozygous
HRP	Horseradish peroxidase
IF	Immunofluorescence
IHC	*Immunohistochemistry*
Kana	Kanamycin
kbp	Kilobase pair
kDa	Kilodalton
Ki	Knockin
Ko	Knockout
KOH	Potassium hydroxide
LB	Lysogeny broth
M	Molar
Mef	Mouse embryonic fibroblasts
Mg	Milligram
MilliQ	Highly purified and deionized water
min	Minutes
ml	Milliliter
mm	Millimeter
mM	Millimolar
mRNA	Messenger ribonucleic acid
ms	Mouse
Mt	Mutant
Mut	Mutation
NCC	Neural crest cells
Neo	Neomycin
nm	Nanometer
NP-40	Nonidet P40

NPG	N-propyl gallate
NTC	Neural tube closure
NTD	Neural tube closure defect
NTS	Nuclear translocation signal
Nuc	Referring to the mouse line carrying the mutation in the NTS of Cofilin1
o.n.	Over night
OD	Optical density
PAGE	Polyacrylamide gel electrophoresis
PBS	Phosphate buffered saline
PCNA	*Proliferating cell nuclear antigen*
PCR	Polymerase chain reaction
Pen	Penicillin
PFA	Paraformaldehyde
pH	The negative logarithm (base 10) of the molar concentration of dissolved hydronium ions
PI	Propidium iodide
pmol	Picomol
rb	Rabbit
RNA	Ribonucleic acid
rpm	Rounds per minute
RT	Room temperature
SDS	Sodium dodecyl sulphate
Strep	Streptomycin
TAE	Tris-acetate-EDTA-buffer
Taq	DNA polymerase
TC	Tissue culture
Tris	Tris(hydroxymethyl)-aminomethane
U	Enzyme unit
UV	Ultraviolet
V	Volt
v/v	Volume per volume
vs.	Versus
w/v	Weight per volume
Wt	Wildtype
X-Gal	5-bromo-4-chloro-3-indolyl P3-D-galactoside
ø	Diameter

List of figures

1. Introduction

1.1 The cytoskeleton

The cytoskeleton of eukaryotic cells comprises different protein polymers. They generate cell movement and provide mechanical support for the cell. Cells have three different types of cytoskeletal protein families: microtubules, intermediate filaments and actin filaments. Each of these polymers is made up of an indefinite number of subunits which form filaments that are dynamic. The cytoskeletal polymers share general features though each is suited for specific tasks in the cell because of the unique characteristics they carry (Lewin et al., 2007). Dynamic rearrangement of actin filaments is essential for their involvement in motility, vesicle trafficking, maintenance and change of cellular shape and structure, cytokinesis, endo- and exocytosis, synaptic plasticity, cell signaling and chromosome congression (Jordan and Wilson, 1998; Lenart et al., 2005).

1.2 Actin

Actin is highly conserved and the most abundant protein in many eukaryotic cells. Multiple actin genes for varying isoforms were found in higher organisms that are differentially expressed in various tissues and also differ in function (e.g. mammalians have six actin genes, alpha actins are found in muscle cells, whereas beta and gamma isoforms are prominent in non-muscle cells like Mefs) (Pollard et al., 1994; Khaitlina, 2001). Actin-like proteins could also be found in bacteria. These highly conserved structural homologs of actin indicate that the prokaryotic cytoskeleton is similar to the eukaryotic cytoskeleton (Campbell and Mullins, 2007; Orlova et al., 2007). In the cell globular (G-) actin and filamentous (F-) actin exist in a reversible equilibrium. G- actin, the actin monomer, is a 42 kDa protein that polymerizes into F-actin (Hofmann and de Lanerolle, 2006). G-actin carries an intrinsic ATPase activity, hydrolyzing ATP after polymerization. The monomer consists of four subdomains (1-4), two subdomains (1+2 and 3+4) form a lobe (Figure 1). The lobes are connected by extensions between subdomain 1 and 3. Subdomain 2 comprises the DNase I binding loop. This characteristic allows the specific identification of G-actin. In the form of F-actin the subdomain 2 is blocked and DNase I is unable to bind. In the center of the actin

monomer molecule a nucleotide (ADP or ATP) and a divalent ion (Ca^{2+} or Mg^{2+}) can be bound (Figure 1). The binding of nucleotide and ion to actin is reversible.

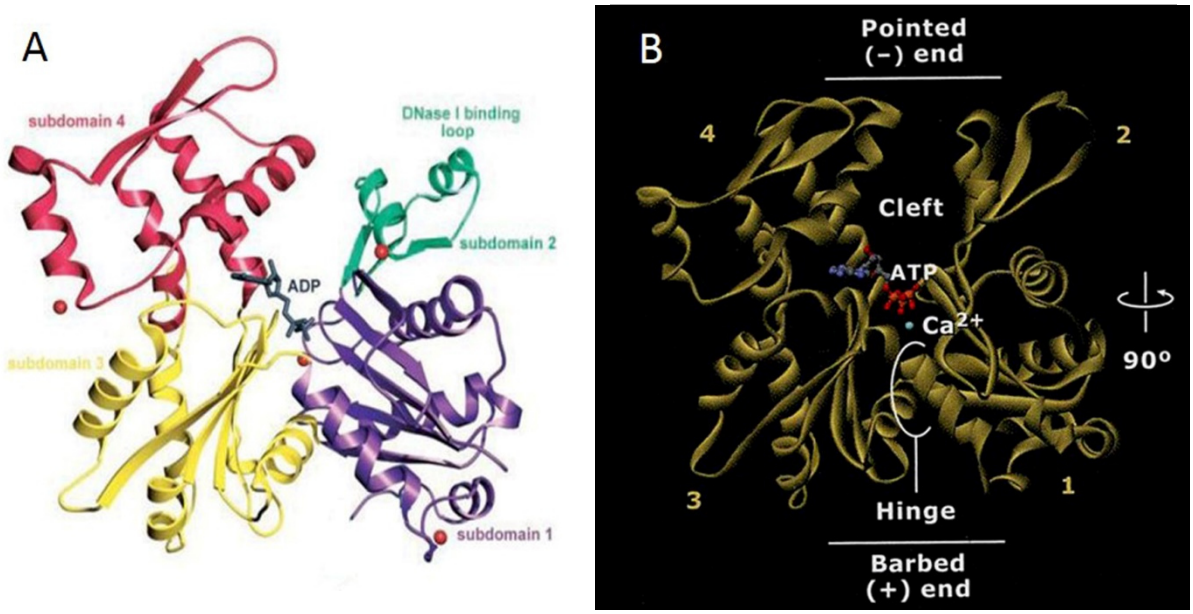

Fig. 1: Ribbon structure of uncomplexed actin in the ADP state (A) and crystal structure of the actin monomer binding ATP (B) A: Ribbon representation of the structure of uncomplexed actin in the ADP state. The four subdomains of actin are represented in different colors: subdomains 1 (purple), 2 (green), 3 (yellow), and 4 (red). The DNase I binding loop, which is folded as a helix in this structure, is located toward the upper part of subdomain 2. ADP is bound at the center of the molecule, where the four actin subdomains meet. Four Ca^{2+} ions bound to the actin monomer in the crystals are represented as red dots. One of the Ca^{2+} ions, termed primary or catalytic, is bound in close association with the nucleotide. The other three Ca^{2+} ions are bound to subdomains 1, 2, and 4 on the surface of the molecule and may correspond to secondary cation-binding sites of actin (Otterbein et al., 2001). B: Crystal structure of the uncomplexed actin in the ATP state showing the polarized structure of the monomer. The ends are termed barbed end (+) (between subdomain 1 and 3) and pointed end (-) (between subdomains 2 and 4) (Kabsch et al., 1990).

F-actin and G-actin reorganize in response to intracellular and extracellular signals. The formation of actin filaments, by polymerization of actin monomers, can be divided into four steps: 1. activation of the monomer (substitution of Ca^{2+} for Mg^{2+} and conformational changes); 2. nucleation (formation of a trimeric ATP-actin nucleus to increase the probability of filament growth); 3. elongation (extension of the polymers); and 4. annealing (joining of two filaments at the ends) (Pollard and Cooper, 1986). Actin filaments are double stranded, right handed helices with approximately 8 nm in

diameter. The filamentous structure is stabilized by extensive hydrophobic contact and hydrogen bonds between actin subunits (Pollard et al., 1994; Sheterline et al., 1998; Falck, 2004).

Globular actin subunits align in a head-to-tail manner giving the filament a polarized structure in consequence of the polar structure of the monomers. In analogy of the filament the ends are termed barbed end (+) and pointed end (-). The ends differ in their elongation rate. Elongation of F-actin with ATP-actin is favored at the barbed end, while dissociation of ADP-actin at the pointed end is more rapid (Figure 2). The polarity of F-actin is crucial for directional transport of cargo (e.g. myosin motors transport organelles along the uniformly polarized actin filaments, which form bundles that form tracks that for the movement), establishing polarity and actin assembly (Evans and Bridgman, 1995; Tabb et al., 1998; Pollard and Borisy, 2003; Pollard and Cooper, 2009).

Within an actin filament each monomeric subunit is encased by four other monomers: one on each side on the same strand (longitudinal contacts) and two on the opposite strand (lateral contacts). This structure provides a big integral strength to the filament.

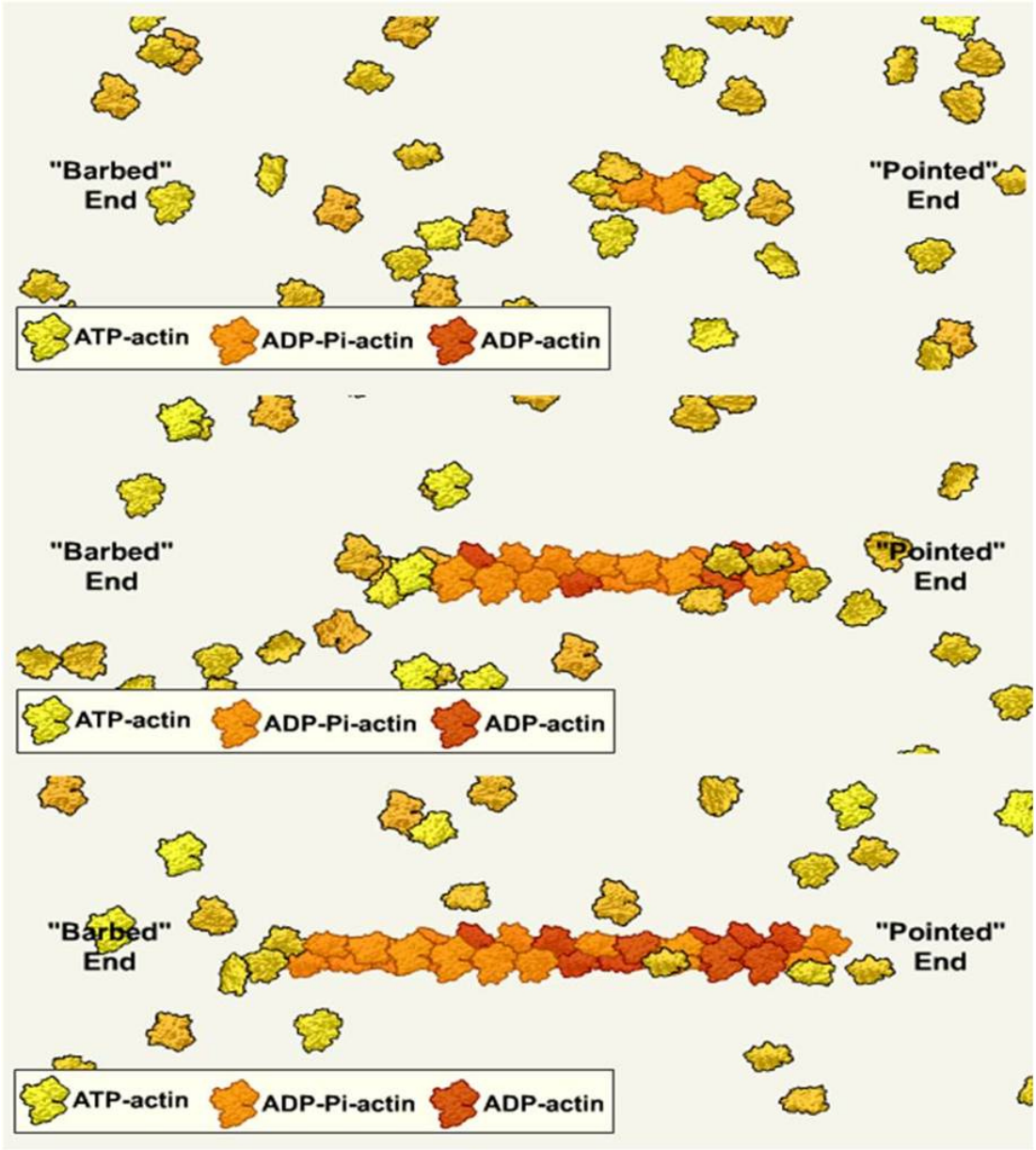

Fig. 2: **Assembly of actin filaments**. ATP-actin subunits preferentially bind to the fast growing **barbed end (+)** of an actin filament, they can also bind to the other, **pointed end (-),** though at a slower rate. After binding to the barbed end of a filament the actin subunit rapidly hydrolyzes its bound ATP into ADP and phosphate (Pi) and slowly releases the hydrolyzed phosphate. ADP-actin filaments disassemble from the pointed end. Released ADP-actin monomers undergo nucleotide exchange. ATP-actin monomers can be used for a new cycle of assembly. This flux is termed treadmilling (Kuhn and Pollard, 2005).

1.2.1 Actin cytoskeleton

The state of polymerization of actin and organization of actin in the cytoplasm are tightly regulated processes that respond to extracellular signals (Jaffe and Hall, 2005). *In vivo* the concentration of actin in the cytoplasm as well as in the nucleus, is above the critical concentration for polymerization. The polymerization process in the cytoplasm is regulated by a vast number of actin-binding proteins. Actin is regulated in by nucleating monomers, crosslinking, bundling as well as severing of filaments, including filament branching and sequestering, all processes regulating actin polymerization and depolymerization (Hofmann, 2009).

1.2.1.1 Actin-binding proteins

Acting-binding proteins (ABPs) are essential for the regulation of actin dynamics and their organization into functional higher order networks (Winder and Ayscough, 2005). ABPs are classified according to their functions, furthermore a distinction between monomer binding and filament binding proteins is made (Figure 3).

1.2.1.1.1 Monomer binding proteins

Monomer binding

The availability of actin monomers is required to be tightly regulated, for their need in rapid growth and reorganization of actin filaments. Over 25 monomer binding proteins are identified in mammalian cells (Winder and Ayscough, 2005). In many higher eukaryotic cells, the two major actin monomer binding proteins are profilin and thymosin β_4. They form 1:1 ratio complexes with actin monomers, while thymosin β_4 inhibits spontaneous polymerization of G-actin and prevents the elongation of existing filaments at both ends, profilin catalyzes the exchange of ADP for ATP and thus recycling ATP-actin subunits to the monomer pool which are then ready to be used for assembly (Pollard and Borisy, 2003).

Nucleation

Nucleation is the first step in the polymerization of new actin filaments; new filaments can be formed on the side of existing filaments or by severing of preexisting filaments. Two primary regulators of nucleation are the Arp2/3 complex and members of the formin family.

The Arp2/3 complex binds G-actin and effectively forms a stable trimer and nucleus for filament elongation. WASP activates the Arp2/3 complex by inducing conformational changes and delivering the first actin monomer of the daughter filament (Padrick et al., 2011). The pointed end is capped by the Arp2/3 complex thus only allowing elongation of the filament at the barbed end. Profilin also binds to G-actin, in consequence preventing nucleation by occupying an actin-actin contact site. Thereby, profilin sequesters monomeric actin from the G-actin pool.

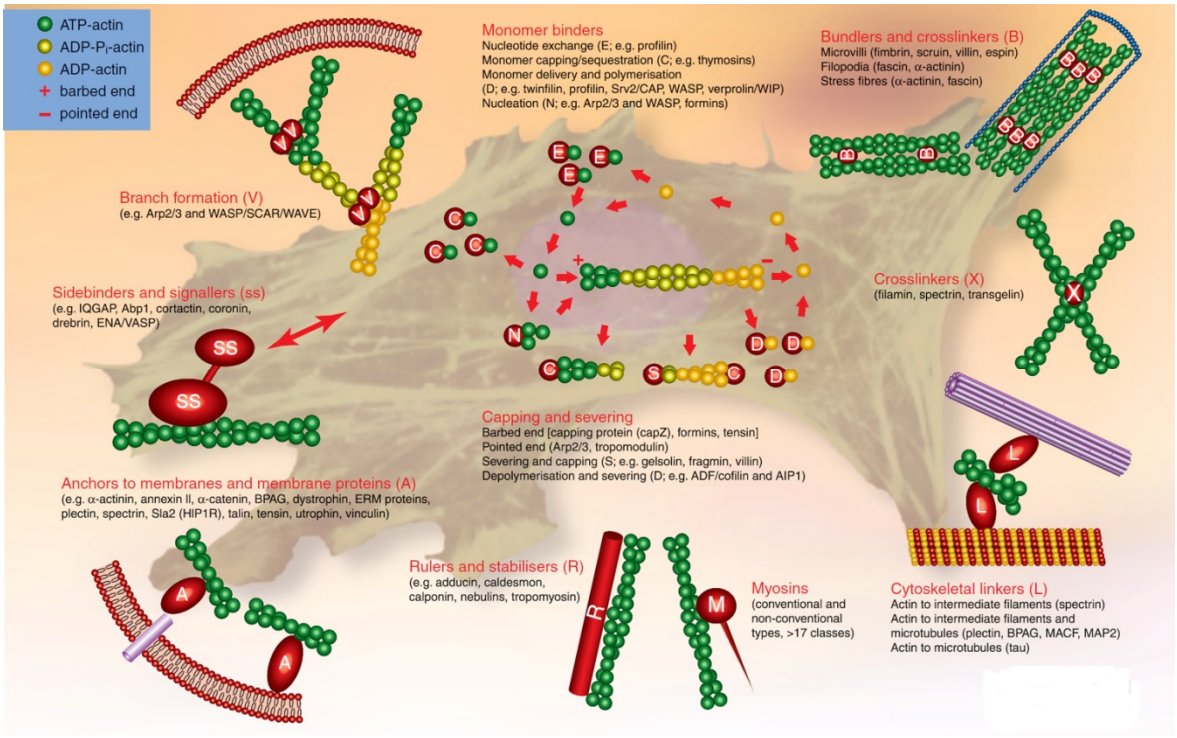

Fig. 3: Overview of actin binding proteins regulating the actin cytoskeleton. Different classes of ABPs with various functions involved in the assembly, disassembly and the regulation of the actin cytoskeleton are shown (Winder and Ayscough, 2005).

The mechanisms of elongation and nucleation for formins are unlike those of the Arp2/3 complex. Formins form a complex with two G-actin monomers and stay associated with the barbed end of the filament, while the addition of further monomers occurs at the barbed end. Formins nucleate non-branching, linear structures, whereas Arp2/3 complexes nucleate branching actin arrays (Lewin et al., 2007).

1.2.1.1.2 Filament binding proteins

Crosslinking and bundling

Higher-order structures and actin networks are indispensable for the shape and function of cells. The higher-order structures of filamentous actin are formed by crosslinking proteins. Transgelin, an actin cross-linking/gelling protein, is found in fibroblasts and smooth muscle. In vitro assays showed that it binds directly to actin filaments and converts the loose, random distribution of filamentous actin into a tangled, cross-linked meshwork (Shapland et al., 1993). In filopodia fascin is the main actin filament bundling protein. In addition to two actin binding sites, it makes secondary contacts with other actin filaments in the bundle (Jansen et al., 2011). The parallel or antiparallel alignment of F-actin into linear arrays is called actin bundling as found in microvilli, whereas among others, the orthogonal linking of actin filaments is called crosslinking and forms actin meshes (Winder and Ayscough, 2005; Lewin et al., 2007).

Cytoskeletal linkers and membrane anchors

These proteins are of great significance for the cell by interconnecting different cytoskeletal elements and connecting actin to the membrane or membrane proteins. This group of proteins is of great importance in the integration of structure and maintenance of cell integrity. Membrane binding proteins as dystrophin and vinculin connect the actin cytoskeleton to cell adhesion receptors (dystroglycan or integrin), whereas plectin, a protein for interconnecting different cytoskeletal elements, links actin to microtubules and intermediate filaments (Winder and Ayscough, 2005).

Capping

Capping proteins determine the length of actin filaments. The length of an actin filament influences its mechanical properties, e.g. short actin filaments are less flexible. While gelsolin and tensin block the addition of monomers to the barbed end thus decreasing, the overall length of the filament, pointed end cappers reduce the dissociation of monomers from the pointed end, leading to rapid filament elongation (Winder and Ayscough, 2005; Lewin et al., 2007).

Contracting

Myosins are actin-dependent motors, using ATP hydrolysis to generate movement and force along actin filaments (Lewin et al., 2007). Actin filaments are used as tracks to move cargo. The majority of myosins moves from the pointed end to the barbed end of the actin filament (Winder and Ayscough, 2005).

Stabilizing, depolymerizing and severing

Severing and depolymerizing proteins regulate actin filament dynamics. Strictly regulated disassembly of actin filaments is necessary to maintain a dynamic turnover of the actin cytoskeleton. Severing increases the number of filament ends for assembly and disassembly while depolymerization is necessary to maintain a pool of actin monomers. Tropomyosins, a highly conserved and important family of ABPs, bind along the length of the filament and stabilize the filament against depolymerization, as well as gelsolin severing. Tropomyosins also regulate the interaction of myosin with the actin filament. Gelsolin, the most potent actin filament severing protein, binds to the side of an actin filament and changes the actin conformation. Upon severing, gelsolin remains attached to the barbed end of the filament as a cap. In consequence, short actin filaments that can not reanneal at their barbed ends are generated (Sun et al., 1999). The best characterized protein family responsible for actin depolymerization is the ADF (actin depolymerizing factor)/Cofilin family (Winder and Ayscough, 2005).

1.2.2 Actin in the nucleus

Actin has been localized in the cytoplasm as well as in the nucleus. Along with actin, growing evidence for actin-related proteins (Arps) in the nucleus was found (Cairns et al., 1998; Harata et al., 1999; 2000; 2002) (Table 2).
Ohnishi et al. were one of the first researchers to report the presence of actin in calf thymus cell nuclei as early as 1963 (Ohnishi et al., 1963; Ohnishi et al., 1964).

While the cytoplasmic functions of actin are well established, the role of actin in the nucleus was not clear and controversial for years (Pederson and Aebi, 2002). In recent years more and more light has been shed on the function of nuclear actin, dismissing the idea of actin being an artefact in the nucleus.

Actin lacks a nuclear translocation signal, but putative nuclear export sequences were identified (Rando et al., 2000), weakening the initially anticipated theory of nuclear actin being an artefact only.

No actin-specific import receptor has been identified so far. With a size of 42 kDa, actin is unable to pass freely through the nuclear pores. Therefore it was suggested that proteins functioning as chaperones are needed to mediate the transport of actin into the nucleus under conditions promoting translocalization of actin from the cytoplasm. Cofilin1, a depolymerizing factor, contains a nuclear translocation sequence and enters the nucleus through the import receptor importin β. A number of other actin- binding proteins (ABPs) have been shown to enter the nucleus either through importin β or through yet unidentified import pathways. Bound to the chaperones, actin is also transported to the nucleus upon nuclear translocation via the import receptor importin β (Hofmann, 2009; Bamburg et al., 2010).

A difference in the immunochemical signature of nuclear and cytoplasmic actin in mammalian cells has been reported (Pederson and Aebi, 2002). It has been established that the polymeric forms of actin in the nucleus are different from those in the cytoplasm (Hofmann and de Lanerolle, 2006).
Phalloidin, a F-actin specific staining reagent, that binds to actin filaments of a minimum size of seven monomers (Visegrady et al., 2005), does not stain actin in the nucleus indicating that, either nuclear actin consist of less than seven monomers in

length or has a different structure that impairs the binding of phalloidin. However, using monoclonal antibodies specifically recognizing G-actin, monomeric actin in the nucleus could be identified (Gonsior et al., 1999). After the treatment of cells with miscellaneous reagents (e.g. DMSO) actin filaments could be detected in the nucleus by phalloidin staining (Sanger et al., 1980), suggesting that filaments longer than seven monomers in length can be formed or that structural changes allowing the binding of phalloidin take place. Nuclear actin has been assigned various functions.

Over the years the existence of nuclear actin could be proven in a variety of species and cell types (Table 1).

Species and/or cell type	**Reference**
Plants	
Allium cepa	(Cruz et al., 2008)
Insects	
Drosophila melanogaster	(Sauman and Berry, 1994)
Amphibians	
Xenopus laevis	(Merriam and Hill, 1976)
Birds	
Duck erythroblasts	(Maundrell and Scherrer, 1979)
Chicken liver	(Crowley and Brasch, 1987)
Mammalian cell types	
Thymus cells	(Ohnishi et al., 1963; Ohnishi et al., 1964)
Liver cells	(Douvas et al., 1975)
Epithelial cells	(Lestourgeon et al., 1975)
Myoblasts	(Paulin et al., 1976)
Kidney cells	(Pagoulatos and Yaniv, 1978)
Ovary cells	(Brunel and Lelay, 1979)
Lymphocytes	(Nakayasu and Ueda, 1983)
Neural cells	(Milankov and De Boni, 1993; Sahlas et al., 1993; Amankwah and De Boni, 1994)
Oocytes	(Funaki et al., 1995)

Table 1: Selected list of species and cell types in which nuclear actin has been identified (modified from Hofmann, 2009)

The vast number of findings of nuclear actin in the mammalian species indicates that nuclear actin is also of importance and can also be found in murine cells.

In the last years actin has been shown to be involved in several nuclear processes such as RNA processing and export, intranuclear movement of euchromatin and nuclear structural maintenance (Figure 4) (Hofmann, 2009). Actin polymerization and translocation to the nucleus are strictly regulated processes involving a number of different proteins and signaling cascades.

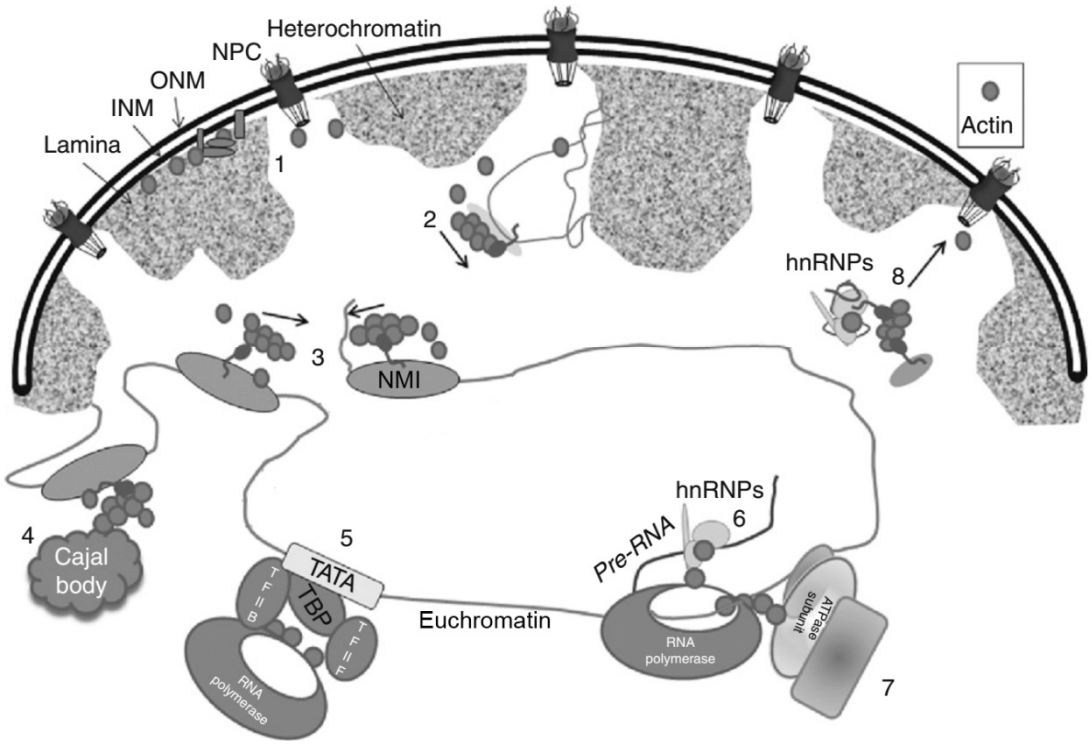

Fig. 4: Proposed nuclear functions of actin. (1) Assembly, stabilization, and connection of nuclear envelope through interactions of actin with emerin and lamin A. (2-4) Actin facilitated intranuclear chromosome movement. (2) Movement of chromosomes away from heterochromatin after activation of transcription. (3) Chromosomal reorganization during transcriptional activation. (4) Movement of chromosome regions towards Cajal bodies. (5) Assembly of transcription initiation complexes. (6-7) Regulation of transcription elongation through recruitment of chromatin modifying complexes and RNA packaging proteins. (8) Nuclear export of proteins and RNA. hnRNP: Heterogeneous nuclear ribonucleoproteins; INM: inner nuclear membrane; NMI: nuclear myosin I; NPC: nuclear pore complex; ONM: outer nuclear membrane; TATA: TATA-box; TBP: TATA-binding-protein; TFIIB: Transcription factor IIB; TFIIF: Transcription factor IIF (Hofmann, 2009).

In addition actin it is fundamental for the nuclear transport of proteins and RNA (de Lanerolle et al., 2005). Actin plays essential roles in gene transcription on several

different levels. Nuclear myosin I (NMI) and actin were shown to be involved in the translocation of activated genes.

Actin directly associates with the RNA- Polymerase II core complex and is necessary for the start of transcription by RNA polymerase II. In the absence of actin preinitiation complexes cannot assemble at the promoter. Furthermore, there is also conclusive evidence that actin plays a role in transcription elongation through a complex interaction with RNA-processing factors and chromatin remodeling factors (Hofmann et al., 2004; Visa, 2005; Chuang et al., 2006). Actin has also been shown to bind to transcription factors and can thus determine their subcellular function. Furthermore, actin is a component of the chromatin remodeling complex involved in the activation of transcription (Olave et al., 2002). It is also required for full transcriptional activity of RNA polymerases I, II and III (Hu et al., 2004; Philimonenko et al., 2004; Percipalle and Visa, 2006). In addition actin associates with nascent mRNPs and participates in the recruitment of histone modifiers to transcribed genes. To date it is unknown whether these functions are general or whether these functions are restricted to certain subtypes of genes (Miralles and Visa, 2006).

So far actin has not only been shown to be involved in intra nuclear processes, but also in stabilizing and maintaining the structure of the nuclear envelope itself. The existence of an actin layer on the inside of the nuclear envelope, colocalizing with lamins, has been described (Clubb and Locke, 1998). Further, a nuclear protein complex consisting of emerin, actin and lamin at the nuclear envelope providing stabilization against mechanical stress has been suggested (Holaska et al., 2004; Holaska and Wilson, 2007).

Protein	Function	Reference
Profilin I	A monomer- binding protein that promotes nucleotide exchange	(Skare et al., 2003; Stuven et al., 2003)
CapG	An abundant protein in macrophages, which binds pointed ends of F-actin	(Onoda et al., 1993; Witke et al., 2001)
Zyxin	Zyxin organizes the actin-polymerization machinery and has actin-polymerization-promoting activity	(Nix and Beckerle, 1997; Fradelizi et al., 2001)
Myopodin	A filamentous (F)-actin-bundling protein	(Weins et al., 2001)
Nrf2	Upon oxidative stress, Nrf2 forms a complex with actin that translocates to the nucleus	(Kang et al., 2002)
NDHII	A helicase that seems to bind F-actin in the nucleus	(Zhang et al., 2002)
hrp36, DBP40, hrp65	Proteins that associate with pre-mRNA to form ribonucleoprotein complexes	(Percipalle et al., 2001; Percipalle et al., 2002; Percipalle et al., 2003)
Emerin	A nuclear-envelope protein that interacts with lamin A and actin	(Fairley et al., 1999; Lattanzi et al., 2003)
Lamin A	A major protein of the nuclear lamina, which binds nuclear actin	(Sasseville and Langelier, 1998; Shumaker et al., 2003)
Exportin-6	A nuclear- export receptor that specifically exports profiling-bound actin	(Stuven et al., 2003)
Cofilin1	Upon physiological stress, Cfl1 forms nuclear rods with actin	(Nebl et al., 1996; Arber et al., 1998)
BRG1	Involved in chromatin remodeling, forms multisubunit complex including actin	(Giansanti et al., 1999)
Anillin	Redistributes during cell cycle, is involved in F-actin bundling	(Field and Alberts, 1995; Giansanti et al., 1999)

Table 2: Identified nuclear actin- binding proteins
Modified from Bettinger et al., 2004 and Rando et al., 2000

1.3 The ADF/Cofilin family

A precise spatially and timely regulated actin turnover by ADF/Cofilin appears to be crucial for cells. Since the discovery of the first actin depolymerizing factor a number of various proteins from different species were added to the ADF/Cofilin family, including Cofilin (cosediments with filamentous actin), ADF (Actin Depolymerizing Factor) or destrin (destroys F-actin). Proteins like coactosin from *Dictyostelium*, *Drosophila* twinstar, AtADF1 from *Arabidopsis thaliana* and porcine ADF share a

considerable (30–40%) amino acid sequence identity (dos Remedios et al., 2003). Members of this protein family can be found in plants as well as through the entire animal kingdom. The number of genes coding for members of the ADF/Cofilin family differs from species to species, while up to three different Cofilin genes have been found in plants (Lopez et al., 1996; Hussey et al., 2002) only one gene coding for two functionally distinct isoforms of ADF/Cofilin has been found in the nematode *Caenorhabditis elegans (McKim et al., 1994; Ono et al., 1999)*.

1.3.1 ADF/Cofilin family in the mouse

Three ADF/Cofilins exist in the mouse and presumably in all other mammalian species as well (Vartiainen et al., 2002). These proteins were termed ADF (actin depolymerizing factor,) n-Cofilin for non-muscle Cofilin (synonymous with Cofilin1) and m-Cofilin abbreviating muscle Cofilin (synonymous with Cofilin2).

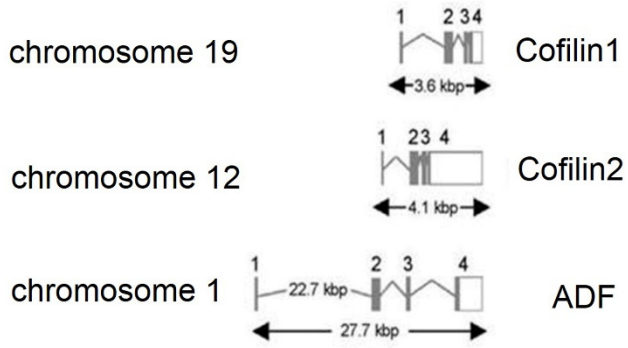

Fig. 5: Genetic structure of the ADF/Cofilin family members. All three ADF/Cofilin genes are composed of four exons with the first exon coding for the start codon ATG. Intron-exon junctions are also conserved among the family members. The genes of Cofilin1 on chromosome 19 and Cofilin2 on chromosome 12 cover about 4 kbp, while ADF on chromosome 2 has an unusually long first intron of almost 23kbp (Gurniak et al., 2005).

Phylogenetic analysis of all known mammalian and avian ADF/Cofilins divided these proteins into the three above mentioned distinct subclasses. On DNA level murine Cofilin1 and Cofilin2 are approximately 80% identical while both are about 70% identical to mouse ADF (Figure 5). In situ hybridization and Northern blot analyses concluded the change of expression patterns of the three ADF/Cofilins during embryonic development. Cofilin1 is expressed in most embryonic tissues and adult cells, Cofilin2 is expressed in muscle cells and brain while the expression of ADF is

restricted to epithelial and endothelial cells. Even though the three ADF/Cofilins are coexpressed in many tissues early in development and show high analogy in their coding sequences (homology on protein level) they differ in function and biochemical characteristics (Vartiainen et al., 2002).

1.3.2 Functions and characteristics of the ADF/Cofilin family members

The most important physiological function of ADF/Cofilins is their involvement in rapid actin turnover. ADF/Cofilins depolymerize F-actin from the pointed end and therefore increase actin dynamics. The total amount of ADF/Cofilins in the cell adds up to 20 µM, about 0,44% of the total amount of protein in the cell (dos Remedios et al., 2003). A number of studies showed species specific differences in the affinity of ADF and Cofilin1 for actin. Murine ADF and Cofilin1 have approximately 5-10 fold higher affinities for actin than previously reported for human and plant ADF/Cofilins (Vartiainen et al., 2002). An approximately two-fold higher affinity of ADF/Cofilins for ADP-actin compared to ATP-actin or ADP-Pi-actin could be assessed thus preventing the binding of ADF/Cofilins to newer filaments (Carlier et al., 1997). Furthermore murine Cofilin2 binds ATP-actin monomers with a 5-10 fold higher affinity than murine ADF and Cofilin1, suggesting differences in their physiological functions. Cofilin2 also shows a smaller difference between the affinity for ADP- and ATP-actin monomers (Vartiainen et al., 2002). The exchange of nucleotides is inhibited in consequence to the binding of ADF/Cofilins to ADP-actin monomers and thereby regulating the recycling of monomeric ADP-actin into ATP-actin (Nishida, 1985). Profilin competes with ADF/Cofilins for ADP-actin and promotes the dissociation of ADP (Pollard and Borisy, 2003). The regulation of the activity of the ADF/Cofilin family members will be discussed in detail in the following chapter (1.3.3).

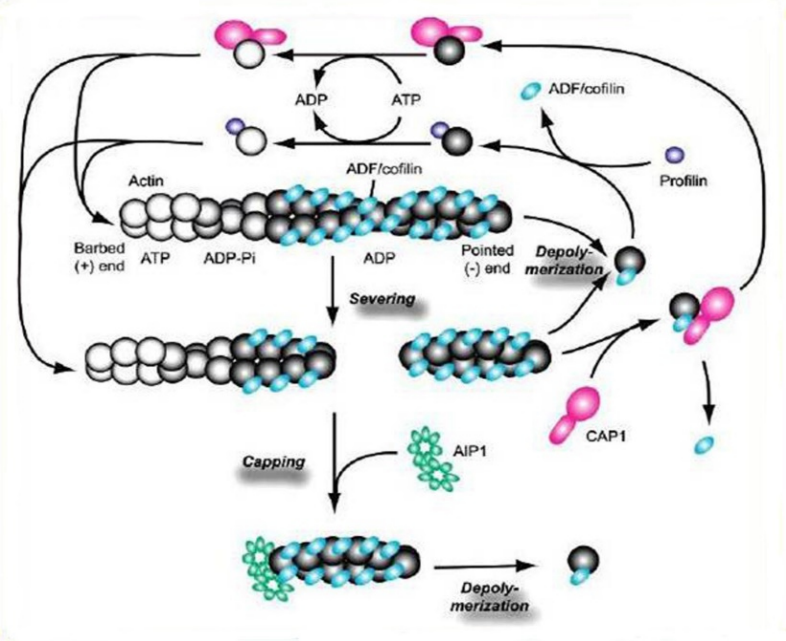

Fig. 6: Model of the regulation of actin dynamics by ADF/Cofilin, CAP1, profilin, and AIP1. ADF/Cofilins preferentially binds to ADP-actin, enhance actin depolymerization from the pointed ends, and sever filaments. Although ADF/Cofilins inhibit the exchange of actin bound nucleotides, profilin and CAP1 enhance exchange of actin-bound ADP with ATP and promote barbed end elongation. AIP1 specifically caps ends of ADF/Cofilin-bound filaments and enhances fragmentation by inhibiting reannealing of monomeric actin of short filamentous actin. AIP1: actin-interacting protein 1; CAP1: cyclase-associated protein 1 (Moriyama and Yahara, 2002; Ono, 2003).

At lower concentration activated ADF/Cofilins bind to F-actin changing the twist about 5° per subunit (McGough and Chiu, 1999), weakening the actin to actin attachments within the filament and initiating severing into small segments increasing the number of ends available for further depolymerization or polymerization as well as increasing the loss of subunits from the pointed end of the filament (Figure 6). AIP1 (Actin-Interacting Protein 1) enhances ADF/Cofilin induced actin dynamics by capping barbed ends and inhibiting annealing of actin monomers (Ono, 2003). ADF/Cofilins are able to nucleate the assembly of actin, a function likely to be important if the barbed end is blocked by proteins like CapZ (dos Remedios, Chhabra et al. 2003).

1.3.3 Regulation of the ADF/Cofilin family members

The members of the ADF/Cofilin family can be regulated in multiple ways. The activity of ADF/Cofilins can be altered by the binding of the membrane lipids phophatidylinositol 4-phosphate (PIP) and phophatidylinositol 4,5-bisphosphate (PIP_2) (Yonezawa et al., 1990) inhibiting the actin-binding (Kusano et al., 1999). Mammalian ADF/Cofilins are inactivated by the phosphorylation of Ser3, thereby also affecting actin binding (Figure 7) (Moriyama et al., 1996). It is suspected that the phosphorylation does not lead to conformational changes but generates charge repulsion inhibiting actin binding (Blanchoin et al., 2000).
Lim kinases (LIMK1 and LIMK2) and TESK (testicular protein kinase) inactivate ADF/Cofilins by phosphorylation. Two phosphatases from unrelated families, involved in the activation of ADF/Cofilins, have been discovered: Slingshot (SSH) and chronophin (Huang et al., 2006).

14-3-3, a family of proteins affecting signaling by modulating localization, causing changes in enzymatic activity, or altering protein-protein interactions (Fu et al., 2000), was also shown to be involved in the regulation of the ADF/Cofilins. The phosphorylated and unphosphorylated forms of ADF/Cofilins both interact with 14-3-3. The binding of 14-3-3 to inactivated ADF/Cofilins is presumably enhanced due to the lack of binding actin. 14-3-3 binding decreases the availability of phosphorylated ADF/Cofilins for activation (i.e. dephosporylation) and therefore has an impact on the rate of ADF/Cofilin phosphocycling. Apart from that a chaperone function to deliver ADF/Cofilins in close proximity to other regulatory molecules (i.e. SSH, LIMK) was suggested for 14-3-3. As mentioned before tropomyosins can protect F-actin from ADF/Cofilins by influencing the actin structure (Sarmiere and Bamburg, 2004).

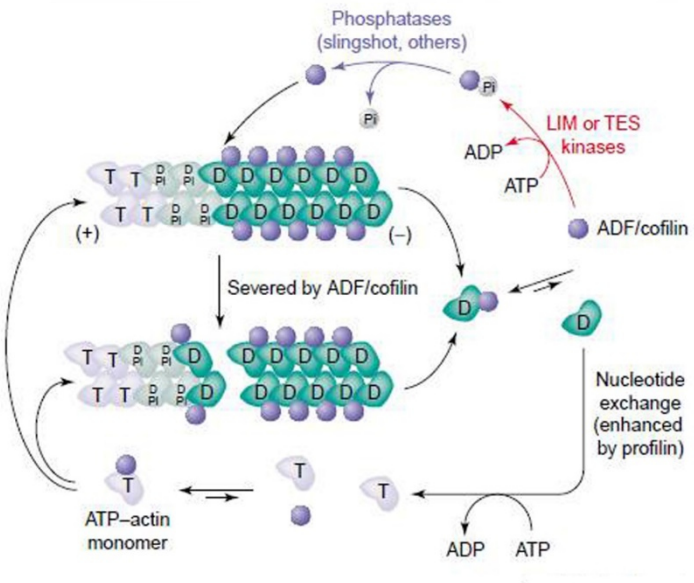

Fig. 7: Regulation of ADF/Cofilins by balance of phosphorylation and dephosphorylation. ADF/Cofilins (purple ball) are inhibited in their activity and dynamics by Lim kinases such as Lin-11/Isl-1/Mec-3 kinases or TESK (testicular protein kinases), which phosphorylate the proteins on their conserved serine 3 residue. Dephosphorylation by the phosphatases chronophin and slingshot activate actin binding of ADF/Cofilins. D: ADP-actin; T: ATP-actin; Pi: inorganic phosphate (Bamburg and Wiggan, 2002; Wiggan et al., 2005).

The pH also has a regulatory effect on the activity of ADF/Cofilins. At acidic conditions (pH less than 6.8) the ability of ADF/Cofilins to stabilize F-actin is enhanced. The mechanism of F-actin stabilization has not been elucidated so far, but it was proposed that the stability is enhanced by a specific twist of the filamentous actin to 162°- 158° (Galkin et al., 2001). At more alkaline conditions (pH higher than 7.3) F-actin can be depolymerized more rapidly (dos Remedios et al., 2003). Whether this regulation by pH alters the structure of actin or ADF/Cofilins is not clear (Bowman et al., 2000).

1.3.3.1 Nuclear translocation signal

All three mammalian ADF/Cofilins contain an amino acid sequence, similar to the core consensus sequence of Simian virus 40 type nuclear translocation signal (NTS), in the form of KKRKK. In Cofilin1 localized at the 30th to 34th amino acid (Nishida et al., 1987). This sequence was proven to function as nuclear translocation signal by site directed

mutagenesis. Iida et al. altered the sequence of Cofilin1 to KTLKK. It was shown that rapid nuclear translocation of Cofilin1 and actin can be induced by various stress stimuli like exposure to heat shock and DMSO (Nishida et al., 1987; Ohta et al., 1989). Upon heat shock KTLKK-Cofilin1 did not translocate to the nucleus and no nuclear actin-Cofilin1 rods were formed (Iida et al., 1992). Cofilin1 is a protein with a molecular weight of approximately 20 kDa and therefore expected to freely pass through nuclear pores (Dingwall and Laskey, 1986) if it exists in a monomeric form, indicating the need of the nuclear translocation signal to chaperone other proteins to the nucleus, for example actin (Hofmann, 2009; Dopie et al., 2012). The NTS of Cofilin1 is also of such importance in consequence to the non-existing nuclear translocation signal of actin (Rando et al., 2000). Upon removal of the stress factor both Cofilin1 and actin translocate back to the cytoplasm. In this thesis the importance, impact and role for nuclear translocation of Cofilin1 was studied with the help of a mouse line carrying a mutated NTS sequence where the wildtype sequence KKRKK was changed to KTRTK. In analogy to mutations in the form of KTLKK for Cofilin1 generated by Iida et al. and the mutated sequence KTKTK in Simian virus 40 previous studies. KTKTK-Cofilin1 was shown to be restricted to the cytoplasm. Both NTS mutants were solely studied in transfected cells (Nakanishi et al., 2002). The Cofilin1$^{KTRTK/KRTK}$ presents the first opportunity to study a Cofilin1-NTS mutant in vivo.

1.3.4 Cofilin1 (Non-muscle Cofilin)

Cofilin1 comprises 166 amino acids in an assortment of species like chicken, mouse, human and pig (Moriyama et al., 1990; Iida et al., 1992).Cofilin1 was shown to comprise two actin binding sides. Cofilin1 is best known for its function as actin depolymerizing factor. In recent studies Cofilin1 has also been linked to a number of cellular processes such as transcription and cytokinesis (Gohla et al., 2005; Kamal et al., 2007; Dopie et al., 2012). To date the *in vivo* function of Cofilin1 is not fully understood. So far several mutants for the members of the ADF/Cofilin have been studied. Disruption of ADF/Cofilin isoforms in *Drosophila melanogaster*, *C. elegans* and *S. cerevisiae* were lethal supporting the importance of the role of the members of the ADF/Cofilin family for cellular mechanisms and actin dynamics. As mentioned

before (1.3.1) the three mammalian ADF/Cofilins (Cofilin1, Cofilin2 and ADF) are similar but show different characteristics. While ADF deficient mice are not distinguishable from wildtype littermates (Bellenchi et al., 2007), the complete deletion of Cofilin1 leads to impaired neural crest cell migration, neural tube closure and is embryonic lethal (Gurniak et al., 2005). Deletion of Cofilin1 in different murine cell types, e.g. podocytes, show phenotypical alterations of morphology or function (Garg et al., 2010). Similar results were shown in zebrafish upon loss of Cofilin1 (Ashworth et al., 2010). The study of the deletion of Cofilin1 under the megakaryocyte-specific PF4 promotor in mice indicates a crucial role for Cofilin1 for the formation of normally sized and discoid-shaped platelets. The deletion of ADF under the same promoter showed normal, fully functional platelets (Bender et al., 2010). Whereas the Cofilin1 knockout is embryonic lethal, the ADF knockout is viable only showing a mild eye phenotype (Bellenchi et al., 2007). Another study on the role of Cofilin1 during early mouse development has shown that decreased Cofilin1 expression is important for compaction during early development. Compaction is the process of cell flattening and polarization by which cellular asymmetry is first established (Ma et al., 2009). The thymocyte specific deletion of Cofilin1 prevents maturation of B-cells. All these studies indicate a crucial role of Cofilin1 during specific stages of embryonic development as well as in adult animals in the function of certain tissues. These data also prove that Cofilin1 plays a fundamental role in development and in adult tissues and that the loss of Cofilin1 cannot always be compensated by ADF and Cofilin2 or other proteins. In this study the function of Cofilin1in the nucleus was the focus of interest.

1.3.4.2 Cofilin1 and Actin

Cofilin1 was shown to directly interact with actin in the nucleus using FRET. This study indicated that there might be more Cofilin1 in a complex with actin in the nucleus than in the cytoplasm in Vero African green monkey fibroblasts (Chhabra and dos Remedios, 2005; Vartiainen, 2008). Chabbrah et al., proposed that almost all G-Actin in the nucleus is bound to Cofilin1, whereas approximately 50% of the cytoplasmic G-Actin is bound to Cofilin1. This would further indicate an importance for Cofilin1 in the nucleus. Another study, performed in yeast, deemed Cofilin1/G-actin complexes unpolymerizable (Du and Frieden, 1998). Further a possible interaction between

Cofilin1 and actin in apoptosis has been suggested. Chua et al. identified the translocation of Cofilin1 from cytosol into mitochondria upon apoptosis induction. Reduction of Cofilin1 protein levels with small-interfering RNA (siRNA) resulted in inhibition of apoptosis. Furthermore, phosphorylated Cofilin1 did not translocate to mitochondria and facilitate apoptosis. It was proposed that the apoptosis-inducing ability of Cofilin1, is dependent on the functional actin-binding domain. Chua et al. concluded that proteins involved in mitochondrial targeting and actin binding are essential for its pro-apoptotic function (Chua et al., 2003). Contrary data was presented by Rehklau et al. They also observed the mitochondrial translocation of Cofilin1 after induction of apoptosis. The study of Cofilin1 deficient mouse embryonic fibroblasts (Mefs) did not show any alterations in apoptosis progression compared to control cells. These data would indicate that Cofilin1 is not essential for apoptosis induction and progression in mammalian cells (Rehklau et al., 2012). Over the years several studies implicated interactions between Cofilin1 and actin beyond depolymerization and severing.

1.3.4.3 Cofilin1 in the nucleus

For years it has been suggested that Cofilin1 may be involved in other processes than the severing and depolymerization of actin filaments. Obrdlik and Percipalle showed that Cofilin1 is in the same complex with actin and phosphorylated RNA polymerase II during the elongation phase of transcription. Chromatin IP assay showed the selective association of Cofilin1 with transcribed regions of active genes. Active genes in Cofilin1 silenced cells were devoid of actin. This indicated that Cofilin1 is indispensable for association of actin and phosphorylated pol II with active genes, presumably through a mechanism that controls and maintains polymerization of gene associated actin. It was suggested that the composition of actin complexes vary dynamically, in polymeric as well as in monomeric forms, along different exonic regions.

Therefore it was hypothesized that Cofilin1 influences RNA-Polymerase II transcription by regulating polymerization of gene associated actin indirectly. By contributing to the local G-actin pool, providing monomeric actin for actin polymers along active genes (Obrdlik and Percipalle, 2011).

1.3.4.4 Cofilin1 in embryonic development

The importance of Cofilin1 for embryonic development has been demonstrated in various studies involving a number of different species.
Cofilin1 is expressed throughout different species often sharing high sequence homologies (Table 3).

	UNC-60	dCfl1	xCfl1	bCfl1	rCfl1	mCfl1	hCfl1	fCfl1	meCfl1	zCfl1
UNC-60		50	44	46	47	**47**	47	46	46	50
TSR			51	52	53	**52**	53	49	51	56
xCfl1				83	83	**83**	83	81	82	82
bCfl1					99	**99**	99	86	85	87
rCfl1						**100**	99	87	86	88
mCfl1							**99**	**87**	**86**	**88**
hCfl1								87	86	88
fCfl1									98	89
meCfl1										90

Table 3: Relative similarity of Cofilin1 amino acid sequences from different species. UNC-60: nematode cfll1; TSR: drosophila melanogaster cfl1; xCfl1: western clawed frog cfl1; bCfl1: bovine cfl1; rCfl1: rat cfl1; mCfl1: mouse cfl1; hCfl1: human Cfl1; fCfl1: fugu cfl1; meCfl1: medaka cfl1; zCfl1: zebrafish cfl1
(Lin et al., 2010).

Murine Cofilin1 (bold numbers) is highly similar to most of the examined Cofilin1 forms from rat, human, cow, western clawed frog for example (100%-83%). It is identical with Cofilin1 from rat and shows a 99% similarity with human Cofilin1. The lowest conformity for mouse Cofilin1 is found when compared to drosophila (52%) and nematode Cofilin1 (47%). Zebrafish and mouse Cofilin1 show a similarity of 88%.

In the phylogenetic tree (Figure 8), Cofilin1 genes were grouped as chordata and in vertebrae. The gene for Cofilin1 is located on different chromosomes in different species (zebrafish: chromosome 14; human: chromosome 11; mouse: chromosome 19), but the same genes are found in the vicinity of the respective Cofilin1 locus, suggesting an evolutionary relationship of the *cfl1* genes in the different species (Lin et al., 2010). The loss of Cofilin1 in zebrafish resulted in severe edema, an abnormal accumulation of fluid around the yolk. Compared to wildtype embryos Cofilin1 deficient

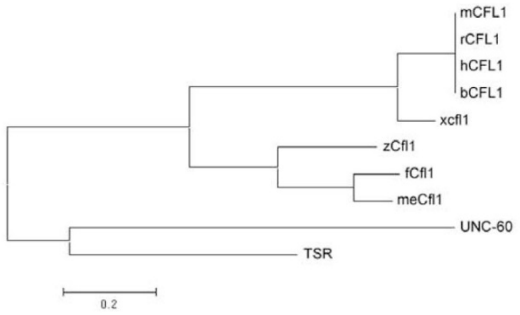

Fig. 8: Phylogenic tree of Cofilin1 amino acid sequences. UNC-60: nematode cfl1; TSR: drosophila cfl1; xCfl1: western clawed frog cfl1; bCfl1: bovine cfl1; rCfl1: rat cfl1; mCfl1: mouse cfl1; hCfl1: human Cfl1; fCfl1: fugu cfl1; meCfl1: medaka cfl1; zCfl1: zebrafish cfl1 (Lin et al., 2010).

zebrafish larvae also showed an absence of a swim bladder, smaller eyes, pericardial effusion, arched backs and altered jaw features (Ashworth et al., 2010). A second group also investigating the loss of Cofilin1 in zebrafish development reported arrested epiboly progression and malformed tail-buds (Lin et al., 2010). Studies in Xenopus showed that Cofilin1 is necessary on the surface of the early cleavage furrow of blastomeres (Tanaka et al., 2005). In *C.elegans*, the loss of Cofilin results in severe aggregation of actin in the developing body-wall muscle (Ono et al., 1999).

The deletion of Cofilin1 in mice leads to embryonic lethality around gestational day 10.5 due to impaired neural crest cell migration and neural tube closure (Gurniak et al., 2005). Further, it has been shown that Cofilin1, but not ADF or Cofilin2, is essential for embryonic development (Bellenchi et al., 2007; Gurniak et al., 2014).

All these data support the importance of Coflin1 in embryonic development of different species.

1.3.4.5 Cofilin1 in neuronal development

The broad expression of Cofilin1 in brain has been shown in a number of different studies (Meberg et al., 1998; Gurniak et al., 2005; Bellenchi et al., 2007; Flynn et al., 2012; Wolf et al., 2014). Direct and indirect alterations of Cofilin1 activity lead to brain-related phenotypes. Modification of LIMK1, a direct regulator of Cofilin1, entail impairment of visuo-spatial constructive cognition (Frangiskakis et al., 1996). The neuronal cell-specific deletion Cofilin1 in a number of different mouse lines, confirmed the importance of Cofilin1 for brain development further. The introduction of Cre-

recombinase driven by the Nestin-promotor into a conditional Cofilin1$^{fl/fl}$, produced a lissencephaly-like phenotype. This brain-restricted Cre-recombinase is (Tronche et al., 1999). Nestin, an intermediate filament protein, is expressed in proliferating cells in the early stages of development in the CNS. Nestin-Cre specific deletion is detectable at E10.5 and marks neuronal progenitor cells in the SVZ. Conditional Cofilin1 Nestin mutants were missing intermediate cortical layers and showed changes in cell shape. (Bellenchi et al., 2007). Emx1, a homeobox gene transcription factor, is specifically expressed in cerebral cortex and hippocampus. In this case the deletion is detectable at E9.5 in principle neurons (Iwasato et al., 2000). The Nex-Cre mouse line is under the control of a neuronal basic-helix-loop-helix transcription factor promotor. Deletion of Cofilin1 in mutants is detectable in postmitotic neurons after E11.5 (Goebbels et al., 2006). The cell-type specific deletion of Cofilin1 using Emx-Cre and Nex-Cre lines, respectively, also rendered neural tissue specific phenotypes, including altered morphology and migration behavior (Schütz and Bläsius, unpublished Data). All these results strongly indicate that Cofilin1 is essential for cortical neuron migration. Bellenchi et al., also reported a significant increase of F-actin accumulation upon the loss of Cofilin1 in neurons.

As mentioned before embryos suffering the complete lack of Cofilin1 enter developmental arrest around E10.5 due to neural crest cell migration impairment and consequently neural tube closure defects (Gurniak et al., 2005). Additional data implicates localization of Cofilin1 in distinct synaptosomal compartments in neuronal cells during development, indicating specific functions (Rust et al., 2010)

The expression pattern of Cofilin1 changes during murine embryonic development. At E8.5 Cofilin1 expression is highest in the neural fold. At E9.5, expression is persistent in the developing nervous system and neural crest. Expression of Cofilin1 can be observed in the somites, the neural tube as well as limb buds after E10.5. In later stages of development localization of Cofilin1 expression becomes restricted to specific tissues. High levels of expression could be observed in the CNS, the trigeminal ganglion and the olfactory lobe among other non-neural tissues at E13.5 and E16.5. In the tissues the expression of Cofilin1 is maintained postnatally (Vartiainen et al., 2002; Gurniak et al., 2005). Summarized it can be said that Cofilin1 plays an essential role in the migration of cortical neurons, since different spatial and temporal deletions of Cofilin1 were shown to be associated with neuronal migration disorders. In humans

a connection between single-nucleotide polymorphism (SNP) of Cofilin1 and an increased risk for spina bifida has been shown (Zhu et al., 2007), affirming the opinion that alteration of Cofilin1 can affect neural tube closure.

1.4 Development of the mouse brain

The development of the brain is one of the most complex processes in nature. The entity of the mechanisms involved in brain development have not been fully elucidated, yet. However, it is known that transcription factors and physiological influences play crucial roles in brain development.

1.4.1 Neural crest cells and neural crest induction

Neural crest cells are a population of transient, multipotent, migratory cells unique to vertebrate embryos giving rise to the neural crest. Originating at the lateral edge of the neural plate, they migrate throughout the embryo, developing a vast variety of cell types like enteric and peripheral neurons and glia, smooth muscle, connective tissue of the face, craniofacial cartilage and bone (Huang and Saint-Jeannet, 2004).
The neural crest, arising at the end of gastrulation, flanks the neural plate and non-neural ectoderm (Figure 9). This border, the neural fold, flanks the neural plate bilaterally.

The neural plates closes during neurulation, bringing together the neural folds at the dorsal midline. Subsequently the cells of the neural crest undergo an epithelial-to-mesenchymal-transition (ETM). Allowing delamination from the neuroepithelium and migration throughout the embryo. The ability to segregate and migrate away from the neuroepithelium is a feature unique to developing neural crest cells (Thiery, 2003). .

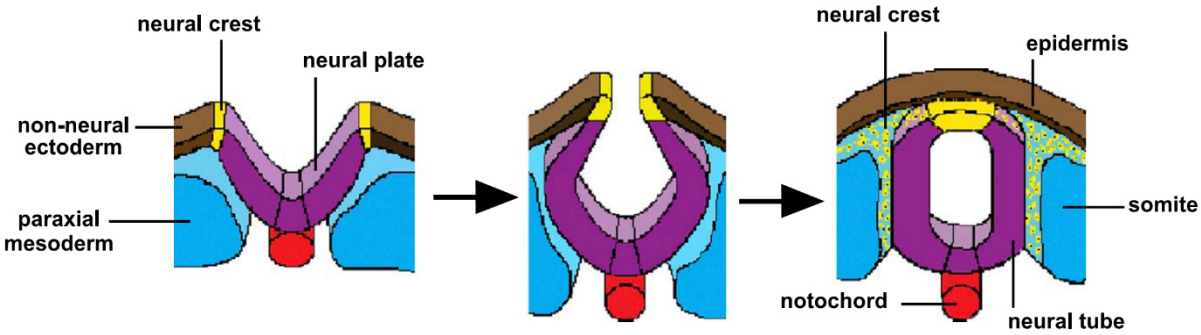

Fig. 9: Neural plate border: The place of neural crest induction. At the beginning of neurulation the neural crest is positioned at the boundary between the neural plate and the non-neural ectoderm. It is positioned at the dorsal aspect of the neural tube, as the neuroectoderm folds. Upon neural tube closure, neural crest delamination and migration start, in most vertebrates including the mouse (Huang and Saint-Jeannet, 2004).

The deletion of Cofilin1 in the murine system causes impairment of neural crest cell migration and neural tube closure defects, resulting in early embryonic lethality (Gurniak et al., 2005).

1.4.2 Neural tube formation

The formation of the neural tube, called neurulation, is a crucial morphogenetic event in development. In mammalian embryos neurulation occurs in two phases named primary and secondary neurulation (Purves, 1985). Studies of mouse models showed that failure of primary neurulation results in exencephaly, craniorachischisis and open spina bifida (1.4.4). Defects in secondary neurulation can result in skin-covered spinal dysraphism (Copp et al., 2013).
The closure of the neural tube is a complex process, taking place early in development (Detrait et al., 2005). One of the first systems to develop and to differentiate during embryonic development is the central nervous system and it is also the one that is last to be completed (Rugh, 1990).

Formation of the brain and spinal cord starts with the neural tube development. In mice the neural tube starts to close around E 8.5 along the ventral line. This process of

neurulation is completed around E10 (Lomaga et al., 2000; Gurniak et al., 2005). The neural plate originates as a thickening from the dorsal surface ectoderm, folds up and fuses in the midline to form the neural tube. Closure of the mammalian neural tube initiates serially at different body axis levels along the spine (Figure 10). Basically, epithelial fusion takes place, creating the neural tube, as the tips of the neural folds are brought into apposition in the dorsal midline. A separate outer surface ectoderm, (forming the future epidermis), and inner neuroepithelial (nervous system) layers are created by epithelial remodeling of the tissues of the dorsal midline (Copp et al., 1990).

Even though neural tube closure is not needed for the subsequent differentiation of specialized neuronal and glia cell types or the connection of nerves, it is an essential step for the development of the brain (Stiefel et al., 2003; Copp, 2005).

Primary and secondary neurulation events are conserved between mammalian species, therefore making the mouse an advantageous model. The closure of the neural tube is a multifactorial process requiring transcription factors and proteins affecting the chromatin structure and protein function. Proteins functioning as part of complexes containing multiple enzymes to ubiquitinate and target proteins for degradation in the proteasome. Loss of these proteins increases neural tube closure defects (Rogner et al., 2000; Copp and Greene, 2010).

Different groups of genes involved in neural tube closure have been identified. Two of the main players in neural tube closure are genes involved in planar cell polarity and folate metabolism.

The closure of the neural tube includes critical cell biological and protein regulatory functions. Cytoskeletal proteins are crucial for cranial closure (Gurniak et al., 2005; Garvalov et al., 2007; Zhu et al., 2007) (Table 4), cell viability-related proteins control apoptosis necessary for neural tube closure, cell cycle/neurogenesis-related proteins ensure a sufficient amount of proliferating cells and avoid premature neuronal formation. The involvement of cell surface-extracellular matrix interactions in neural tube closure still needs to be clarified (Copp and Greene, 2010).

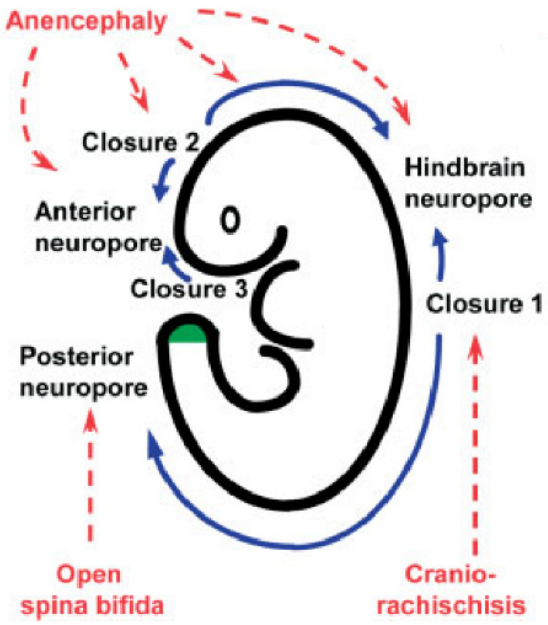

Fig. 10: Diagram representing the process of neural tube closure and the origin of neural tube defects (NTDs). Mouse embryo soon after the completion of cranial neurulation. Initiation events (Closures 1, 2, 3) and completion events (at 'neuropores') are joined by unidirectional or bidirectional neural tube zippering (blue arrows). Events leading to NTDs (red labels) are indicated by red arrows. Secondary neurulation proceeds from the level of the closed posterior neuropore, as a result of canalization within the tail bud (green) (Copp, 2005; Copp and Greene, 2010).

In the mouse the neural folds lift and fuse at the hindbrain/cervical boundary (closure 1), followed by the bidirectional fusion into the hindbrain and along the spinal region. Separate closure initiation sites occur at the midbrain-forebrain boundary (closure 2). In the next step fusion at the rostral extremity of the forebrain takes place (closure 3). For the complete closure of the neural tube fusion continues from these closure sites along the spine completing the process of primary neurulation. In the process of secondary neurulation the formation of the spinal cord at lower sacral and caudal levels is accomplished. The neuropores describe the opening at each end of the neural tube during early embryonic development, leading from the central canal of the neural tube to the exterior (anterior, posterior and hindbrain). A multipotential population of cells in the tail bud differentiates into cells of neural fate. These cells organize themselves in the dorsal part of the tail bud to create a neuroepithelium. The neuroepithelium gives rise to the nervous system (Bu et al., 2007; Copp and Greene, 2010).

1.4.3 Corticogenesis

In the mammalian cortex, patterned structures are formed by neurons and glia cells across six layers. The cortex represents the exterior layer of the telencephalon and is abundant in neuronal cells (Gaspard et al., 2008). The exact mechanism of corticogenesis remains to be elucidated.

Sequential radial migration of neurons, generated from in the subventricular zone, forms the six-layered neocortex. Early generated neurons form the deep cortical layers (V, VI), whereas later generated neurons are destined for upper cortical layers (II, III, IV) a characteristic feature of the inside-out layering of the cortex (Figure 11). Parnavales et al. showed that Cdk5 is involved in preplate splitting, an early step of importance in cortical lamination, setting the foundation for the characteristic inside-out layering of the neocortex. Other studies showed that early preplate neurons preserve a radial relationship to the progenitor cells of the ventricular zone, where they arose from, indicating that a preplate protomap is provided by the ventricular zone (Kriegstein and Parnavelas, 2006). One key player in this process is the extracellular matrix protein, Reelin. It controls radial migration of cortical neurons and also facilitates phosphorylation of Cofilin1 (Chai et al., 2009). Kriegstein et al., also demonstrated that neuronal migration can be regulated by phosphorylation of intracellular substrates (Kriegstein and Parnavelas, 2006).

It was shown in previous studies that in cortical precursor cells the regionalization of cell cycle kinetics appears to play a role in the determination of positioning cortical area borders (Kriegstein and Parnavelas, 2006).

Progenitor cells undergo a distinct pattern of oscillation in the ventricular zone, the interkinetic nuclear migration.

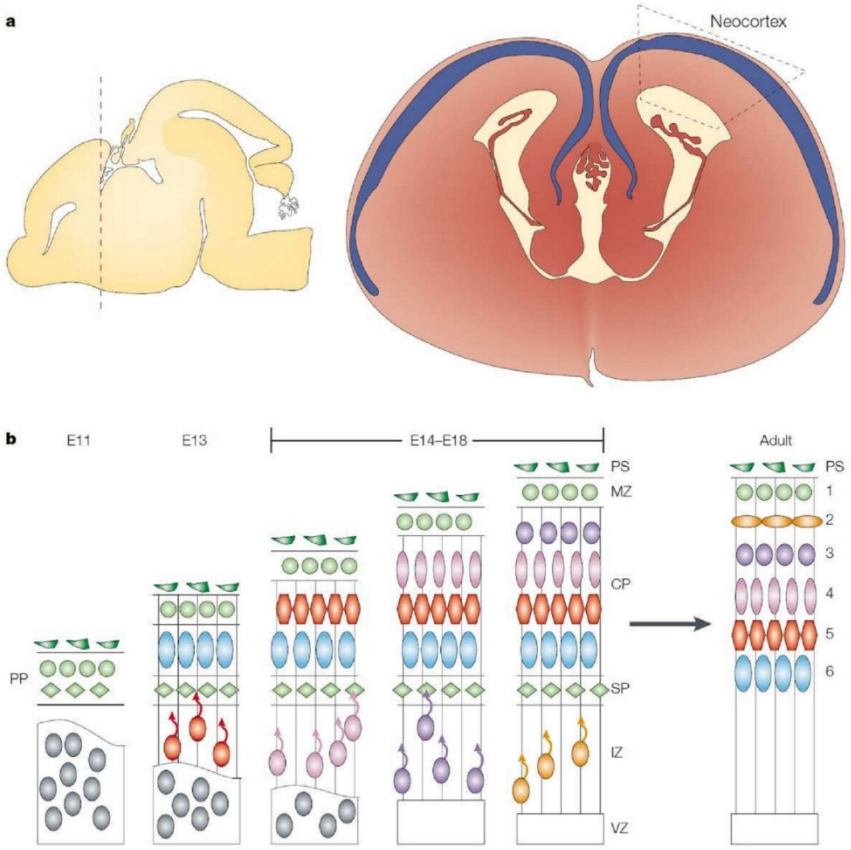

Fig. 11: Formation of the cortical layers during embryonic development. a: Location of the neocortex in the central nervous system. A lateral view of an E16 mouse brain (left). The red dashed line indicates the section plane from which a coronal section (right) has been taken, showing the location of the neocortex. b: The organization of the adult neocortex into distinct neuronal layers. At E11 the preplate is established through the postmitotic migration of neurons from the VZ to the pial surface. A second postmitotic wave migrates through the intermediate zone and splits the preplate into the marginal zone and the more superficial subplate, which generates the cortical plate (E13). During E14- E18 a subsequent wave of neurons from the SVZ (not shown) reaches the cortical plate and expands it in an insight-out-fashion, which means that later born neurons migrate through the existing layers to the pial surface. In the adulthood the subplate degenerates and leaves behind a six-layered cortex. PP: preplate; VZ: ventricular zone; IZ: intermediate zone; SP: subplate; CP: cortical plate; MZ: marginal zone; PS: pial surface; 1-6: referring to the cortical layers I- VI (Gupta et al., 2002).

Cells undergo S-phase at the basal surface of the ventricular zone and then migrate to the apical zone, where mitosis takes place (Gotz and Huttner, 2005).

At E11, first postmitotic cortical neurons migrate out of the ventricular zone and form a transient layer, the preplate. This preplate is split into the marginal zone and the subplate by subsequent waves of migrating neurons at E13. The marginal zone consists of Cajal-Retzius cells, reelin-producing cell types in the marginal zone, while

the subplate consists of remaining primordial cells. Both layers together build the cortical plate. Additional waves of migrating neurons arrive at the cortical plate, bypassing existing layers, migrating to the surface, forming cortical layers I the inside-out fashion (Gupta et al., 2002; Nadarajah and Parnavelas, 2002).

Cortical lamination is established in an inside-out patterning, with cortical neurons migrating from the ventricular zone (VZ) to the marginal Zone (MZ), where Reelin is located. It acts as positional signal for migrating neurons and is essential for correct formation of the six-layered cortex. Reelin deficient mice suffer from inverted cortical lamination, with many neurons located in the MZ and others unable to migrate, accumulating beneath their predecessors (Chai et al., 2009). Reelin was shown to induce phosphorylation of Cofilin1 in migrating neurons as they locate toward the MZ. The inactivation of Cofilin1 affects the stability of the neuronal actin network, stopping migration and positioning cortical neurons in specific layers (Chai et al., 2009). Patterning results from a complex sequence of cell cycle progression in the VZ and migration of neuronal precursor cells from there toward the pial surface (Nadarajah and Parnavelas, 2002). The first post-mitotic neurons leave the germinal VZ to form the preplate early in development. In the next step it is split by infiltrating cortical plate (CP) neurons into the outer MZ and the inner subplate (SP). The MZ and SP present early structures, whereas the intermediate layers, are formed between E13 and E19 in the “inside-out” fashion. Further, interneurons, originated in the medial and lateral ganglionic eminence, migrate long distances into the cortex and hippocampus. Early tangential migration begins around E11 and peaks around E13.5 (Bellenchi et al., 2007).

Previous studies showed that alterations affecting actin cytoskeleton regulator Cofilin1, impact the pathology of cortex development by impaired formation of intermediate layers (1.3.4.5).

1.4.4 Neural tube closure defects (NTDs)

To this date the cellular and molecular mechanisms causing human neural tube closure defects are poorly understood.

Neural tube closure defects can result in a diverse set of birth defects (Figure 12). In humans not all of them are lethal if treated correctly.

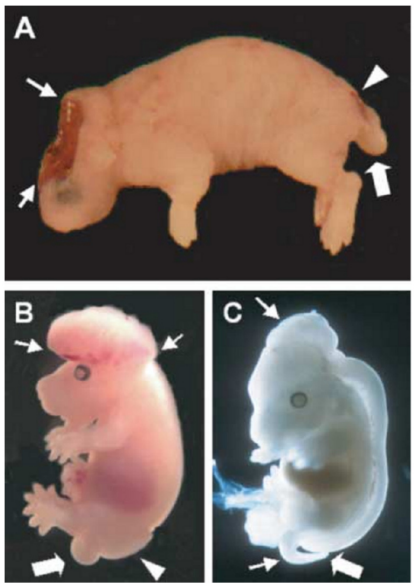

Fig. 12: Murine newborn (A) and E15.5 fetuses (B, C) showing the main cranial neural tube defects. (A) Anencephaly in a curly tail mutant. A lack of skull vault is obvious indicated between small arrows. The skull base is overlaid by the 'area cerebrovasculosa', the remnant of the degenerate brain tissue. Open spina bifida (strictly, myelocele) is present in the lumbosacral region (arrowhead). (B) Exencephaly of the midbrain in a curly tail mutant, showing the everted cranial neural folds (between small arrows). Open spina bifida is also present, affecting the lumbosacral region (arrowhead). (C) Craniorachischisis in a Celsr1 mutant, in which the neural tube is open from midbrain to low spine (indicated between small arrows). Presence of a curled tail can be noted in all cases (large arrows in A–C) (Copp, 2005).

The most frequent NTDs observed are spina bifida and anencephaly, the human counterpart to exencephaly in mouse. Anencephaly presents the less common but most severe manifestation of neural tube closure defects in humans (Detrait et al., 2005). The etiology of malformations of the neural tube are vast and complex. In humans they are thought to arise during the third and fourth week after conception. It is known that genetic along with environmental factors influence this developmental process. Maternal diabetes, maternal obesity and the exposure to hyperthermia in early phases of pregnancy can lead to NTDs (Soler et al., 1976; Webster and Edwards, 1984; Moretti et al., 2005; Rasmussen et al., 2008). It is known that the intake of folic acid reduces the risk of NTD by 50 -70% (Milunsky et al., 1989), indicating that genes involved in the metabolism of folate also have a role in neural tube closure. Folate acts as a cofactor for an enzyme involved in DNA and RNA biosynthesis and also acts as a supplier of methyl groups to the methylation cycle (Scott et al., 1994). Due to the

historical link between NTDs and folic acid, genes involved in folate pathway have been studied most intensively. Another group of genes involved in neural tube closure defects are genes involved in planar cell polarity (Copp et al., 2013).

The leading cause for lethality in human embryos and newborns are congenital anomalies. The most abundant form of birth defects are congenital heart defects followed by congenital malformations of the neural tube affecting 0,5 to 2 out of 1000 established pregnancies in humans along with genitourinary defects (Detrait et al., 2005; Mitchell, 2005; Dolk et al., 2010).

There are approximately 250 known genetic alterations resulting in neural tube closure aberrations in mice offering a vast number of methods to analyze neurulation events at physiological, cellular and even molecular levels (Fairbridge et al., 2010; Harris and Juriloff, 2010).

The wide range of functions of genes whose alterations result in exencephaly implicates that a wide range of cellular activities is crucial to cranial fold elevation (Harris and Juriloff, 1997). A number of different studies show a preponderant occurrence of exencephaly in female embryos, in both mice and humans. In 1986 Hall (Hall, 1986) hypothesized that a temporary functional aneuploidy caused by late X-inactivation could interfere with development and increase the risks for NTDs.

Factors regulating the cytoskeleton have been connected to the formation of neural tube closure defects (Table 4).

Gene symbol(s)	Mouse genes producing NTDs	NTD type	Protein function	Reference
Abl1, Abl2	Abl/Arg double mutant	Ex	Non-receptor tyrosine kinases	(Koleske et al., 1998)
Grlf1	RhoGAP P190	Ex	Glucocorticoid receptor DNA binding factor	(Brouns et al., 2000)
Mapk8; Mapk9	Jnk 1/Jnk2 double mutant	Ex	c-Jun-N-terminal kinases	(Sabapathy et al., 1999)
Marcks	MARCKS (myristoylated alanine rich C-kinase substrate)	Ex	Cytoskeleton-related protein with function in signal transduction	(Stumpo et al., 1995)
Mena, Profilin	Mena/profilin 1 double mutant	Ex	Regulation of actin polymerization	(Lanier et al., 1999)
Mena; Vasp	Mena/Vasp double mutant	Ex	Member of Mena/Vasp/Evl family of cytoskeletal regulators	(Menzies et al., 2004)
Mlp	MARCKS-like protein	Ex±Sb	Cytoskeleton-related protein with function in signal transduction	(Wu et al., 1996)
Cofilin1	Cofilin1	Sb	Actin depolymerizing factor	(Gurniak et al., 2005)
Palladin	Palladin	Ex	Actin cytoskeleton-associated protein	(Luo et al., 2005)
Shrm	Shroom	Ex+Sb	PDZ-containing cytoskeletal protein	(Hildebrand and Soriano, 1999)
Vcl	Vinculin	Ex	Cytoskeletal protein	(Xu et al., 1998)

Table 4: Mouse genes causing NTD (neural tube closure defects) via mechanism involving disturbance of the cytoskeleton. Ex: Exencephaly; Sb: Spina bifida; NTD: Neural tube closure defect (Copp and Greene, 2010).

Many of these mouse lines show autosomal recessive inheritance unlike the majority of human cases. Even though the mutant gene in these mouse lines are identified, the mechanism by which neural tube closure defects arise are generally not clear (Harris and Juriloff, 1997; Harris and Juriloff, 1999; Copp et al., 2003)

1.5 Aim of thesis

In previous *in vitro* studies it was shown that the amino acid sequence KKRKK of Cofilin1 functions as the nuclear translocation signal (NTS), allowing the translocation of Cofilin1 into the nucleus upon certain stress stimuli like DMSO or heat shock. Cofilin1 deficient mice show a failure of neural tube closure and go into developmental arrest around embryonic day 10. In humans mutations and alterations of Cofilin1 have been associated with the neural tube closure defect termed spina bifida.

A knock in mouse line with the mutated NTS of Cofilin1, which was mutated from the wildtype sequence KKRKK to KTRTK was created (2.1). Previous studies in vitro showed that GFP-KTRTK-Cofilin1 was unable to translocate to the nucleus upon induction. Homozygous mutants, Cofilin1$^{KTRTK/KTRTK}$ embryos, showed cranial tube closure defects (Gurniak, unpublished data).
The aim of this thesis was to elucidate the biochemical properties and characteristics of KTRTK-Cofilin1.
In the initial step the depolymerizing activity and actin binding capacity of the mutant protein were analyzed.

The focus of this study was the closer analysis of the malformation of the brain, with the help of histology and immunohistochemistry, to gain more detailed information concerning structures to understand the origin of the deformity. To gain insight of the process that causes the observed malformations, early stages of development, as soon as the exencephalic phenotype was distinguishable, were prepared. To analyze whether also internal structures were affected by the mutation of the NTS of Cofilin1 sagittal whole body sections and skeletal isolations were prepared and analyzed in detail.

In vitro studies of mouse embryonic fibroblasts (Mefs) isolated from Cofilin1$^{KTRTK/KTRTK}$ embryos indicated the involvement of Cofilin1 in cytokinesis. To allow further analysis and characterization of KTRTK-Cofilin1, *in vitro* and *in vivo* studies, particularly with regard to morphological and biochemical characteristics were performed. Furthermore, gene expression profiles for embryonic brain and Mefs were analyzed.

2. Materials

2.1 Mouse line

Name	Description	Reference
KTRTK-Cofilin1	Transgenic mouse line, in which wildtype Cofilin1 was substituted with KTRTK-Cofilin1	Christine Gurniak

The Cofilin1 locus spans 2.8 kbp and comprises 4 exons, the first exon solely encodes the start codon ATG. Previous studies have shown that Cofilin1 has a nuclear translocation signal, located in exon 2, crucial for the entrance of Cofilin1 in the nucleus. The role of nuclear translocation is unknown. To analyze the function of this sequence, it was targeted in the mouse line used in this study (Table 5), analogue to prior studies. In the targeting construct two loxP sites flanking a neomycin resistance cassette were introduced in the first intron. Neomycine resistance facilitates the selection of homologous recombination in ES cells. Previous gene targetings showed that the insertion of loxP sites in the first intron does not interfere with the expression of Cofilin1. The mutation of the nuclear translocation signal (Figure 13) was introduced in exon 2. Wildtype Cofilin1 has a core nuclear translocation signal consisting of the five amino acids KKRKK, which is located in exon 2. The adenines at position two in the codon triplets coding for lysines at position two and four of the wildtype KKRKK sequence were substituted for cytosines, causing the substitution of the lysines at the positions two and four by threonines on the amino acid level in the KTRTK allele for the KTRTK- Cofilin1 mice.

Wt-Cfl1	GAA GAA GTG **AAG AAA CGC AAG AAG** GCG GTG E E V **K K R K K** A V
KTRTK-Cfl1	GAA GAA GTG **AAG ACA CGC ACG AAG** GCG GTG E E V **K T R T K** A V

Table 5: Wildtype and mutated nuclear translocation signal (bold letters) of Cofilin1. Panel 1 (on top) shows the wildtype amino acid and nucleotide sequence of Cofilin1. The mutated sequence for KTRTK-Cofilin1 is shown in panel 2. Lysines at the position 2 and 4 of the wt NTS sequence were substituted for threonines. Exchange was attained by the replacement of adenines on nucleotide level with cytosines (red letters) at the second position of the triplet.

In a gene targeting experiment the wt Cofilin1 allele was replaced by the KTRTK/neo Cofilin1 allele by homologous recombination. Chimeras were produced transmitting the KTRTK/neo-Cfl1 allele through the germline. To induce the deletion of the neomycin resistance cassette heterozygous KTRTK/neo-cfl1 mice were crossed to Cre-deleter mice (Schwenk et al., 1995).

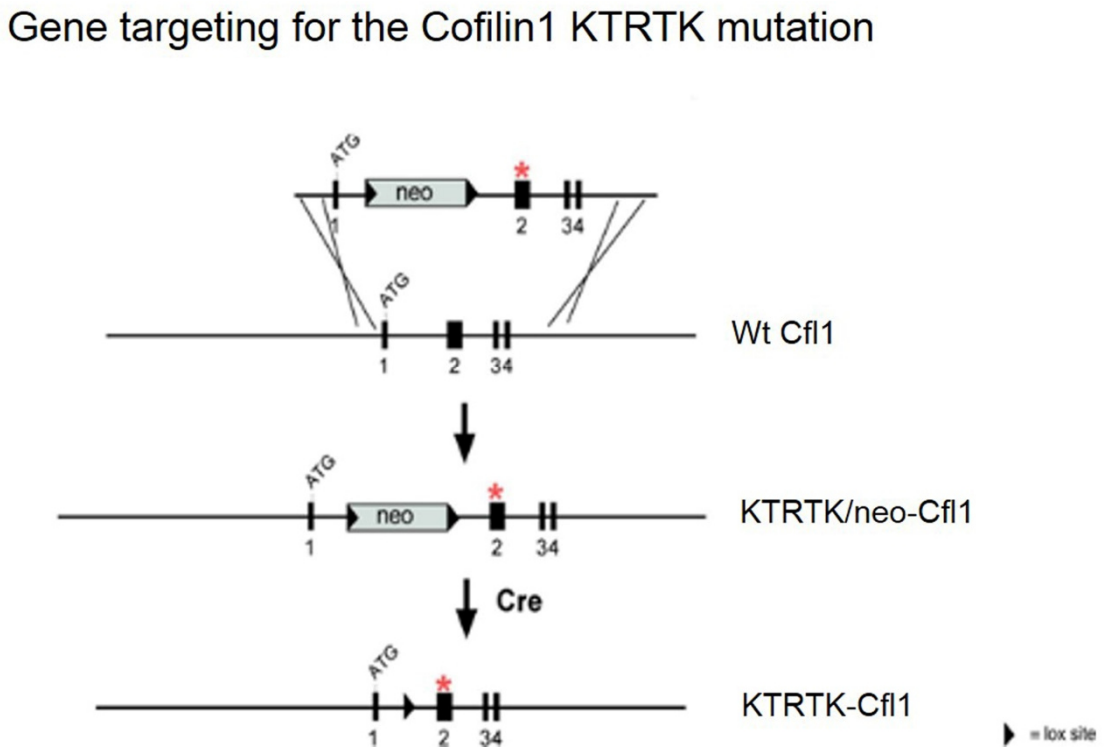

Fig 13: Generation of KTRTK- Cofilin1 mice. The schematic drawing shows the gene targeting construct for the Cofilin1 gene (top) and the genomic map of the Cofilin1 gene (wt cof 1) comprising four exons (black boxes, 1-4). LoxP-sites (black arrow heads) flanking the neomycin resistance gene (neo) were inserted between exon 1 and exon 2 (KTRTK/neo-cof 1). Exon 1 of Cofilin1 comprises exclusively the start codon of the coding region, methionine.The red asterisk indicates the position of the introduced mutation of the nuclear taregt sequence in exon 2. Upon Cre recombinase activity the neomycin resistance cassette is deleted.

To obtain homozygous Cofilin1$^{KTRTK/KTRTK}$ mutants, heterozygous Cofilin1$^{wt/KTRTK}$ mice were crossed. Embryos were analyzed using PCR or Southern blot.

2.2 Commercial solutions

2.2.1 Commercial solutions for nucleic acid analysis

Name	Supplier
dNTPs	Promega
$MgCl_2$	Promega
PCR-flexi-buffer (5x)	Promega
DNAse buffer (10x)	Invitrogen

2.2.2 Commercial enzymes for nucleic acid analysis and modification

Name	Supplier
Taq-Polymerase	Promega
RQ1 DNase	Invitrogen

2.2.3 Commercial solutions and reagents for tissue culture

Name	Supplier
DMEM	Gibco
Fetal calf serum (FCS)	PAA
HEPES pH 7.2 (100x)	Gibco
L-Glutamine (100x)	Gibco
Non- essential amino acids (100x)	Gibco
Penicillin/Streptomycin antibiotics (100x)	Gibco
Sodium pyruvate (100x)	Gibco
PBS^- (tissue culture grade)	Gibco
Trypsin-EDTA (0.05%)	Gibco
Trypsin (2.5%)	Gibco
DMSO	Sigma
Neurobasal medium	Gibco
B-27 supplement	Gibco

MEM (10x)	Gibco
MEM essential amino acids (50x)	Gibco
MEM non- essential amino acids (100x)	Gibco
AraC	Calbiochem
DNAse grade II	Roche
HBSS	Gibco
Distilled water (tissue culture grade)	Gibco
G418	Sigma
Doxorubicin	Alfa Aesar

2.2.4 Commercial solutions for protein analysis

Name	**Supplier**
Bradford 5x solution	BIO-RAD
Broad Range Standard	BIO-RAD
SeeBlue Plus2 Prestained Standard	Invitrogen

2.2.5 Commercial solutions and dyes for histology

Name	**Supplier**
4% Histofix	Roth
Eosin Y (0.5%)	Sigma
Mayer’s haemalaun solution	Merck
Gill’s Haemalaun solution	Thermo scientific
Alizarin Red	BDH Laboratory Supplies England
Alcian Blue 8GX	BDH Laboratory Supplies England
Cresyl violet acetate	Sigma
DAB peroxidase substrate tablet	Sigma immuno chemicals

2.3 Commercial chemicals and reagents

2.3.1 Liquids

Name	Supplier
Acetic acid	Merck
Acetone	Merck
Acrylamide (30%)	AppliChem
Bovine serum albumin (BSA), (10mg/ml)	New England Biolabs
Chloroform	Merck
Dimethyl sulfoxide (DMSO)	Merck
Ethanol (analysis grade)	Merck
Ethanol (technical)	Merck
Ethidium bromide (1%)	BIO-RAD
Fish gelatin	Sigma
Formaldehyde (37%)	Merck
Glutaraldehyde (25%)	Sigma
Glycerol	AppliChem
Hydrochloric acid (HCl, 37%)	Merck
Hydrogen peroxide (30%)	Merck
Isopropanol	Merck
Methanol	VWR
N,N- Dimethylformamide (DMF)	Sigma
Nitric acid (HNO_3)	AppliChem
Nitrogen (liquid)	German-Cryo
NP-40	Sigma
Phenol	Merck
SDS (20%)	AppliChem
Sodium hydrogen carbonate ($NaHCaO_3$)	Sigma
TEMED	Sigma
Triton®X-100	Roche
Trizol®	Life Technologies
Tween®20	Sigma
Xylene	VWR
β-mercaptoethanol	Sigma

2.3.2 Solids

Name	Supplier
Agar	AppliChem
UltraPure agarose (gel electrophoresis)	Invitrogen
Ampicilin	AppliChem
APS	Fischer Scientific
Bovine serum albumin (BSA)	Merck
Bromphenol blue	BIO-RAD
Citrate acid	BDH Laboratory Supplies England
Coomassie Brilliant Blue	BIO-RAD
EDTA	Sigma
Gelatin	Sigma
Glucose	Merck
Glycine	Grüssing
HEPES	Sigma
Luminol	Sigma
Magnesium chloride ($MgCl_2$)	Merck
Milk powder (non-fat)	Roth
MOPS	Sigma
Moviol	Roth
$NaHCO_3$	Merck
NPG	Sigma
PBS^-	Sigma
p-hydroxy-coumarin	Sigma
PIPES	Sigma
Potassium ferricyanide (K3[Fe(CN)6])	Sigma
Potassium ferrocyanide (K4[Fe(CN)6])	Sigma
Potassium hydroxide (KOH)	Merck
Protease inhibitor cocktail tablets, complete mini, EGTA free	Roche
Proteinase K	Sigma
SDS	Merck
Sodium chloride (NaCl)	Merck
Sodium citrate	Sigma
Thrombin, bovine	Calbiochem
Tris Base Ultra Quality	Roth
X-Gal	Sigma

2.4 Commercial Kits

Name	Supplier
Vybrant® CFDA SE Cell Tracer Kit	Invitrogen
BrdU Labeling and detection Kit II	Roche
VECTOR® M.O.M. Immunodetection Kit	VECTOR Laboratories
PureLink® HiPure Plasmid Filter Purification Kits	Invitrogen
SuperScript™ III First-Strand Synthesis System for RT-PCR	Invitrogen

2.5 General stock solutions, buffers and media

2.5.1 General solutions

Solution	Composition
PBS^- (no Ca^{2+}, no Mg^{2+}) (1x)	9.6 g Dubelcco's PBS → add MilliQ to 1 liter → autoclave
4% paraformaldehyde (PFA)	4% (w/v) PFA → heat 1x PBS^- in microwave → add PFA and stir → cool down and sterile filtrate → store aliquots at -20°C
TBS (10x)	1.47 M NaCl 0.4M Tris/HCl (pH 8.0)

2.5.2 Solutions for the analysis of nucleic acids

Solution	Composition
TENT buffer (stock)	20 mM Tris-HCl, pH 8.3 0.1 mM EDTA 1% Tween®20 0.2% Triton®X-100 → autoclave
Proteinase K solution (stock)	10 µg/µl Proteinase K in MilliQ → store aliquots at -20°C
Genomic DNA extraction buffer	10 ml TENT buffer (stock) 160 µl Proteinase K solution (stock) → 200 µl aliquots → store at -20°C
TE buffer	100 mM Tris-HCl, pH 8.0 1 mM EDTA → autoclave
TAE (50x)	242 g Tris base 57.1 ml acidic acid 100 ml 0.5 M EDTA, pH 8.0 → add MilliQ to 1 liter
DNA loading buffer (100ml)	40% (w/v) Saccharose 0.5% (w/v) SDS 0.25% (w/v) Bromphenol blue → add TE buffer to 100 ml
DNA ladder PhiX 174 (HAEIII)	100 µl marker 100 µl Fermentas loading buffer (1:6) 400 µl MilliQ → store aliquots at 4°C
DNA lambda phage ladder Eco911 (BstEII)	100 µl marker 100 µl Fermentas loading buffer(1:6) 400 µl MilliQ → heat for 5 minutes at 65°C → incubate 3 minutes on ice → store aliquots at 4°C
RNA Isolation	
DEPC H_2O	100 ml MilliQ 0.1 ml DEPC → stir o.n. under fume hood → autoclave one hour

RNA sample buffer	50% (v/v) Formamide 6% (v/v) Formaldehyde 10 µg/ml EtBr in 1x RNA gel buffer
RNA loading buffer	50% (w/v) Saccharose 0.25% (w/v) Bromphenol blue → add DEPC H_2O to 100 ml
RNA gel buffer (pH8.0)	20 mM MOPS/NaOH 5 mM Sodium-acetate 1 mM EDTA in DEPC H_2O
RNA running buffer (pH 7.0)	20 mM MOPS/NaOH 5 mM Sodium-acetate 1 mM EDTA in DEPC H_2O

2.5.3 Solutions and media for the tissue culture

2.5.3.1 General Media for tissue culture

Solution	**Composition**
HeLa/Mef- medium	425 ml Dulbecco's modified Eagle's medium (DMEM) 50 ml fetal calf serum (FCS) 5 ml L-Glutamine (100x) 5 ml Penicillin/Streptomycin (100x) 5 ml Non-essential amino acids (100x) 5 ml Sodium pyruvate (100x) 5 ml HEPES pH 7.2 (100x) → sterile filtrate
Freezing medium	HeLa/Mef- medium 10% (v/v) DMSO (tissue culture grade)

20% Moviol + NPG	20 % (w/v) Moviol 2.5 mg/ml NPG → stir Moviol in MilliQ in the dark until completely dissolved → add NPG → stir → store aliquots at -20°C

2.5.3.2 Solutions and media for cultivating and analyzing Mefs

Solution	**Composition**
Concentrated Trypsin	Trypsin-EDTA 1:20 (v/v) 2.5% Trypsin
Gelatin (0.2%)	0.2% (w/v) 'porcine skin gelatin' in MilliQ → autoclave
PI wash	1x PBS^- 1 g/l Glucose 0.1 mM EDTA ➔ filter
PI staining solution	8 ml 1x PBS^- 12.5 µl PI-slurry 12.5 µl RNaseA 10mg/ml ➔ store in the dark ➔ prepare fresh

2.5.3.3 Solutions and media for analyzing cultured cells

Solution	**Composition**
MACS cell separation buffer	2 mM EDTA 0.5% FCS in 1x PBS^- → store at 4°C
MACS blocking solution	1% (v/v) fish gelatin in MACS cell separation buffer

2.5.3.4 Solutions and media for cultivating and analyzing neural cells

Solution	Composition
BSA stock solution (5%)	1x PBS^- (TC grade) 5% (w/v) BSA → store at 4°C
HEPES stock solution (1M, pH 7.25)	1 M HEPES powder →dissolve in distilled water (TC grade) →adjust pH → store at 4°C
HBSS /HEPES solution (7mM)	500 ml HBSS 3.5 ml 1 M HEPES stock solution → store at 4°C
Trypsin/ HEPES solution	100 ml 0.05% Trypsin-EDTA 700 µl 1M HEPES stock solution → store 10 ml aliquots at -20°C
HBSS + Dnase	100 ml HBSS /HEPES solution (7mM) 1 ml Dnase → store aliquots at -20°C
Neurobasal medium complete	94 ml neurobasal medium 2 ml B-27 1 ml L-Glutamine 1 ml Pen/Strep 2 ml FCS → sterile filtrate
Ara-C (stock)	12 mg Ara-C →dissolve in 50 ml distilled water (TC grade)
Astrocyte inhibition medium	Neurobasal medium complete → add 1:200 AraC (stock)
2% PFA +2% sucrose	2% (w/v) PFA 2% (w/v) sucrose in PBS^- → store 10 ml aliquots at -20°C

MEM–FCS medium	300 ml distilled water 50 ml 10x MEM 20 ml 5.5% $NaHCaO_3$ 15 ml 20%(w/v) Glucose 5 ml L-Glutamine (100x) 10 ml 50x MEM essential amino acids 10 ml 100x MEM non-essential amino acids 50 ml FCS → adjust pH to 7.3 using 1M NaOH → fill up with distilled water (TC grade) to 500 ml → filter sterile

2.5.4 Solutions and media for bacterial culture

Solution	**Composition**
Ampicillin (stock)	50 mg/ml Ampicillin in MilliQ → sterile filter → store aliquots at -20°C
IPTG (stock)	1 M IPTG in MilliQ → store aliquots at -20°C
LB_0 medium	10 g Bacto-Tryptone 5 g Bacto-yeast extract 10 g NaCl → add MilliQ to 1 liter → autoclave
LB_{Amp} medium	Dilute Ampicillin (stock) 1:1000 to LB_0 medium
LB_0-plates	15 g Agar → add LB_0 medium to 1 liter → autoclave → cool to 55°C and pour plates → store plates at 4°C
LB_{Amp}-plates	15 g Agar → add LB_0 medium to 1 liter → autoclave → cool to 55°C and add Ampicillin stock (1:1000) → pour plates → store plates in the dark at 4°C

GST lysis buffer	5 mM EDTA 0.5% (v/v) Triton®X-100 10% Sucrose → in PBS → add 1 tablet complete protease-inhibitor in 50 ml directly before use
GST washing buffer	0.5% (v/v) Triton®X-100 → in PBS

2.5.5 Solutions for protein analysis

Solution	**Composition**
SDS running buffer (10x)	250 mM Tris 1.9 M Glycine 1% (w/v) SDS in MilliQ
SDS-PAGE separation gel (15%; for 7gels)	25 ml 30% Acrylamide 9.4 ml 2 M Tris-HCl, pH 8.8 0.5 ml 10% SDS 15 ml MilliQ 240 µl 10% APS 45 µl TEMED
SDS-PAGE stacking gel (15%; for 7gels)	4.8 ml 30% Acrylamide 0.3 ml 10% SDS 17.4 ml MilliQ 7.5 ml 0.5 M Tris-HCl, pH 6.8 150 µl 10% APS 30 µl TEMED
Fractionation buffer A	5 mM MgCl 100 mM NaCl 50 mM HEPES, pH 7.0 → sterile filter → store at 4°C
Fractionation buffer B	Fractionation buffer A 1% NP-40 → store at 4°C

PEB	20 mM Tris, pH 8.0 100 mM NaCl 5 mM EGTA 2 mM EDTA 0.5% (v/v)Triton®X-100 1 tablet Protease-Inhibitor in 10 ml PEB → store at 4°C
PHEM (10x, pH 7.0)	600 mM PIPES 200 mM HEPES 100 mM EGTA 20 mM $MgCl_2$ → store at 4°C
G/ F-actin separation buffer	1% (v/v) Triton®X-100 in 1x PHEM
SDS sample buffer (5x)	110 mM Tris, pH6.8 20% (v/v) Glycerol 3.8% (w/v) SDS 8% (v/v)ß-Mercaptoethanol Bromphenol blue *ad libidum* in MilliQ
Coomassie Brilliant Blue staining solution	0.1% (w/v) Coomassie Brilliant Blue 50% (v/v) Methanol 10% (v/v) Acetic acid in MilliQ → stir o.n. → filter
Rapid destain	30% (v/v) Isopropanol 6% (v/v) Acetic acid in MilliQ
Towbin transfer buffer (1x)	25 mM Tris/HCl, pH8.5 190 mM Glycine 20% (v/v)Methanol → add MilliQ to 1 liter
NCP- azide, pH 8.0 (10x)	600 mM Tris/HCl 1.5 M NaCl 0.5% (v/v)Tween® 20 → add MilliQ to 1 liter
NCP + azide, pH 8.0 (10x)	600 mM Tris/HCl 1.5 M NaCl 0.5% (v/v) Tween® 20 2 g Sodium azide → add MilliQ to 1 liter

Western Blot blocking solution	5% (w/v) Milk powder in 1x NCP + azide
Primary antibody solution (Western Blot)	1:x antibody in Western blot blocking solution
Secondary antibody solution (Western Blot)	1:x antibody in 1x NCP- azide 5% (w/v) Milk powder
Luminol stock solution	0.44 g Luminol in 10 ml DMSO → store at -20°C
p-hydroxy-coumarin stock	150 mg p-hydroxy-coumarin in 1 ml DMSO → store at -20°C
ECL	Solution A: 200 ml 0.1 M Tris-HCl, pH 8.6 4 ml luminol stock 0.1ml p-hydroxy-coumarin stock → store solution in the dark at 4°C Solution B: 200 ml 0.1 M Tris-HCL, pH 8.6 0.2 ml H_2O_2 (from 30-35% stock solution) → store solution in the dark at 4°C
BSA stock solution (5%)	1x PBS^- 5% (w/v) BSA → store aliquots at -20°C
BSA solution (1%)	1x PBS^- 20% (v/v) BSA stock solution
IF permeabilizing solution	0.1 % (v/v) Triton®X-100 in PBS
IF blocking solution	BSA solution (1%) 5% (v/v) goat serum
IF antibody solution (primary and secondary antibody)	1:x antibody 0.5% (v/v) goat serum BSA solution (1%)
G-buffer (10x)	20 mM Tris 2 mM CaCl2 0,1% sodium acide

G-buffer (1x)	After dilution: → add 0,2 mM ATP → adjust pH to 8,0 with 1 M HCl → add 0,1 mM DTT
Actin polymerization buffer (50x)	2,5 M KCl 0,1 M MgCl2 1 mM ATP → adjust pH to 7, with 1 M NaOH

2.6 Buffers for actin assays

Solution	**Composition**
Pyrene assay	
G assay buffer	2 mM Tris-HCl, pH8.0 0.5 mM DTT 0.2 mM ATP 0.1 mM $CaCl_2$ 0.01% NaN_3
KMEI (10x)	500 mM KCl 10 mM MgCl2 10 mM EGTA 100 mM imidazole, pH 7.0
Falling ball assay	
G-Mg assay buffer	2 mM Tris-HCl, pH8.0 0.5 mM DTT 0.2 mM ATP 0.1 mM $MgCl_2$ 0.01% NaN_3
K50MEI (10x)	50 mM KCl 10 mM MgCl2 10 mM EGTA 100 mM imidazole, pH 7.0
Assay binding buffer	1.1ml K50MEI (10x) 8.9 ml G-Mg assay buffer

2.7 Solutions for histology

Solution	Composition
Dye stainings	
Eosin Y (0.05%)	1% (v/v) Eosin Y (5%) in 96% EtOH
Mayer's haemalaun solution (50%)	50% (v/v) Mayer's haemalaun solution (stock) in 50% (v/v) distilled water
Acetic acid (3%, pH 2.5)	3% (v/v) acetic acid in Elix H_2O
Alcian Blue staining solution (0.8 -1%, sections)	0.8 -1% (w/v) Alcian Blue → fill up with 3% acetic acid → stir for at least 30 minutes → protect solution from light
Alizarin Red staining solution (0.015%, whole mount)	0.015% (w/v) Alizarin Red → fill up with 1% KOH solution → stir for at least 30 minutes → protect solution from light
Alcian Blue staining solution (0.05%, whole mount)	0.05% (w/v) Alcian Blue 30% (v/v) glacial acetic acid 70% (v/v) absolute ethanol (analysis grade) → stir for at least 30 minutes → protect solution from light
KOH solution (2%, stock)	2% (w/v) KOH → fill up with MilliQ
Nissl staining solution (100 ml)	0.1 g cresyl violet acetate 100 ml Elix (pre-warmed to 37°C) → stir for approx. 90 min →protect from light → add 300µl glacial acetic acid → filtrate →warm up to 37°C before use

Senescence staining solutions

Senescence fixing solutions	1% FA + 0.2% GA in PBS
	1% FA in PBS
	0.2% GA in PBS → always prepare freshly
X-Gal solution (Dimri)	20 mg/ml X-Gal →dissolve in DMF → store at -20°C → protect from light
Potassium ferricyanide solution	100 mM Potassium ferricyanide in MilliQ → protect solution from light → store at 4°C
Potassium ferrocyanide solution	100 mM Potassium ferrocyanide in MilliQ → protect solution from light → store at 4°C
Sodium phosphate buffer	M Dibasic sodium phosphate in MilliQ
Citric acid buffer (Dimri)	0.1 M Citric acid in MilliQ
Citric acid/ sodium phosphate buffer (200mM; pH4.0, 5.0, 5.5, 6.0, Dimri)	36.85 ml 0.1 M citric acid 63.15 ml 0.2 M dibasic sodium phosphate → use 1 M citric acid to adjust pH
X-Gal staining solution (Dimri) (pH 6.0, 5.5, 5.0, 4.0)	1 mg/ml X-Gal solution 40 mM citric acid/sodium phosphate, (pH 6.0, 5.5, 5.0, 4.0) 150 mM NaCl 2 mM $MgCl_2$ 5 mM Potassium ferricyanide solution 5 mM Potassium ferrocyanide solution → fill up with MilliQ →protect from light → prepare directly before use

Antibody stainings

Citrate buffer (10x, pH 6.0, epitope retriever)	100 mM sodium citrate in MilliQ → adjust pH 1M using citric acid → store at 4°C
Oldenburg buffer (1x, pH 7.4)	50 mM Tris 1.5% NaCl → add 800ml MilliQ → adjust pH to 7.4 → add 0.4% (v/v) Triton®-X-100 → fill up to 1l
Primary antibody solution for IHC	5% (v/v) NGS 1% (v/v) BSA in Oldenburg buffer
Secondary antibody solution for IHC	0.5% (v/v) NGS 1% (v/v) BSA in Oldenburg buffer
DAB	9 ml MilliQ →dissolve tablet in MilliQ → protect from light →add 1ml 10x TBS →store aliquots at -20°C

2.8 Antibodies

2.8.1 Primary antibodies

Name	Antigen	Clone	Origin	Dilution	Source
7D10	ADF	Monoclonal	Mouse	WB: 1:5	Witke lab
AC74	Actin	Monoclonal	Mouse	IF: 1:1000	Sigma
β-III-tub	β-III-tubulin	Monoclonal	Mouse	IF: 1:500 IHC: 1:200	Promega
BrdU	BrdU	Monoclonal	Mouse	IHC 1:10	Roche
C4	Actin	Monoclonal	Mouse	WB: 1:5000	MP Biomedicals
Ctip2	**Ctip2**	Monoclonal	Rat	IF: 1:100	Abcam
Cux1	Cux1	Monoclonal	Mouse	IF: 1:100	Abcam
FHU1	Cofilin 2	Polyclonal	Rabbit	WB: 1:500	Witke lab
GAPDH	GAPDH	Monoclonal	Mouse	WB: 1:10.000	Calbiochem
GFAP	GFAP	Monoclonal	Mouse	IF: 1:500	Millipore
KG60	Cofilin1	Polyclonal	Rabbit	WB: 1:500 IF: 1:100	Witke lab
NeuN	NeuN	Monoclonal	Mouse	IHC: 1:100	Millipore
PCNA	PCNA	Monoclonal	Mouse	WB: 1:500	Biosource
Reelin	Reelin	Monoclonal	Mouse	IF: 1:100	Millipore

2.8.2 Secondary antibodies

Antigen	Clone	Species	Labeling	Dilution	Source
Mouse	Polyclonal	Goat	FITC (green)	IF: 1:400	Invitrogen
Rabbit	Polyclonal	Goat	FITC (green)	IF: 1:400	Invitrogen
Rat	Polyclonal	Goat	(FITC (green)	IF: 1:400	Invitrogen
Mouse	Polyclonal	Goat	Alkaline phosphatase	IHC: 1:250	DAKO
Mouse	Polyclonal	Goat	Horseradish peroxidase	WB:1:1000	Thermo Scientific
Rabbit	Polyclonal	Goat	Horseradish peroxidase	WB: 1:1000	Thermo Scientific

2.8.3 Staining reagents

Name	Dilution	Supplier
Phalloidin Alexa – 488	IF: 1:200	Merck
DAPI	1:1000	Sigma
Draq5	1:1000	Abcam

Name	Excitation/ Emission	Final concentration/ Dilution	Supplier
CFDA-SE	Green (FL1)	Flow-Cyt: 1µM	Invitrogen
DNase I	Alexa- 488 (FL1)	Flow-Cyt: 1:500	Merck
Phalloidin	Alexa – 680 (FL4)	Flow- Cyt: 1:200	Merck

2.9 General laboratory, tissue culture, bacterial culture and histology materials

2.9.1 Plastic ware

Name	Supplier
Safe seal tubes (1.5ml/ 2ml)	Sarstedt
Tubes (15ml, 50 ml)	Sarstedt
Snapshot tubes (3ml, 12ml)	BD Falcon
PCR tubes	Bioplastics
Pipettes (5ml, 10ml, 25ml, 50ml)	BD Falcon
Pipette tips (20µl, 200µl, 1000µl)	Sarstedt
Pipette tips plugged	Molecular Bio Products
Pasteur pipettes	Sarstedt

2.9.2 Glass ware

Name	Supplier
Glass bottles (50ml, 100ml, 250ml, 500ml, 1000ml)	Schott
Glass pipettes (5ml, 10ml, 50ml)	Brandt
Microscope slides	VWR
Glass pasteur pipettes	Volcan
Glass pasteur pipettes (plugged)	Volcan

2.9.3 General tissue culture material

Name	Supplier
Accu-jet (electronic pipette boy)	Brandt
Eppendorf tubes (1.5ml/ 2ml)	Eppendorf
Filter (for medium filtration; 0.2 µm)	Millipore
Plastic pipettes (1ml, 2ml, 5ml, 10ml, 25ml, 50ml)	BD Falcon
Plastic tubes (15ml, 50 ml, Mefs, HeLa)	Sarstedt
Cell culture flasks (25cm^2, 75cm^2, 175cm^2, Mefs, HeLa)	Corning Life Sciences
Petri dishes (Ø : 3cm; 10cm; Mefs , HeLa)	BD Falcon
Well plates (96- ; 48- ; 24-; 12- and 6-well)	Corning Life Sciences
Plastic tubes (15ml, neural culture)	Corning Life Sciences
Cell culture flasks (25cm^2, 75cm^2; neural culture)	Nunc
Petri dishes (Ø : 6cm; neural culture)	Nunc
Cryotubes	Nunc
Coverslips (Ø; 13 + 18mm)	VWR
Coverslip holder (porcelain, for neural culture)	Thomas- scientific

2.9.4 General bacterial culture material

Name	Supplier
Petri dishes (10cm)	VWR
Erlenmeyer flask (100ml, 500ml)	VWR

2.9.5 General histology material

Name	Supplier
Embedding cassettes	Leica
Embedding molds	VWR
Entellan	Merck
Microscope slides	VWR
Microscope slides, Superfrost plus	Thermo Scientific
Paraffin Paraplus	Sigma
Razor blades	Apollo

2.10 Further material

Name	Supplier
Transfer membrane Immobilon-P	Millipore
Parafilm	Brandt

2.11 Technical equipment

Description	Supplier
Accu-jet® (electronic Pipette-Boy)	Brandt
Binocular MS 5 +	Leica
camera ConProgRes C10 plus + light source KL 1500 LCD	JENOPTIK Germany
BioChem VacuuCenter BVC 21 +	BioChem
VacuuHandConrol VHC	BioChem
Centrifuge 5415 D	Eppendorf
Centrifuge 5417 R	Eppendorf
Centrifuge tissue culture	Beckmann
CTR 5500 + camera DFC 420 C	Leica
Epitope retriever 2100	Prestige™ Medical
FACS C6 Flow Cytometer	Accuri
Freezer (-80 °C)	Thermo Scientific
Gel-electrophoresis running chamber	European Molecular Biology Laboratory
Glass-Teflon tissue grinders	Kontess Glass Co. Duall®
Heating block	Grant/QBT
Heating block for histology	VWR

Heating plate for histology	Leica
Homogenizer apparatus	Bosch
Incubator for bacterial culture	Heraeus
Incubator for tissue culture	Heraeus
BZ-900 Biorevo microscope	Keyence
ImageQuant LAS4000 mini imager	GE Healthcare
LSM	Zeiss
Magnetic stir plate	Heidolph
Microscope tissue culture	Leitz
Microtome	Microm
Oven for drying sections	Heraeus
Oven in histology	Heraeus
PCR machine PTC-200 Peltier thermal cycler	MJ Research
pH-meter, pH Level 2	InoLab
Pipettes	Gilson
Power supply (for agarose gels)	Pharmacia
Power supply Power PAC 200	BIO-RAD
Rocker	Heidolph
SDS gel apparatus SE250	Pharmacia Biotech
Semi-dry blotting chamber	BIO-RAD
Shaker	New Brunswick Scientific
Spectrophotometer UV-DU 640	Beckmann
Vortex-Genie 2	Scientific Industries
Water purifier	Millipore

2.12 Nucleic acids

2.12.1 Oligonucleotides for PCR

Name	Sequence (5' to 3')	Binding site	PCR
Mut-Nuc 3' (#669)	CCA GAA GAA GTG AAG ACC CGC A	Binds to the 5' region, ends in the KTRTK mutation	KTRTK Mutation
Cof1 1-250-5' (#17)	CTT GGT CTC ATA GGT TG	Anneals to the 3' region downstream of the KTRTK mutation sequence	KTRTK Mutation
Coin sma 3' (#347)	CGC TGG ACC AGA GCA CGC GGC ATC	Binds upstream of the loxP site in the first intron	Cof1-lox
Coin1-5' (#619)	CGA GGT ACA GTG ACT ACA GAA TG	Anneals downstream of the loxP site in the first intron	Cof1-lox

2.12.2 TaqMan probes for qPCR

Name	Sequence (5' to 3')	Label	ID
TaqMan Cofilin1	AGA AGC TGA CAG GAA TCA AGC ATG A	FAM	Mm03057591_g1 life technologies
TaqMan GAPDH	GGTGTGAACGGATTTGGCCGTATTG	Vic	Mm99999915_g1 Life technologies

2.13 Recombinant plasmids

Name (Plasmid number)	Description	Reference
GST-wt-Cofilin1(101)	Wt Cofilin1 cloned into pGex-2T at BamHI restriction site	Christine Gurniak
GST-KTRTK-Cofilin1 (494)	KTRTK-Cofilin1 cloned into pGex-2T at BamHI restriction site	Melanie Jokwitz
GFP-wt- Cofilin1 (99)	Wt Cofilin1 cloned into pEFG-C3 at SmaI restriction site	Christine Gurniak
GFP-KTRTK-cofilin1 (483)	KTRTK-Cofilin1 cloned into pEFG-C3 at SmaI restriction site	Christine Gurniak

2.14 Strains of bacteria

Name	Reference
XL1-Blue (for plasmid 483)	(Bullock et al., 1987)
JM105 (for plasmid 99)	(de Taxis du Poet et al., 1987)

2.15 Eukaryotic cell lines

Name	Description	Reference
HeLa wt	Well established cell line originally derived from human cervix carcinoma	(Hsu et al., 1976)
HeLa A12	Lamin producing HeLa cells	Witke Lab
HeLa GFP- Cofilin1 wt	Transfected HeLa wt cells, expressing GFP- Cofilin1 wt stably	Witke Lab
HeLa GFP-KTRTK-Cofilin1	Transfected HeLa wt cells, expressing GFP-KTRTK- Cofilin1 stably	(Roy, 2011)
Mef Cofilin1$^{wt/wt}$ **Mef Cofilin1$^{wt/KTRTK}$** **Mef Cofilin1$^{KTRTK/KTRTK}$**	Mouse embryonic fibro-blasts isolated from embryos of heterozygous mated KTRTK-Cofilin1 mice	(Roy, 2011)

2.16 Marker

DNA marker

Lambda-BstEII
Fermentas

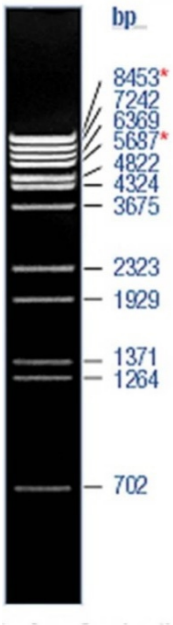

PhiX-174- HaeIII
Fermentas

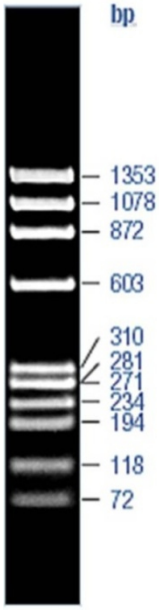

Protein marker

Broad Range Standard
BIO-RAD

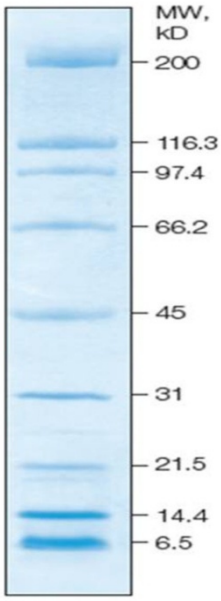

SeeBlue Plus2 Prestained Standard
Invitrogen

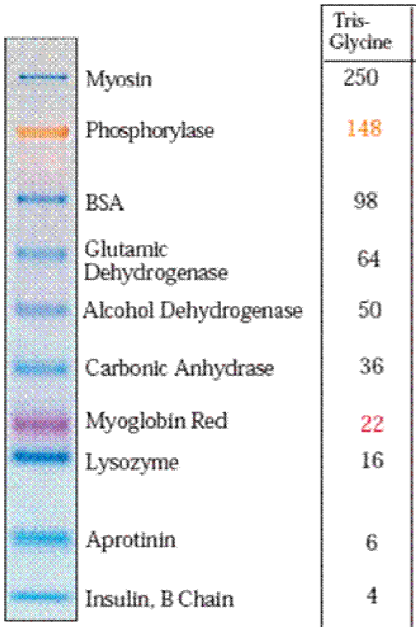

3. Methods

3.1 Molecular Biology

3.1.1 Genotyping by PCR

The polymerase chain reaction (PCR) provides a means of exponentially amplifying DNA (Mullis and Faloona, 1987). Using the enzyme Taq-Polymerase, originally isolated from *Thermus aquaticus*, a pre-existing DNA template and short single stranded oligonucleotides (Primer) allow the amplification of a chosen target sequence from the template DNA. The used oligonucleotides are complementary to the sequences at either end of the target DNA. Each synthesized DNA molecule becomes a template for the synthesis of a new DNA molecule therefore creating a chain reaction. Every PCR cycle consist of three steps: denaturation, annealing and elongation.

The denaturation of the DNA at 94° C is the first step of the PCR cycle. In this phase the strands of the template DNA are separated. In the second phase, the annealing phase, the reaction temperature is lowered to 55 – 72°C allowing the hybridization of the complementary oligonucleotides (primers) to the DNA template. Oligonucleotides usually consist of 18-30 bases, containing a guanine and cytosine content of 40-60%. The sequence of oligonucleotides should be specific to ensure a specific hybridization to the target sequence and avoid unspecific DNA products. They are essential because Taq-Polymerase cannot start a *de novo* synthesis, a starting molecule is required to start elongation. In the following phase the temperature is maintained at 72°C, the optimal temperature for the Taq-Polymerase, to allow the elongation of the new synthesized DNA strands in 5' -> 3' from the oligonucleotides. At the end of the cycle the amount of DNA is multiplied by the factor of two. To initiate a new cycle the temperature is raised to 94°C again. This cycle of denaturation, annealing and elongation is repeated 35 times for the PCRs used in this work.

In this thesis PCR was used to determine the genotypes of embryos and adult mice.

3.1.1.1 Genotyping of mice by PCR

To determine the genotype of transgenic mice 2-4 mm tail biopsies were taken from pups at postnatal day 21-28 or from adult animals used in experiments in order to confirm the genotype. The tail biopsies were digested over night (o.n.) in 200 µl genomic DNA extraction (2.5.2) buffer at 55°C in a heating block. The following day the tubes were vortexed vigorously before boiling at 95°C for 10 minutes. Afterwards the tubes were centrifuged at 13.200 rpm for 10 minutes. 1 µl of the supernatant was used for PCR. The tail biopsies were stored at 4°C or RT.

3.1.1.2 Genotyping of embryos by PCR

To analyze the development of the embryos more precisely the developmental stages had to be exactly determined. Therefore timed matings were set up, offering the opportunity to analyze the embryos at defined stages in their development. One to two females were placed in a cage with a male o.n. Mating was determined by the existence of a vaginal plug. The morning after the mating was defined as E (embryonic day) 0.5 of pregnancy. The stages E10.5 to E18.5 were further analyzed. To determine the genotype of embryos at various developmental stages a tissue sample of the amnion or the tail was used. The tissue was digested in genomic DNA extraction buffer and treated as mentioned above. 1 µl of the supernatant was used for PCR.

3.1.1.3 Genotyping PCRs

3.1.1.3.1 Cof1-lox- PCR

This PCR was generally used for genotyping pups, adult mice and embryos of the KTRTK-Cofilin1 mouse line. The oligonucleotides (see 2.12.1) used in this PCR anneal in the first intron of the Cofilin1 gene. The upstream primer (Coin sma 3') binds in front of the loxP site in the first intron, while the downstream primer (Coin1-5') binds behind

the loxP site (Figure 14), resulting in a band of 391 bp. In the wildtype allele there is no loxP site therefore the expected band has a size of 347 bp.

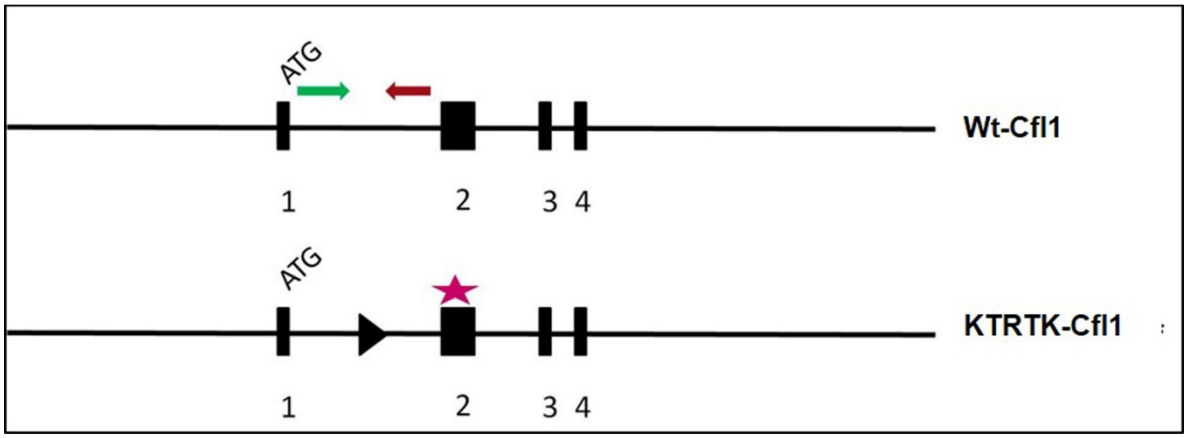

Fig.14: Schematic diagram of wildtype (Wt) and mutant (KTRTK) Cofilin1 alleles analyzed by PCR. The oligonucleotides are indicated as arrows. Coin sma 3' (green arrow) anneals upstream of the loxP site (black arrow head), while Coin1-5' (red arrow) binds downstream of the loxP site. For KTRTK-Cofilin1 the amplified fragment has a size of 391 bp, for wt Cofilin1 347 bp. Cofilin1 comprises 4 exons (black boxes, 1-4), exon 1 encodes the start codon ATG exclusively, the pink asterisk indicates the position of the inserted mutation in exon 2

Cof1-lox PCR mix

PCR mix for one PCR sample		
1.0	µl	DNA
8.87	µl	H_2O
4.0	µl	PCR-Flexi-buffer (5x)
1.5	µl	$MgCl_2$ (25 mM)
1.5	µl	dNTPs mix (2.5 mM)
1.5	µl	Primer 1 (5 pmol/µl)
1.5	µl	Primer 2 (5 pmol/µl)
0.13	µl	Taq- polymerase (5 U/ µl)

20 µl per reaction

PCR program for the Cof1-lox PCR		
94°C	2 min	
94°C	30 sec	
55°C	40 sec	35
72°C	40 sec	cycles
72°C	5 min	

3.1.1.3.2 KTRTK-Mutation PCR

To ensure the mutation of the nuclear translocation signal of Cofilin1 was present this PCR was used to confirm the results of the Cof1-lox PCR. The upstream oligonucleotide (Mut-Nuc 3') (2.12.1.) anneals to the template ending in the mutation and does not amplify the wildtype allele. The downstream oligonucleotide (Cof1 1-250-5') (2.12.1.) binds to the 3' region downstream of the KTRTK mutation sequence (Figure 15). This PCR allowed the identification of one or two KTRTK-Cofilin1 mutant alleles. The PCR product was expected at a size of 200 bp.

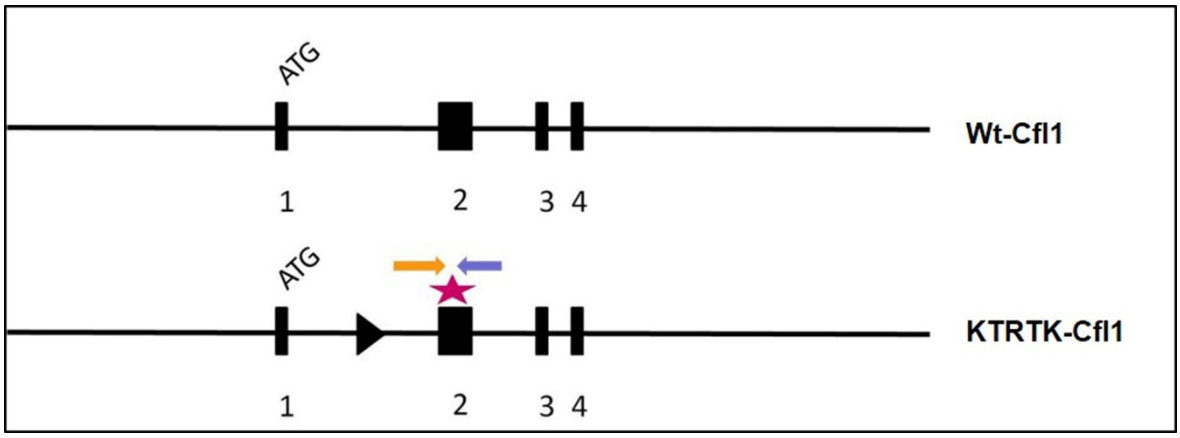

Fig.15: Schematic diagram of wildtype (Wt) and mutant (KTRTK) Cofilin1 alleles analyzed by KTRTK-Mut PCR. Wt and KTRTK-Cofilin1 each comprise 4 exons (black boxes, 1-4), the inserted loxP site (black arrow head) is located in the first intron. Exon 1 solely encodes the start codon ATG, the mutation of the nuclear translocation signal is localized within exon 2 (pink asterisk). Primer Nuc-Mut 3' (orange arrow) ends in the KTRTK mutation. Cof1 1-250-5' (blue arrow) anneals downstream of the KTRTK mutation. There was no DNA fragment amplified for the wt Cofilin1 allele. The amplified product has a size of 200 bp.

KTRTK-Mutation PCR mix

PCR mix for one PCR sample			PCR program for the KTRTK-Mut PCR		
1.0	µl	DNA	94°C	3 min	
8.87	µl	H_2O			
4.0	µl	PCR-Flexi-buffer (5x)	94°C	40 sec	
1.5	µl	$MgCl_2$ (25 mM)	55°C	75 sec	35 cycles
1.5	µl	dNTPs mix (2.5 mM)	72°C	60 sec	
1.5	µl	Primer 1 (5 pmol/µl)			
1.5	µl	Primer 2 (5 pmol/µl)	72°C	5 min	
0.13	µl	Taq- polymerase (5 U/ µl)			

20 µl per reaction

3.1.2 Gel electrophoresis

The amplified DNA fragments can be visualized by agarose- gel electrophoresis. This method is based on the separation of molecules according to their intrinsic electrical charge (Clark, 2006). It allows a qualitative and quantitative analysis of the products. In an electrophoresis DNA moves to the anode due to the negative charge of the DNA resulting from the phosphate groups in the backbone. Depending on the size of the respective DNA fragments 0.8- 1.5 % (w/v) agarose gels were prepared. 1.5 µl ethidium bromide were added per 100 ml of gel. Agarose was boiled in 1x TAE until the agarose was completely melted. The gel was poured into a running chamber, combs were inserted and later the gel was covered with 1x TAE (2.5.2) after polymerization. Gels were run at constant voltage of 50-70 Volts for 30-45 minutes. Afterwards the results were documented using an UV-light based imager system.

3.1.3 RNA isolation

To investigate mRNA expression levels in mutant and control, RNA was isolated from E14.5 Mefs and embryos at the developmental stages E10.5 to E18 for qPCR and microarray analyses.

3.1.3.1 Isolation of RNA from mouse tissues for qPCR

Shock-frozen tissue was homogenized in appropriate volume of Trizol® using a Polytron at full speed. All purification steps were performed under a fume hood. Upon complete dissociation of the tissue 1/4 volume of chloroform/isoamyl alcohol (24:1) was added. Next, samples were vortexed at full speed. After ten minutes of incubation at room temperature, samples were centrifuged at 3000 rpm for 15 minutes at 4°C to achieve phase separation. The upper aqueous phase, containing the RNA, was carefully transferred to a fresh tube. Proteins and DNA are mainly contained to the interphase and phenol phase, respectively.

Following the addition of 1 volume of chloroform to the aqueous phase, samples were vortexed, incubated and spun down once more.

Upon transfer of the aqueous phase to a fresh tube 1 volume of isopropanol was added. Samples were mixed and incubated on ice for 5 minutes in the next step. After centrifugation at 4000 rpm at 4°C for 20 minutes, supernatant was removed and pellet was washed with 70% EtOH/ DEPC H_2O and left to dry at room temperature. Pellets were resuspended in appropriate volume of DEPC H_2O/ 0.1% SDS.

In order to remove any remaining DNA contamination, samples underwent DNAse digestion for 45 minutes at 37°C. To achieve highest purity and quality of RNA, phenol/ chloroform (1:1, pH7.4) extraction was repeated. RNA was mixed with 1 volume of phenol/ chloroform, vortexed, incubated and spun down to achieve phase separation. Aqueous phase was transferred to a fresh tube and one volume of chloroform was added. After incubation, the samples were centrifuged. The aqueous phase was transferred to a fresh tube and another chloroform extraction step was performed.

Upon centrifugation, upper phase was transferred to a fresh tube, 1/10 volume of 2M NaOAc (pH 4.5) was added and mixed before adding 2.5 volume of absolute ethanol for precipitation at -20°C over night.

On the following day, RNA samples were spun down at full speed at 4°C for 20 minutes. Upon removal of supernatant, pellets were left to dry at room temperature. In the final step RNA pellets for resuspended in an appropriate volume of 10mM Tris/HCl (pH 7.4).

In order to analyze integrity, quantity and quality of isolated RNA, NanoVue measurements were performed along with the run of a denaturing RNA gel.

This extensive protocol for RNA isolation yields a high quality and purity outcome, allowing the use of this RNA for highly sensitive experiments such as qPCR. Shock-frozen tissue E10 total embryos and E13.5, E16.5 and E18 brains were homogenized in an appropriate volume of Trizol® using a Polytron at full speed. Upon complete dissociation of the tissue 1/4 volume of chloroform/ isoamyl alcohol (24:1) was added, samples were vortexed and incubated at room temperature for 10 minutes and afterwards centrifuged at 3000 rpm for 15 minutes at 4°C to achieve phase separation. The upper aqueous phase, containing the RNA, was carefully transferred to a fresh tube.

Following the addition of 1 volume of chloroform to the aqueous phase, samples were vortexed, incubated and spun down once more.

The aqueous phase was mixed with 1 volume of, incubated on ice for 5 minutes and centrifuged at 4000 rpm at 4°C for 20 minutes. The pellet was washed with 70% EtOH/ DEPC H_2O and left to dry at room temperature. Pellets were resuspended in an appropriate volume of DEPC H_2O/ 0.1% SDS.

In order to remove any remaining DNA contamination, samples underwent DNAse digestion for 45 minutes at 37°C. To achieve highest purity and quality of RNA, a phenol/ chloroform (1:1, pH7.4) extraction was performed followed by two extractions with chloroform. The aqueous phase was transferred to a fresh tube, 1/10 volume of 2M NaOAc (pH 4.5) was added and mixed before adding 2.5 volume of absolute ethanol for precipitation at -20°C o.n.

On the following day, RNA samples were spun down at full speed at 4°C for 20 minutes, pellets were left to dry at room temperature and resuspended in an appropriate volume of 10mM Tris/HCl (pH 7.4).

In order to analyze the integrity, quantity and quality of isolated RNA, measurements using a NanoVue were performed along with a denaturing RNA gel.

This extensive protocol for RNA isolation yields a high quality and purity outcome, allowing the use of this RNA for highly sensitive experiments such as qPCR and microarray.

3.1.3.2 cDNA synthesis

Before a qPCR could be performed, a cDNA had to be synthesized on the respective mRNA using the SuperScript™ III First-Strand Synthesis System. Every sample was prepared in duplicate, to control for DNA contaminations reactions without reverse transcriptase (-RT) and reactions plus reverse transcriptase (+RT). In the denaturing step RNA, hexamer primers and dNTPs were incubated at 65°C for 5 minutes and then put on ice for 1-2 minutes before the cDNA synthesis mix was added, followed by an incubation at 50°C for 50 minutes. To terminate the synthesis reaction, samples were exposed to a heat shock at 85°C for 5 minutes and then kept on ice. To eliminate any remaining RNA contamination of the cDNA, RNase H was added. Digestion took place at 37°C for 20 minutes. Synthesized cDNA was stored at -20°C.

3.1.3.3 qPCR RT-PCR from mouse tissue

Quantitative PCR (qPCR) allows you the gathering of information regarding the levels of RNA expression of specific gene of interest. Along with the gene of interest, so called housekeeper genes, are always tested. They are used for normalization. Genes, which behave the same in control and mutation and are not influenced by mutations, are qualified as so called housekeeper genes and used for normalization. In this experiment GAPDH was used as reference. qPCRs are quite sensitive and react to a

diversity of factors such as contamination, deviations in pipetting and concentrations. In order to analyze the mRNA levels of wt-Cofilin1 compared to KTRTK-Cofilin1, TaqMan probes annealing independent of the NTS were used, Vic labeled Cofilin1 (2.12.2) and FAM labeled GAPDH probes were used.

The principle of TaqMan probes is based on the 5´- 3´ *Taq*-polymerase exonuclease activity. In TaqMan probes a fluorophore is covalently attached to the 5´-end of the oligonucleotide probe while a quencher is attached to the 3´- end. During hybridization to the complementary target sequence, the *Taq*-polymerase cleaves the dually labeled probe, resulting in an emitting fluorescence signal. As long as the quencher and the fluorophore are in proximity, any fluorescence signal is inhibited by the quencher. This fluorescence signal allows quantitative measurements in regard to the accumulating product during the exponential phase of the PCR. A number of different fluorophores as available. In this case FAM (excitation: 492 nm; emission: 516 nm) and VIC (excitation: 535 nm; emission: 555 nm) were used (Aldrich, 2008).

PCR mix for one PCR sample

4.0	µl	cDNA (1:10)
0.5	µl	GAPDH- TaqMan FAM
0.5	µl	Cfl1- TaqMan Vic
5	µl	TaqMan mastermix

10 µl per reaction

PCR program for the Cofilin1 qPCR

1.	95°C	10 min	
2.	95°C	10 sec	
3.	60°C	30 sec	
4.		Acquisition	
5.		Go to 2.	39x

Program: TAQMAN AB

To analyze possible deviations all +RT samples were measured in triplicates for more detailed analysis.

3.1.3.4 qPCR RT-PCR from mouse tissue

The acquired data was analyzed using the ΔCT-method, a form of relative quantification.

Relative quantification can provide information regarding changes and differences in gene expression. For this form of quantification a reference gene (GAPDH) for normalization is needed, that should not be influenced by the introduced mutation, in this experiment (C_T- reference).

For each sample the ΔCT-method uses calculations for the difference between reference C_T (GAPPDH) and target gene C_T (Cofilin1) values. The first step in analysis required the normalization of Cofilin1 expression, determining the relative expression of both genes for each sample.

$$1)\ Relative\ expression\colon 2^{(CT(GAPDH)-CT(Cofilin\ 1))}$$

This value represents the expression of Cofilin1 relative to GAPDH in the respective sample. In the subsequent step the ratio of expression between wildtype and mutant is calculated.

$$2)\ \frac{Relative\ expression\ (mt)}{Relative\ expression\ (wt)}$$

3.1.4 Microarray

Microarrays allow high-throughput molecular profiling, screening the expression of thousands of genes at the same time (Duggan et al., 1999). In this control and mutant embryonic mouse brains (E16.5) and Mefs (E14.5) were analyzed with the goal to identify critically altered genes. Microarray analyses were performed in collaboration with the laboratory of Prof. Schultz at the University of Bonn, using the Illumina® bead chip system.

3.1.4.1 Isolation of RNA from Mefs and embryonic brains for microarray analysis

Mefs from one confluent T75 cell culture flask were washed with PBS^-, trypsinized and pelleted. Upon removal of supernatant, pellets were carefully resuspended in 2ml Trizol®, and divided into two parts. Samples were vortexed at full speed for a minute. After an incubation of 15 to 20 minutes at RT, samples were frozen at -20°C until further processing.

Embryos at developmental stage E16.5 were prepared on ice and washed several times in ice cold PBS^-. Brains were removed from the skull vault, shock-frozen in liquid nitrogen and stored at -80°C until further processing. Samples were delivered to collaborator in this state.

All the following steps in this section were conducted by the collaborator and are only mentioned shortly for precision.

RNA extraction was achieved using the miRNeasy Mini Kit (Qiagen), followed by a concentration quantification and a test run on a denaturing gel to analyze integrity.

This purification step was followed by c-RNA-synthesis utilizing the TargetAmp™ Nano-g™ Biotin-aRNA Labeling Kit for the Illumina® System (Epicentre). After a quality control in the form of a PCR, c-RNA (750 -1500 ng) was ready to be used for the Illumina® beadchip arrays.

All the following steps were conducted by the collaborators and are briefly summarized below.

RNA extraction was achieved using the miRNeasy Mini Kit (Qiagen), followed by a concentration quantification and a test run on a denaturing gel to analyze integrity.

This purification step was followed by c-RNA-synthesis utilizing the TargetAmp™ Nano-g™ Biotin-aRNA Labeling Kit for the Illumina® System (Epicentre). After a quality control in the form of a PCR, c-RNA (750 -1500 ng) was ready to be used for the Illumina® beadchip arrays.

3.2 Cell biology

3.2.1 Tissue culture

In this thesis primary mouse embryonic fibroblasts (Mef) of the Cofilin1$^{KTRTK/KTRTK}$ mouse line showing late embryonic lethality were taken into culture. All procedures were performed under sterile conditions using sterile plastic and glass ware in a sterile hood. Cells were incubated in an incubator set at 37°C with 5% CO_2. Before use, all media and solutions were pre-warmed in a water bath at 37°C (or at room temperature). Cells were seeded in tissue culture flasks, well plates or tissue culture plates for culturing.

3.2.1.1 Culture of cells

Cells attached to the surface of a tissue culture flask or a plate usually within 2 to 3 hours. Close to confluence, Mef-medium (2.2.3) was removed for passaging. After washing with phosphate buffered saline (PBS^-, (tissue culture grade)), cells were incubated for 5 minutes at 37°C with 5% CO_2 in Trypsin-EDTA. Trypsinization was stopped by adding Mef-medium and the cells were resuspended. Next, the cell suspension was transferred to a 15 ml tube and centrifuged at 1000rpm for 5 minutes at RT. The pellet was resuspended in fresh medium to obtain a single cell suspension. The cell suspension was split adequately into a new flask and resuspended in an appropriate volume of Mef-medium.

3.2.1.2 Freezing and thawing of cells

To freeze cells, the cell suspension was pelleted after trypsinization (5 minutes at 1000 rpm at RT). The pellet was resuspended in cold freezing medium (2.5.3.1) and 1 ml transferred to cryo vials. After leaving the vials on ice for 5 minutes they were moved

to the -80°C freezer. The following day the vials were transferred to the liquid nitrogen tank for storage.

To thaw cells, cell aliquots vials were taken from the liquid nitrogen tank and immediately transferred to a water bath set at 37°C. Cells were resuspended in warm Mef-Medium directly after thawing and transferred to a 15 ml tube. After centrifugation for 5 minutes at 1000 rpm at RT the pellet was resuspended in warm Mef medium. In the next step the cell suspension was transferred to a prepared flask and incubated at 37°C with 5% CO_2.

3.2.1.3 Treatment of coverslips for mouse embryonic fibroblasts (Mef)

The coverslips were incubated in 4M HCl o.n. at room temperature. On the following day upon removal of HCl coverslips were boiled three times in autoclaved MilliQ water before being transferred to 70% EtOH. Before use coverslips were flame-scarfed and then placed into 12 well plates.

Preparation of coverslips for Mefs

Cells were plated on glass coverslips for stainings and subsequent microscopy. Coverslips were treated as described above. Afterwards coverslips were coated a 0.2% gelatin solution for 15 minutes at room temperature. The gelatin solution was removed before plating cells. After trypsinization usually 2-3 drops of the cell suspension was diluted in 45 ml of medium. 1.5 ml of this dilution was transferred to each 12 well. Well plates were incubated at 37°C with 5% CO_2.

3.2.1.4 Fixation of plated Mefs

Depending on their growth rate the cells were fixed 2-4 days after plating. After removing the medium the cells were washed twice with generous amounts of pre-warmed PBS^-. The cells were fixed for 10-15 minutes with 500 µl 4% paraformaldehyde (PFA) at room temperature. Next, the cells were washed twice with PBS^- and stored in fresh PBS^- at 4°C.

3.2.2 Primary cultures

3.2.2.1 Isolation of primary mouse embryonic fibroblasts

Animals which carry the mutation of the NTS of Cofilin1 on both alleles are not viable. In order to perform studies on live cells mouse embryonic fibroblasts (Mefs) were prepared.
Embryos from timed matings at the stages E13.5 to E18.5 were used for the preparation of Mefs. Before starting the dissection all instruments were sterilized with 70% EtOH. The uterus of the pregnant female was transferred to a tissue culture plate with PBS^- and transferred to a sterile hood. After removing the uterus and the yolk sac a piece of the amnion was transferred to 200 µl genomic DNA extraction buffer for genotyping. Alternatively, a piece of the head could be used.

After cutting the umbilical cord and removing the remaining amnion completely the embryos were transferred to separate dishes containing PBS^-. The head and liver were removed. In the next step the remaining bodies were washed in fresh PBS^- before being transferred to a 3 cm tissue culture plate with 4 ml of concentrated Trypsin (2.5% Trypsin 1:20 in Trypsin-EDTA). Using forceps and scissors the tissues were cut into small pieces and incubated at 37°C with 5% CO_2 for 25 minutes. Afterwards 4 ml Mef medium was added to the tissue culture plate to stop the Trypsin reaction. The content of the tissue culture plate was transferred to a 15 ml tube and resuspended thoroughly.

After tissue pieces sank to the bottom of the tube, the supernatant was transferred to a fresh 15 ml tube and resuspended again. After a short period of time in which

remaining pieces of tissue were allowed to sink to the bottom of the tube, the supernatant was then transferred to a 175 cm^2 cell culture flask, which already contained 25 ml Mef-medium, and resuspended well. Cells were incubated at 37°C with 5% CO_2.

3.2.2.1.1 Culturing and splitting of Mefs

In the early passages Mefs were split 1:20, in the progress of culturing the splitting ratio was adequately adjusted (usually to 1:5). After the second passage Mefs were transferred from 175 cm^2 cell culture flask to 75cm^2 flasks.

3.2.2.1.1.1 Extracellular matrix

After loss of the mutant Mefs in the early passages an extracellular matrix was provided after the first passage in future Mef preparations. Cell culture flasks (75cm^2) were incubated with an adequate amount of 0.2% gelatin (2.2.3.1) for 15 minutes. After removing the gelatin Mefs were treated as mentioned above.

3.2.2.1.2 IF staining of Mefs

For further microscopic analysis the Mefs plated on coverslips were stained with a number of different primary antibodies and fluorophore labeled phalloidins.
After fixation with 4% PFA (see 3.2.1.4) for 10 minutes, cells were washed with PBS^- three times. In this state cells could be stored at 4°C.

To continue staining, cells were incubated in permeabilizing solution (2.5.5) for 60 seconds. Subsequently, they were washed three times with PBS^- and transferred to a humid chamber cell side facing downwards in a 50 µl drop of blocking solution (2.5.5) which was placed on a layer of parafilm. Cells were incubated for 60 minutes at room temperature. Next 200 µl of PBS^- were carefully pipetted under the coverslips from the side. The afloat coverslips were carefully placed on 50 µl drops of staining solution.

Primary antibodies (2.8.1) were diluted in IF antibody solution (2.5.5.) after removing excess fluid carefully. Antibody stainings were incubated o.n. at 4°C. Following this step of incubation 200 µl of PBS^- were carefully pipetted under the coverslips from the side. Next, coverslips were washed three times by carefully dipping them into PBS^-. Afterwards coverslips were carefully placed on staining drops containing secondary antibody and phalloidin diluted in IF antibody solution (2.5.5). Phalloidin and secondary antibody staining were incubated for 60 minutes at room temperature. Following another washing step with PBS^-, cells were incubated with DAPI (1:1000 in PBS) for nuclear staining for 10 minutes. Afterwards coverslips were carefully washed two times with PBS^- and once with H_2O. After getting rid of excess liquid coverslips were mounted with pre-warmed Moviol (2.5.3.1) and left to dry at 4°C in the dark.

3.2.2.1.3 Senescence-associated β-galactosidase *in vitro* assay

This assay allows the differentiation between senescent and quiescent cells using a histochemical staining with the artificial substrate X-gal. Senescence-associated β-galactosidase (SA-β-gal) is not induced in quiescence or terminal differentiation. SA-β-gal is a biomarker only reacting to senescent cells. The exact function remains unclear. Depending on the cell type, enzyme activity is measured between pH 5.0- 6.0. Activity of the endogenous β-galactosidase activity is measured at pH 4.0 (Dimri et al., 1995).
For analysis of cellular senescence a protocol based on literature was slightly modified (Itahana et al., 2007). In order to determine whether the loss of mutant Mefs, after a definite number of passages, was caused by cellular senescence this assays was performed. Different passages of wildtype and KTRTK-mutant Mefs were stained on coverslips.

As positive controls plated wt Mefs were treated with doxorubicin (Dox), at a final concentration of 100ng/ml, 300ng/ml and 600ng/ml for 20 hours. Doxorubicin (Dox), an extremely toxic and light sensitive DNA-intercalating chemical substance, is known to induce senescence. Stock of doxorubicin was prepared at a concentration of 1mg/ml in DMSO. Aliquots were stored at -80°C. Different fixation solutions were used to optimize the protocol and preserve cell morphology (2.7).

Additionally different pH values of the X-Gal staining solution were tested to optimize staining conditions. Previous studies reported, that staining of SA-β-gal is dependent on pH and fixation method and can differ from cell type to cell type. In order not to lose any information three different fixation methods (senescence fixation solutions, 1% FA, 0.2% GA, 1% FA+ 0.2% GA; 2.7) in combination with four different pH values in the staining solution (X-Gal staining solution, pH 6.0, 5.5, 5.0, 4.0; 2.7) were conducted.

Cells were washed twice with PBS. Next, cells were fixed using the respective senescence fixing solution for 150 seconds at RT. After removal of fixation solution, cells were washed twice with PBS. Afterwards respective X-Gal staining solution was added to each well. Cells were incubated at 37°C without CO_2 for 12-16 hours in the dark. To protect the X-Gal staining solution from light, well plates were wrapped in tinfoil during incubation. On the following day, coverslips were carefully washed with PBS twice, before final rinse with MilliQ water. Coverslips were mounted with pre-warmed Moviol and left to dry o. n. at RT in the dark. For analysis phase contrast images were acquired.

3.2.2.2 Preparations for primary neural cultures

For the isolation of neural cells it is important to use tissue culture plastic from Nunc, 2.9.3), a different extracellular matrix (laminin, 2.15) and specially treated coverslips (3.2.2.2.2). In this thesis neurons and astrocytes cultures from Cofilin1$^{wt/wt}$ and Cofilin1$^{KTRTK/KTRTK}$ embryos were prepared.

3.2.2.2.1 Preparation of laminin from A12 cells

Adhesion of neurons on glass coverslips is dependent on the extracellular matrix protein laminin which A12 cells secrete into the medium.
A12 cells were cultivated in 75cm^2 flasks with HeLa-medium upon thawing. After cells grew as a confluent layer, they were split in a 1:4 dilution into several 175cm^2 flasks with HeLa-medium.

Cells were grown for several days, until the color of the medium changed from red to gold-yellow. This change of color indicated a high production of laminin. Cell supernatants were collected, pooled and filtered through a 0.2 µm pore filter. Aliquots were stored at -20°C.

3.2.2.2.2 Preparation of coverslips for neurons and astrocytes

For neural culture 13 mm diameter coverslips were loaded into a porcelain holder and incubated o.n. in nitric acid at room temperature. The next day nitric acid was removed, coverslips were washed three times with MilliQ water and incubated at 220°C for six hours. After coverslips were allowed to cool down, they were transferred into sterile tissue culture dishes under the TC hood and stored at room temperature.

3.2.2.2.2.1 Coverslips coated with laminin for neuronal culture

For neuron cultures 13 mm coverslips (3.2.2.2.2) were transferred to 24 well plates. Two days before neuron culture preparation glass coverslips were coated with 200 µl of lamin. Well plates were sealed with parafilm and incubated over night in a wet chamber at room temperature.
On the next day the lamin was removed and well plate was directly filled with 500 µl Neurobasal medium complete (2.5.3.4). Well plate were placed in the incubator until neuron culture preparation.

3.2.2.3 Isolation of embryonic neurons

Embryos from timed matings at the stages E14.5 to E18.5 were used for the preparation of neurons. Before starting the dissection all instruments involved were autoclaved. The uterus of the pregnant female was transferred to a tissue culture plate. After removing the uterus and the yolk sac a piece of the tail was transferred to 200 µl genomic DNA extraction buffer (2.5.2) for genotyping. After isolation of the cortex, tissue was transferred to a 3 cm tissue culture plate with 1.5 ml of HBSS/HEPES (2.5.3.4). The following steps were performed under the tissue culture hood. All used glass pasteur pipettes were coated with 5%BSA/PBS^- to avoid cell adhesion. After transfer of neural tissue to 15 ml Falcon tubes (Corning), the tissue was sheared by pipetting up and down. After pieces of tissue sank to the bottom, excess buffer was carefully removed and discarded. 1ml Trypsin/DNase solution (2.5.3.4) was added. Tubes were incubated in a water bath set at 37°C for 30 minutes. After pieces of tissue sank to the bottom, supernatant was removed carefully. Tissue was washed twice with 1 ml HBSS/HEPES solution. After removal of supernatant, 2 ml complete Neurobasal medium (2.5.3.4) was added. One untreated and one fire abolished plugged pasteur pipette was used to dissociate the tissue in the medium.

Cell suspension was transferred to laminin coated 25cm^2 flasks (Nunc) and laminin-coated coverslips in different dilutions. 25µl to 50µl of cell suspension was used for each 24- well. Cells were incubated at 37°C with 5% CO_2.

3.2.2.3.1 Culturing of neurons

Neurons can not be split like HeLa cells or astrocytes, so no passaging was possible. After 24 hours in culture half of the medium was replaced by fresh medium. In order to remove any astrocyte contamination after approx. 5-7 days the Neurobasal medium complete was replaced by astrocyte inhibition medium (2.5.3.4).
To analyze development coverslips were fixed every 24 hours.

3.2.2.4 Isolation of embryonic astrocytes

Embryos from timed matings at stages E16.5 to E18.5 were used for the preparation of astrocytes. Before starting the dissection all instruments involved were autoclaved. The uterus of the pregnant female was transferred to a tissue culture plate. After removing the uterus and the yolk sac a piece of the tail was transferred to 200 µl genomic DNA extraction buffer (2.5.2) for genotyping. After isolation of the cortex, tissue was transferred to a 3 cm tissue culture plate with 1.5 ml of HBSS/HEPES (2.5.3.4). The following steps were performed under the tissue culture hood.

Using a coated (5%BSA/PBS^-) plugged glass pasteur pipette, neural tissue was transferred to 15 ml Falcons (Corning). Tissue was sheared by pipetting up and down. After tissue pieces sank to the bottom, supernatant was removed. 1ml Trypsin/ HEPES solution (2.5.3.4) was added. Tubes were incubated in water bath set at 37°C for 10 minutes. After pieces of tissue sank to the bottom, supernatant was removed carefully. Tissue was washed with 1 ml HBSS/DNase solution (2.5.3.4). After removal of supernatant, remaining tissue was washed once more with 1 ml HBSS/HEPES. Upon removal of the supernatant, 3 ml MEM-FCS medium was added. One untreated and one fire abolished plugged pasteur pipette was used to dissociate the tissue in the medium. Both glass pasteur pipettes were coated with 5%BSA/PBS^- to avoid cell adhesion.

Cell suspension was transferred to 25cm^2 flasks (Nunc). Cells were incubated at 37°C with 5% CO_2.

3.2.2.4.1 Culturing and splitting of astrocytes

Close to confluence, MEM-FCS medium (2.5.3.4) was removed for passaging. After washing with PBS cells were incubated for 5 minutes at 37°C with 5% CO_2 in Trypsin-EDTA. Trypsinization was stopped by adding MEM-FCS medium and cells were resuspended. Cells should not be centrifuged at any time. Cell suspension was split adequately into a new flask and resuspended in an appropriate volume of MEM-FCS medium.

3.2.2.4.2 Plating astrocytes on coverslips

For astrocyte cultures 13 mm coverslips (3.2.2.2.2) were transferred to 24 well plates. No further coating was necessary. After trypsinization and resuspension of the pellet usually 2-3 drops of cell suspension were diluted in 25 ml of MEM-FCS medium. 1 ml of this dilution was transferred into each well. Well plates were incubated at 37°C with 5% CO_2.

3.2.2.5 Fixation of plated neural cells

After removal of medium, cells neurons and astrocytes were fixed with pre-warmed 2% PFA/2% sucrose fixing solution (2.5.3.4) for 20 minutes at room temperature. After fixation cells were washed twice with HBSS/HEPES (2.5.3.4). Cells were stored at 4°C in HBSS/HEPES until further use.

3.2.2.6 Staining of neural cells

The staining procedure for neural cells does not differ much from other cells. One main difference that should be noted though is the extremely weak staining efficiency for phalloidin in neurons. Phalloidin for neurons was used at a dilution of 1:100 in IF antibody solution (2.5.5) for up to 3 hours at room temperature. Though it should be noted that in this case the staining solution contained no antibody. Other than that, cells were incubated in permeabelizing solution (2.5.5) for 60 seconds. Subsequently, they were washed three times with PBS^- and transferred to a humid chamber cell side facing downwards in a 30 µl drop of blocking solution (2.5.5) which was placed on a layer of parafilm. Cells were incubated for 60 minutes at room temperature.
Next 150 µl of PBS^- were carefully pipetted under the coverslips from the side. The afloat coverslips were carefully placed on 30 µl drops of staining solution. Primary antibodies were diluted in IF antibody solution (2.5.5) after removing excess fluid carefully. Antibody staining were incubated o.n. at 4°C. Following this step of

incubation 150 µl of PBS^- were carefully pipetted under the coverslips from the side. Next, coverslips were washed three times by carefully dipping them into PBS^-. Afterwards coverslips were carefully placed on staining drops containing secondary antibody (for astrocytes also Phalloidin) diluted in IF antibody solution (2.5.5). Secondary antibody staining were incubated for approx. 90 minutes at room temperature. Following another washing step, cells were incubated with DAPI (1:1000 in PBS) for nuclear staining for 10 minutes. Afterwards, coverslips were carefully washed, two times with PBS^- and once with H_2O. After removing excess fluid carefully coverslips were mounted with pre-warmed Moviol (2.5.3.1) and left to dry at 4°C in the dark.

3.2.3 FACS analyses

3.2.3.1 Cell cycle analysis of Mefs

Propidium iodide (PI) is a fluorescent dye that stains DNA, used for the analysis of cell cycle and cell death. The fluorescence emission is proportional to the nucleic acid content, because PI binds stoichiometrically to nucleic acids. This fluorogenic compound binds as well to RNA as to DNA. To distinguish between DNA and RNA and to avoid unwanted double signal of DNA and RNA samples have to be treated with RNaseA. PI can be detected at 562-588 nm band pass filter, after excitation at 488 nm.

To characterize wildtype and mutant Mefs a cell cycle analysis using FACS was performed, 10.000 cells were measured for each sample. In each passaging a sufficient amount of cells was centrifuged at 1000 rpm for 5 minutes in a 15 ml tube after trypsinization. The pellet was resuspended twice in 2 ml of PI wash (2.5.3.2) and centrifuged at 1000 rpm for 5 minutes at RT. After the second wash approximately 300 µl of PI wash were left behind. Next, the cells were vortexed very gently while 1 ml of cold 70% EtOH was added dropwise to fix the cells. The cells were stored at 4°C.

To prepare the cells for the PI-staining, they were centrifuged at 1800 rpm for 5 minutes at 4°C. Cell pellets were washed in MASC + 0.2% (v/v) Tween® 20 (2.5.3.3),

centrifuged for 5 minutes at 1800 rpm at RT, resuspended in 500 µl to 1000 µl of PI staining solution (2.5.3.2) depending on the size of the cell pellet and incubated o.n. in the dark at room temperature.

On the following day cells were centrifuged at 1800 rpm for 5 minutes washed with PBS^- and resuspended in an adequate amount of PBS^-. Cells were kept in the dark and on ice for the measurements with ACCURI flow cytometer. Cell cycle analysis was performed with ACCURI software.

3.2.3.2 Proliferation analysis of Mefs

CFDA-SE (carboxyfluorescein diacetate, succinimidyl ester) presents a versatile and simple way to study cell proliferation. The dye itself is colorless and non-fluorescent. CFDA-SE enters cells by diffusion. Green fluorescence is detected using flow cytometry. Each resulting peak in FL1 represents a round of cell division. The peak area represents cells in the respective division cycle (Robinson et al., 1998). For the proliferation assay cells were plated on non-coated 6-wells and harvested at different time points (0h, 8h, 24h, 48h and 72h). Cells were left to adhere over night. Three wells were prepared for each sample (2x stained cells, 1x unstained control).On the following day all samples (not the control samples) were labeled with pre-warmed CFDA-SE staining solution (final concentration: 1 µM CFDA-SE in Mef-medium). After an incubation of 15 minutes in the tissue culture incubator labeling medium was removed and replaced by fresh Mef-medium, then cells were incubated for another 30 minutes. Afterwards, the medium was replaced with fresh Mef-medium once more. At this point the time measurement started. Samples for 0h were processed immediately.

Cells were washed, trypsinized and centrifuged (10 minutes, 1000 rpm, RT). Pellets were resuspended in MACS buffer (2.5.3.3) and centrifuged at 1000 rpm for 10 minutes at 4°C. Unstained and CFDA-SE samples were resuspended in MACS buffer. 13.000 cells were measured for each sample.

3.2.3.3 G-Actin to F-actin ratio analysis of Mefs

The G-Actin to F- actin ratio of Mefs was analyzed using flow cytometry performing a Phalloidin/DNase I staining. While Phalloidin specifically binds to F-actin, DNase I exclusively binds G-actin. Cells were fixed in 300 µl 4%PFA for 10 minutes on ice upon trypsinization and pelleting. Next 400 µl MACS-buffer (2.5.3.3) were added and subsequently cells were spun down in a swing-out centrifuge for 10 minutes at 1000 rpm at 4°C. After removal of supernatant cells were resuspended in 300 µl MACS-buffer + 0.5% Tween20 to avoid the stickiness of the cells. This washing step was repeated once more. After centrifugation, pellet was resuspended in 300µl MACS-buffer + 0.1% TritonX-100. For permeabilization cells were incubated for 10 minutes on ice. Following centrifugation at 1000 rpm at 4°C for 10 minutes pellet was resuspended in 400 µl MACS-buffer + 0.5% Tween20 and spun down again. In the subsequent step the cell pellet was resuspended in MACS blocking solution (2.5.3.3) and incubated for 45 minutes on ice at 4°C.

Phalloidin-680 (1:200) and DNaseI-488 (1: 500) were diluted in MACS- buffer. Following centrifugation cell pellets were resuspended in 100 µl of staining solution and incubated at 4°C on ice for 45 minutes in the dark.

Upon incubation 400 µl MACS buffer were added to each sample. After centrifugation at 10000 rpm for 10 minutes at 4°C pellets were washed with 200 µl MACS buffer. In the final step pellets were resuspended in an appropriate volume of MACS-buffer and analyzed with the AccuriC6.

Along with double stainings, single stainings for F-actin and G-actin were performed as well as un-stained controls. Each sample was prepared as triplicate.

3.3 Biochemical analysis

3.3.3 Protein isolation

3.3.3.1 Preparation of protein lysates from mouse tissues

Embryos and mouse organs were dissected and shock frozen in liquid nitrogen. The tissues were stored at -80°C.

Depending on the size of the tissue an appropriate amount of PEB lysis buffer (2.5.5) was added before homogenization on ice. The frozen tissue was placed in cold PEB in a glass-teflon douncer (e.g. 0.7 ml for a kidney) and several strokes were applied until the tissue was homogenized completely; samples were kept on ice. Next the homogenized tissue was transferred to an Eppendorf tube and centrifuged for 10 minutes at 10000 rpm at 4°C. The supernatant soluble protein was transferred to a fresh tube and the protein concentration was determined using a Bradford assay (3.3.4). The pellet was frozen at –20°C. Lysates were stored at -80 °C. Lysates diluted with 5x SDS sample buffer was added (2.5.5) to an end concentration of 1x SDS sample buffer were boiled at 95°C for 10 minutes and stored at -20°C. After thawing and before loading samples were centrifuged at 4°C for 10 minutes at 10.000 rpm.

3.3.3.2 Determination of G- actin to F-actin ratio in murine tissue according to McRobbie

In order to survey whether changing levels of Cofilin1 were also reflected in altering actin ratios, a G- and F-actin separation from mouse tissues was performed. The separation protocol was adapted from McRobbie and Newell (1983) and Pilo Boyl et al. (2007). This simple method allows a fast separation of G-actin in the supernatant fraction from F-actin in the pellet fraction.

Frozen tissue was dounced in G-/F-actin separation buffer (2.5.5) on ice. Afterwards lysate was left on ice to incubate for 15 minutes. Next lysates were spun down in a swing-out centrifuge at 10.000 rpm for 10 minutes at 4°C. 80% of the supernatant, containing the G-actin, were transferred into a fresh tube and the appropriate amount of 5x SDS sample buffer was added. Samples were boiled for 10 minutes at 95°C. The remaining supernatant in the pellet fraction was discarded. Next was washed twice with G-/F-actin separation buffer to remove any G-actin contamination from the F-actin fraction. Subsequently the pellet was resuspended in the original volume of G-/F-actin separation buffer. Upon addition of 5x SDS sample buffer final 1x and boiling, samples were cooled down on ice and stored at -20°C.

After a Bradford quantification assay equal volumes of paired supernatant and pellet fractions were loaded.

3.3.3.3 Preparation of protein lysates from cultured cells

Following trypsinization, the single cell suspension was centrifuged at 1000 rpm for 5 min.

The pellet was washed twice with PBS^-. To be able to compare the total lysate with the lysates of the nuclear and cytoplasmic fraction it was necessary to start with the same amount of cells. In the second wash step the cell suspension was divided equally and transferred to 1.5 ml Eppendorf tubes and spun down at 3500 rpm for 5 minutes at 4°C. For the following steps of the experiment one tube was used for the total lysate and the remaining one for the fractionation.

3.3.3.3.1 Total lysates

After removing the supernatant the cell pellet was resuspended with H_2O and diluted with 5x SDS sample buffer until an end concentration of 1x SDS sample buffer was obtained.

3.3.3.3.2 Fractionation of cytoplasmic and nuclear lysates

For the fractionation the pellet was resuspended in equal parts of fractionation buffer A and B (2.5.5), adding up to the same volume as the volume of H_2O in, which the pellet for the total lysate was resuspended, and incubated on ice for 1 minute. Following centrifugation at 3500 rpm for 5 minutes at 4°C the nuclei were pelleted and the supernatant consisted of the cytoplasmic fraction. The supernatant was transferred to a fresh tube and diluted with 5x SDS sample buffer until a 1x SDS sample buffer end concentration was obtained. The nuclear pellet was washed with equal parts of fractionation buffer A and B. After centrifugation at 3500 rpm for 5 minutes at 4°C the nuclear pellet was resuspended in a mix of fractionation buffer A and B, in the same volume as the cytoplasm and the total lysate, and diluted with 5x SDS sample buffer.

Subsequently all samples were boiled for 10 minutes at 95°C and the protein concentration was determined via a Bradford assay (3.3.4). The lysates were stored at -20°C.

3.3.3.4 Purification of actin from acetone powder

Purified actin is needed for functional analysis of Cofilin1 and KTRTK-Cofilin1 *in vitro* assays.

Actin was purified from acetone powder (provided by Jan Faix, Hannover Medical School), which was prepared from rabbit muscle. The actin assays shown in this thesis were performed in a methods course, in which purified actin was provided. The following protocol describes the basics of actin purification according to Spudich and Watt 1971.

6g Acetone powder was mixed with 100ml 1x G-buffer (2.5.5) and incubated for 30min at 4°C while stirring. First a piece of gauze (“cheese cloth”) was equilibrated with 1x G-buffer.

The following steps were conducted 10 times: The acetone powder/G-buffer mix was pushed through the cheesecloth. The flow-through was saved and a sample was taken

in every round. The remaining acetone powder was again mixed with 1x G-buffer and incubated for 30min at 4°C while stirring. Samples of the flow-through fractions were analyzed on SDS-PAGE.

Flow-through fractions, showing adequate actin concentrations, were pooled and centrifuged at 8.000 rpm at 4°C for 30 minutes (rotor JA-14) to remove gross contaminations.

Supernatant was mixed with 50x actin polymerization buffer (2.5.5) to a final concentration of 1x. Mixture was incubated 2 hours at 4°C while stirring.

KCl was slowly added until a final concentration of 0.8 M KCl was reached. An incubation for 30min at 4°C while stirring followed. The mix was centrifuged for 3h at 38.000rpm at 4°C (rotor TI-45).

Supernatant was discarded. Pellet was carefully transferred to a douncer and 1x G-buffer was added. After a homogenous liquid was attained, actin solution was filled into a dialysis membrane (pore size 6.000-8.000) and dialyzed against 1x G-buffer over night at 4°C while stirring. On the following day, 1x G-buffer was replaced every six hours. On the third day, the 1x G-buffer was once again refreshed and the actin solution was centrifuged for 2h at 35.000rpm at 4°C (rotor TI-45).

Phase separation consisting of three different layers was achieved. A milky, fatty phase (lipids), the middle phase (actin) and the pellet.

The middle phase was saved, quantified and dialyzed against 1x G-Buffer at 4°C while stirring. Buffer was replaced on a weekly basis.

3.3.3.5 Purification of proteins from bacteria

Isolated proteins allow versatile applications like a number of *in vitro* assays to test for functionality. These experiments also enable to analyze the repercussions of variability of parameters as protein concentration and pH.

3.3.3.5.1 Isolation of GST-fusion proteins from bacteria for functional in vitro assays

To study the function in a number of different *in vitro* assays, GST-wt-Cofilin1 and GST-KTRTK-Cofilin1 were isolated.

3.3.3.5.2 Cultivation and lysis of transformed bacteria

40ml LB_{Amp} (2.5.4) pre-culture was inoculated and incubated o. n. at 37°C on the shaker (200rpm). On the following day 4 liters of pre-warmed LB_{Amp} medium was inoculated with the pre-culture from the previous night. 5 ml pre-culture were used for inoculation of 8x 500 ml of main culture. Bacteria were grown at 37°C until OD of 0.7 was obtained.

IPTG (1M) was added to a final concentration of 0.5 µM to each main culture to induce protein expression. Culture were incubated over night at 22°C to avoid inclusion bodies.

All following steps were performed on ice. To harvest the bacteria, cultures were centrifuged at 4500 rpm for 15 minutes at 4°C (rotor JA-14). Supernatant was discarded completely.
Pellets were resuspended in 40 ml GST lysis buffer (2.5.4) and lysed by ultrasound in repeated steps for 1 min, with 30 second gaps in between. Afterwards cell suspension was dounced, approx. 40 times, followed by a 30 minute centrifugation at 35000 rpm at 4°C (rotor TI-45). The cleared lysate was used for further purification.

3.3.3.5.3 Purification of GST-wt-Cofilin1 and GST-KTRTK-Cofilin1 fusion proteins

For purification columns filled with glutathione-linked agarose beads (approximately 4ml) were used. Before use, columns were equilibrated with GST lysis buffer. The 40ml

cleared lysate (from 3.3.3.5.2) was loaded onto the column. The flow-through was saved and applied to the column a second time.

In the subsequent step, the column was washed several times using GST wash buffer (2.5.4), the flow-through was discarded.
Following a washing step with PBS, beads were extracted from the column using PBS and transferred to a fresh tube.

3.3.3.5.4 Cleavage of GST-tag

In order to work with the respective native protein in assays the GST-tags had to be removed from the fusion proteins. Beads were incubated with 400U of thrombin o. n. on a rotating wheel at 4°C.
On the following day, the bead suspension was transferred back to the column, the flow-through was saved. Beads were washed with PBS, flow-through was saved.

Flow-through fractions contained the cleaved proteins. Samples of proteins in the flow-through were used for SDS-PAGE and Bradford quantification.

Aliquots of proteins were frozen in liquid nitrogen and stored at –80°C until further use.

3.3.4 Protein quantification

To ascertain the protein content of lysates two different forms of the Bradford assay were performed. The Bradford assay is a colorimetric analytical procedure to determine the concentration of protein in solution. Upon binding to protein the absorption maximum of Coomassie Brilliant Blue G-250 shifts from 465 nm to 595 nm (Bradford, 1976). The increase in absorption at 595 nm is a measure for the protein concentration in a solution. The protein amount was calculated based on BSA based calibration curve, which was performed before each measurement.

3.3.4.1 Quantification of bacterial or tissue lysates

2-3 µl of cleared bacterial and tissue lysates were diluted in a total volume of 100 µl H_2O and mixed well. Before measuring the protein concentration at 595 nm, 900 µl of diluted Bradford reagent (1:5 with H_2O) were added.

3.3.4.2 Quantification of cultured cell lysates

To determine the amount of protein in the lysates of the cell fractionation experiment, which were already boiled in SDS sample buffer, a different protocol was chosen. 5µl of the respective lysate was diluted in 45 µl H_2O. 1000 µl diluted (1:5 in H_2O) Bradford reagent were added to 12.5 µl of the diluted protein lysate and mixed well. Subsequently, the protein concentration was measured at 595 nm. The protein amount was calculated based on the calibration curve performed with BSA.

3.3.5 Discontinuous SDS-Polyacrylamide gel electrophoresis

Based on their amino acid sequences proteins have varying electrical charges, which affect their running behavior.

Sodium dodecyl sulphate (SDS) is an anionic detergent, which denatures proteins by breaking hydrogen bonds and reducing them to their primary structure. Negative charges are applied to the proteins according to their mass. Consequently the charge/mass ratio is the same in all the linearized protein-SDS-complexes. Therefore, their running behavior in the gel is only influenced by their molecular weight. The SDS sample buffer (Laemmli buffer) also contains bromphenol blue and β-mercaptoethanol. β-mercaptoethanol reduces inter- and intra-molecular disulfide bonds while bromphenol blue marks the running front.

A discontinuous sodium dodecyl sulfate polyacrylamide gel electrophoresis, short SDS-PAGE, consists of a separating gel and a stacking gel. They differ from each other in pH and the pore size of the gel. The stacking gel allows the focusing of the samples before entering the separating gel. The discontinuous SDS-PAGE allows a higher resolution of proteins according to their electrophoretic mobility (Laemmli, 1970).

The molecular weight of the protein of interest determines the percentage of the gel to use. For Cofilin1, with a molecular weight of 20 kDa, 15 % Tris-glycine acrylamide gels (2.5.5) were prepared and run in 1x SDS running buffer (2.5.5). After protein quantification 10 µg of the samples were loaded into the sample wells. To identify the sizes of the respective protein 5 µl Broad range Standard was loaded for Coomassie stained gels, while 5 µl Sea Blue Plus 2 Prestained Standard was separated for Western blotting. The electrophoretic separation was accomplished at 60 V through the stacking gel and regulated up to 100 V for the separation gel. The electrophoresis was stopped when the 4 kDa marker band of the Prestained marker reached the bottom of the gel. Coomassie gels were stopped, when the blue running front reached the bottom of the gel.

3.3.5.1 Coomassie staining of protein gels

After gel electrophoresis or even after transfer to membrane Coomassie staining of gels was used to visualize the protein bands. This method is commonly used in analytical biochemistry for optical quantification of protein concentrations.

The gels were incubated rocking for 30 minutes in Coomassie Brilliant Blue staining solution (2.2.5) at room temperature. Afterwards the gels were incubated for 90 to 120 minutes in ‘rapid destain’ solution (2.5.5) at room temperature on a rocker. The gels were stored in H_2O and scanned for documentation.

3.3.6 Western Blot analysis

Western Blot analysis allows the detection of specific proteins in a mixture of proteins in a sample. After separation of the proteins according to their electrophoretic mobility by gel electrophoresis the proteins are transferred to an “Immobilon” (polyvinylidene difluoride, PVDF), where specific antibodies can be used to detect proteins of interest (Towbin et al., 1979).

3.3.6.1 Semi dry blotting procedure

Electroblotting was used to transfer proteins to “Immobilon” membranes. In this method electric current is used to transfer the proteins from the gel to the membrane. The binding of the proteins to the membrane is based on charged and hydrophobic interactions. After electrophoresis the “Immobilon” membrane was activated in methanol first and together with the gel and Whatman paper sheets equilibrated in Towbin transfer buffer (2.5.5). For the set-up of the blotting the gel and membrane were positioned between two layers of Whatman paper sheets. The transfer takes place from cathode to anode. The transfer to the anode was performed at 20 Volts for 60 minutes at room temperature. Following the transfer the membranes were incubated 1-2 hours at room temperature or o.n. at 4°C in Western blot blocking solution (2.5.5) to avoid unspecific binding.

3.3.6.3 Western blot analysis using chemo luminescence

To detect proteins by Western blot analysis antigen specific primary antibodies are used. The primary antibody carries species specific Fc-regions, which are recognized by the horseradish peroxidase (HRP) linked secondary antibody. Horseradish peroxidase catalyzes the oxidation of luminol. The product of this reaction causes chemiluminescence proportional to the amount of antibody bound which reflects the amount of protein present. This luminescence can be visualized after exposing x-ray films to the membrane or by detection of the chemiluminescence signal with the ImageQuant LAS 4000 mini.

After blocking the membrane the primary antibodies were diluted in Western blot blocking solution (2.5.5, for information about utilized primary and secondary antibodies see 2.8.). The blot was incubated either for 3 hours at room temperature or over night at 4°C. Afterwards the blot was washed 5 times for 10 minutes in 1xNCP without azide (2.5.5). In the next step the secondary antibody was diluted 1:1000 in the secondary antibody solution (2.5.5) and the blot was incubated for one hour. The membrane was washed 5 times for 10 minutes in 1xNCP without azide. After rinsing the membrane briefly in water it was incubated for 1 minute in a 1:1 mixture of the ECL solutions (2.5.5). The excess ECL was removed from the blot before it was wrapped in Saran-Wrap. The detection time with the ImageQuant LAS 4000 was adjusted according to signal.

3.3.7 Actin assays

There is a variety of actin assays, each one gaining information regarding a protein of interest. All of these assays need purified protein of interest along with purified actin.

3.3.7.1 Falling ball assay

In this assay actin depolymerization/ polymerization can be measured by a change in viscosity. The time it takes a ball to fall a specific distance at a specific angle in the capillary is noted (Figure 16). Actin alone without any additional proteins functions as negative control. One of the main advantages of this assay is the low amount of protein required.

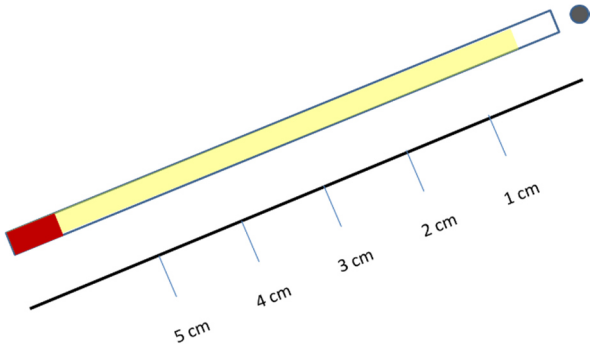

Fig.16: Principle of falling ball assay

KTRTK-Cofilin1 (251.3 µM) and Cofilin1 wt (204.9 µM) (see 3.3.3.5.3) were each diluted to a final concentration of 3 µM in assay binding buffer (2.6). Polymerization reactions were set up by mixing 9 µM actin and the different final concentrations of wt-

Cofilin1 and KTRTK-Cofilin1 (3 µM, 1.5 µM and 0.75µM), respectively. Mixtures were transferred to glass capillaries with capped end. Samples were left to polymerize for 60 minutes at RT.

Little metal balls were applied and the time of the falling ball at a 17° angle was measured.

3.3.7.2 Pyrene assay

This assay requires pyrene-labeled actin. Pyrene does not affect the binding kinetics of actin. This assay facilitates the measurement of F-actin quenching kinetics by monitoring changes in pyrene fluorescence. Labeled G-actin is only weakly fluorescent, but upon polymerization the fluorescence is enhanced about 20 times. The binding capacity of the protein of interest can correlated to the measured change in fluorescence using suitable wavelengths (for pyrene: excitation: 365 nm; emission: 410 nm) in a microplate reader. The binding of the protein quenches the pyrene fluorescence signal. Pyrene assay also allow the analysis of depolymerization and polymerization activity. Set-up for both approaches is basically the same, but for analyses of depolymerization and polymerization activity measurements fluorescence signal data has to be acquired over a longer period of time. Also here only a low percentage of pyrene actin is required.

To polymerize actin 4.4 ml G assay buffer (2.6), 500 µl KMEI (10x) (2.6), 98 µl unlabeled actin (102 µM) and 33 µl pyrene actin (34 µM) were mixed and left to incubate at RT for 2 hours.

For the binding reactions the wt Cofilin1 and KTRTK-Cofilin1 were diluted in Assay binding buffer (2.6) to a final concentration of 8 µM and added to the polymerized actin respectively. Assays were performed in 96 well plates, polymerized actin was always added last.

In this assay different condition were tested. The final measurements were performed with 2 µM polymerized actin and 4 µM of the respective Cofilin. Read-out was performed every 3 seconds for 30 minutes.

3.4 Histology

3.4.1 Dissection of mouse embryos

Females from timed matings were sacrificed at embryonic days E10 to E18. The uterus was placed in ice cold PBS. After removing the uterus and yolk sac including the placenta and umbilical cord, tissue samples of amnion were used for genotyping.

After a subsequent wash in fresh PBS, embryos were treated according to their age and use in following experiments.

3.4.2 Bone and cartilage staining and isolation (Alizarin Red-Alcian Blue staining)

The basic concept of differential staining of cartilage and bone in mouse fetuses has been reported as early as 1980 (McLeod, 1980), allowing the detection of developmental malformations. Alizarin Red in combination with Alcian Blue allows a staining of cartilage in blue and bone in red.

For this staining animals older than E16.5 should be used for optimal results.

Upon preparation embryos were placed in 95% EtOH for fixation o.n. at 4°C on a rocker. On the next day the skin of the embryos was removed carefully, paying special attention to the paws and the tail. After that the viscera were removed with extreme caution as not to injure the thoracic area. For the continuance of the staining the samples were protected from light. Embryos were transferred to 12 ml snapshot tubes containing 0.05% Alcian Blue staining solution for cartilage staining (2.7) and incubated for 48 hours at 4°C on a rocker. Subsequently embryos were rinsed twice with 95%EtOH at RT for an hour each.

To remove soft tissue and due to their increasing fragility the embryos were placed in 6 cm plastic dishes for the following steps.

For removal of any soft tissue the embryos were incubated in 2% KOH at RT for 24-48 hours depending on the size of the embryos. After the first 6-8 hours the KOH solution was replaced. After the KOH treatment the skeletons should be treated with extreme caution due to their fragile state.

In order to stain bones the skeletons were incubated in 0.015% Alizarin Red staining solution for 72 hours at RT (2.7). Upon removal of the staining solution, skeletons were cleared by subsequent incubations in the following KOH:Glycerol solutions at RT (80% 1% KOH: 20% Glycerol; 60% 1% KOH: 40% Glycerol; 40% 1% KOH: 60% Glycerol; 20% 1% KOH: 80% Glycerol). In each clearing steps skeletons were incubated for 60-90 minutes.

For the final step skeletons were transferred to 100% Glycerol and stored at 4°C.

3.4.3 Fixation and dehydration for microtome sections of mouse embryos

Depending on the age of the embryos the duration of the incubation steps had to be modified. The following steps were performed for all embryos older than E10.5. During fixation, washing and dehydration the volumes used were approximately 10 times that of the tissue, for incubations tubes were placed on a rocker.

After preparation embryos were washed with PBS before being transferred to tubes with cold 4% Histofix and fixed at 4°C over night. Afterwards embryos were washed twice with PBS for 30 minutes each at 4°C and left in fresh PBS over night at 4°C. On the following day the embryos were washed two times for 30 minutes each with 50% EtOH at 4°C. Next they were washed twice with 70% EtOH 30 minutes each at 4°C. After exchanging the 70% EtOH once again the embryos were left over night at 4°C. At this point 70% EtOH can also be used for storage of the embryos at 4°C.On the following day the embryos were washed once in 96% EtOH and then twice in absolute Ethanol at room temperature for an hour each. The embryos were transferred into glass vessels and incubated with xylene for 30 minutes. This step was repeated two more times and performed under the fume hood.

3.4.3.1 Paraffin embedding of mouse embryos

The day before use the paraffin was melted in an oven at 58.5°C. After replacing the xylene with paraffin the embryos were left in a heating block at 58°C. The paraffin was changed two more times after 30-45 minutes each before leaving the embryos in fresh paraffin o.n. in the heating block. On the following day the paraffin was exchanged once again using approximately 3 ml, an amount that fits into the embedding molds. After incubation for 15 minutes embryos were transferred to the embedding molds. Hot forceps were used to orient the embryos within the molds. Afterwards the paraffin blocks were left to solidify at room temperature. For storage the solidified paraffin blocks were kept at RT.

3.4.4 Fixation and dehydration process for paraffin embedding of E10.5 mouse embryos

Embryos younger than E10.5 were treated specially in order to attain best histological results. After preparation and washing with PBS embryos were fixed with 4% Histofix for 15 minutes at room temperature rotating on a wheel. Next, the embryos were washed in 70% EtOH which was replaced after five minutes. At this point embryos could also be stored in 70% EtOH at 4°C. For further dehydration the embryos were incubated in 80% EtOH for two minutes. To simplify the following steps and increase visibility, embryos were placed in 0.5% Eosin/90% EtOH for two minutes. Next, embryos were washed in 96% EtOH and absolute ethanol for two minutes each. Using cut plastic Pasteur pipettes embryos were placed in pre-warmed embedding molds. Any excess ethanol was removed. Embedding molds were filled up with liquid paraffin and put in the oven to incubate at 58.5 °C for 120 minutes to allow increased penetration of the tissue. Then embedding molds were placed at room temperature to solidify slowly.

3.4.5 Mounting and sectioning of paraffin embedded tissue

Paraffin blocks were removed from the embedding molds and mounted onto plastic embedding cassettes using melted paraffin. The paraffin blocks were oriented according to the desired cutting plane. To trim the embedded tissues thin layers of paraffin were sliced off with razor blades (a narrow zone of paraffin was left around the tissue).

The trimmed paraffin blocks were fixed at the embedding cassette holder of the microtome. The head on the microtome was orientated until the right position for the right cutting plane was acquired. Sections were cut with a thickness of 10 µm. The cut ribbons were placed on a layer of 10% EtOH onto superfrost slides and transferred to a heating plate set at 35°C. Slides were left on the heating plate until the sections had stretched and the paraffin had turned white. If necessary more ethanol was added carefully from the sides. After stretching excess ethanol was drained and the slides were moved back to the heating plate. Over night slides were left upright in an open box in an oven set at 37°C to remove any remaining moisture and to dry the sections completely. Slides were stored at room temperature.

3.4.6 Staining protocols for paraffin sections

In this thesis a number of different stainings on embryonic tissue sections were performed. The following chapter describes a number of different staining procedures.

3.4.6.1 Stainings of paraffin embedded sections

One of the main advantages of paraffin sections is the well maintained morphology, but all paraffin section have to be de-paraffinated and rehydrated before any further staining is possible. The following de-paraffination protocols have been established to accommodate the subsequent stainings. All following steps were performed under the fume hood.

Deparaffination process preceding color stainings

3 x	10 min	xylene
1 x	5 min	absolute ethanol
1 x	5 min	96 % EtOH
1 x	5 min	70 % EtOH
1 x	5 min	50 % EtOH
1 x	10 min	distilled H_2O

For antibody stainings the H_2O in the final step was substituted with PBS. Following the deparaffination sections for antibody stainings are treated in the epitope retriever for 60 minutes in 1x citrate buffer.

3.4.7 Color staining

All the following stainings using color dyes were performed on paraffin sections.

3.4.7.1 Haematoxylin and Eosin staining (H+E)

Haematoxylin and eosin stainings provide an overview of tissue structure. Haematoxylin has a deep blue-purple color. The oxidation product of haematoxylin is haematin. In acidic conditions metal-haematin complexes bind to lysine residues of nuclear histones. Eosin is a derivative of fluorescein. It stains cytoplasm, collagen, keratin and erythrocytes. Eosin was used for counterstaining. It is pink and stains proteins un-specifically (Fischer et al., 2008). Since haematoxylin (Mayer's haemalaun) is sensitive to light the glass cuvettes used for stainings were wrapped in tinfoil. All following table shows the staining protocol following up the deparaffination.

	20 sec	Mayer's haemalaun solution (50%)
		Rinse cuvette with tap water
	5 min	Wash in running tap water
	5 min	Eosin Y (0.05%)
		Rinse cuvette with tap water
	30 sec	Dehydrate with 96% EtOH
	2 min	Dehydrate absolute EtOH
	2 min	Dehydrate Xylene
		Mount with Entellan

3.4.7.2 Alcian Blue staining

Here Alcian blue is used to identify cartilage on sections. The staining is pH dependent and only stains sulfated polysaccharides at pH1.0. At pH 2.5 it also stains carboxyl group containing sugars. Alcian blue stains acid mucosubstances and acetic mucins (Scott et al., 1964). Sections have to be deparaffinized as shown above before staining (3.4.8.1).

	30 min	Alcian Blue staining solution (1%, sections; 2.7)
		Rinse cuvette with tap water
2x	2 min	Wash in running tap water
		Rinse cuvette with distilled water
1x	3 min	Dehydrate with 96% EtOH
2x	3 min	Dehydrate absolute EtOH
	5 min	Clear in xylene
		Mount with Entellan

3.4.7.2.1 Alcian Blue + Eosin staining

To optimize the staining an alternative version for cartilage staining including a counterstain was established. This staining allows a better overview of the tissue, but bears the risk of obscuring weak Alcian blue staining of the loose connective tissue. The staining follows up deparaffination (3.4.8.1).

	40 min	Alcian Blue staining solution (0.8%, sections; 2.7)
2x	2min	Rinse with running tap water
1x	2min	Rinse with Elix
	2 min	Eosin Y (0.05%; 2.7)
	30 sec	Rehydrate with 96% EtOH
	2 min	Rehydrate absolute EtOH
	2-5 min	Clear in xylene
		Mount with Entellan

3.4.7.3 Nissl cresyl violet staining

The cresyl violet staining was performed to gain insight into the layering of the embryonic cortex and the overall distribution of neurons in the brain.

The Nissl staining is most commonly used to identify basic neural structures in brain tissue. It is a classic nucleic acid staining that is most abundantly used on nervous tissue. The basic dye binds to the negatively charged RNA and DNA.

Cresyl violet acetate stains Nissl substance, consisting of granular endoplasmic reticulum and ribosomes, occurring in nerve cell bodies and dendrites of neurons. Neuropil, any area in the nervous system composed of un-myelinated axons, dendrites and glial cell processes forming synaptically dense regions containing relatively low number of cell bodies, will be stained granularly purple blue (Purves, 2012). This method utilizes basic aniline dye.

The following protocol was established for 10µm paraffin sections of embryonic brain. For this specific staining the de-paraffination process had to be adjusted. The staining solution was prepared 2 hours prior to use due to low solubility of the dye. After filtration cresyl violet solution was pre-warmed to 37°C to increase staining efficiency and penetration. This staining can be performed as early as E13.5 on murine brain.

3x	10 min	Xylene
2x	5 min	absolute ethanol
1x	3 min	96% EtOH
1x	3 min	70% EtOH
		Rinse cuvette twice with tap water
		Rinse cuvette 3x with Elix
		Transfer slides to pre-warmed cuvette with pre-warmed 0.1% cresyl violet solution
	6-8 min	Cresyl violet solution at 40°C in the dark
		Rinse cuvette at least twice with Elix
	5-15 min	Differentiate in 95% EtOH
2x	5 min	Rehydrate absolute EtOH
2x	5 min	Clear in xylene
		Mount slides with Entellan

3.4.7.4 Mounting of paraffin sections after color stainings

The sections were mounted using Entellan, distributing 2-3 drops with a glass pipette on the slides. To avoid air bubbles the entire coverslips were dipped in xylene before being placed on the slides. Slides were left to dry at room temperature and stored at RT.

3.4.8 BrdU staining

BrdU (5-Bromo-2´-deoxy-uridine), a thymidine analog, is incorporates into DNA during replication in the S-Phase of the cell cycle. It serves as an exogenous cell tracer, allowing the tracking of cell proliferation. Incorporated BrdU features long-term retention and during cell division is passaged on to daughter cells diluting out with every division cycle. This naturally incorporated nucleoside analog can be detected with an anti-BrdU antibody (Wojtowicz and Kee, 2006).

To study proliferation in embryonic E13.5 brain *in vivo* labeling was necessary. Pregnant females were injected with 100 µl BrdU labeling reagent (10µmol/l) intraperitoneally one to two hours prior to dissection. All used solutions were provided by the 5-Bromo-2´-deoxy-uridine Labeling and Detection Kit II and prepared according

to manual (Roche, 2.4). The staining protocol was modified from the original manual to obtain better results based on previous studies (Kee et al., 2002). After dissection embryos were treated according to the protocol for paraffin sections (3.4.5.1). 10 µm sections were prepared. After de-paraffination and equilibration in PBS (3.4.8), sections were treated in the antigen retriever for 1 hour in 1x citrate buffer. After a short cooling period (approx. 15 minutes), slides were washed twice in PBS for a total of 10 minutes. Next slides were incubated in pre-warmed 4M HCl at 37°C for 1 hour. This step improved immunohistochemical detection of incorporated BrdU, by denaturing DNA and therefore exposing the antigen further. Following a 10 minute incubation in 0.1M sodium borate at RT, sections were blocked with 5% NGS/ Oldenburg buffer at RT for an hour. Afterwards sections were incubated in a 1:10 dilution of the primary mouse anti-BrdU antibody in primary antibody solution for IHC (2.7). First incubation took place at 37°C for 60 minutes in a humid chamber, then was moved to 4°C for o.n. incubation. On the following day slides were washed in Oldenburg buffer for 15 minutes at RT. During this time buffer was refreshed twice. An incubation in a 1:250 dilution of anti-mouse-IgG-alkaline phosphatase-coupled secondary antibody in secondary antibody solution for IHC (2.7) followed. After incubation in a humid chamber for 30-60 minutes at 37°C, slides were washed in Oldenburg buffer as described above. In the following step sections were incubated in a sufficient amount of fresh color-substrate solution at RT. This color-substrate solution contains NBT (nitroblue tetrazolium) along with X-phosphate/ BCIP (5-bromo-4-chloro-3-indolyl phosphate). BCIP acts as an artificial chromogenic substrate. It is often used in combination with NBT. Alkaline phosphatase hydrolyses BCIP to 5-bromo-4-chloro-3-indolyl and inorganic phosphate. 5-bromo-4-chloro-3-indolyl is oxidized by NBT to form an insoluble dark diformazan precipitate after reduction (Horwitz et al., 1966). After 30 minutes, solution was carefully removed, slides were rinsed in washing buffer and mounted with Entellan. Mounted sections were allowed to dry at RT over night.

3.4.9 Antibody stainings

Immunohistochemistry (IHC) and immunofluorescence (IF) stainings both work with primary and secondary antibodies. Whereas immunofluorescence works with fluorophore-labeled secondary antibodies the IHC reaction is based on horseradish peroxidase reaction, the use of color substrates (DAB) and amplifier complexes (ABC-complex; M.O.M Kit; 2.4). The ABC complex (Avidin/Bioton complex) comprises Avidin and Biotin. The specific primary antibody will bind an antigen. Then, a biotinylated secondary antibody will attach to the primary antibody. The Avidin/Biotin complex (ABC) with Horseradish Peroxidase (HRP) will affix to the biotinylated secondary antibody forming an enzyme complex, allowing the detection of DAB a substrate of the enzyme complex.

3.4.9.1 IF stainings of paraffin sections

		Deparaffinize to PBS
	60 min	Antigen retriever in 1x citrate buffer, pH6.0
3x	5 min	Oldenburg buffer
		Slides were transferred to humid chamber
	1 h	IF blocking solution at RT(2.5.5)
	o.n.	IF antibody solution with primary antibody at 4°C (2.5.5)
3x	10 min	Oldenburg buffer
	2 h	IF antibody solution with secondary antibody at RT (2.5.5)
3x	5 min	Oldenburg buffer
	30 min	Draq5 in Oldenburg buffer (1:2000) at RT
		Rinse in Oldenburg buffer
	15 min	DAPI in Oldenburg buffer (1:1000) at RT
2x	5 min	PBS^-
	2 min	MilliQ
		Mount with pre-warmed Moviol (2.5.3.1)

Draq5 as well as DAPI serve as nuclear markers. After mounting slides were left to dry at RT and stored at 4°C protected from light.

3.4.9.2 IHC stainings

The procedure for IHC stainings differs slightly from the IF protocol. In order to avoid false positive stainings the endogenous peroxidase in the tissue has to be inactivated in one of the steps. The purchased M.O.M Kit (2.4) is to be used for mouse primary antibodies. In the first step the sections have to be deparaffinized to the final step in PBS.

	60 min	Antigen retriever in 1x citrate buffer, pH6.0
3x	5 min	Oldenburg buffer
	30 min	3% H_2O_2 in tap water (peroxidase inactivation)
		Slides were transferred to humid chamber

3.4.9.2.2 IHC staining with M.O.M. Kit for mouse primary antibodies

In the following procedure sections were treated according to kit manual.

	1 h	M.O.M Ig blocking in Oldenburg buffer at RT
2x	2 min	PBS^-
	5 min	M.O.M diluent without primary antibody
	o.n.	Primary antibody in M.O.M diluent at 4°C
4x	10 min	Oldenburg buffer
	90 min	Secondary antibody (Kit) in M.O.M diluent at RT
4x	10 min	Oldenburg buffer
	60 min	ABC-complex (Kit) at RT
3x	5 min	0.05 M Tris-HCl, pH 7.4
		DAB color reaction+
2x	5 min	0.05 M Tris-HCl, pH 7.4
	5 min	MilliQ
		Mount with Entellan

Next, slides were incubated with DAB reagent (2.7). To start the color reaction small volumes (20-50 µl) of different dilutions of 3% H_2O_2 in tap water (1:50, 1:100 and 1:200) can be added to the DAB reagent, starting with the highest dilution. Section are incubated in DAB solution until staining of desired intensity was obtained. Following the color reaction a number of washing steps were performed. DAB is highly toxic and needs to be treated with extreme care.

Slides were left to dry o.n. and stored at room temperature.

4. Results

In previous *in vitro* studies the amino acid sequence KKRKK of Cofilin1, positioned at the 30th to 34th amino acids, was proven to be functioning as the nuclear translocation signal (NTS), allowing the translocation of Cofilin1 into the nucleus upon certain stress stimuli. The role of Cofilin1 in the nucleus is not completely understood, yet. One function that has been observed is the formation of nuclear actin/Cofilin1 rods after the exposure of cells to various stress factors (e.g. DMSO) (Fukui and Katsumaru, 1979). Rods are composed of ADF/Cofilin and actin in a 1:1 ratio and vary in filament length from 22 to 1448 nm (Minamide et al., 2010). Experiments in which the NTS KKRKK of Cofilin1 was mutated to KTLKK, showed the inability of the mutated protein of active nuclear translocation (Iida et al., 1992). The mutation of the KKRKK sequence to KTKTK of capsid proteins in Simian virus 40 (SV40) showed, that the capsid proteins direct viral DNA nuclear entry. The mutation led to impaired delivery of the viral DNA to the nucleus in the host, resulting in reduced viability of the virus (Nakanishi et al., 2002). In analogy to these studies Cofilin1 carrying the mutated sequence KTRTK was generated for analyses *in vitro* and *in vivo*. Prior experiments concluded that KTRTK-Cofilin1, expressed as GFP fusion protein in HeLa cells, was unable to form actin/Cofilin1 rods in the nucleus (Gurniak, unpublished) whereas wildtype Cofilin1 formed distinct actin/Cofilin1 rods upon stimulation. The mouse line in which Cofilin1 was replaced by KTRTK-Cofilin1, as well as the constructs for expression of GFP fusion proteins in eukaryotic cell lines used in this thesis, were generated and provided by Christine Gurniak.

4.1 GFP-KTRTK-Cofilin1 fusion protein did not form nuclear actin/KTRTK-Cofilin1 rods *in vitro*

Previous data from the diploma thesis showed that the nuclear translocation sequence (NTS) of Cofilin1 serves as transport signal to the nucleus. For this study the mutant KTRTK-Cofilin1 was analyzed in comparison to wt-Cofillin1(Roy, 2011). HeLa cells were transfected with GFP-wt-Cofilin1 and GFP-KTRTK-Cofilin, respectively.

Stably transfected HeLa cells were exposed to a stress stimulus in the form of DMSO to induce nuclear translocation of actin and Cofilin1 and the subsequent formation of rods. In agreement to previous studies that showed the inability of nuclear translocation of NTS mutants along with failure of chaperoning other molecules (i.e. viral DNA) to the nucleus (Iida et al., 1992; Nakanishi et al., 2002), KTRTK-Cofilin1 should not locate to the nucleus. Upon DMSO treatment, transfected HeLa cells were fixed and stained for DAPI (Figure 17).

After DMSO treatment nuclear actin/Cofilin1 rods were clearly discernable in HeLa cells transfected with GFP-wt-Cofilin1, whereas no comparable structures could be detected in GFP-KTRTK-Cofilin1 transfected HeLa cells (Figure 17).

A clear co-localization of actin and GFP-wt-Cofilin1 could also be observed (data not shown), verifying the association Cofilin1 and actin in rods.

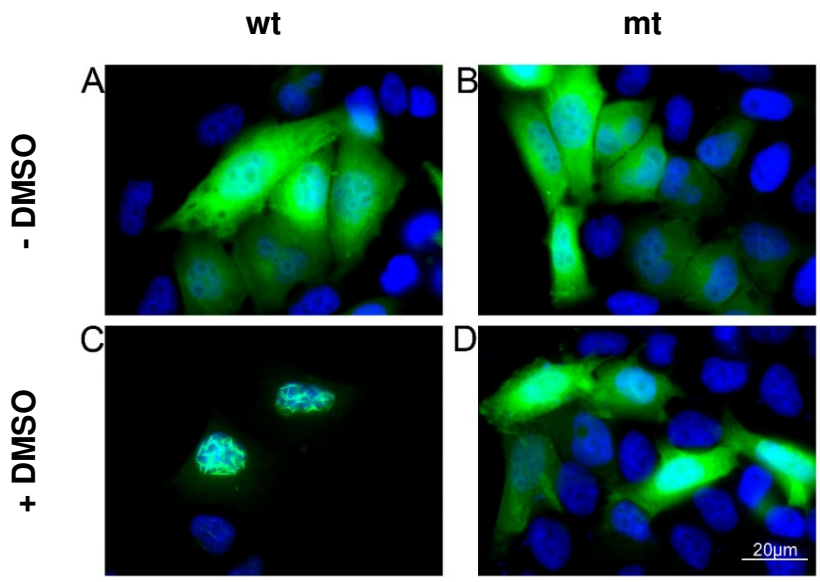

Fig. 17: Immunofluorescence of GFP-wt-Cofilin1 (wt) and GFP-KTRTK-Cofilin1 (mt) transfected HeLa cells after DMSO treatment. Cells were stained with DAPI (blue). Nuclear actin/Cofilin1 rods were detected in GFP-wt-Cofilin1 HeLa cells after DMSO treatment (lower panel; wt). No nuclear actin/Cofilin1 rods were detectable in DMSO treated HeLa cells transfected with the mutant construct GFP-KTRTK-Cofilin1 (lower panel, mt). The overlay shows the GFP signal (green) and the DAPI signal (blue). Scale: 20 µm.

These results confirmed the inability of KTRTK-Cofilin1 to form nuclear rods, due to the mutation of the NTS.

4.1.1 Mutant protein KTRTK-Cofilin1 showed reduced depolymerization activity

In order to conclude if the depolymerizing activity of the mutated protein was altered, a number of actin *in vitro* assays were performed to compare wt-Cofilin1 to KTRTK-Cofilin1.

4.1.1.1 Decreased F-actin depolymerizing activity of KTRTK-Cofillin1 in falling ball assay

A falling ball assay measures actin depolymerization activities by determining a change in viscosity (3.3.7.1) (Pollard and Cooper, 1982). The time it took the ball to cross a specific distance, here 4 cm, at a specific angle (17° angle) in the capillary was noted (Figure 18). Purified actin along with purified Cofilin1 (wt) and KTRTK-Cofilin1 (mt) was used. Polymerization reactions were set up by mixing 9 µM actin and the different final concentrations of wt-Cofilin1 and KTRTK-Cofilin1 (3 µM, 1.5 µM and 0.75µM), respectively. Actin, without any additional proteins functioned as reference. With the highest viscosity, that did not change during the experimental set-up, it allowed conclusions regarding the depolymerization activity of wt-Cofilin1 and KTRTK-Cofilin1,

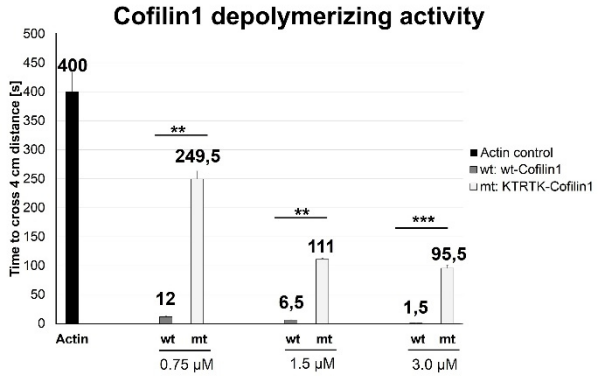

Fig. 18: Cofilin1 and KTRTK-Cofilin1 depolymerizing activity in a falling ball assay. Different final concentrations (0.75 µM, 1.5 µM and 3 µM) of wt-Cofilin1 and KTRTK-Cofilin1, respectively, were mixed to F-actin. Time of the falling ball in actin alone was used as reference. Depolymerizing activity of the mutant protein (light gray) was significantly lower at the studied concentrations. Wt: wt-Cofilin1; mt: KTRTK-Cofilin1. Levels of significance: 0.05 >p≥ 0.01 (*); 0.01>p≥0.001 (**); p>0.001 (***).

respectively, in comparison. The depolymerizing activity of the analyzed protein correlated with the viscosity of the sample. Therefore the faster the ball crossed the defined distance, the higher the depolymerizing capacity of the protein of interest.

Polymerization reactions were set up by mixing KTRTK-Cofilin1 and Cofilin1, diluted to different final concentrations, with 9 µM actin. Mixtures were transferred to glass capillaries with capped end and left to polymerize before the metal ball was added. The sample containing only actin was used as reference (Figure 18, black). It took significantly longer for the ball to cross the predetermined distance in the samples containing KTRTK-Cofilin1 (light gray). At a final concentration of 0.75 and 1.5 µM of the respective protein, the ball crossed the distance in the samples containing the wildtype protein (dark gray) approximately 20 times faster than in the mutant counterparts. The biggest difference of depolymerizing activity was observed at a concentration of 3 µM of wt and mt protein. The ball in the mt sample took about 63 times longer to cross the specified distance. The highest difference in depolymerizing activity was observed at a concentration of 3 µM of wt-Cofilin1. This suggests that depolymerizing activity of wt-Cofilin1 increases with rising concentration, whereas the depolymerizing activity of KTRTK-Coflin1 does not. Regarding, the crossing time of the actin reference in comparison to the mt samples, differences in migrating behavior could be noted. Therefore, these data indicated that KTRTK-Cofilin1 has a reduced F-actin depolymerizing activity in comparison to wt-Cofilin1 but depolymerizing ability was not completely lost.

4.1.1.2 Mutant protein KTRTK-Cofilin1 displayed reduced quenching capacity in pyrene actin assay

This assay provides further information regarding F-actin binding kinetics by monitoring changes in pyrene actin fluorescence (Figure 19). Labeled G-actin is only weakly fluorescent, but upon polymerization the fluorescence is enhanced about 20 times. Binding of the analyzed protein basically blocks the fluorescence signal of pyrene actin (Mustonen et al., 1987). Therefore binding kinetics could be traced by the quenching of fluorescence intensity signal. (3.3.7.2).

For the final reaction, 4 µM Cofilin1 (wt and mt, respectively) was added to 2 µM polymerized actin. Actin, without any additional proteins represented the reference. Data acquisition was performed every 1.8 seconds for 90 seconds, approximately 60 seconds after proteins of interest were added (Figure 19).

The lower the remaining fluorescence, the higher the binding capacity of the protein of interest. The detected fluorescence in the samples containing KTRTK-Cofilin1 (light gray) remained significantly higher than in the samples containing wt-Cofilin1 (dark gray). While the fluorescence in the wildtype samples was reduced to one-fifth of the reference, the mutant samples showed only a slight decrease of approximately 9% in comparison to the actin reference.

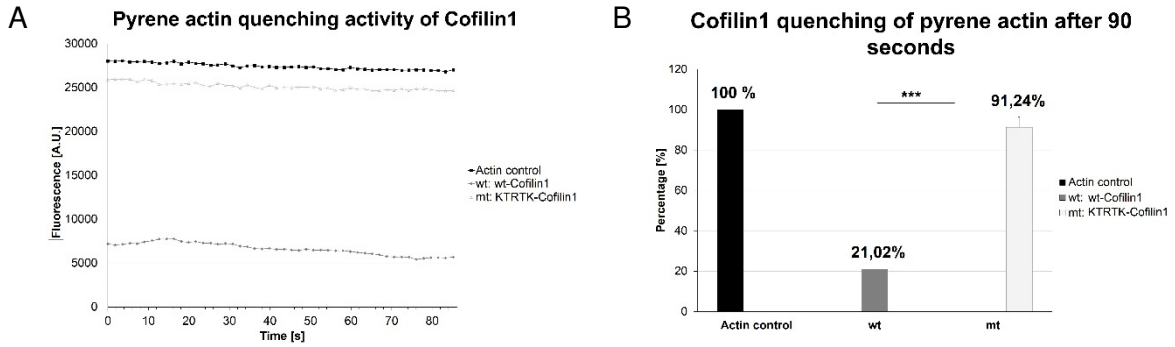

Fig. 19: Wt-Cofilin1 and KTRTK-Cofilin1 quenching activity of pyrene F-actin. A) Pyrene actin fluorescence signal in the course of 90 seconds. **B**) Relative fluorescence signal after 90 seconds in comparison to the actin reference. Wt and mt Cofilin1, respectively, were added to F-actin. Data acquisition was started approx. 60 s after proteins of interest were added fluorescence was measured every 1.8 seconds for 90 seconds. Actin alone was used as reference. Binding activity of the mutant protein (light gray) was significantly lower than in the wt (dark gray). Wt: Cofilin1; mt: KTRTK-Cofilin1. Levels of significance: 0.05 >p≥ 0.01 (*); 0.01>p≥0.001 (**); p>0.001 (***).

In this experiment the quenching capacity and thereby the binding activity of wt-Cofilin1 was four times higher than of the mutant. These *in vitro* assay data indicate that KTRTK-Cofilin1 did preserve some of the depolymerizing function (4.1.1.1) but that the binding capacity of the mutant protein was affected compared to wt-Cofilin1.

4.2 Cofilin1$^{KTRTK/KTRTK}$ embryos showed exencephalic phenotype

The role of Cofilin1 in the nucleus and the function of the nuclear translocation signal *in vivo* was studied in this thesis. It is known that Cofilin1 is essential for embryonic development. Deletion of Cofilin1 results in embryonic lethality around embryonic day 10.5 (E10.5). Cofilin1$^{-/-}$ embryos bear a total lack of neural tube closure along with altered neural crest cell migration and cell proliferation (Gurniak et al., 2005; Bellenchi et al., 2007). To elucidate the role of Cofilin1 *in vivo* the KTRTK-Cofilin1 mouse line was created by Christine Gurniak (2.1).
Heterozygous (Cofilin1$^{wt/KTRTK}$) animals showed no phenotype and were not distinguishable from wildtype (Cofilin1$^{wt/wt}$) animals. Homozygous mutants (Cofilin1$^{KTRTK/KTRTK}$), however were not viable, therefore embryos at different gestational stages were analyzed.

Timed matings were set up to obtain embryos at developmental stages from E10 to E19.5. Mating of heterozygous males and females allowed the generation and analysis of all possible genotypes (wt: Cofilin1$^{wt/wt}$; het: Cofilin1$^{wt/KTRTK}$, mt: Cofilin1$^{KTRTK/KTRTK}$).

4.2.1 Exencephaly could be detected starting at E10 at all embryonic stages

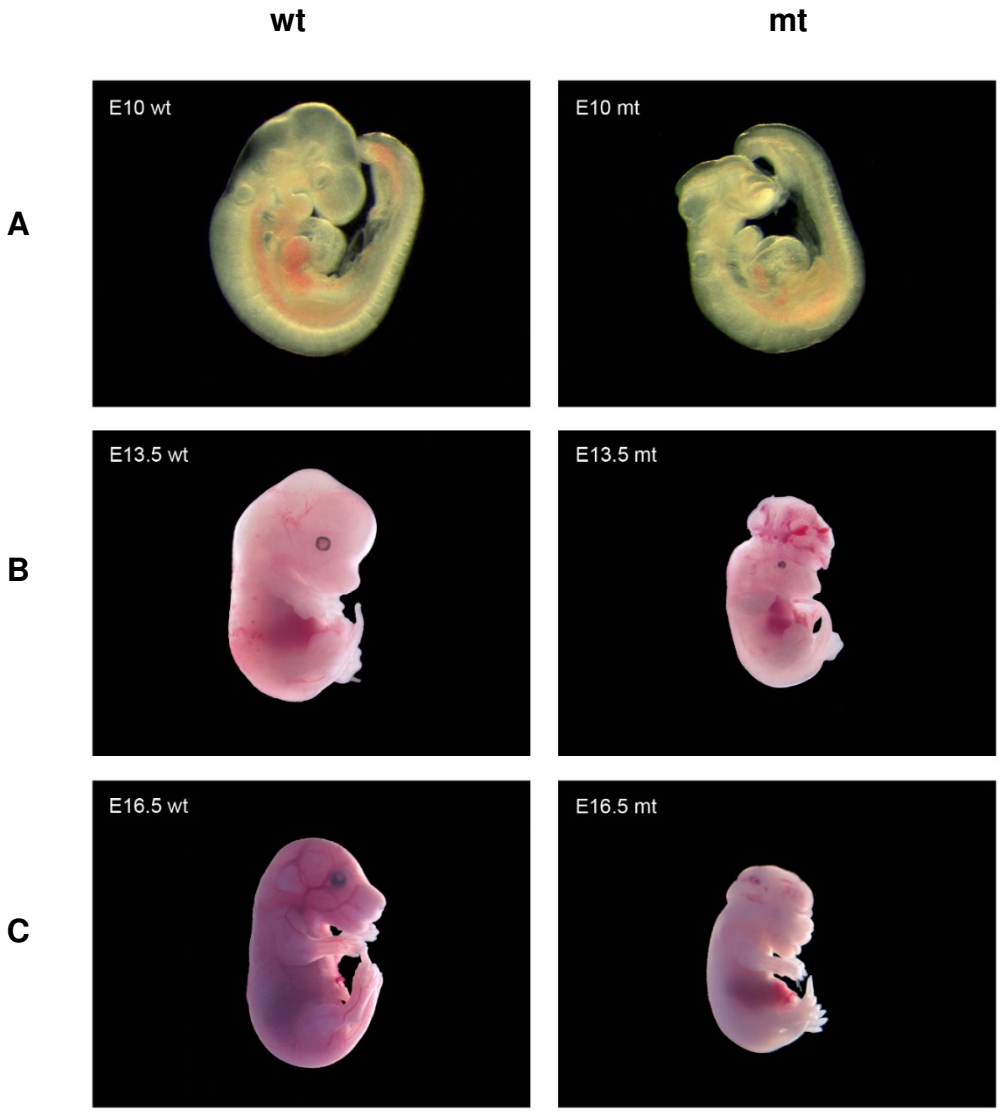

Fig. 20: Wildtype and KTRTK–Cofilin1 embryos at different developmental stages. A) Cofilin1$^{wt/wt}$ (wt) and Cofilin1$^{KTRTK/KTRTK}$ (mt) embryos at E10.; **B)** wt and mt embryos at E13.5 and **C)** wt and mt embryos at E16.5. Images were acquired at different magnifications (4.0x - 1x), the same magnification was used for littermates. wt: Cofilin1$^{wt/wt}$; mt: Cofilin1$^{KTRTK/KTRTK}$.

Cofilin1$^{KTRTK/KTRTK}$ embryos showed distinct defects in cranial tube closure. The exencephalic phenotype could be detected as early as E10, the earliest developmental stage analyzed. All mutants showed a very conspicuous phenotype in the form of the

absence of skull structures featuring the extrusion of the brain (Figure 20). The severity of exencephaly varied, whereas some embryos showed a mild form of brain extrusion, others appeared more severe, in which the brain overlapped facial structures completely (Figure 20; Panel C mt).

All mutant embryos were smaller than their wildtype or heterozygous littermates (Figure 20), but showed no other obvious defects.

When isolated mutant brains, revealed massive malformations. Besides an apparent lack of defined structure of the cerebral hemisphere, mutant brains were significantly bigger than wildtype brains in comparison (Figure 21). The olfactory bulb, a prominent protrusion at E15.5 in wildtype brains, is poorly developed barely identifiable in the mutant. The mutant brain morphology will be analyzed in detail in a later chapter (4.5.2).

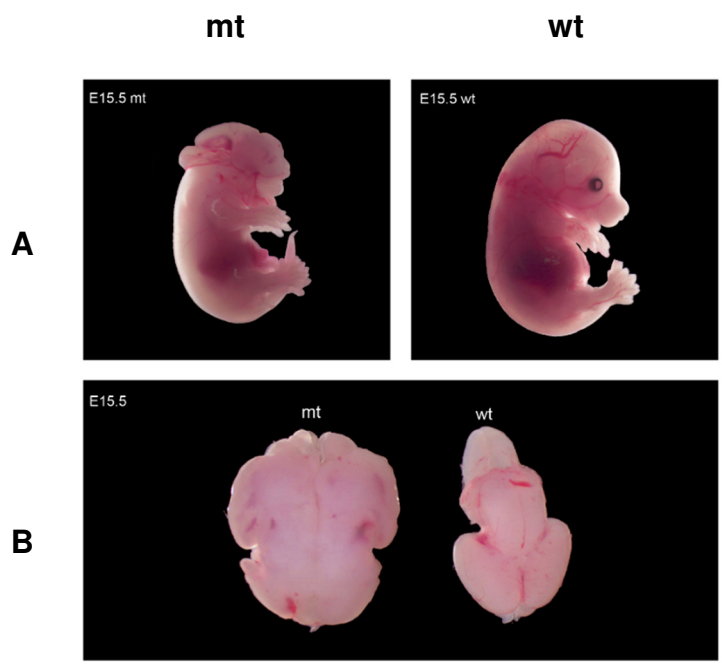

Fig. 21: KTRTK – Cofilin1 and wildtype embryos at E15.5. **A)** Cofilin1$^{KTRTK/KTRTK}$ (mt) and Cofilin1$^{wt/wt}$ (wt) embryos at E15.5; **B)** isolated brains of E15.5 mt and wt embryos. Images were acquired at different magnifications (1.6x – 2.5x), same magnification was used for littermates. mt: Cofilin1$^{KTRTK/KTRTK}$; wt: Cofilin1$^{wt/wt}$

Further, not all mutant embryos carried both eyes, especially in embryos displaying more severe forms of exencephaly the number of eyes was observed to vary.

Collected embryos were used for the isolation of primary cultures (mouse embryonic fibroblasts (Mefs), neurons and astrocytes), the preparation of tissue lysates, RNA isolation, morphological analyses and gene expression analyses.

4.2.2 KTRTK-Cofilin1 showed no dominant negative effect

In order to conclude whether the KTRTK-Cofilin1 mutation might affect the distribution of the respective genotypes (wt, het and mt) among all embryos was determined. Genotype of the collected embryos was determined on embryonic tissue samples (see 3.1.1). In the course of this study 654 embryos at various developmental stages were analyzed (Figure 22).

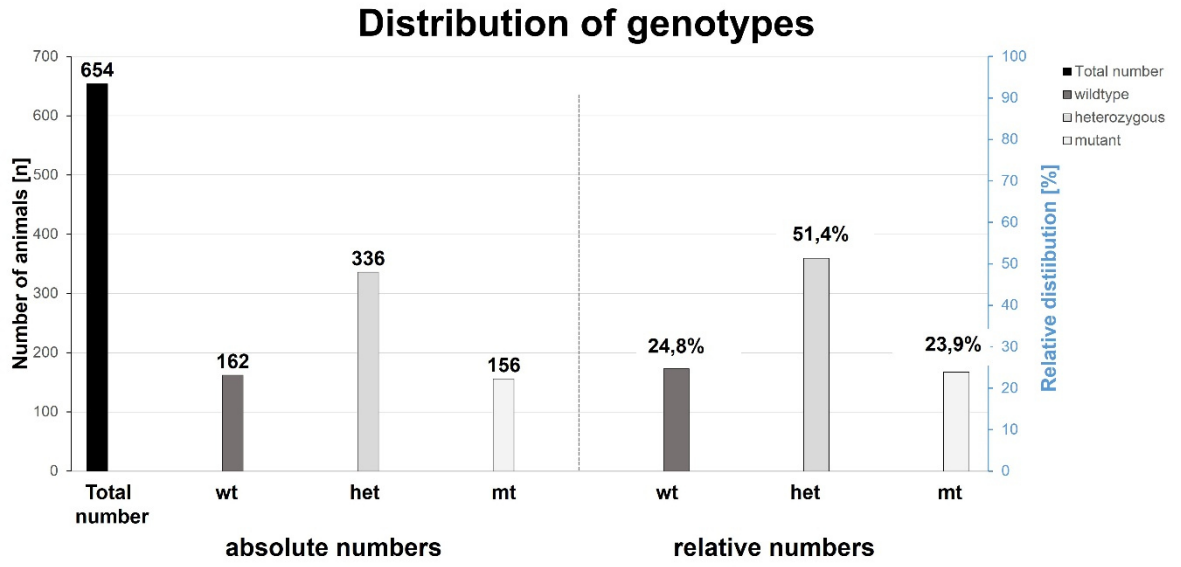

Fig. 22: Distribution of embryonic genotypes and the relative percentage. In the course of this thesis 654 embryos were isolated. The respective percentages (blue axis, right) were calculated based on the total number of embryos (N=654, black). The distribution of genotypes among embryos (N=654) followed Mendelian law. Wildtype/ wt: Cofilin1$^{wt/wt}$ (dark gray); heterozygous/ het: Cofilin1 $^{wt/KTRTK}$ (gray); mutant/ mt: Cofilin1$^{KTRTK/KTRTK}$ (light gray).

Analysis of the embryonic genotypes (Figure 22) showed that the distribution of the genotypes occurred almost perfectly according to Mendelian inheritance law. A ratio of 1: 2: 1 (wt: het: mt) for the different genotypes was expected among the progenies. The ratio that applies here was 24.8%: 51.4%: 23.9%, indicating that the resorption rate or the frequency of the respective genotypes were not affected by the mutation of the nuclear translocation signal of Cofilin1.

Phenotypic analysis of embryos at different developmental stages concluded, that only the Cofilin1$^{KTRTK/KTRTK}$ embryos showed the exencephalic phenotype (4.2.1),

demonstrating a recessive phenotype. Furthermore, 100% penetrance of the phenotype was observed in Cofilin1$^{KTRTK/KTRTK}$ embryos. Cofilin1$^{wt/KTRTK}$ embryos showed no phenotype and were not distinguishable from wt littermates. Cofilin1$^{wt/KTRTK}$ animals were viable. No viable Cofilin1$^{KTRTK/KTRTK}$ animals were found.

4.3 KTRTK-Cofilin1 protein expression level decreased during embryonic development

4.3.1 ADF/Cofilin members in embryonic tissues

To analyze the protein expression levels of KTRTK-Cofilin1 in mutant (mt: Cofilin1$^{KTRTK/KTRTK}$) and heterozygous (het: Cofilin1$^{wt/KTRTK}$) embryos in comparison to Cofilin1 in wt embryos (wt: Cofilin1$^{wt/wt}$) lysates at different developmental stages were prepared. Furthermore, protein expression in brain and body tissue was of interest in consequence to the restriction of the phenotype to the brain.
E10.5, E13.5, E16.5 and E18 embryo lysates for all three genotypes (wt, het and mt) were prepared and the respective Western blots were probed for all members of the ADF/Cofilin family: Cofilin1 (KG60), Cofilin2 (FHU1) and ADF (7D10). In the diploma thesis the expression levels of the ADF/Cofilin family members between genotypes were observed to vary in brain depending on developmental stage and genotype (Figure 23+24) (Roy, 2011).

Cofilin1$^{KTRTK/KTRTK}$ embryos were alive at E18, the beating heart was observed. Other than an exencephalic phenotype, variations of the number of eyes and the slightly smaller overall size, the embryos showed no further obvious phenotype. Cofilin1$^{wt/KTRTK}$ embryos were not distinguishable from Cofilin1$^{wt/wt}$ embryos.

4.3.1.1 Levels of ADF/Cofilin family members during development

At E10.5 total embryos were analyzed, since at this stage in development it was not possible to isolate a brain. E10.5 total embryos showed no differences in the levels of Cofilin2 and Cofilin1. The expression level of ADF appeared to be slightly decreased in the mutant (Figure 23, A). The antibody (KG60) used for Cofilin1 recognized KTRTK-Cofilin1 as well as wildtype Cofilin1. Efficiency of the antibody was tested with GFP-KTRTK-Cofilin1 and GFP-wt-Cofilin1 in comparison (data not shown). At E18, almost no Cofilin1 could be detected in the mutant brain, in Cofilin1$^{wt/KTRTK}$ Cofillin1 was also decreased compared to Cofilin1$^{wt/wt}$ brains at E18 Figure 23, B. The Cofilin1 pool in the heterozygous animal both wt-Cofilin1 and KTRTK-Cofilin1 are present. The decreasing level of KTRTK-Cofilin1 observed in the embryonic Western blot analysis could indicate that the ratio of Cofilin1 to KTRTK-Cofilin1 is not equimolar in heterozygous tissues. The expression of Cofilin2 was up-regulated both in the mutant and the heterozygous brain, compared to wildtype brain. Expression of Cofilin2 was also up-regulated in the heterozygous brain.

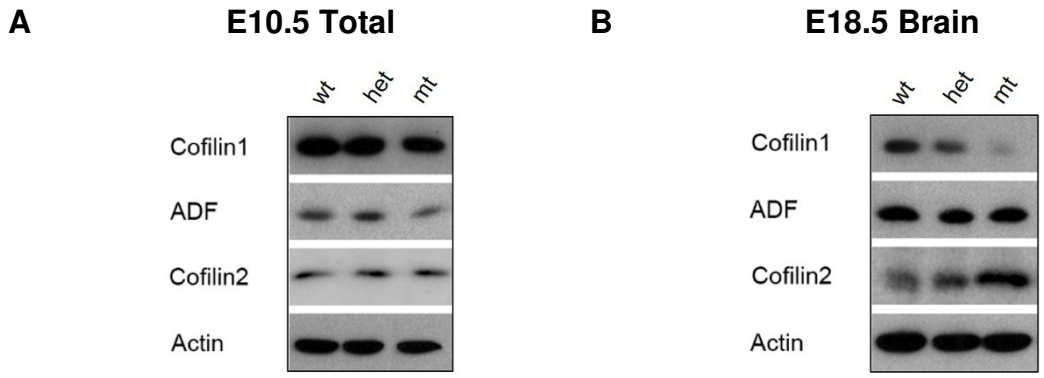

Fig. 23: Expression of the ADF/Cofilin family members in E10.5 embryo (A) and E18 brain lysates (B). A) The antibody KG60 recognizes Cofilin1 as well as KTRTK-Cofilin1. E10.5 total embryo lysates from wt, het and mt samples showed the same levels of Cofilin1 (KG60) and Cofilin2 (FHU1) protein. The level of ADF (7D10) expression appeared to be slightly decreased in the mt. B) In E18 mutant brain lysate only a very weak signal for Cofilin1 could be detected (mt). Cofilin2 showed increasing expression levels from wt to mt. The Western blots were probed with anti-actin (C4) as loading control. 10 µg of protein was loaded for each sample. wt: Cofilin1$^{wt/wt}$; het: Cofilin1$^{wt/KTRTK}$; mt: Cofilin1$^{KTRTK/KTRTK}$.

These results indicated the decrease of KTRTK-Cofilin1 expression between gestational stages E10 and E18. This experiment repeatedly showed a massive decrease or even complete loss of KTRTK-Cofilin1 protein in E18 mutant brains.

To determine the point of decrease of KTRTK-Cofilin1 level of protein expression more accurately, lysates of brain and body of E13.5 and E16.5 embryos were prepared respectively (Figure 24). Western blots were probed with antibodies for the members of the ADF/ Cofilin family.

The Western blot analyses for the E13.5 and E16.5 brain and body tissues showed differences of the protein expression levels of the ADF/Cofilin family members between genotypes and developmental stages (Figure 24). GAPDH levels showed equal loading within one group (e.g. E13.5, brain). In E13.5 brain lysates the level of Cofilin1 decreased slightly from wt to het to mt. In exchange the ADF expression level increased from wt to het to mt. The expression of Cofilin2 did appear to be slightly higher in the wt than in het and mt (Figure 24, black).

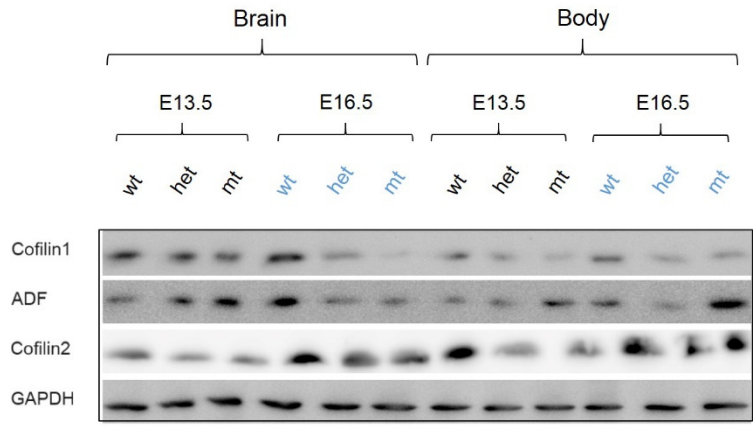

Fig. 24: Expression of the members of the ADF/Cofilin family in E13.5 and E16.5 body and brain. Lysates from brain and body of E13.5 (black) and E16.5 (blue) embryos showed differences in the levels of Cofilin1 (KG60), ADF (7D10) and Cofilin2 (FHU1) protein expression. GAPDH was used as loading control. 10 µg of protein was loaded for each sample. wt: Cofilin1$^{wt/wt}$; het: Cofilin1$^{wt/KTRTK}$; mt: Cofilin1$^{KTRTK/KTRTK}$.

In E16.5 brain lysates distinctly weaker signals for Cofilin1 were detected in the heterozygous and mutant brain than in the wt brain lysate. The detected levels of ADF and Cofilin2 were decreased in the heterozygous and mutant brain compared to wildtype (Figure 24, blue).

Next the corresponding bodies were analyzed to determine whether the altered expression levels could also be found in the respective bodies. The bodies of Cofilin1$^{KTRTK/KTRTK}$ embryos showed no obvious phenotype. The same tendencies of

decreasing expression levels, as in the brain lysates for both E13.5 and E16.5, could be observed for Cofilin1. At both developmental stages an up-regulation of ADF in mutant bodies was detected. The level of Cofilin2 in wt of E13.5 body was noticeably higher than in the het and mt tissues, whereas the level of Cofilin2 in E16.5 bodies of all three genotypes seemed to be same. The expression levels of Cofilin1, ADF and Cofilin2 differed from brain to body lysates and from E13.5 to E16.5. The difference in expression was especially explicit for ADF in E16.5 brain compared to E16.5 body. Whereas ADF is down-regulated in the mutant brain to compared het and wt brain, ADF expression level is up-regulated in the mutant body compared to het and wt body.

The members of the ADF/Cofilin family vary in their expression patterns. Cofilin2 is found in muscle, the CNS and brain (Gurniak et al., 2014). The expression level of Cofilin2 is up-regulated in later steps of development (Vartiainen et al., 2002), coinciding with the higher levels of Cofilin2 observed in E16.5 tissues. Analyses of the expression patterns of the ADF/Cofilin family members at different developmental stages was repeated three times confirming decreasing levels of KTRTK-Cofilin1 during the course of embryonic development.

The reason for the decrease of KTRTK-Cofilin1 protein level with increasing developmental age is not clear. Cofilin1 is expressed in all tissues but skeletal muscle during embryonic development (Vartiainen et al., 2002). The decrease in KTRTK-Cofilin1 level could be the consequence of different factors. Three possible hypotheses for the decrease of the level of mutant protein regarded the decrease of KTRTK-Cofilin1 at RNA level, proteasomal degradation due to altered stability and alterations of solubility characteristics.

4.3.1.2 KTRTK-Cofilin1 is not lost on transcriptional level

To elucidate whether the observed decrease of KTRTK-Cofilin1 occurs on transcriptional level, total RNA from E10.5 total embryos and E13.5, E16.5 and E18 brains, corresponding to the brain and body tissues analyzed by western blot, was isolated (4.3.1.1). RNA was prepared for quantitative PCR (qPCR) and analyzed for amounts of GAPDH (reference gene) and wt-Cofilin1 and KTRTK-Cofilin1 (target) transcripts (3.3.1.3).

The chosen probe for Cofilin1 did not interfere with the NTS. The efficiencies of the used probes were tested in prior experiments. Probes bound to KTRTK-Cofilin1 with the same efficiency as to the wildtype Cofilin1.

In conventional PCR the amplicon is detected by end-point analysis whereas in real-time quantitative PCR (qPCR) the amplicon accumulation is detected and measured while the reaction progresses in real time. This method is based on the detection of fluorescence proportional to the amplified product. In qPCR the data that are generated are the C_T-values (threshold cycle). The C_T-value describes the cycle number at which a detectable signal is achieved, representing the threshold. The amount of template present at the start of the amplification reaction mainly determines the threshold cycle. The lower the amount of template in the sample, the higher the threshold cycle. This ratio forms the basis for the quantitative aspect of qPCR.

For this experiment RNA was derived from E10 total embryo along with brains from E13.5, E16.5 and E18 (Cofilin1$^{wt/wt}$ and Cofilin1$^{KTRTK/KTRTK}$). Cofilin1$^{wt/KTRTK}$ were not tested. The chosen Cofilin1 probe did not distinguish between wt-Cofilin1 RNA and KTRTK-Cofilin1 RNA. Therefore, heterozygous samples would not have allowed any conclusions regarding the KTRTK-Cofilin1 RNA portion of the detected Cofilin1 RNA. The acquired data was analyzed using the ΔCT-method, a form of relative quantification (3.3.1.4).

Relative quantification can provide information regarding changes and differences in gene expression.

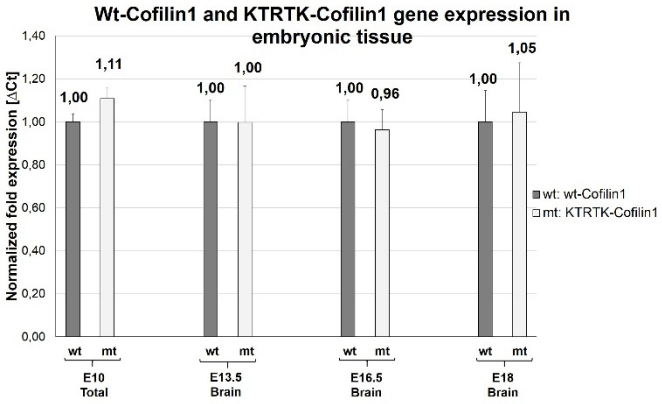

Fig. 25: Gene expression levels of wt-Cofilin1 and KTRTK-Cofilin1 at different stages of embryonic development. RNA derived from E10 embryo along with brains of E13.5, E16.5 and E18 brain was analyzed for expression of GAPDH (reference gene) and Cofilin1 (target). Acquired data was analyzed using the ΔCT-method. No significant differences between the mRNA expression levels of KTRTK-Cofilin1 and Cofilin1 were detected in the respective samples. Wt: Cofilin1$^{wt/wt}$; mt: Cofilin1$^{KTRTK/KTRTK}$.

In the ΔCT-method the expression of the target gene (Cofilin1) in the wt sample is normalized to 1. The expression of the target gene in the mutant is calculated according to the respective normalized value of the wildtype counterpart. Data of quantitative PCR is presented in Figure 25. At every developmental stage analyzed (E10, E13.5. E16.5 and E18) a gene expression level close to 1 could be detected for KTRTK-Cofilin1 RNA in reference to the wildtype sample. At no age significant differences in gene expression were observed that would cause the observed decrease in KTRTK-Cofilin1 protein level. After the decrease of KTRTK-Cofilin1 on RNA level could be excluded, the decrease could be originated from alterations in translation.

A possible change of solubility of the mutant protein was analyzed next.

4.3.1.3 The KTRTK mutation of Cofilin1 does not alter protein solubility

Previous studies showed that a mutation in the form of an alanine to threonine substitution directly behind the KKRKK sequence (wt: KKRKKAVLFCLS; mt: KKRKKTVLFCLS) in Cofilin2 resulted in significantly lower protein levels in the mutant muscle tissue than in wildtype tissue, even though the mutant tissue contained 4-20 fold more Cofilin2 mRNA, indicating a reduced stability or altered solubility of the mutant protein (Agrawal et al., 2007).

In the prior western blots (Figure 23+24) soluble protein fractions were analyzed, therefore in the case of altered solubility KTRTK-Cofilin1 could be in the pellet. Developmental day E12.5 embryos were chosen for analyses, a stage in development in which the KTRTK-Cofilin1 protein was still present in the mutant but less than in wildtype (Figure 26).

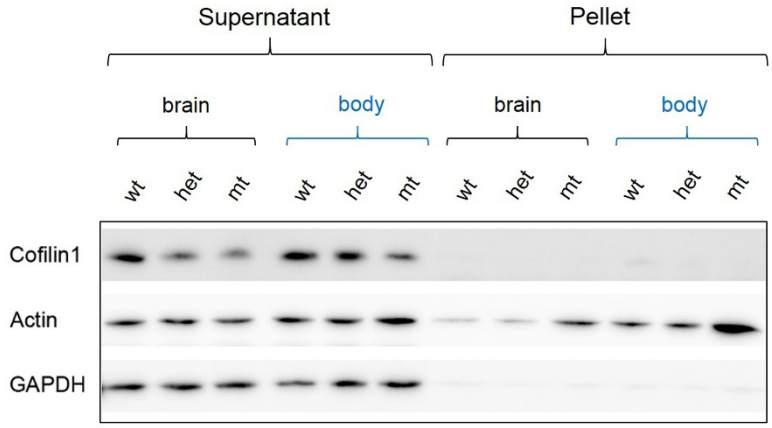

Fig. 26: Analysis of KTRTK-Cofilin1 solubility properties in E12.5 embryos. Supernatant (soluble) and pellet (insoluble) fractions of wt, het and mt brains (black) and bodies (blue) of E12.5 embryos were prepared. Actin (C4) was detected in all fractions at different levels. Mutant insoluble fractions showed considerably more actin. Western Blot was probed for anti-GAPDH as soluble contamination control. Cofilin1 (KG60) was detected in all soluble fractions, whereas Cofilin1 could not be detected in any pellet fraction. Soluble fractions of E12.5 brains and bodies showed differences in the levels of Cofilin1 (KG60) between genotypes and tissues. 10µg for the supernatant lysates were loaded with equivalent volumes of the insoluble fractions. Wt: Cofilin1$^{wt/wt}$; het: Cofilin1$^{wt/KTRTK}$; mt: Cofilin1$^{KTRTK/KTRTK}$;

To study possible alterations of the solubility of the KTRTK-mutant protein, supernatant (soluble) and pellet (insoluble) fractions of E12.5 bodies and brains were prepared of wildtype, heterozygous and mutant embryos. This way insoluble proteins would have been detected in the pellet fractions. GAPDH was used to exclude the possibility of soluble contamination of the insoluble fractions. This was of importance to verify that no possibly detected signal was a result of soluble contamination. Figure 26 shows that a clean fractionation of supernatant and pellet fractions was achieved. Cofilin1 was only detected in the soluble fractions of all three genotypes in both tissues. The

detected levels of Cofilin1 decreased from wildtype to heterozygous to mutant. An observation that had already been made in various other western blot analyses for embryos of different gestational stages (4.3.1.1). Actin was detected in all samples. It should be noted that in the insoluble fractions the level of actin increases from wildtype to heterozygous to mutant. It is feasible that this detected level of insoluble actin reflects the reduced depolymerization of F-actin (4.1.1) and the increased amount of F-actin that have been observed in later experiments (4.4.6). The method used to prepare supernatant and pellet fractions is not designed to efficiently separate G-actin from F-actin. The data acquired in this experiment showed that KTRTK-Cofilin1 protein level did not decrease due to altered solubility.

To verify whether solubility might be altered depending on developmental stage, embryonic stages E11.5 to E18 were analyzed. At no time point of development the mutant protein KTRTK-Cofilin1 was detected in insoluble fractions.

Since the decrease of KTRTK-Cofilin1 protein due to a change of solubility could be eliminated, possible decrease of KTRTK-Cofilin1 in consequence to protein stability was analyzed.

4.3.1.4 KTRTK-Cofilin1 protein is not lost to proteasome degradation

If the stability of the mutant protein was changed by the introduction of the KTRTK sequence, KTRTK-Cofilin1 proteasomal degradation may be increased. In this experiment the possible loss of the mutant protein due to proteasomal degradation was studied.

Proteasomes degrade unnecessary or damaged proteins by proteolysis. These protein complexes are part of major mechanisms by which the concentration of particular proteins in cells is regulated and misfolded proteins are degraded (Peters et al., 1994).

In this experiment proteasomal degradation was blocked with the proteasome inhibitor MG132, to find out whether an accumulation of KTRTK-Cofilin1 could be detected. MG132, is a specific, reversible cell permeable proteasome inhibitor. It effectively blocks the proteolytic activity of the 26S proteasome complex. Previous studies

showed that successful proteasome inhibition via MG132 induces intracellular overexpression of heat shock protein 70 (Hsp70) (Grossin et al., 2004).

For this *in vitro* experiment, mouse embryonic fibroblasts (Mefs) were derived from E18.5 embryos. Mefs provide an ideal model system to study functional genetics and cellular mechanisms. At this stage of mutant embryonic development the lowest KTRTK-Cofilin1 protein level had been observed. Should degradation take place this extremely low level would simplify the detection of a rise in protein level due to a block in proteasomal degradation.

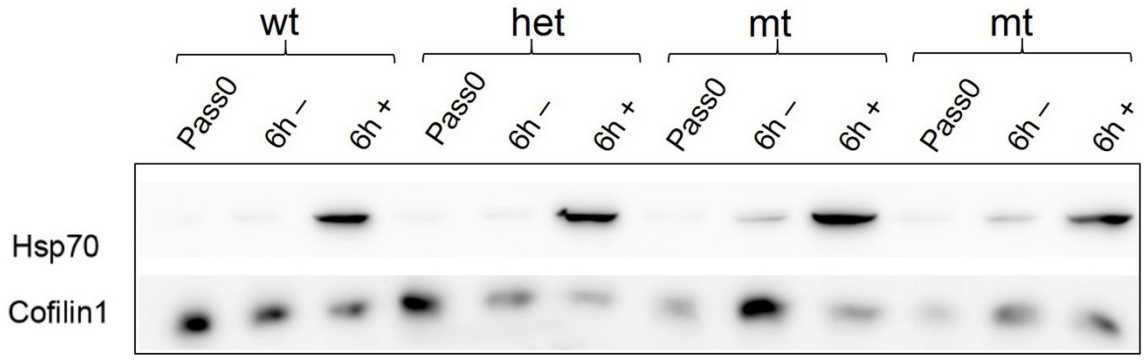

Fig. 27: Proteasome inhibition by MG132 treatment of E18.5 mouse embryonic fibroblasts (Mefs). Mefs derived from E18.5 embryos were treated with 20 µM MG132 for 6 hours. Western blots were probed for anti-heat shock protein 70 (Hsp70) to verify successful proteasome inhibition. Pass0 cells were analyzed to determine starting expression level of Cofilin1 (KG60). No increased Cofilin1 levels were detected after 6 hours proteasomal inhibition (6h +). Coomassie gels verified equal loading (data not shown). P0: Passage 0; 6h -: untreated Mefs after 6 hours; 6h +: Mefs treated with 20µM MG132 for 6 hours; wt: Cofilin1$^{wt/wt}$; het: Cofilin1$^{wt/KTRTK}$; mt: Cofilin1$^{KTRTK/KTRTK}$;

Directly after isolation and before plating embryonic cells were defined as passage number 0 (Pass0). Lysates of passage 0 cells were prepared to determine the starting protein expression level, before cells were taken into culture, of Cofilin1 and KTRTK-Cofilin1, respectively (Figure 27). At Pass0 the amount of Cofilin1 decreased from wildtype to heterozygous to mutant. The same phenomenon had been observed before in E13.5 and E16.5 brains (4.3.1.1). “6h+” represent Mefs that were treated with 20 µM MG132 for 6 hours, whereas the “6h –“ lane indicates Mefs that remained untreated during the same time period. As expected after 6 hours MG132 incubation a distinct up-regulation of heat shock protein 70 (Hsp70) in all MG132 treated samples was detected. The protein expression level of Cofilin1 was up-regulated in all “6h –“

samples compared to the Pass0 expression level. This characteristic had been observed in Cofilin1$^{KTRTK/KTRTK}$ Mefs before. Mefs of certain developmental age (E15.5+E16.5) increase their level of Cofilin1 expression in culture after seeding (4.4.7). The up-regulation in mutant 1 (lanes 7-9) was noticeably higher than in mutant 2 (lanes 10-12). Therefore it was of importance in this experiment to compare Mefs that were plated for the same amount of time. The Cofilin1 protein expression level in "6h +" was decreased in the wildtype, heterozygous and mutant 1 samples compared to the level in "6h –". Mutant 2 showed approximately the same KTRTK-Cofilin1 protein expression level in treated and untreated cells, but no accumulation of KTRTK-Cofilin1 in the MG132 treated sample was detected. GAPDH expression levels were affected by MG132 treatment of the Mefs, but Coomassie gels verified equal loading of all samples (data not shown). The detected level for Cofilin1 in the treated cells was distinctly lower than in the untreated cells. Considering the successful proteasomal inhibition and the decreasing and unchanged protein levels of KTRTK-Cofilin1 in the treated mutant, concluded that the mutated protein is not decreased due to instability and thereby increased proteasomal degradation.

MG1332 treatment over night, including different concentrations showed the same results (data not shown). These data showed that KTRTK-Cofilin1 is not lost due to changes on transcriptional level (4.3.1.2), alterations of solubility (4.3.1.3) or altered stability (4.3.1.4.)

The reasons for the decrease in KTRTK-Cofilin1 protein level remain to be elucidated.

4.4. Cofilin1$^{KTRTK/KTRTK}$ mouse embryonic fibroblasts show distinctly affected multinucleate morphology and cellular functional mechanisms

In consequence to the embryonic lethality of Cofilin1$^{KTRTK/KTRTK}$ mutants at the point of birth, mouse embryonic fibroblasts (Mefs) were isolated to obtain living cells to facilitate analyses of cellular processes and morphology.
Mefs provide an ideal model system to study functional genetics and cellular mechanisms in cases of embryonic lethality (Lengner et al., 2004).

Embryonic fibroblasts were derived from Cofilin1$^{wt/wt}$ and Cofilin1$^{KTRTK/KTRTK}$ embryos at various developmental stages ranging from E13.5 to E18.5. All analyzed Cofilin1$^{KTRTK/KTRTK}$ Mefs, independent of gestational stage of isolation, displayed the same phenotype. The Mefs that are shown here were all isolated from E14.5 embryos.

4.4.1 Members of the ADF/Cofilin family are expressed differently in Cofilin1$^{KTRTK/KTRTK}$ Mefs

The expression of the mutant protein KTRTK-Cofilin1 is decreased in embryonic brain and body. To find out whether this differential expression level could also be observed in Mefs the expression levels of the members of the ADF/Cofilin family were determined in this chapter.
Mefs derived from E14.5 Cofilin1$^{wt/wt}$ and Cofilin1$^{KTRTK/KTRTK}$ embryos were studied. Mefs were grown in uncoated flasks. Lysates of consecutive passages were prepared in order to analyze *in vitro* expression levels.
Western blots were probed for all members of the ADF/Cofilin family, Cofilin1 (KG60), Cofilin2 (FHU1) and ADF (7D10). GAPDH (GAPDH) was used to control equal loading control (Figure 28).
Passage 0 defined cells directly isolated from the embryos. Lysates of passage 0 (Pass0) cells were prepared to determine the starting expression level of wt-Cofilin1 and KTRTK-Cofilin1, respectively (Figure 28). At Pass0 mt Mefs showed decreased

protein level of Cofilin1 (KG60) compared to wt. The expression of ADF, Cofilin2 and Cofilin1 in wt and mt is very low in Pass0. In the course of the culture from passage 0 (Pass0) to passage 3 (Pass3) a distinct up-regulation for ADF and Cofilin2 was detected in the mt starting in passage 1(Pass1). In the wt an up-regulation of ADF could only be observed in passage 3 (Pass3). In the wt an increase in expression of Cofilin2 was detected in Pass1 and Pass2. In Pass3 the level of Cofilin2 decreased again. In the mutant Cofilin2 rose in Pass1 and remained at a constant level afterwards. The reason for the high amount of ADF and Cofilin2 in the mutant is not clear, the possibility of a compensatory function of ADF and Cofilin2 for KTRTK-Cofilin1 in Mefs needs to be clarified.

Additionally to the members of the ADF/ Cofilin family the blots were probed with anti-PCNA (PCNA). Alterations of growth behavior and kinetics along with a striking multinuclearity have been observed in mt Mefs, giving rise to the question whether DNA replication might also be affected. The proliferating cell nuclear antigen (PCNA), a DNA clamp, is essential for replication and acts as processivity factor for DNA polymerase δ, therefore PCNA can be used as proliferation marker (Kelman, 1997). The impression was that the PCNA level at Pass2 was lower than in Pass1 in the mt. A considerable down-regulation of PCNA was detected in Pass3 for both genotypes. Which fits *in vitro* the observations of slowed down growth of wt and mt Mef cultures.

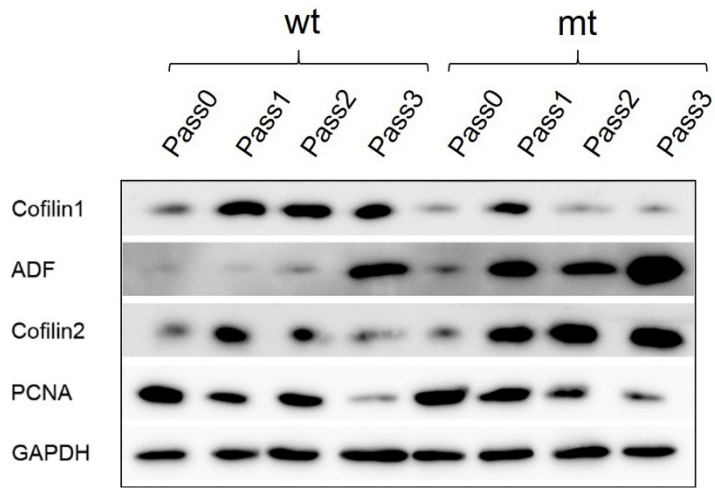

Fig. 28: Detection of ADF/Cofilin family members in E14.5 Mefs. Genotypes showed distinct differences for the expression pattern of the members of the ADF/Cofilin family, Cofilin1 (KG60), ADF (7D10), Cofilin2 (FHUI), respectively. Expression of PCNA (PCNA) was down- regulated in Pass3, indicating a decrease in proliferation. Blot was probed for anti-GAPDH to verify equal loading. 10µg of protein for the total lysates were loaded. Wt: Cofilin1$^{wt/wt}$; mt: Cofilin1$^{KTRTK/KTRTK}$; Pass0: Passage 0; Pass: Passage 1; Pass2: Passage 2; Pass3: Passage 3

The differences of expression pattern of the ADF/ Cofilin family could be observed in Mefs isolated from different gestational stages as well (data not shown). Mutants showed up-regulation for Cofilin2 and ADF starting in passage 1, whereas the expression of the mutant protein KTRTK-Cofilin1 was less than in the wt. The up-regulation of ADF could only be observed in passage 3 of the wt. Also, Cofilin1$^{KTRTK/KTRTK}$ Mefs showed a different morphology that Cofillin1$^{wt/wt}$ Mefs. Whether ADF and Cofilin2 assume a possible compensatory function to a certain extent due to loss of KTRTK-Cofilin1, needs to be elucidated.

4.4.2 Cofilin1$^{KTRTK/KTRTK}$ Mefs were significantly enlarged in cell size compared to Cofilin1$^{wt/wt}$ *in vitro*

From previous experiments it was known that Mefs derived from Cofilin1$^{wt/wt}$ (wt) and Cofilin1$^{KTRTK/KTRTK}$ (mt) embryos showed differences in culturing behavior, the growth rate of mutant Mefs was noticeably slower than the rate of wildtype Mefs after the second passage in culture.

One passage was counted when confluent cells were trypsinized and diluted for subsequent seeding.

Mefs of both wildtype and mutant went into crisis, usually after the second or third passage (depending on gelatin coating), characterized by slowed down division rate for approximately 10 to 14 days. Afterwards, wildtype Mefs recovered fully and permanent cultures could be established. Mutant Mefs could only be sustained in culture for one to two more passages after recovery. Afterwards mutant Mefs were lost.

When plated on gelatin as extracellular matrix, mutant Mefs could be obtained in culture until after the fifth passage. Differences in the ability of wildtype and mutant Mefs to attach to glass coverslips were observed. It was problematic to plate a sufficient number of cells on glass coverslips after the first passage, especially in the case of the mutant. Therefore, glass coverslips coated with an extracellular matrix (gelatin) were provided. All morphological studies were performed on Mefs grown on

gelatin coated glass coverslips. Analyses was performed by microscope at different time points in culture.

Morphological comparison of wildtype and mutant cells grown on uncoated with gelatin coated grown Mefs revealed no alteration of morphological characteristics.
To further elucidate the morphological differences and the in culture behavior of mutant Mefs, cell cycle progression, cell proliferation and G-Actin- F-Actin ratio were analyzed among others.

4.4.2.1 Mutant Mefs were multinuclear and increased in cell size

Protein expression analyses of bodies from E16.5 and E13.5 embryos revealed the decreased expression of KTRTK-Cofilin1 in mutant bodies compared to the expression level of wt-Cofilin1 in wildtype bodies (Figure 24). Mefs are fibroblast derived from body tissue. Therefore a closer look at the morphology of the isolated Mefs was taken. Cofilin1$^{KTRTK/KTRTK}$ displayed distinct morphological differences. In general, the cells and the nuclei of the mutant cells were bigger (Figure 29).

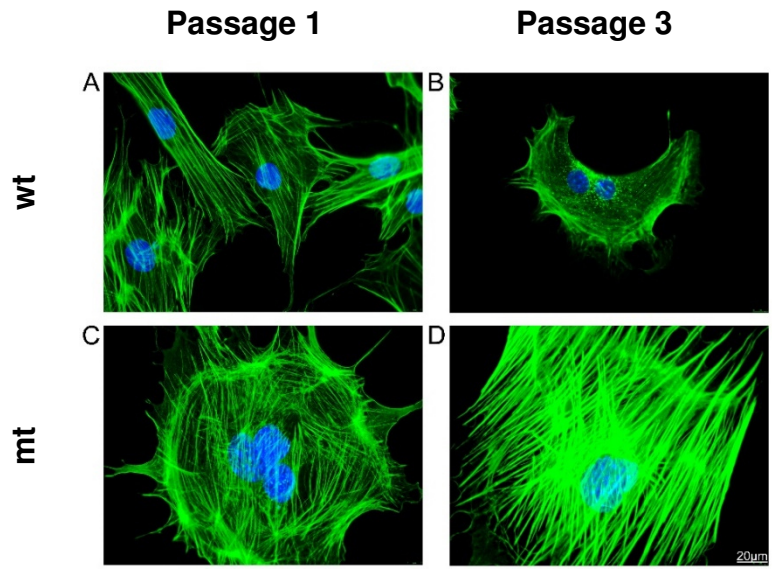

Fig. 29: F-actin staining of Cofilin1$^{wt/wt}$ and Cofilin1$^{KTRTK/KTRTK}$ E14.5 at passages 1 and 3. Mefs were plated on gelatin coated coverslips and stained for F-actin (Phalloidin Alexa-488, green) and DAPI (blue). Passage 1 (A+C) and passage 3 (B+D) revealed significant differences in cell size and the presence of multinuclearity. Images were acquired at 63x magnification. wt: Cofilin1$^{wt/wt}$; mt: Cofilin1$^{KTRTK/KTRTK}$

Cofilin1 depolymerizes F-actin. Depolymerizing *in vitro* activity assays with purified protein showed decreased F-actin depolymerization capacity of KTRTK-Cofilin1 (4.1.1). This would indicate increased F-actin levels in tissue and isolated cells. Phalloidin is a bicyclic peptide that binds selectively to F-actin. It was originally derived

from the fungus *Amanita phalloides*. These labeled conjugates bind in a stoichiometric ratio of about one phallotoxin per actin subunit. It is a widely used staining reagent to visualize the actin cytoskeleton of cells.

Phalloidin stainings were conducted to observe the general morphology of the cells more closely and look at F-actin. In order to gain further reliable information whether the mutation of the NTS also affected the ability to depolymerize F-actin in the cell (see 4.1.1) further experiments were needed (see 4.4.3.3.1).

In consideration of the decrease of the mutant protein with increasing age (see 4.3), E14.5, an embryonic stage at which the mutant protein was still present at a comparable level to wt-Cofilin1 was chosen, in order to ensure that the observed phenotype was dependent on the mutated protein and not the reduced protein levels (Figure 28).

All following experiments were all carried out on Mefs derived from E14.5 embryos unless otherwise noted.

To further characterize the increase in cell size and multinuclearity, wt and mutant Mefs derived from two different embryos (n=2), were examined for statistical analysis (Figure 30). Emphasis was put on cell size, number and size of nuclei.

300 Mefs for each genotype and passage were analyzed. The acquired data for each question (cell size, number of nuclei and nuclear size) was derived from the same 300 Mefs for each time point of analyses. Due to the observed morphological changes of the cells during culture, Mefs from passage 1 and 3 were chosen for analysis.

Closer analysis of cell size, by point to point measurement determining the diameter, showed significant differences for wildtype and mutant Mefs in passage 1(Figure 30, left) and passage 3 (Figure 30, right) (Figure 30; A+B). For examination Mefs were assigned to different groups according to diameter size range 0-60 µm; 61-100 µm; 101- 200 µm; 201-450 µm and 450 µm<.

In passage 1 the analysis revealed highly significant difference for the first 4 groups of size range. Four fold increased number of wt Mefs could be found in the group 0-60 µm compared mt Mefs. In the group of 61-100 µm number of wt Mefs was increased

by 1.7-fold compared to mutant Mefs. In the size range groups 101- 200 µm (increased by 1.5-fold in the mt) and 201-450 µm (increased by 10-fold in the mt), the number of mutant Mefs exceed the number of wildtype Mefs in the respective group. The same size ranges were analyzed for passage 3 (Figure 30, B).

A shift towards increasing cell sizes could be observed for both genotypes, though the differences in cell size became even more pronounced in passage 3. Only 0.82% of the mt Mefs were smaller than 101 µm at this point. In the wt 24-times more Mefs were met the criteria of this group. Whereas the majority of the wt Mefs could be found in the group of 101-200 µm (67.96%), the majority of the mt Mefs was found in the group of 201-450 µm (73.66%). Mutant Mefs bigger than 450µm could be observed (5.35%), while no wt Mefs fulfilling this criteria were found. In general in can be said, that mutant Mefs were significantly bigger.

Next, multinuclearity (Figure 30, C+D) and nuclear size (Figure 30, E+F) were analyzed. In passage 1 a significantly higher number of mt Mefs comprising two nuclei (29.33%) could be found compared to wt Mefs (Figure 30, C). Whereas in P3 the number of mt cells with three nuclei was significantly increased compared to wt cells, (4.94% (mt) vs. 0.35% (wt)), an increase of 11-fold (Figure 30, D).

Also significant differences in nuclear size could be observed for wt and mt Mefs in passage 1 and 3 (Figure 30, E+F). For analysis nuclei were sub-classified into groups according to size range 5-20 µm; 21-35 µm; 36- 50 µm; 51-65 µm and 66 µm<.

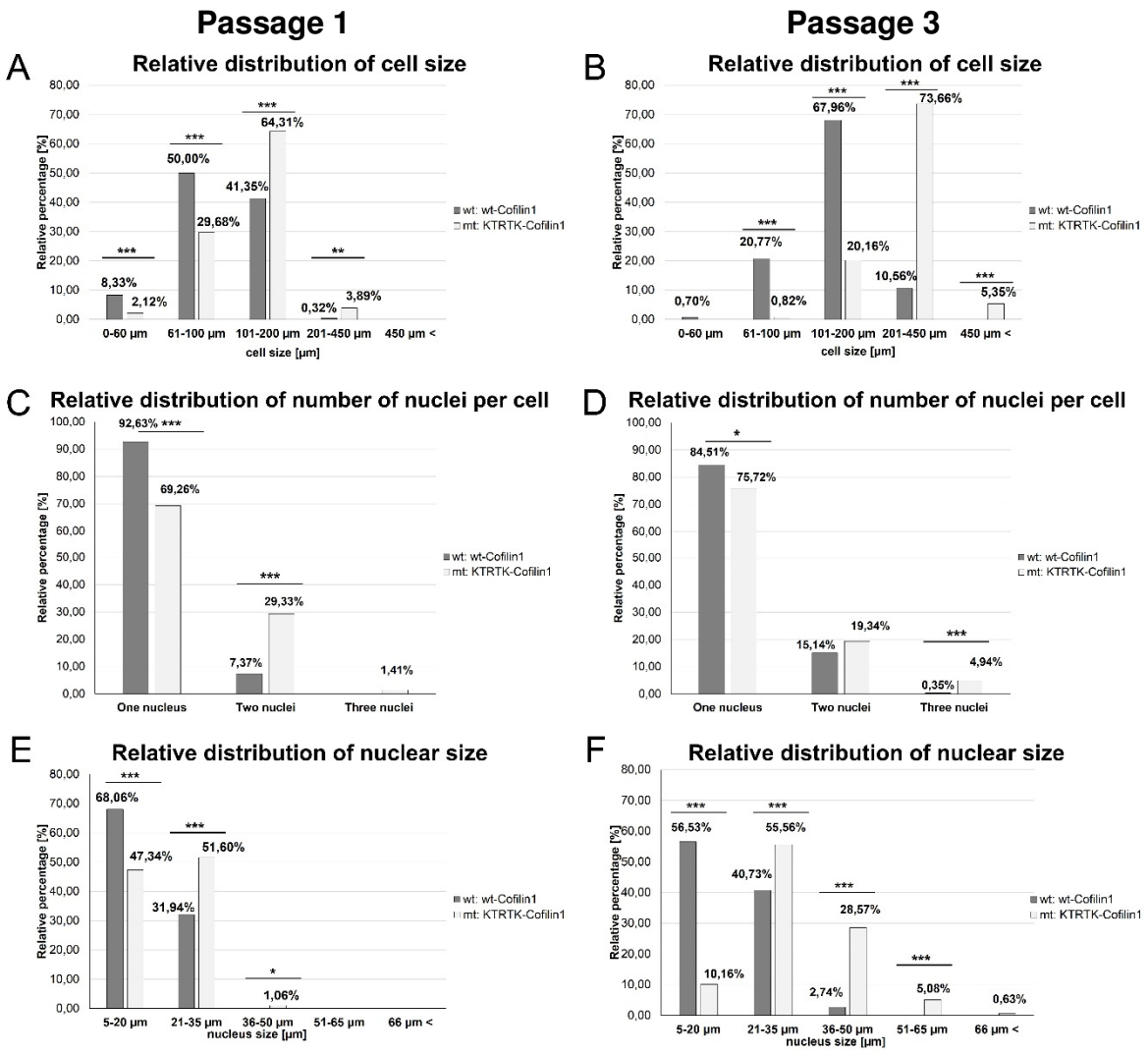

Fig. 30: Statistical morphological analyses of passage 1 (left) and passage 3 (right) of E14.5 Mefs. Relative percentages were calculated based on the total number of cells counted for each genotype and passage (n=300). **(A+B) Cell size:** significant differences could be observed for wt and mt Mefs in passage 1 and 3. **(C+D) Multinuclearity:** in passage 1 significantly more mt Mefs had two nuclei, whereas in passage 3 the number of mt Mefs with three nuclei was significantly increased compared to wt cells. **(E+F) size of nuclei:** nuclear size was examined (approx. n=400). Significant differences in nuclear size could be observed for wt and mt cells in P1 and P3. Generally, KTRTK-Cofilin1 Mefs had bigger nuclei. A difference that was even more pronounced in P3. Note: increased number of analyzed nuclei was a consequence to multinuclearity. Wt: Cofilin1$^{wt/wt}$; mt: Cofilin1$^{KTRTK/KTRTK}$; Levels of significance: 0.05 >p≥ 0.01 (*); 0.01>p≥0.001 (**); p>0.001 (***)

Measurement was performed by point to point measurement determining the diameter of the nuclei. Note, the total number of nuclei varied between wt and mt since a higher percentage of the mt Mefs (n=300) was multinuclear, consequently increasing the number of nuclei in the mutant. All nuclei of the 300 analyzed Mefs, for each point of time, were included in the analysis. Respective percentages were calculated, based on the total number of nuclei counted for each genotype and passage (approx. n=400). In passage 1, 68.06% of the nuclei in the wt could be assigned to the group of 5-20 µm, whereas only 1.4-times less of the mutant nuclei were classified in this size range. Significantly more nuclei of mt Mefs were found in the range of 21-35µm (51.6%), compared to nuclei of wt Mefs (31.94%) (Figure 30, E).

A shift towards increasing nuclear sizes could be observed for both genotypes, when the same groups were for analyzed for passage 3 (Figure 30, F). At this point only 5-times less of the nuclei of mt Mefs could be classified in the group of 5-20 µm, in comparison to the wt nuclei. Significantly more nuclei of mutant cells met the criteria for a size range of 21-65 µm. 43% of the wt nuclei were bigger ≥35 µm, whereas 90% of the mt nuclei were bigger than 35 µm.
Analysis showed the possible cell size did not correlate to nuclear number or nuclear size.

The observed differences in nuclear size became even more pronounced in passage 3. In summary, KTRTK-Cofilin1 Mefs had significantly bigger nuclei.

The above described morphological differences of increased cell size and multinuclearity could be observed in all prepared Mefs, regardless of developmental stages of isolation.

4.4.2.2 Cofilin1$^{KTRTK/KTRTK}$ Mefs displayed a cytokinesis defects

Several previous studies suggested a role for Cofilin1 in the cell cycle. Alteration of Cofilin1 activity resulted in the formation of multinuclear cells, probably resulting from defects in cytokinesis (Gohla et al., 2005).

The differences in growth rate and the high frequency of multinuclear cells suggested cytokinesis disturbances in Cofilin1$^{KTRTK/KTRTK}$ Mefs. In order to quantify and analyze possible changes in growth kinetics, propidium iodide stainings were conducted and analyzed via flow cytometry.

Propidium iodide (PI), a fluorescent dye, binds DNA and RNA stoichiometrically. To avoid a RNA signal, cells were additionally treated with RNaseA. PI stainings provide information regarding the cell cycle phases of the analyzed cells. The cell cycle leads to the duplication of the DNA content and division of a cell with the intent to produce a daughter cell, which is an identical copy of the original cell. The cell cycle consists of four phases: G1-phase, S-phase, G2-phase and the M-phase. In the G1-phase (first gap phase) the cell grows in mass. Following the S-phase (synthetic phase), in which the centrosome duplication starts and chromosome duplication takes place, comes the G2-phase (second gap phase). Here cells check for completion of DNA replication and damaged DNA. In the last phase of the cell cycle the chromosomes condense and the duplicated pairs are separated in preparation of the cytokinesis (Pollard and Earnshaw, 2008).

Along with cell cycle analysis, cell were also analyzed for size and granularity using forward scatter (FSC) and sideward scatter (SSC) in flow cytometry.

PI was detected by FL2 channel, after excitation at 488 nm. The forward vs. sideward scatter plot, provided a graphical representation of the size and complexity distribution within the analyzed cell population. Smaller cells appear to the lower end of the axis and larger cells towards the upper end in the forward scatter (FSC). Conclusions concerning the granularity and complexity within a cell are provided by the sideward scatter (SSC). The higher the granularity of the cell the higher it appeared on the end of the axis it appears in the plot. Each cell is represented by a dot.

For this experiment four passages of wt and mt Mefs derived from E14.5 embryos were analyzed. Figure 31 shows reanalyzed data from the diploma thesis (Roy, 2011).

A total number of 10.000 cells was acquired for each sample. First step, was the selection of the live cells based on distribution in forward vs. sideward scatter plot (Figure 31, A1 – A4, “live cells”; representative data for passage 1 and 3 shown). This process is also called “gating”. Gate was set to exclude debris (lower, left corner).

For the next step the area of fluorescence channel 2 (FL2-A) was depicted versus the height of fluorescence channel 2 (FL2-H) and cells within the gate “live cells” were factored in (data not shown). These plots provide information on whether cells are present as single ones or aggregates of multiple cells.
In consideration of the phenotype of the Cofilin1$^{KTRTK/KTRTK}$ Mefs and results from the diploma thesis it could be deduced that the cells localized towards the upper end of the axis represent the multinucleate cells (data not shown). Therefore, in this analysis this cell population of interest was included in the analysis (data not shown; gate: P). The number of cells that lie within the gates “live cells” and “P” are shown in the last plots (Figure 31; plots B1-B4). The first peak represents the G1-phase (G: gap) of the cell cycle, a phase in which RNA-synthesis and protein synthesis take place at a high level immediately after mitosis. In this phase no DNA synthesis occurs. The DNA content of diploid cells is 2n. The area between the first and second peaks represents the S-phase (S: synthesis of DNA). RNA and protein synthesis are very low during S-phase. In this cell cycle phase DNA synthesis occurs, the DNA content of a cell is doubled to 4n indicative for an increasing fluorescence until it reaches the second G2/M (M: mitosis) peak which has twice the fluorescence level of the G1 peak. The G2-phase lasts until the cell enters mitosis. In the G2-phase protein- and RNA-synthesis is up-regulated again, mainly for proteins required during mitosis. The amount of DNA remains at the level of the G2/M-phase (4n) until the cell finishes mitosis (Munk, 2000). Polyploidy is a state of multiple sets of chromosomes beyond the basic set, it occurs in consequence to abnormal cell division and would result in a fluorescence shift to the right. The peaks to the right of the G2/M-peak represent multinuclear cells with a DNA content of 8n and 16n, respectively (Figure 32, indicated by arrows).

In the course of the passages only slight differences in the cell cycle results could be observed for wt Mefs. A shift of 2.3% for the amount of cells in the G1-phase in comparison of passage 1 and passage 3 was seen. A more noticeable shift of the cells could be detected for the G2/M-phase where an increase of 5.8% was observed from the first to the third passage. A slight shift for the amount of multinuclear cells (Mn-peak) could be detected. Cells in culture showed a change in growth rate following the crisis after the third passage. After recovery the growth rate was noticeably slower. Also cells increased in size and multinuclear cells (Figure 30) were found more often after the third passage of wildtype Mefs. The number of viable cells remained stable in the course of the passages from 89.0% and 92.7% (passage 1 and passage 3) (Figure 31, A1+ A2).

The same analyses were carried out for the mutant Mefs. Between the passages of the Mefs isolated from Cofilin1$^{KTRTK/KTRTK}$ embryos remarkable differences in the characteristics of the cells could be observed (Figure 31, mt). The number of viable cells slightly decreased from 86.0% in the first passage to 77.2% in the third passage (Figure 31, A3+A4). Further, a change in the distribution of the cells in the FSC/SSC (Figure 31, A3+A4) could be observed. In passage 3 mutant Mefs were increasingly scattered, varying more in size and granularity than wildtype Mefs, coinciding with microscopic observations (Figure29+30).

The cell cycle results showed remarkable shifts of the percentages of mutant Mefs in the respective cell cycle phases (Figure 31, B1-B4). A decrease of 21.3% for the amount of cells in the G1-phase from of passage 1 to passage 3 could be detected, a shift approximately 9 times higher than the shift observed in the wildtype Mefs in this cell cycle phase. The second noticeable change occurred in the G2/M-phase. In the first passage the amount of Mefs in the G2/M-phase of the cell cycle in the mutant was (9.6%) and in wildtype (6.7%).

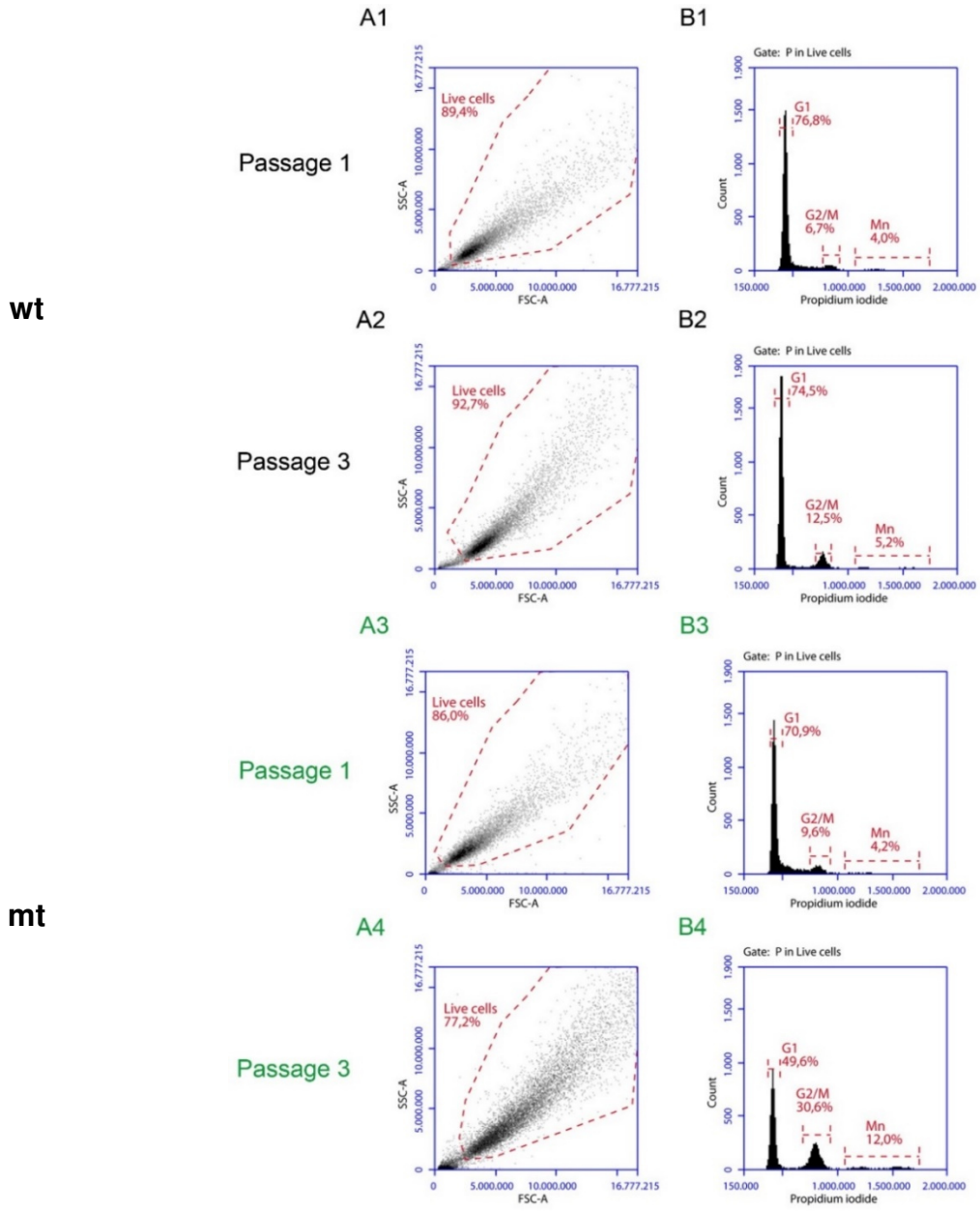

Fig. 31: Cell cycle analysis of E14.5 Cofilin1$^{wt/wt}$ (wt) and Cofilin1$^{KTRTK/KTRTK}$ (mt) Mefs. Mefs, grown on gelatin, were fixed and stained with PI for cell cycle analysis. Representative data for wt (black) and mt (green) for passage 1 and 3 is shown. A total number of 10.000 cells for each passage was measured, followed by the gating, adjusted individually according to sample, of live cells (column A). The percentage information next to the selected gates, indicates the amount of cells within the gate based on the total amount of cells measured (n=10.000). Cells were selected based on size and complexity. In the next step single and multinuclear cell were determined in gate “P” individually for each sample (data not shown) Cells chosen in gates “live cells” and “P” were further analyzed for their propidium iodide (PI) signal in FL2 (column B). The given percentage indicates the number of cells in the respective gate and the cell cycle phase, respectively.G1: G1 phase of cell cycle; G2/M: G2/M; Mn: Multinuclear cells; SSC-A: Sideward scatter- area; FSC-A: Forward scatter- area; FL2-H: Fluorescence2- height; FL2-A: Fluorescence2- area

In the third passage 30.6% of mutant Mefs were part of the G2/M-phase. A shift approximately 1.5 times higher than for wildtype Mefs. The number of cells in the G2/M phase in the mutant is increased in consequence to the reduction of the G1-phase cells. All cells together account for approximately 100%. The amount of Mn-cells increased from 2.6% in passage 1 to 12.0% in passage 3 (Figure 31, B3+B4).

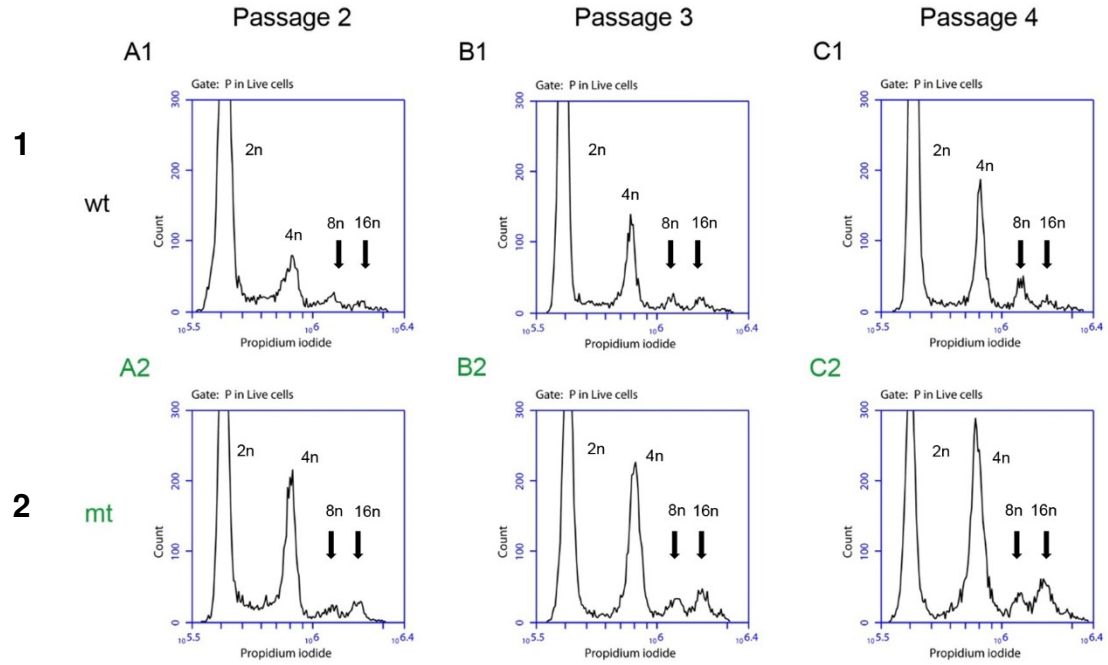

Fig. 32: DNA content analyses of E14.5 Cofilin1$^{wt/wt}$ (wt) and Cofilin1$^{KTRTK/KTRTK}$ (mt) Mefs. Shown are the alternative illustrations corresponding to column B in Figure 31, focusing on the Mn-peaks. Representation of Propidium iodide (x-axis) was changed to logarithmic presentation. Plots for passage 2 (A) and passage 3 (B) and passage 4 (C) are presented. Cofilin1$^{wt/wt}$ Mefs are presented in black while Cofilin1$^{KTRTK/KTRTK}$ Mefs are depicted in green. This optimized illustration allows closer analysis of the Mn-peaks from Figure 31; C1-C4. First two peaks represent G1- and G2/M peaks (2n and 4n). The adjacent peaks present cells with 8n and 16 DNA content, which lay within the Mn-peak in Figure 31. It could be noted that the amount of 8n and 16n positive cells, was higher in mt Mefs, especially in passage 2 and 3. 2n, 4n, 8n and 16n: DNA content of cells.

One of the morphological main characteristics of Cofilin1$^{KTRTK/KTRTK}$ Mefs lay within the multinuclearity. On account of these findings, multinuclear cells that could normally be mistaken for cell aggregates were included in the analysis.
These multinuclear cells, with increased DNA contents, were illustrated in the Mn-peaks (Figure 31, C, gate: “Mn”). For closer analysis and better illustration of the polyploidy, the representation of the PI staining (x-axis) was changed to logarithmic presentation (Figure 32). Data for passage 2 to 4 is shown.

Four peaks could be detected, representing cells with DNA content of 2n (G1- peak), 4n (G2/M- peak), 8n and 16n, respectively (Figure 32, indicated by black arrows). In this step of analysis, 8n and 16n peaks were of main interest, due to the observed multinucleate phenotype.

The peaks for 8n and 16n cells were more distinct in passage 3 and 4 (Figure 32, B + C). Though the 16n- peak was already more pronounced in the mutant (Figure 32, A2) than in the wt in passage 2. In passage 3 the difference of the 8n and 16n peaks between wt and mt was most striking. Cofilin1$^{KTRTK/KTRTK}$ Mefs in passage 3 include definitely more polyploid cells. These results confirm microscopic observations.

The cell cycle analysis experiment was repeated several times also using wt and mt Mefs which were cultivated in un-coated flasks. For those Mefs only three passages of cells were available for measurements due to loss of the lines after the third passage. The analyzed cells (data not shown) showed the same tendencies as the Mefs shown here. An accumulation of cells in the G2/M-phase peak and Mn-peak (multinuclear cell) with increasing number of passages which was more pronounced in mt Mefs. The same results could also be observed in Mefs derived from E16.5 embryos.

These data indicate that KTRTK-Cofilin1, which carries a mutation in the NTS, does affect the cytokinesis of mouse embryonic fibroblasts (Mefs). In coincidence with our data, cytokinesis defects in the form of multinuclearity after alterations of Cofilin1 have been reported before (Gohla et al., 2005).

The cytokinesis defect indicated proliferation problems. In the next chapter proliferation rates of Cofilin1$^{wt/wt}$ and Cofilin1$^{KTRTK/KTRTK}$ E14.5 Mefs were studied.

4.4.2.3 KTRTK-Cofilin1 Mefs displayed lower proliferation rates

Cell proliferation is a complicated process, involving cell growth followed by cell division to produce daughter cells. In culture the growth rate of mutant Mefs was noticed to be slower than the rate of wildtype Mefs after passage 2. In order to quantify and analyze this observation, CFDA-SE assays were performed (3.2.3.2.).

CFDA-SE (carboxyfluorescein diacetate, succinimidyl ester) provides a fairly easy method to trace cell proliferation. CFDA-SE enters cell by diffusion. Acetate groups cleaved by intracellular esterase enzymes form an amine-reactive product, carboxyfluorescein succinimidyl ester (CFSE). This product yields detectable fluorescence and binds covalently to intracellular lysine residues and other amine sources. Labeled cells retain the dye throughout development, also passing it on to daughter cells after cell division but not to adjacent cells. An important key element in the principle of function of CFDA-SE. The concentration of the dye decreases from mother to daughter cell by approx. 50%, causing a decrease in fluorescence that can be detected via flow cytometry. CFDA-SE signal was detected in FL1 at 517 nm, after excitation at 492 nm. Each shifting peak represented a round of cell division. The area of the peak provided information regarding number of cells in the respective division cycle. Cells stained with CFDA-SE can be kept in culture for several days.

For this experiment wt and mt Mefs were grown in non-coated 6-well plates. Each sample was prepared in triplicates including untreated controls. After settling of the cells over night, samples were labeled with 1µM CFDA-SE. Following a recovery period preparation for measurement was started beginning with the starting sample labeled “0h” representing the initial value.

In this experiment Mefs, derived from four Cofilin1$^{wt/wt}$ and four Cofilin1$^{KTRTK/KTRTK}$ E14.5 embryos, were used. Proliferation rates for passages 0 to 3 were analyzed. Representative data for wt and mt Mefs for passage 0 and passage 3 are shown. Cells directly plated in 6-well plates immediately after isolation from the embryo were defined as passage 0. Purpose of this step was to analyze possible proliferation rate alterations immediately upon isolation. A total number of 13.000 cells was measured, followed by the exclusion of dead cells and cell debris (gate: “live cells” data not shown).

The further the peak is shifted to the left, the lower the detected CFDA signal was, because fluorescence decreased in dividing cells. Therefore, in the course of the time points the CFDA fluorescence intensity was expected to shift from the right to the left. In the progress of the experiment distinct shifts of the CFDA-peak from 0h to 24h to 72h for both wt and mt could be detected (Figure 33, top panel).

To point out the shift of the CFDA-peak during the course of time in the different passages for wt and mt Mefs, Figure 33 shows histograms illustrating the overlays of CFDA-signal at 0h, 24h and 72h, respectively. In passage 0, 1 and 2 noticeable shifts of the peaks in wt and mt could be detected (Figure 33, top panel).

Following the crisis after the second passage, cells in culture showed a noticeably slower growth rate after recovery. Mefs also showed phenotypic changes regarding cell size and multinuclearity (Figure 30). In passage 3 the CFDA-peak from 0h to 24h to 72h for both wt and mt Mefs could also be detected, though shifts of CFDA signal intensity seemed less distinct than in passage 1 (Figure 33, top panel). Also CFDA peaks in the mutant were less defined in height but broader. At this point the detection of explicit peaks and shifts of CFDA signal in mt cells was difficult (Figure 33, D2). Therefore, in the next step proliferation rates of wt and mt cells from passage 0 to 3 were mathematically analyzed (Figure 33, lower panel).

It had to be taken into consideration that the starting intensity for time point 0h was not the same in each sample, due to different labeling efficiencies, therefore the shift of CFDA signal at the measured points of time had to be calculated for each sample individually, respective to the starting signal at 0h (Figure 33, lower panel).

1

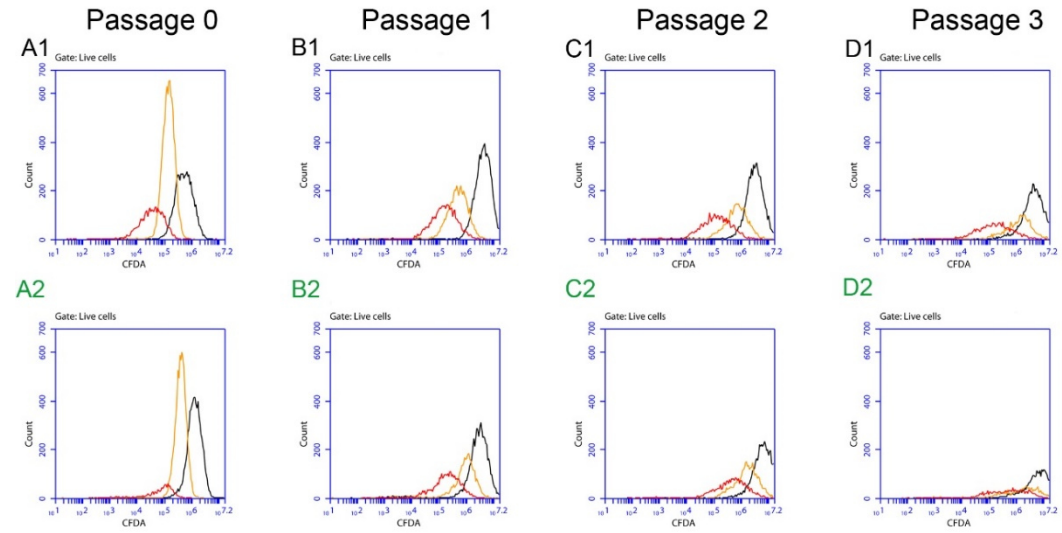

2

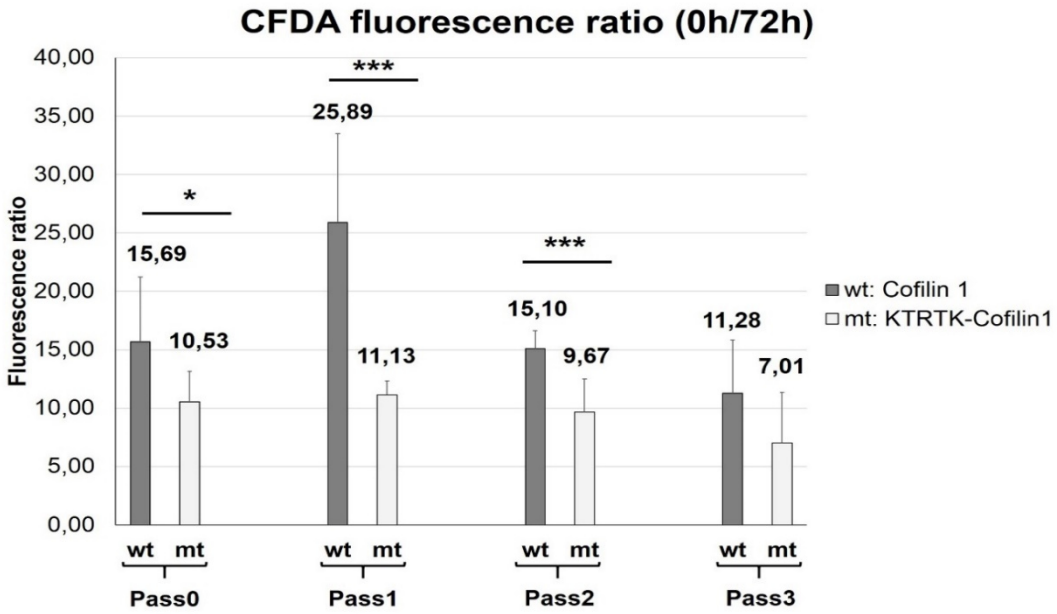

Fig. 33: 1) Overlay of cell proliferation analyses of E14.5 Cofilin1$^{wt/wt}$ (wt) and Cofilin1$^{KTRTK/KTRTK}$ (mt) Mefs. Shown are the overlays of the passages 1 to 3 for the time points 0h (black), 24h (yellow) and 72h (red). Cofilin1$^{wt/wt}$ Mefs are presented in black (top panel, A1-D1) while Cofilin1$^{KTRTK/KTRTK}$ Mefs are depicted in green (bottom panel, A2-D2). In passage 0 to 2 (A-C), distinct shifts of CFDA peaks could be observed. Shifts in passage 3 for the mt (D2) were less pronounced, while shifts in the wt were more clearly detectable (D1). **2) Statistical analysis of cell proliferation rates of E14.5 Cofilin1$^{wt/wt}$ (wt) and Cofilin1$^{KTRTK/KTRTK}$ (mt) Mefs.** Ratio of CFDA signal of 0h with 72h was calculated for each passage and triplicate samples. Medians of the CFDA peaks were used for calculations. The higher the ratio, the higher was the proliferation rate. Significant differences in proliferation rates in passage 0 to 2 could be detected. In passage 3 the proliferation rate of the wt Mefs was still 1.6 times higher than the one of the mutant Mefs. CFDA-SE: CFDA signal, Pass0: Passage 0; Pass1: Passage 1; Pass2: Passage 2; Pass3: Passage 3; wt: Cofilin1$^{wt/wt}$; mt: Cofilin1$^{KTRTK/KTRTK}$. Levels of significance: 0.05 >p≥ 0.01 (*); 0.01>p≥0.001 (**); p>0.001 (***)

It could be noted that the proliferation rate in wt cells was higher in all passages, but the difference of ratios between wt and mt changed. In passage 1 the difference was most pronounced. Wildtype Mefs divided twice as much as the mutant Mefs. In wt Mefs the proliferation rate was increased by a factor of 1.5 in passages 0, 2 and 3 compared to mutant Mefs.

These results confirmed the observations regarding differences in cell growth and proliferation in Cofilin1$^{wt/wt}$ and Cofilin1$^{KTRTK/KTRTK}$ Mefs.
The data indicates that the protein KTRTK-Cofilin1, does affect the cell proliferation rates of mouse embryonic fibroblasts. Proliferation depends on cell growth and cell division, two factors that were also shown to be altered in Cofilin1$^{KTRTK/KTRTK}$ Mefs (Figure 30 and Figure 31).

4.4.2.4 An earlier and increased occurrence of senescence was observed in Cofilin1$^{KTRTK/KTRTK}$ Mefs

Senescent cells have a large, flat morphology accompanied by profound growth defects, a characteristic clearly featured in mutant Mefs (Figure 29 -31). To determine whether the loss of mutant Mefs, after a definite number of passages, was caused by cellular senescence this assays was performed. An irreversible growth arrest and certain altered functions are characteristic for cellular senescence. *In vitro*, senescent cells can be identified by their inability to undergo DNA synthesis, a feature also quiescent cells share. Senescent and quiescent cells share important characteristics, making it hard to distinguish them. Both are viable and metabolically active, but do not undergo mitosis and cytokinesis. Quiescence is defined as a state in which cells are dormant but can re-enter cell cycle. This assay could distinguished senescent from quiescent cells, relying on the activity of senescence-associated beta-galactosidase (SA-β-gal), which can only be found in senescent cells. The presence of SA-β-gal is independent from DNA synthesis. To this day, origin and function of the enzyme in senescent cells remains unknown. Unlike average beta-galactosidase, SA-β-gal can only be detected at a pH range between 6.0- 4.0 with a

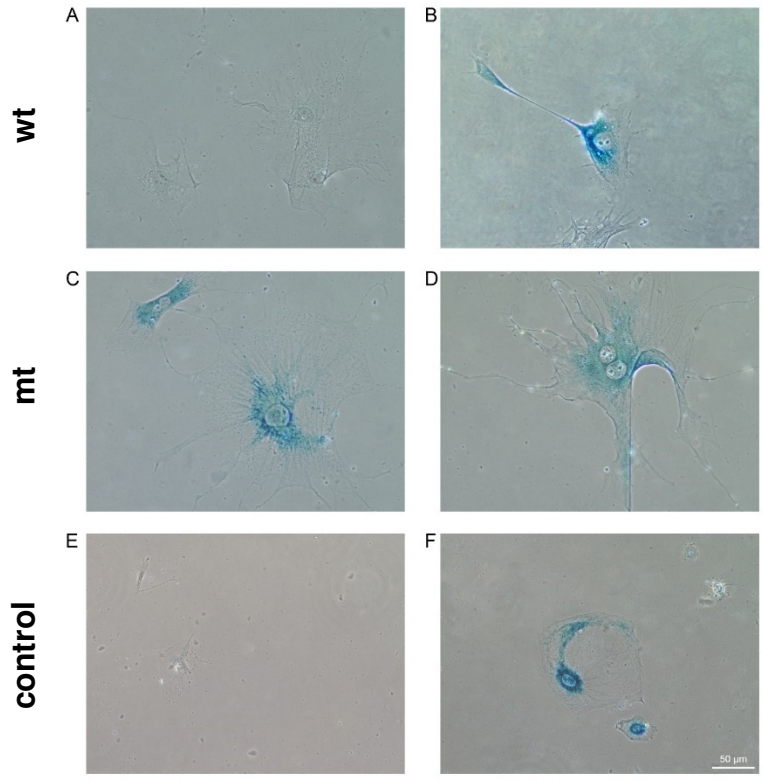

Fig. 34: Senescence-associated beta-galactosidase (SA-β-gal) staining of E14.5 wt and mt Mefs (passage 4). SA-β-gal positive cells stained blue. Wt (A+B) and KTRTK-Cofilin1 (C+D) Mefs were stained. An increased number of mutant cells were senescent in passage 4 compared to wildtype. As controls, wt cells from passage 1 were used. Doxorubicin treated cells presented the pos. control (F), whereas untreated cells served as neg. control (E). Wt: Cofilin1$^{wt/wt}$; mt: Cofilin1$^{KTRTK/KTRTK}$

X-Gal staining solution (3.2.2.1.4) (Dimri et al., 1995; Itahana et al., 2007). Different passages of Cofilin1$^{wt/wt}$ and Cofilin1$^{KTRTK/KTRTK}$ Mefs, grown in gelatin-coated flasks, were seeded on coverslips and stained.

Cells positive for senescence-associated beta-galactosidase (SA-β-gal) were detected by a perinuclear blue stain after the crisis (Figure 34). In order to verify the specificity of the assay, passage 1 wt cells were used as controls. In order to attain a positive control, cells from passage 1 were treated with 300 ng/ml doxorubicin for 20h, a chemical compound that was shown to induce senescence *in vitro*. Only doxorubicin treated wt cells from passage 1 stained positive (Figure 34, F), confirming the specificity of the assay. Wt and mutant Mefs in passage 1 did not stain positive for SA-β-gal (data not shown).

Passage 4 was of main interest, since at this point KTRTK-Cofilin1 Mefs grown on gelatin-coated surfaces were usually lost. Wildtype as well as mutant cells were positive for SA-β-gal at this point (Figure 34, A-D), more mt than wt cells appeared to be senescent. In order to determine whether there was an actual difference in SA-β-gal positive cells, a total number of 180 cells (n= 180) for wt and mt each were analyzed. In passage 4 (Figure 35), 32.98% of Mefs derived from Cofilin1$^{wt/wt}$ embryos were senescent compared to 53.44% of Cofilin1$^{KTRTK/KTRTK}$ Mefs. This highly significant difference also coincides with the observations made *in vitro*, the failure to recover after crisis and massive distinctions in cell size and multinuclearity. It was of interest if KTRTK-Cofilin1 also lead to senescence *in vivo*. Whole body cryo sections of E19.5 Cofilin1$^{wt/wt}$ and Cofilin1$^{KTRTK/KTRTK}$ embryos were prepared

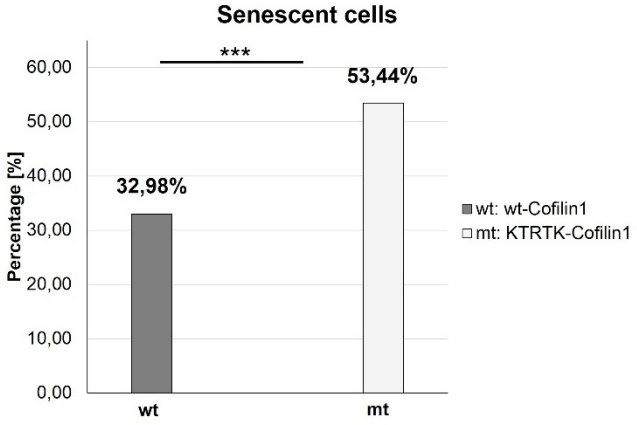

Fig. 35: Analysis of senescence positive E14.5 wt and mt Mefs in relative numbers (passage 4). A total number of 180 cells was analyzed for each genotype. Significantly more mt Mefs were SA-β-gal positive in passage 3 compared to wt Mefs at this stage. The number of senescent cells was increased by 1.6- fold compared to wt. Wt: Cofilin1$^{wt/wt}$; mt: Cofilin1$^{KTRTK/KTRTK}$; Levels of significance: 0.05 >p≥ 0.01 (*); 0.01>p≥0.001 (**); p>0.001 (***)

and stained for senescence-associated beta-galactosidase. No senescent tissue was detected in either wt or mt bodies or brains (data not shown).

4.4.3 KTRTK-Cofilin1 affected G-and F-actin levels differently *in vivo* and *in vitro*

IF imaging did not allow quantification of F-actin in Mefs. Biochemical analysis of KTRTK-Cofilin1 showed reduced depolymerizing and F-actin binding capacity of mutant protein compared to wildtype (Figure 18+19). Therefore, the levels of G-Actin and F-actin in cultured Mefs and in brain tissue were of interest.

4.4.3.1 KTRTK-Cofilin1 Mefs expressed increased levels of F-actin

Stainings of Cofilin1$^{KTRTK/KTRTK}$ Mefs showed massively increased size of cells (Figure 29). Based on the intensity of the fluorescence signal it was difficult to determine whether Cofilin1$^{KTRTK/KTRTK}$ cells comprised more F-actin than wt cells of the same size. Further, actin assays showed reduced depolymerizing activity for KTRTK-Cofilin1 *in vitro* (4.1.1), raising the question, whether the same characteristics would be observed in cells and in consequence increasing the F-actin levels.
For further analysis, F-actin levels for cells of an equivalent cell size range were analyzed using flow cytometry. A simple method to analyze the levels of F-actin, since Phalloidin exclusively binds to F-actin (3.2.3.3).

Furthermore, a G-actin/F-actin ratio was determined by G/F-actin fractionation. This simple method allows a separation of G-actin in a supernatant fraction from F-actin in a pellet fraction.For this experiment three Cofilin1$^{wt/wt}$ and Cofilin1$^{KTRTK/KTRTK}$ Mefs from passage 3 derived from E14.5 were used.

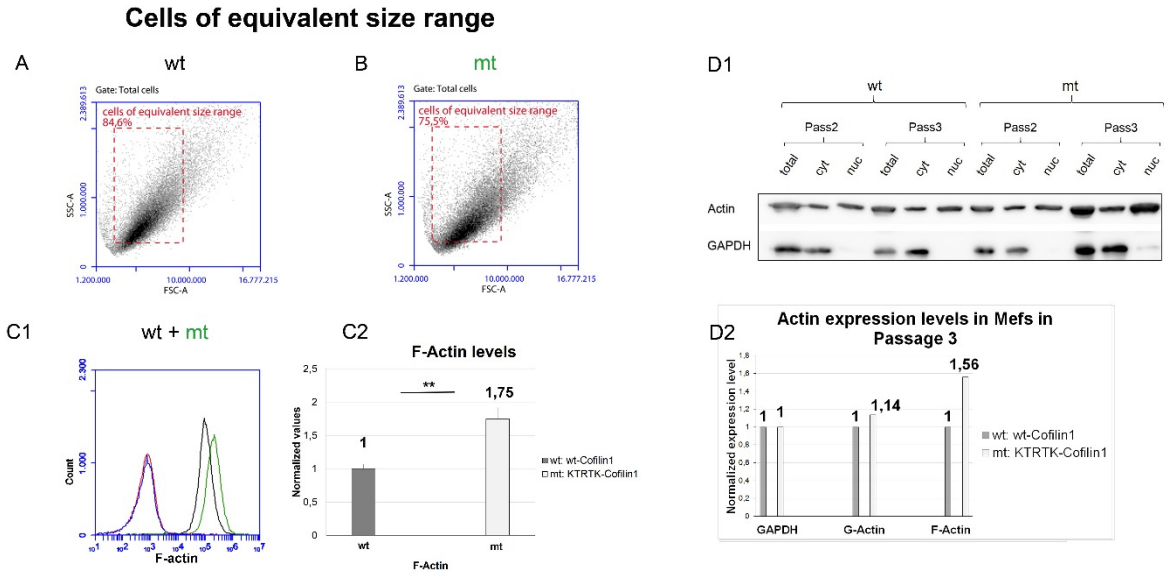

Fig. 36: Analysis of G-actin/F-actin expression levels in E14.5 Cofilin1$^{KTRTK/KTRTK}$ (mt) compared to Cofilin1$^{wt/wt}$ (wt) and Mefs (passage 3). Cells were stained with Phalloidin-680 (F-actin), allowing the determination of the F-actin levels. A total number of 13.000 live cells was acquired per sample, respectively. **A+B)** Cells were depicted in forward vs. sideward scatter for wt (A) and mt (B) Mefs, respectively. Gate "cells of equivalent size range" marks cells of the cell size. G-actin and F-actin levels were determined for cells within the gate. **C1)** Overlay of F-actin signal for wt and mt cells. Cofilin1$^{wt/wt}$ Mefs are presented in black while Cofilin1$^{KTRTK/KTRTK}$ Mefs are depicted in green. Unstained wt cells are illustrated in red, whereas the mt counterpart is presented in blue. Auto-fluorescence signal intensity of unstained wt and mt Mefs were almost identical. A distinct shift of F-actin signal in the mt Mefs (green), compared to wt Mefs could be detected, indicating a higher amount of F-actin in mt Mefs at the same size. **C2)** Normalized quantification of F-actin in cells of the equivalent size range. F-actin signals of wt Mefs was normalized to value 1. Values for mt Mefs were calculated according to wt values. It can be noted that analyzing the same size wt and mt Mefs, Cofilin1$^{KTRTK/KTRTK}$ Mefs comprised significantly more F-actin. The amount of F-actin was increased by 1.75-fold in the mt compared to wt. **D1)** G- (supernatant) and F-actin (pellet) fractions of wt and mt of E14.5 Mefs at passage 2+3 were prepared. Actin (C4) could be detected in all fractions. Western Blot was incubated with anti-GAPDH to verify equal loading and exclude soluble contamination of the F-actin fraction. 5µg for the supernatant lysates were loaded with equivalent volumes of the pellet lysates. **D2)** For densitometric analysis G-and F-actin the wt was normalized to 1. Mt values were calculated in reference to the wildtype for passage 3. Mt Mefs showed increased levels by 1.56-fold of F-actin compared wt. Levels of G-actin were only slightly increased by 1.14-fold in mt Mefs in reference to wt Mefs. G-Actin: G-actin signal; F-Actin: F-actin signal; FSC-A: forward scatter- area; Wt: Cofilin1$^{wt/wt}$; mt: Cofilin1$^{KTRTK/KTRTK}$; Levels of significance: 0.05 >p≥ 0.01 (*); 0.01>p≥0.001 (**); p>0.001 (***)

A total number of 13.000 live cells were acquired and analyzed for F-actin levels.
In Figure 36, the F-actin (C1+2) content of the selected cells is illustrated (A+B). The further the peaks are shifted to the right, the higher the detected fluorescence signals for F-actin were, respectively. In both plots also unstained wt (red) and mt (blue) are depicted, to detect the auto-fluorescence of Cofilin1$^{wt/wt}$ and Cofilin1$^{KTRTK/KTRTK}$ Mefs which was almost identical for wildtype and mutant in F-actin analyses.

Considering the decreased depolymerizing activity of KTRTK-Cofilin1 that was observed in actin *in vitro* assays (Figure 18), the question whether mutant Mefs of the same size also comprise more F-actin compared to the wildtype had to be considered. In order to study the amount of F-actin (Figure 36; C1+2) as parameters of cell size, cells were depicted in a forward vs. sideward scatter for wildtype (Figure 36, A) and mutant Mefs (Figure 36, B), respectively. The gate “cells of equivalent size range” in Figure 36, A and B marks cells of exactly the same size The gate was chosen in a size range, in which a high density and number of cells could be found in both wildtype (84.6%) and mutant (75.5%) Mefs. In ranges of higher size range the mutant was predominant but only few wildtype Mefs could be analyzed.

In order to quantify the F-actin amount in relation to cell size, only the cells within gate “cell of equivalent size range” were taken into account in the following analysis. Therefore, F-actin fluorescence signals were determined for cells from gates “cell of equivalent size range”, respectively. Distinct shifts of the F-actin fluorescence signal (Figure 36; C1) for Cofilin1$^{KTRTK/KTRTK}$ Mefs (green) could be detected compared to wt Mefs. Medians of the respective fluorescence signal peaks were used for calculations. Values for F-actin in Cofilin1$^{wt/wt}$ Mefs was normalized (wt= 1).
Values for the Cofilin1$^{KTRTK/KTRTK}$ Mefs were calculated according to the normalized wt values, respectively (Figure 36, C2). These data clearly showed that mutant Mefs of equivalent cell size as wt Mefs contained significantly more F-actin. The amount of F-actin was increased by 1.75- old compared to wt. These results are in accordance to data acquired in actin assays, showing decreased KTRTK-Cofilin1 F-actin binding and depolymerizing activity (Figure 18+19).

In order to quantify the G-actin and F-actin levels in wt and mt Mefs, E14.5 Mefs from passages 2+3 were fractionated to determine the respective expression levels and analyzed by western blot (Figure 36, D1). This method allowed a separation of G-actin in a supernatant fraction from F-actin in a pellet fraction. For specific determination of G-/F-actin expression levels densitometric evaluation of the western blot was performed (data for passage 3 shown). Values for GAPDH in Cofilin1$^{wt/wt}$ Mefs was normalized (wt= 1). Values for the Cofilin1$^{KTRTK/KTRTK}$ Mefs were mathematically adapted to GAPDH expression level in the wildtype. G-actin and F-actin values were adapted according to GAPDH expression level and afterward normalized in reference to wildtype levels. The results illustrated a shift of G-Actin/F-actin ratio between the genotypes. Whereas the G-actin level in the wildtype and the mutant Mefs remained constant, the F-actin protein level in the mutant was increased by 56% compared to wildtype. Densitometric examination of the G-actin/F-actin ratio revealed an increased shift of the total amount of actin in mutant Mefs. Even though F-actin increased the amount of G-actin remained constant, reflecting the increase of total actin in Cofilin1 $^{KTRTK/KTRTK}$ Mefs. Analysis of passage 2 G-actin/F-actin ratios showed the same tendencies (data not shown). F-actin was increased be 1.4-fold, whereas G-actin was increased by 1.18-fold in reference to the wildtype levels, also indicating an increase of total actin in mutant Mefs. It should be considered that in passage 3 mt Mefs are bigger than in passage 2, potentially elucidating the added increase of F-actin in passage 3.
Comparable results could be observed for Mefs derived from E13.5 and E16.5 mouse embryos.

Analysis of G-/F-actin levels indicated an increase of total actin in mutant Mefs. An up-regulation of actin isoforms was also detected in microarray analysis of wt and mt Mefs (4.7).

4.4.3.2 The G-actin/F-actin ratio was reduced in KTRTK-Cofilin1 embryos compared to wildtype embryos

After an increase in F-actin and G-actin levels could be detected *in vitro*, in cells derived from Cofilin1$^{wt/wt}$ and Cofilin1$^{KTRTK/KTRTK}$ embryos, the question whether the same phenomenon occurred *in vivo* arose. The analysis of E12.5 pellet fractions showed an increase of actin in the mutant brain and body (Figure 26). This experiment determined the G-actin/F-actin ratio in E16.5 brain tissue of Cofilin1$^{wt/wt}$, Cofilin1$^{wt/KTRTK}$ and Cofilin1$^{KTRTK/KTRTK}$ embryos. An adapted separation protocol was from McRobbie and Newell (1983) and Pilo Boyl et al. (2007) was used for G/F-actin separation. This simple method allows a separation of G-actin in a supernatant fraction from F-actin in a pellet fraction (3.3.3.2).

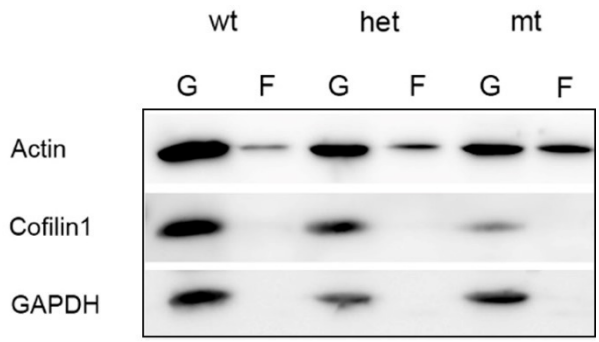

Fig. 37: G-actin/ F-actin *in vivo* separation in E16.5 brain tissue (McRobbie). G- (supernatant) and F-actin (pellet) fractions of wt, het and mt brains of E16.5 embryos were prepared according to an adapted McRobbie protocol. Actin (C4) could be detected in all fractions. Densitometric analysis showed increasing levels of F-actin from wt to het to mt. Levels of G-actin were reduced from reduced form wt to het to mt. F-actin level was increased. 3.9-fold in Cofilin1$^{KTRTK/KTRTK}$ brain compared to Cofilin1$^{wt/wt}$. Western Blot was incubated with anti-GAPDH to verify equal loading and exclude soluble contamination of the F-actin fraction. 10µg for the supernatant lysates were loaded with equivalent volumes of the pellet lysates. Wt: Cofilin1$^{wt/wt}$; het: Cofilin1$^{wt/KTRTK}$; mt: Cofilin1$^{KTRTK/KTRTK}$; G: G-actin; F: F-actin;

The separation of G- and F-actin was performed for embryonic brain isolated from E16.5 embryos. The same stage of development was also used for *in vivo* microarray analysis (4.7). The Western blot for the G-actin/F-actin separation of E16.5 brains showed differences of the amounts G- and F-actin between genotypes (Figure 37). G-actin was up-regulated in the wildtype compared to the mt. Densitometric evaluation of the western blot illustrated a shift of G-Actin/F-actin ratio between the genotypes. Whereas the G-actin level in the wildtype and the heterozygous brain remained constant, the G-actin protein level in the

mutant was decreased by 29% compared to wildtype. The F-actin on the other hand was the strongest in the mt. The weakest signal for F-actin was detected in the wildtype. This has been observed several times before (4.3). Densitometric examination of the G-actin/F-actin ratio revealed distinct shifts in the distribution of the total amount of actin. In Cofilin1$^{wt/wt}$ brain 90% of the total amount of actin consisted of G-actin, while the remaining 10% percent were presented by F-actin. The heterozygous brain displays a ratio of 77% G-actin/ 23% F-actin. The shift was even more explicit in the mutant with a ratio of 62% G-actin/ 38% F-actin. In Cofilin1$^{KTRTK/KTRTK}$ brain the portion of F-actin, in regard to the total amount of actin, was increased by 3.8 fold compared to wildtype, representing the smallest G-/F-actin ratio in comparison of Cofilin1$^{wt/wt}$, Cofilin1$^{wt/KTRTK}$ and Cofilin1$^{KTRTK/KTRTK}$ brains. A decrease of the protein level of Cofilin1 (KG60) in the het and mt compared to wildtype could be noted. The expression of ADF (7D10) and Cofilin2 (FHUI) was up-regulated in the mutant (data not shown). In Mefs F-actin levels were up-regulated in the mutant. G-actin levels remained constant. In vivo G-actin levels were decreased in mutant brain compared to wildtype. This was not necessarily surprising though. Culture behavior and metabolic requirements for Mefs differ from neural tissue. Also Mefs present a uniform cell population whereas brains consist of a variety of cell types and extracellular matrix proteins. The increase of detected F-actin in the mt conforms to *in vitro* results for Mefs (4.4.3.1). In this experiment it appears that F-actin levels increased in response to decreasing Cofilin1 levels, regardless of ADF and Cofilin2 expression. These data indicate that the influence of KTRTK-Cofilin1 may affect G-actin/F- actin levels differently *in vivo* compared to *in vitro* and may also be dependent on cell type.

4.5 Morphological studies of the Cofilin1$^{KTRTK/KTRTK}$ embryos

Cofilin1$^{KTRTK/KTRTK}$ embryos were clearly distinguishable from wildtype and heterozygous littermates due to the neural tube closure defect. Mutants were smaller than controls and showed no other obvious malformations. The expression of Cofilin1 in embryonic development is not restricted to the brain but can also be detected in somites, limb buds, the neural tube, liver and heart (Vartiainen et al., 2002; Gurniak et al., 2005).

To understand defects in brain development and to study the morphology of the exencephalic phenotype of Cofilin1$^{KTRTK/KTRTK}$ embryos, mutant and wildtype embryos at developmental stages E10 to E17.5 were prepared for histochemistry, immunohistochemistry and immunofluorescence stainings (3.4).

4.5.1 Analysis of Cofilin1$^{KTRTK/KTRTK}$ anatomy

One of the most striking features of Cofilin1$^{KTRTK/KTRTK}$ embryos is the absence of skull structures enclosing the brain. To determine whether the mutation also affected further organs, bones and cartilaginous structures, E17.5 and E16.5 embryos were isolated and studied (Figure 38-40).

4.5.1.1 The mutant protein KTRTK-Cofilin1 impacts cartilaginous tissue and bone formation

Embryonic skeletons were isolated to analyze the skeletal state. The basic concept of differential staining of cartilage and bone in mouse fetuses allows the detection of developmental malformations. Alizarin Red is used to study bone and calcium deposits, in combination with Alcian blue, which stains cartilage, this staining allows the skeletal isolation and the differential staining of cartilage and bone (3.4.2).
Skeletal isolation revealed malformation of the mutant skeleton (Figure 38). In the malformed skull (Figure 38, B), the entity of the parietal and frontal bones were missing. Examination of the side of the head (Figure 38, B+D) revealed cartilaginous tissue in the mutant, at the back of the head, that was not detected in the wildtype. Further, obvious malformations of craniofacial structures, primarily consisting of cartilage and bone, were observed in coronal sections (Figure 47). That may indicate disruptions of osteoblast differentiation, in consequence to the protein KTRTK-Cofilin1, causing malformations of the skeleton. The dorsal and ventral segments of the ribs (Figure 38, F) and the skeletal structure (ulna and radius) along with the cartilaginous segments of the front paws (Figure 38, E) showed no morphological differences. The faint cartilage staining of the mutant front paw and the control and mutant hind paws, was a consequence to the excess tissue still surrounding the paws (Figure 38, E+G). Closer examination of the hind paws revealed a missing phalanx in all claws (Figure 38, G) in the mutant combined with an upturned aberrant malformed morphology of the claws. It should be noted that the absence of a phalanx in the paw was not detected in all analyzed mutants. It has to be verified whether a missing phalanx is the result of the KTRTK-Cofilin1 mutation or a coincidence detected malformation independent of the introduced mutation. It could be speculated if the morphology of the top cervical vertebrae (C1) in the mutant was affected (Figure 38, C+D). In the mutant C1 appeared to be enlarged in comparison to the top cervical vertebrae in wildtype. Closer examination of the lumbar vertebrae (Figure 38, H), caudal vertebrae and thoracic vertebrae (data not shown) showed no morphological differences between mutant and control.

4.5.1.1.1 Skeletal differences are observed in KTRTK-Cofilin1 embryos

Fig. 38: Skeletal isolation of Cofilin1$^{wt/wt}$ (wt) and Cofilin1$^{KTRTK/KTRTK}$ (mt) embryos at E17.5. Cartilage is stained in blue, bone is stained in purple. Figure shows comparisons of wt and mt skeletal structures. (A): whole body, (B): skull (top view), (C): neck and shoulder, (D): head (side view), (E): front paws, (F): rib cage, (G): hind paws, (H): lumbar vertebrae. Striking differences in the skull (B) were observed, the parietal and frontal bones were absent. Further, missing of phalanges in claws was observed in the hind paw in combination with a malformed morphology in the mutant (G). C1: cervical vertebrae 1; Cav: caudal vertebrae; Cv: cervical vertebrae; Ds: dorsal segment of rib; Fr: frontal bone; Lv: lumbar vertebrae; Par: parietal bone; Ph: phalanges; Ra: radius; Tv: thoracic vertebrae; Ul: ulna; Vs: ventral segment of rib; wt: Cofilin1$^{wt/wt}$; mt: Cofilin1$^{KTRTK/KTRTK}$. Images were acquired at different magnifications (0.7x- 4.0x).

4.5.1.1.2 Internal structures of bones and cartilaginous tissue were not affected by the mutant protein KTRTK-Cofilin1

To study whether bone or cartilage structures were affected on an internal level, sagittal paraffin sections of E16.5 Cofilin1$^{wt/wt}$ and Cofilin1$^{KTRTK/KTRTK}$ embryos were stained with Alcian blue (cartilage) and Alizarin red (bone), respectively. The staining of bone and calcified structures of wt and mt showed no structural differences within the body (data not shown). Staining of cartilaginous tissue showed no altered accumulation within the body (Figure 39). Closer examination of the head revealed a positive staining for cartilaginous tissue in the mutant brain (Figure 39, B, black arrow). The loose tissue, which was also detected at several gestational stages, stained blue. It was also shown in E13.5 (Figure 45) that the loose, low density tissue featured cartilaginous characteristics. This loose tissue could also be detected in the wildtype and is known to be connective tissue. In the mutant embryo this tissue could be found throughout development, whereas it vanished in the wildtype embryo. The loose tissue in the mutant corresponds to the connective tissue in the control and will be analyzed in more detail in later chapters. The mutant protein KTRTK-Cofilin1 did not affect the internal structure of bones and cartilaginous tissues, but had an effect on the morphology and development of bones.

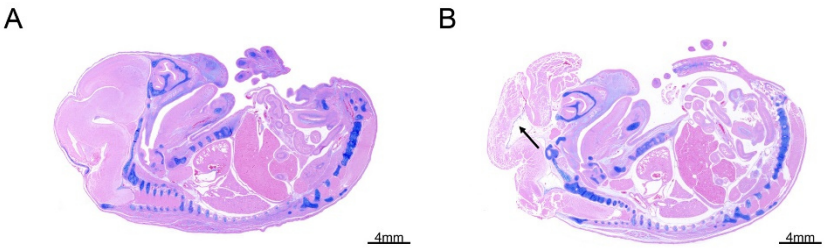

Fig. 39: Cartilaginous tissue in E16.5 Cofilin1$^{wt/wt}$ (A) and Cofilin1$^{KTRTK/KTRTK}$ (B) embryos. 10 µm sagittal whole body paraffin sections were stained with Alcian blue (cartilage, blue) and eosin (cytoplasm, pink). Staining of cartilaginous tissue showed no altered accumulation within the mutant body (B). Loose, low density tissue in the mutant featured cartilaginous characteristics (B, black arrow). Images were acquired at 1x magnification. Wt: Cofilin1$^{wt/wt}$; mt: Cofilin1$^{KTRTK/KTRTK}$.

4.5.1.1.3 Organs in Cofilin1 $^{KTRTK/KTRTK}$ embryos were not affected

To see whether the mutation of Cofilin1 had any impact on internal structures (organs, e.g.), sagittal whole body sections of Cofilin1$^{wt/wt}$ and Cofilin1$^{KTRTK/KTRTK}$ littermates at embryonic day E16.5 were stained for haematoxylin and eosin (Figure 40).
Based on peritoneal organs and jaw structures, comparable planes for wt and mt were stained. In the wt the eye (E) was easy to detect, the eye in the mt (E) was shifted in position. The morphological variation could be a result of different angles during sectioning. No further anatomical malformation could be detected in the H+E staining. No structural differences were detected in the dorsal area (1). Lung (Ln), heart (H), liver (Lv) and intestines (In) were correctly positioned and showed to conspicuous traits. In this plane the kidney was not visible in the mutant due to the angle during sectioning (B). Examination of whole body sections at different gestational stages confirmed the presence of kidneys in the Cofilin1$^{KTRTK/KTRTK}$ embryos (data not shown).

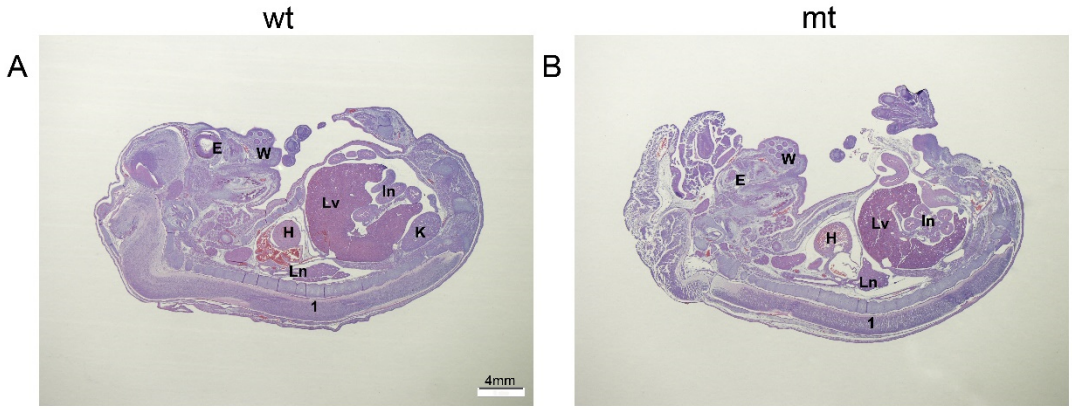

Fig. 40: Sagittal whole body sections of E16.5 Cofilin1$^{wt/wt}$ (A) and Cofilin1$^{KTRTK/KTRTK}$ (B). Paraffin sections were stained with haematoxylin and eosin. The mutant brain (B) showed significant structural differences compared to Cofilin1$^{wt/wt}$ brain. Structure of the eye (E), appeared to be different. Based on morphology and localization the remaining body was unaffected by the introduction of the KTRTK-Cofilin1 mutation. No malformations in the dorsal area (1) or other organs could be detected. E: eye; H: heart; In: intestine; Ln: lung; Lv: liver; K: kidney; W: whisker pad; wt: Cofilin1$^{wt/wt}$; mt: Cofilin1$^{KTRTK/KTRTK}$.

Staining of whole body sagittal sections revealed the restriction of morphological malformations in Cofilin1$^{KTRTK/KTRTK}$ embryos to the head.

4.5.2 Histological analysis of Cofilin1$^{KTRTK/KTRTK}$ embryonic brain

After analyzing whole mount embryos, coronal and sagittal 10 µm paraffin sections of brains were prepared and stained with a number of color dyes and antibodies to extend morphological studies and gain further information regarding the function of KTRTK-Cofilin1 during embryonic development.

4.5.2.1 Brain morphology of Cofilin1$^{KTRTK/KTRTK}$ embryos from E10.5 to E13.5

In the course of isolation of the embryos, the exencephalic phenotype could be detected as early as E10.5 (Figure 20). For more detailed analysis, coronal and sagittal paraffin sections of wt and mt at various developmental from E10.5 to E16.5 were analyzed with the help of different color stainings.
To analyze the severity of the malformations at the early stage in development, in which cranial neural tube closure in the wildtype embryo is completed, sagittal sections of eosin stained E10.5 along with E13.5 wt and mt embryos were prepared (Figure 41).

At E10.5, massive structural differences were detected in Cofilin1 $^{KTRTK/KTRTK}$ brain. No distinct structures could be identified at this stage (Figure 41, B), whereas the midbrain and hindbrain were clearly distinguishable in Cofilin1 $^{wt/wt}$ brain (Figure 41, A). The entity of the mutant brain was filled with a loose, low density tissue that was identified as connective tissue (Figure 45). Connective tissue was also detected in the wildtype, with a higher density, restricted to the cavity between the midbrain and the future prosencephalon. The entire head of the mutant was surrounded by a thick outer cell layer. Examination of E13.5 sagittal section showed similar morphological characteristics (Figure 41, C+D). In the mt the brain area was also filled up with connective tissue. The morphology of the low density tissue at E13.5 differed from the detected tissue at E10.5. The tissue stained differently and appeared to have decreased in density.

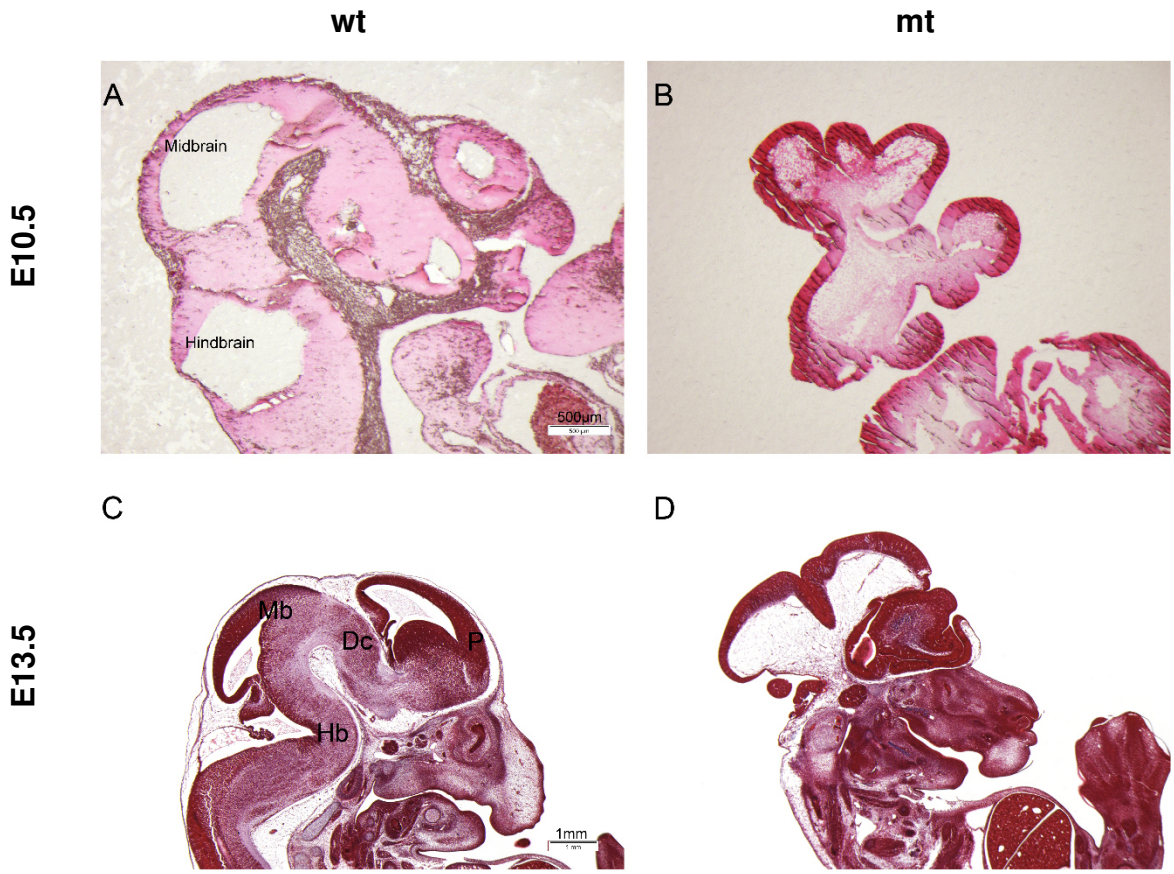

Fig. 41: Sagittal sections of E10.5 (A+B) E13.5 (C+D) Cofilin1$^{wt/wt}$ and Cofilin1$^{KTRTK/KTRTK}$ heads. 10 µm sections were cut from paraffin embedded eosin stained embryos. The mutant brain (B+D) showed severe morphological malformations. No defined structure could be detected within the brain at E10. Cofilin1$^{KTRTK/KTRTK}$, entire cavity was filled with connective tissue. At E10.5 distinct structures of the hindbrain, the midbrain and the eye could be identified in the wt. At E13.5 the mutant brain showed severe malformation of the prosencephalon (D).The hindbrain was not detectable in the mt. The prosencephalon showed severe malformations. Images were acquired at 2.5 x magnification. Dc: diencephalon; Hb: hindbrain; Mb: Midbrain; P: prosencephalon; wt: Cofilin1$^{wt/wt}$; mt: Cofilin1$^{KTRTK/KTRTK}$;

In the mutant the prosencephalon appeared to have suffered from severe malformation, whereas the hindbrain was not even detectable. The malformation of the prosencephalon may be caused in consequence to alterations of the diencephalon, which was also not clearly detectable. It appeared as if though in the mutant brain the midbrain fused to the prosencephalon and the diencephalon, the hypothalamus and part of the prosencephalon merged into one not distinguishable structure. It was mentioned before, that the severity of the phenotype differs (Figure 36), but the

morphological alterations could be observed in other embryos as well in different stages of severity and appeared to be conserved (also see Figure 42 and 45).

To extend the morphological studies of the mutant exencephalic phenotype further Cofilin1$^{wt/wt}$ and Cofilin1$^{KTRTK/KTRTK}$ littermates at E13.5 were prepared for paraffin sections and haematoxylin and eosin staining next (Figure 42).

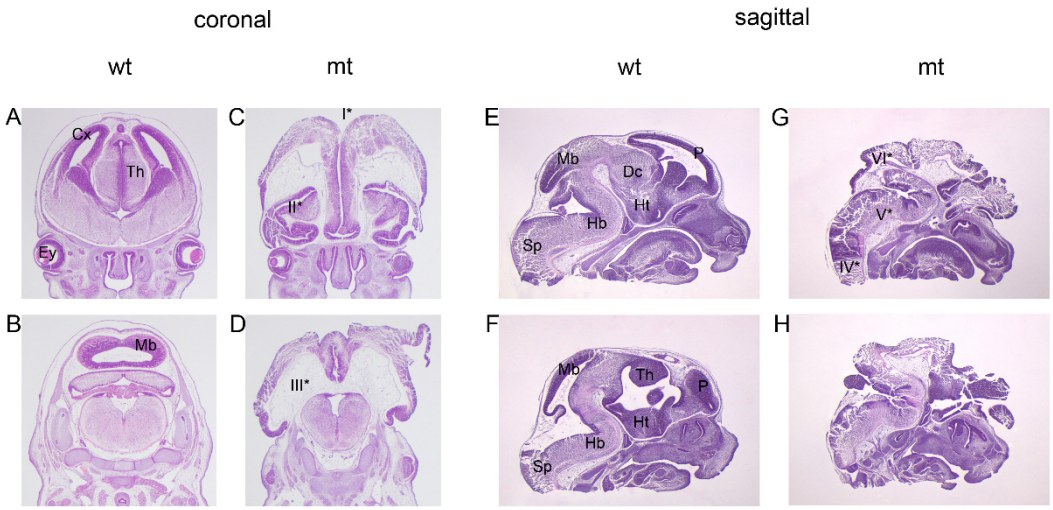

Fig.: 42: Coronal (A-D) and sagittal (E-H) sections of E13.5 Cofilin1$^{wt/wt}$ and Cofilin1$^{KTRTK/KTRTK}$ brains. 10 µm paraffin sections were stained with haematoxylin and eosin (H+E). Coronal sections showed severe malformation of the cortex and thalamus in Cofilin1$^{KTRTK/KTRTK}$ E13.5 brain (C). Distinct malformation of the prosencephalon in the mutant brain was shown in sagittal sections (G+H). I*-III*: presumptive cranial structures in the mutant brain (see text); Cx: cortex; Dc: diencephalon; Ey: eye; Hb: hindbrain; Ht: hypothalamus; Mb: midbrain; P: prosencephalon; Sp: spinal cord; Th: thalamus; wt: Cofilin1 $^{wt/wt}$; mt: Cofilin1$^{KTRTK/KTRTK}$.

Coronal and sagittal sections of chosen planes of wt brain to mutant brain were compared for morphology. Comparable sections were chosen based topographic array of oral cavities and craniofacial features. Development and morphology of E13.5 Cofilin1$^{wt/wt}$ brain took place according to literature (Schambra, 2008).

Figure 42, A-D show coronal sections of wildtype (A+B) and mutant brain (C+D). The chosen sections shift from ventral to dorsal. Here, well defined structures could be observed in the mutant brain (compare to Figure 41). Chosen structures (cortex,

thalamus and midbrain) were labeled in the wildtype for orientation and to facilitate comparison. Structures in the mutant brain were not labeled, since it was not possible to determine brain areas specifically based on the haematoxylin and eosin staining. Image C shows two spheres (indicated by I*), that fused at the top in the course of the movement towards the dorsal side. No comparable structure was detected in the wildtype, structures were fused at all times (A+C). In the mutant (Figure 42, C), folded finger-like structures (indicated by II*) on either side of the brain above the eyes were observed. These folded structures could correspond to the cortex in the wildtype regarding the layering. This structure was not detected in more dorsal sections. Inside the mutant brain the loose tissue, with a low density of nuclei, was detected (indicated by III*), filling up the internal cavity, that was identified as connective tissue.
The outer layer on top in the Cofilin1$^{KTRTK/KTRTK}$ brain, could be assumed to be thalamic tissue or a cortical structure.

Figure 42, E-H show sagittal sections of wildtype (E+F) and mutant brain (G+H) of E13.5 embryos. Well defined, distinct structures could be observed in the mutant brain (Figure 42, G+H). Structures in the mutant brain were not labeled, since it was not possible to determine brain areas specifically based on the haematoxylin and eosin staining. The connective tissue, in the mutant brain was also detected in the sagittal sections. Sagittal sections allowed easier identification of structures inside the mutant brain based on morphology. Supposed spinal cord and hindbrain (V*) could be identified in the mutant. The morphology of the spinal cord and the hindbrain appeared to have been unaffected by KTRTK-Cofilin1. Identification of midbrain (*VI) could be assumed based on localization.

Regarding the observed morphology in sagittal sections, it could be speculated that in Cofilin1$^{KTRTK/KTRTK}$ embryos, brain structures shift to the anterior. Figure 43 presents a hypothetical sagittal schematic model of area specification in the mutant brain. In this scheme the midbrain in the mutant brain is morphologically altered and repositioned (Figure 43, Mb, green). The repositioned midbrain is connected to the structure, corresponding to the diencephalon (Figure 43, Dc, orange). In the mutant, the fusion of midbrain and diencephalon, takes place without the curved manner, subsequently enlarging the ventricle, filled with connective tissue (Figure 43, pink dots). Adjacent to the diencephalon the prosencephalon would be positioned (Figure 43, P, red). The

presumed prosencephalon in the mutant appeared to be enlarged and less compartmentalized.

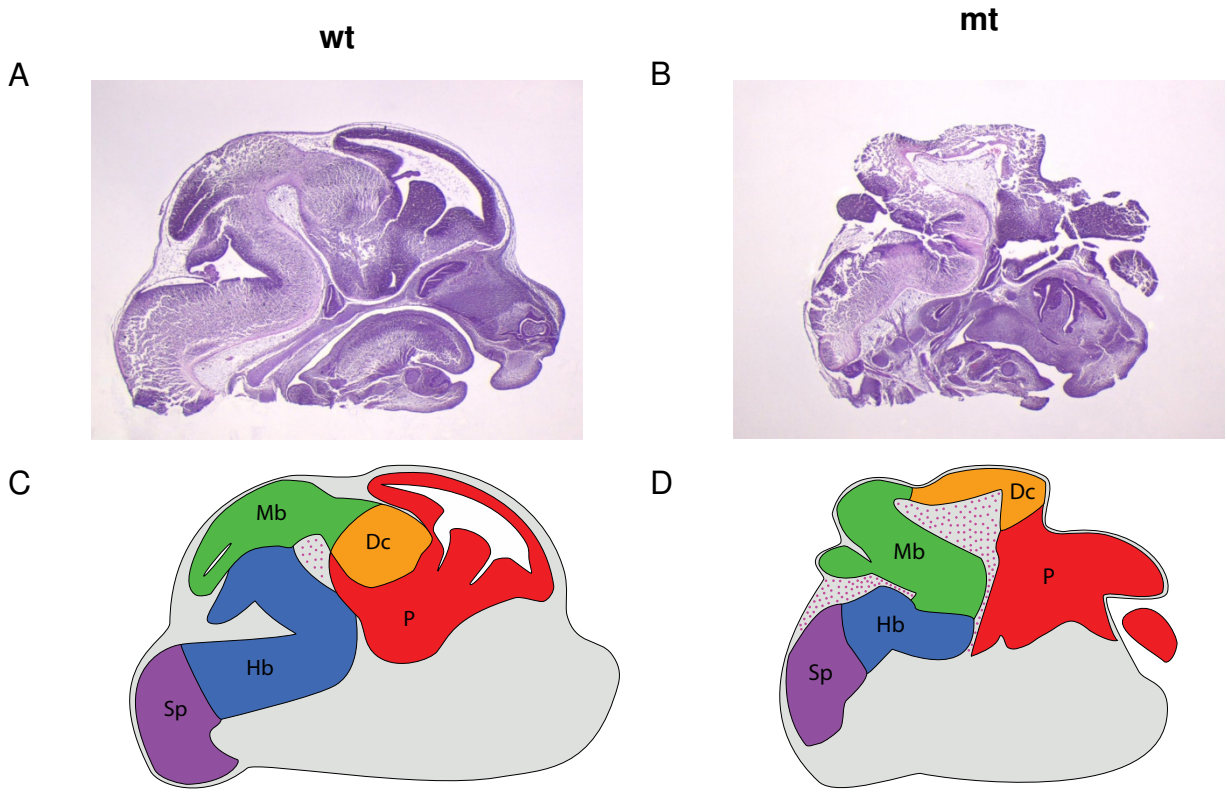

Fig. 43: Hypothetical sagittal schematic model of brain areas in Cofilin1$^{KTRTK/KTRTK}$ brain. Sagittal, haematoxylin and eosin stained sections of E13.5 Cofilin1$^{wt/wt}$ (A) and Cofilin1$^{KTRTK/KTRTK}$ (B) brains. C shows corresponding schematic sagittal model of brain areas in wildtype brain. D shows a hypothetical sagittal schematic model of brain areas in the mutant brain. In the mutant all brain areas are conserved but the prosencephalon is shifted to the anterior and less compartmentalized. Connective tissue: pink dots Dc: diencephalon; Hb: hindbrain; Mb: midbrain; P: prosencephalon; Sp: spinal cord; wt: Cofilin1$^{wt/wt}$; mt: Cofilin1$^{KTRTK/KTRTK}$.

Morphology in sagittal section indicated a preservation of the brain areas but a repositioning in consequence to a shift to the anterior of brain areas.

4.5.2.1.1 Amount of connective tissue was increased in the mutant brain

The loose tissue inside the mutant brain had been observed at several stages of development, taking a predominant role within the KTRTK-Cofilin1 brain. The next step was the identification of the tissue.

Embryos of different gestational stages were stained to identify the loose, low density tissue (Figure 44). In order to identify the tissue of interest and to gain additional information regarding its composition, a number of different color stainings were performed.

Figure 44 shows a close-up of the low density tissue in E12.5 brain. This loose appearance was characteristic for this tissue at all analyzed developmental stages. It shared morphological features of mesenchymal connective tissue, a part of embryonic connective tissue, from which bone, cartilage and muscle originate during development.

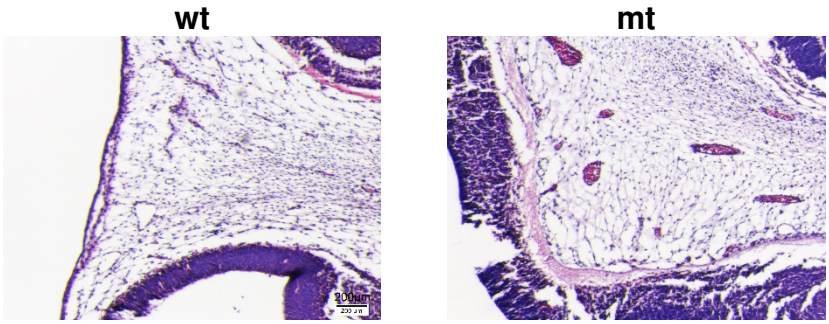

Fig. 44: Close-up of loose, low density tissue in E12.5 brains in mt and wt embryos. Coronal paraffin sections were stained for H+E. At this point in development the low density tissue was detected in both genotypes and shared same morphological features. Picture were taken at 11.5x magnification. Wt: Cofilin1$^{wt/wt}$; mt: Cofilin1$^{KTRTK/KTRTK}$;

This lead to the assumption, that the tissue in question originated from the same source, but due to alterations in regulation and brain morphology the occurrence in the mt was prolonged and increased. One of the next steps was the identification of this tissue.

Alcian blue can used be stain connective tissue that contains collagen. The staining of connective tissue is based on a different pH-dependent chemical reaction that is also independent of developmental stage. In the next step paraffin sections of Cofilin1$^{wt/wt}$ and Cofilin1$^{KTRTK/KTRTK}$ brains were stained to characterize the loose tissue (Figure 45).

Distinct blue staining could be detected in the loose, low density tissue in the wildtype as well as in the mutant (Figure 45), verifying a connective tissue character. Staining was easier to detect in areas, where the tissue showed higher density. Repeated stainings with Alcian blue of different animals at different developmental stages always revealed a positive staining of the low density tissue, which is maintained in the mutant throughout development.

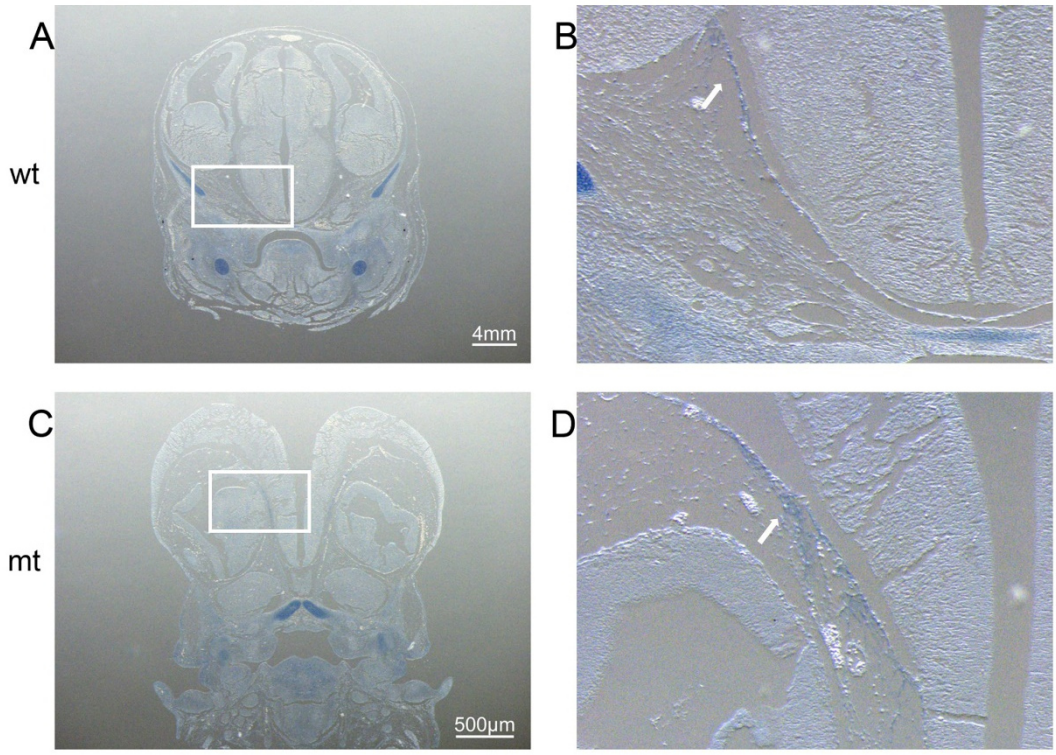

Fig. 45: Collagen staining of E13.5 Cofilin1$^{wt/wt}$ (A+B) and Cofilin1$^{KTRTK/KTRTK}$ (C+D) brains. 10 µm coronal paraffin sections were stained with Alcian blue (blue).The loose, low density tissue in mutant stained blue, indicating the connective tissue character of the tissue. Image A and C show overview images of the heads (1.25x). Images B and D show a higher magnification of the area of interest (6.3x). The connective tissue is maintained throughout the entire development in the mt but vanished in the wt. White rectangles present area of magnification. wt: Cofilin1 $^{wt/wt}$; mt: Cofilin1$^{KTRTK/KTRTK}$

The loose, low density tissue, predominant in Cofilin1$^{KTRTK/KTRTK}$ brain, could be identified as connective tissue.

4.5.2.2 Cofilin1$^{KTRTK/KTRTK}$ brains showed cortical-like layering

Nissl staining allows the visualization of cortical layering. One aim was to identify structures, such as the cortex and understanding more regarding the morphology, within Cofilin1$^{KTRTK/KTRTK}$ brains.

The laminated structure of the cerebral cortex could clearly be detected in Cofilin1$^{wt/wt}$ brains at the E16.5. Figure 46 compares coronal (A-D) and sagittal (E-H) sections of Cofilin1$^{wt/wt}$ (wt) and Cofilin1$^{KTRTK/KTRTK}$ (mt) with Cresyl violet Nissl staining at the embryonic age E16.5. In the wildtype the layers of the marginal zone (MZ), cortical plate (CP), subplate (SP), intermediate zone (IZ), subventricular zone (SVZ) and ventricular zone (VZ) were distinctly developed from outer layers toward the inside (Figure 46, B+F, indicated in red). The thick outer layer in the Cofilin1$^{KTRTK/KTRTK}$ brain (Figure 46, C), showed no explicit lamination. Close-up showed a layering within the cell accumulation in the brain (Figure 46, D). Layers within those cell knobs showed classical characteristics of cortical layering from high density to low density back to high density. This would indicate an upward and outward shift of brain structures. This would coincide with the proposed hypothetical scheme shown in Figure 49.

Layers in the mutant were not labeled, since it was not possible to determine specific layers in the structures based on morphology and localization.
Examination of sagittal sections (Figure 46, E-H), implicated a layering in the frontal folded structures of the mutant brain (Figure 46, G+H). The layering did not allow distinguishing of specific cortical layers in the mutant. The detected layers showed classical characteristics of cortical layering from high density to low density back to high density. This would indicate an anterior shift of brain structures. This would coincide with the proposed hypothetical scheme shown in Figure 43. Also, apparently layered structures were observed within the brain toward the dorsal side (Figure 46, H).

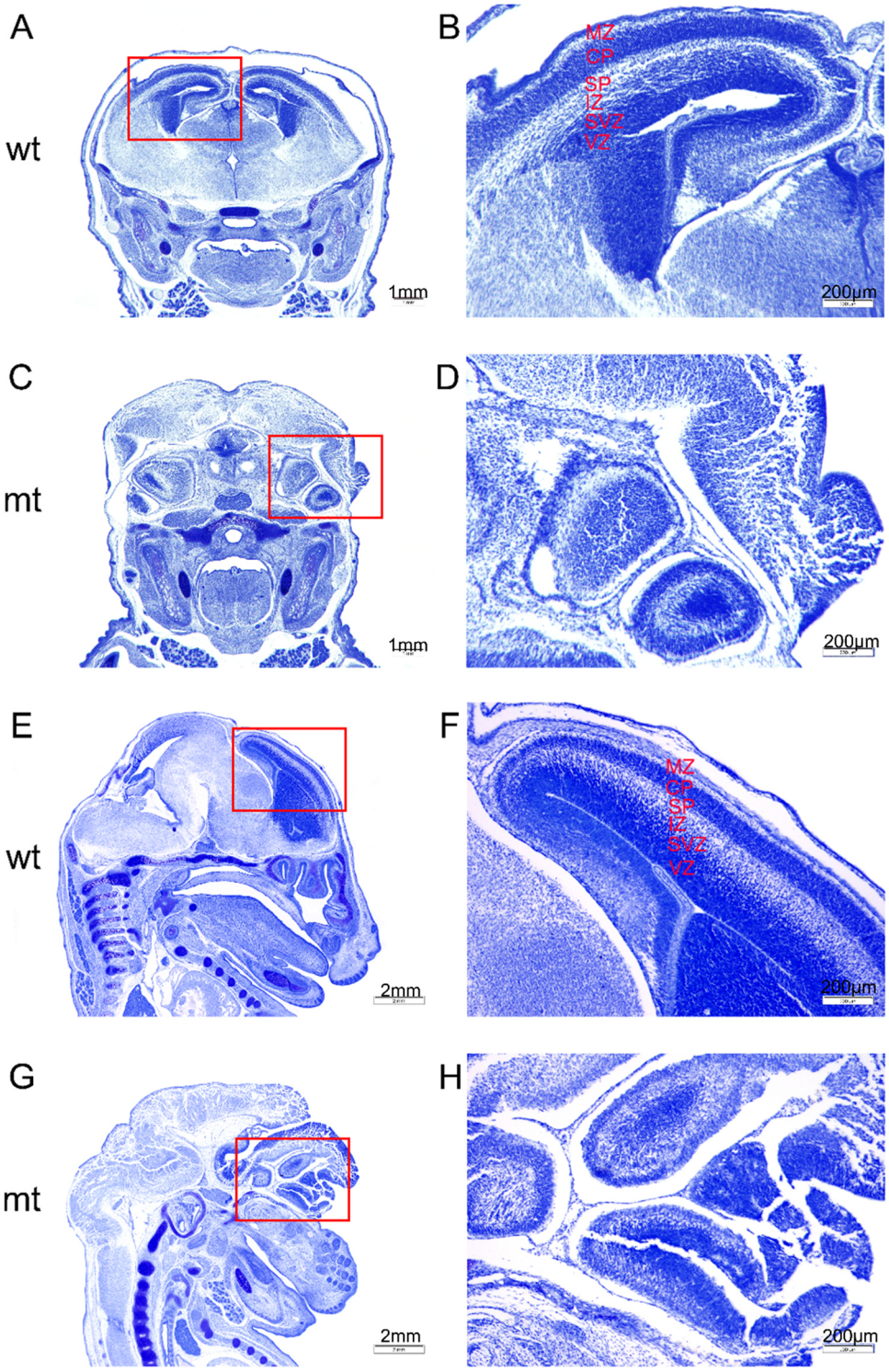

Fig. 46: Cortical layering of E16.5 Cofilin1$^{wt/wt}$ and Cofilin1$^{KTRTK/KTRTK}$ brains. 10 µm coronal (A-D) and sagittal (E-H) paraffin sections were stained with Cresyl violet Nissl dye. Wildtype brains showed distinct cortical lamination (A+E), The thick outer layer of the mutant brain (C), showed no explicit layering. Layers could be specified in structures within the mutant brain. Red rectangles present area of magnification. MZ: marginal zone CP; cortical plate SP: subplate IZ:; intermediate zone SVZ: subventricular zone VZ: ventricular zone; wt: Cofilin1 $^{wt/wt}$; mt: Cofilin1$^{KTRTK/KTRTK}$

After cortical layering could be detected in the mutant brain, it was attempted to determine where neurons were located in the KTRTK-Cofilin1 brain.

4.5.2.3 Localization of neurons in the Cofilin1$^{KTRTK/KTRTK}$ brain

NeuN (Neuronal Nuclei), a neuron-specific nuclear protein, reacts in most neuronal cell types in mice including cerebellum, cerebral cortex and thalamus. NeuN can be detected at E16.5 or later stages in embryonic development and adulthood.

To obtain more specific results, regarding localization of neurons in the brain, NeuN immunohistochemistry staining on paraffin sections of E16.5 wt and mt brains was conducted (Figure 47, bottom panel). NeuN staining in the wildtype showed distinct cortical lamination and NeuN- positive cells. Even with the NeuN staining no cortical layering was detected in the outer layer in mutant, but NeuN- positive cells were observed in the outer layer. This indicated that neurons are located in the outer layer of the mutant brain but form no distinct cortical layering (data now shown). Closer examination of folded “finger-like” structures (Figure 47, D) showed NeuN positive cell and indicated layering.

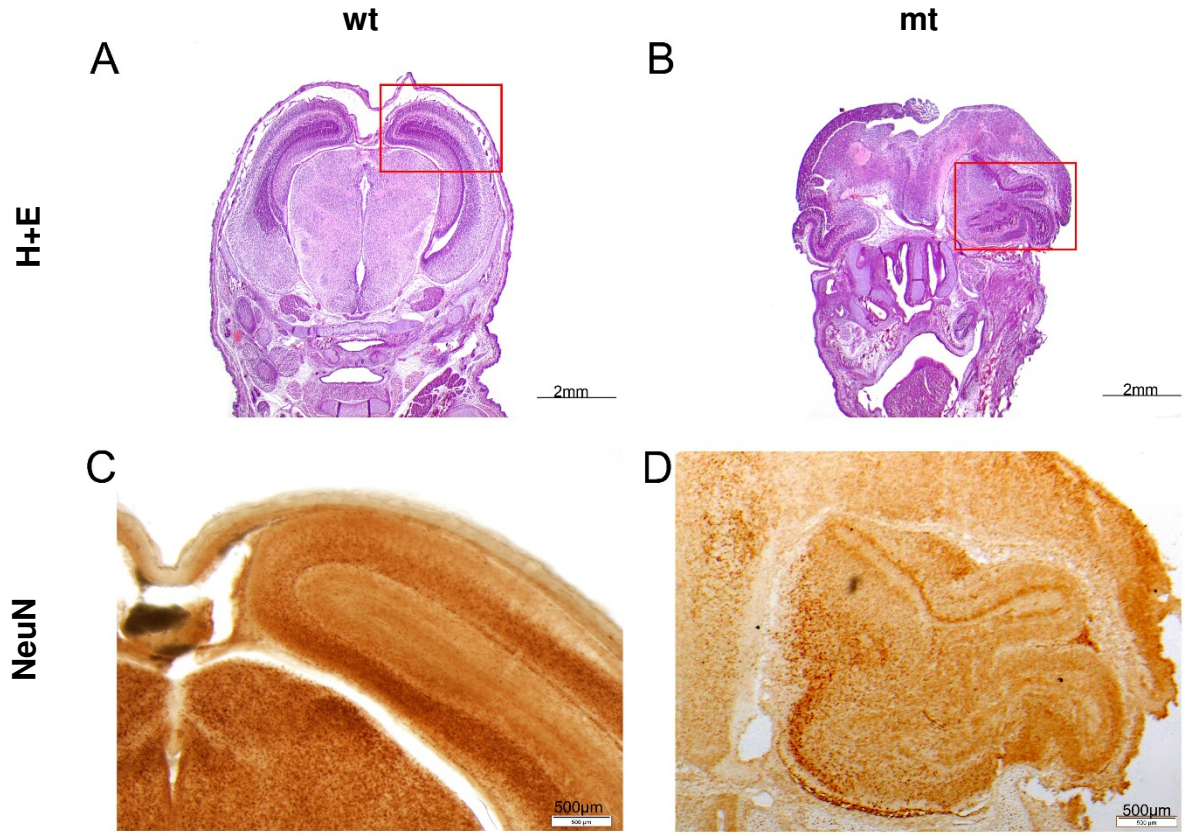

Fig 47: Neuron staining of embryonic Cofilin1$^{wt/wt}$ and Cofilin1$^{KTRTK/KTRTK}$ E16.5 brains. (B) IHC with NeuN (NeuN) on paraffin sections of E16.5 wt and mutant brains. Distinct cortical lamination was observed in the wildtype brain. No explicit cortical lamination comparable to wildtype lamination was observed in the mt. Folded “finger-like” structure suggested rudimental layering. NeuN positive cells were also detected in the outer layer of the mt brain. Red rectangles present area of magnification. wt: Cofilin1 $^{wt/wt}$; mt: Cofilin1$^{KTRTK/KTRTK}$.

These results clearly implicate that the introduction of the KTRTK- mutation massively disrupts the topographic array of the brain in Cofilin1$^{KTRTK/KTRTK}$ mutants.

4.5.2.4 Temporal and spatial expression patterns of cortical layer marker in Cofilin1$^{KTRTK/KTRTK}$ brain were affected

After an alteration of cortical layering in the Cofilin1$^{KTRTK/KTRTK}$ brain was detected, expression patterns of transcriptional regulation factors, involved in cortical layering, along with Reelin were analyzed. Cortical paraffin sections of E16.5 Cofilin1$^{wt/wt}$ and Cofilin1$^{KTRTK/KTRTK}$ brains were stained with specific antibodies for Ctip2, Cux1 and

Reelin (3.4.12.3) Panel 4 indicates the area of interest for the antibodies, respectively (Figure 48). Reelin, an extracellular matrix protein, located in the marginal zone (MZ), is involved in the regulation of neuronal migration. Mice lacking Reelin, show a disruption of cortical layering due to lack of specific positioning of neurons within cortical layers (Rice and Curran, 2001). Staining of the mutant brain revealed no Reelin layer adjacent to the outer layer of the mutant brain (Figure 48, panel 1, C+D). Further, no Reelin could be detected in the folded “finger-like” structures (data not shown). At the same age Reelin (green) was clearly detectable in the marginal zone of the cortex in the wildtype littermate (Figure 48, panel 1, A+B). In past studies, reelin was also shown to regulate migration of neurons by controlling the activity of Cofilin1 and acting as a “stop signal” (Chai et al., 2009). Cux1, drosophila cut like homeobox 1 gene, is associated with regulation of gene expression, morphogenesis and migration, and localized in the cortical plate (CP) of the developing murine cortex (Nieto et al., 2004). Cux1, was not observed in the cortical plate of the wildtype brain (Figure 48, panel 2, A+B). In the mutant brain, Cux1, was clearly detected in the top layer of the outer layer (Figure 48, panel 2, C+D). Cux1 could also be weakly detected in the folded “finger-like” structures (data not shown). This would indicate that the on-set of Cux1 expression took occurred earlier in development in Cofilin1 KTRTK/KTRTK brain. Literature regarding the on-set of Cux1 expression differs from E14.5 to E18.5. Ctip2 (Chicken ovalbumin upstream promoter transcription factor-interacting proteins 2), is expressed in the subventricular zone (SVZ) and is expressed as early as E14.5 (Arnold et al., 2008). Ctip2 positive cells could be detected in SVZ of wildtype (Figure 48, panel 3, A+B). Whereas the layering of positive cells in the wildtype was more defined (Figure 48, panel 3, A+B), the localization in the mutant was more diffuse and less cells appeared to be Ctip2- positive in the outer layer (data not shown). Ctip2 positive cells were also detected in the folded “finger-like” structures (Figure 48, panel 3, C+D). Ctip2 positive cell were arranged in a circular motive, coinciding with the circular cortical layering detected in the Nissl staining (Figure 46).

The results indicated alternated expression patterns of cortical layer markers in consequence to the introduction of KTRTK-Cofilin1.

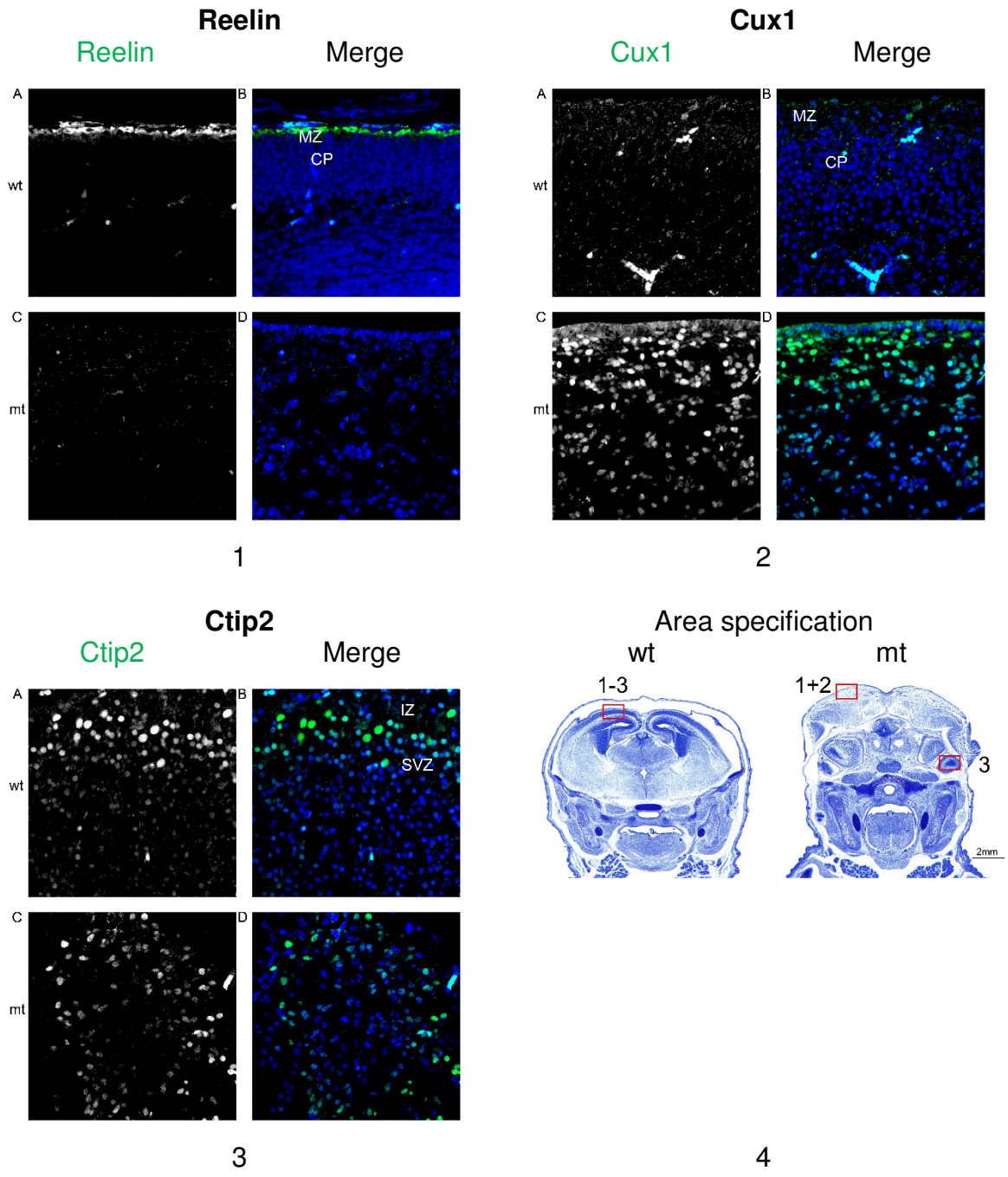

Fig. 48: Expression patterns of cortical layer marker in E16.5 Cofilin1$^{wt/wt}$ and Cofilin1$^{KTRTK/KTRTK}$ brains. 10 µm coronal paraffin sections were stained with Reelin (panel 1), Cux1 (panel 2), Ctip2 (panel 3) and Draq5 for nuclear labeling (blue). Cortical layer marker were labeled with secondary Alexa-488 antibody, respectively (green). Conspicuous changes of expression patterns of cortical layer marker were observed in the mutant brain. Panel 4: red rectangles present area of magnification in panel 1-3. MZ: marginal zone CP; cortical plate SP: subplate IZ: intermediate zone SVZ: subventricular zone; wt: Cofilin1 $^{wt/wt}$; mt: Cofilin1$^{KTRTK/KTRTK}$.

4.5.2.5 Is the Cofilin1$^{KTRTK/KTRTK}$ brain everted?

Beta-III- tubulin presents a neuron specific marker, allowing visualization of the distribution of neurons. It is known that beta-III-tubulin plays a critical role in proper axon guidance and maintenance (Roskams et al., 1998).

The expression pattern of beta-III- tubulin (bIIItub) was severely altered in the Cofilin1$^{KTRTK/KTRTK}$ (mt) brain in comparison to the wt brain (Figure 49, top panel). The mutant brain appeared to have suffered an inside-out shift. Whereas beta-III- tubulin is localized in the outer layers of the wt brain, beta-III-tubulin positive cells are mainly localized in the inner part of the mutant brain, in an everted manner.

4.5.2.5.1 Proliferative zone is increased in Cofilin1$^{KTRTK/KTRTK}$ brain

In vitro analysis of Mefs showed an alteration in proliferation caused by the introduction of KTRTK-Cofilin1. The thickened outer layer in mutant brains and increased connective tissue (Figure 42, D, III*) may also indicate an alteration in proliferation *in vivo*.

BrdU labelling allowed the *in vivo* tracking of proliferating cells after a short- impulse labeling of one hour prior to sacrificing the pregnant female (3.4.12). Proliferating cells were detected in wt and mutant (Figure. 49, middle panel).Localization of proliferating cells was slightly altered, due to structural malformations in the mutant. The area around the assumed third ventricle (Tv) is shown. Number of detected proliferative cells was higher in the mutant in this area, also proliferating cells appeared denser and less spread in the adjacent tissue. This proliferative zone, starting at the supposed ventricle, expanded over the complete outer layer.

The area of the cortex (Cx) in wildtype (Figure 49, C) and the assumed counterpart in the mutant were studied next. Morphology of the analyzed structure was completely different. This structure had been observed before (Figure 42) and was described as folded “finger-like” structures. Density of proliferating cells was high and localization appeared to be very distinct. The cortex in the wt (Figure 49, C) was also abundant of distinctly localized cells.

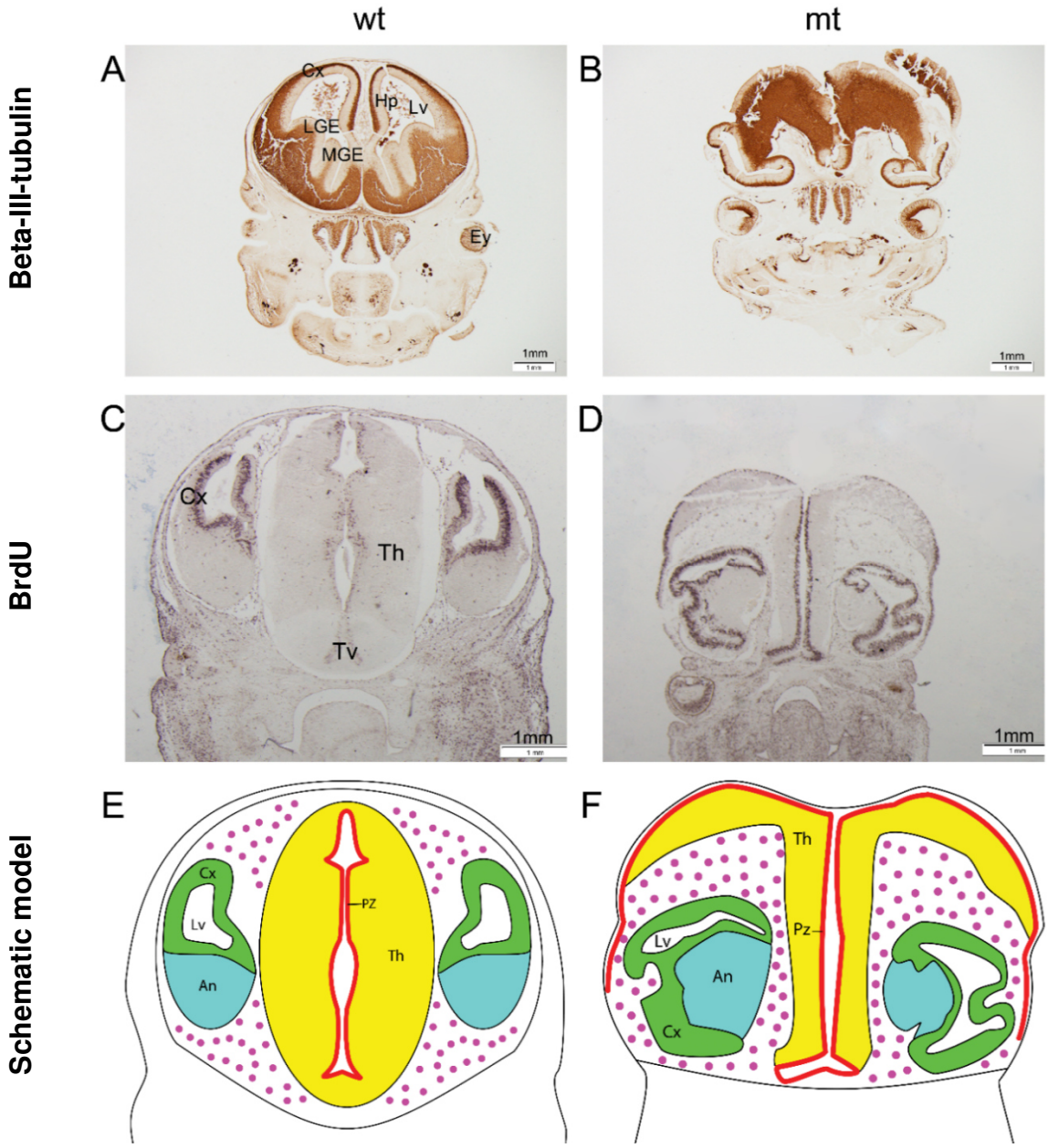

Fig. 49: IHC of coronal sections of E13.5 Cofilin1$^{wt/wt}$ and Cofilin1$^{KTRTK/KTRTK}$ brains. 10 µm paraffin sections were stained with beta-III-tubulin (bIIItub, **A+B**). Everted expression pattern could be observed in the mutant brain (mt) compared to Cofilin1$^{wt/wt}$ E13.5 brain (wt). For proliferation analysis, pregnant females were injected with BrdU one hour prior to sacrifice. Coronal paraffin brain sections were prepared and stained with BrdU, allowing visualization of proliferating cells (**C+D**). Number of proliferating cells was increased and localized differently in the mutant due to shift of structures. Based on the BrdU staining a hypothetical schematic coronal model, showing proliferative zone and presumed brain areas, was created (**F**). Compared to wildtype (**E**), proliferative zone and brain areas in the mutant seem to shift upward and laterally. An: amygdaloid nucleus Cx: cortex; Ey: eye; Hp: hippocampus; LGE: lateral ganglionic eminence; Lv: lateral ventricle; MGE: medial ganglionic eminence; PZ: proliferative zone; Th: thalamus; Tv: third ventricle; wt: Cofilin1 $^{wt/wt}$; mt: Cofilin1$^{KTRTK/KTRTK}$.

Under the consideration of morphology and localization of proliferative zones in coronal sections, an upward and lateral shift of brain structures in Cofilin1$^{KTRTK/KTRTK}$ embryos could be assumed. Figure 49, F presents a hypothetical coronal schematic model of supposed brain areas and proliferative zone in the mutant. In this scheme the hypothetical cortex in the mutant brain is morphologically altered and repositioned (Figure 49, Cx, green), thereby also affecting the suggested lateral ventricle (Figure 49, Lv). The assumed thalamic area (Figure 49, Th, yellow) and the proliferative zone surrounding it (Figure 49, Pz, red) are enlarged and shifted upwards and laterally in the mutant compared to the wildtype.

Beta-III-tubulin staining showed an altered, everted patterning of Cofilin1$^{KTRTK/KTRTK}$ brain. The number of proliferative cell in the mutant was increased. Proliferative zones in the mutant were enlarged and showed an upward and lateral shift.

4.6 Cofilin1$^{KTRTK/KTRTK}$ neurons showed increased neurite growth *in vitro*

The exencephalic phenotype induced by the introduction of the mutation of the NTS in Cofilin1 has been analyzed histologically and was complemented by neural *in vitro* studies to determine the type of neuronal cells in the Cofilin1$^{KTRTK/KTRTK}$ brain. Neural cell culture studies allowed the analyses of morphological features of neurons and astrocytes. The morphology *in vitro* differs from *in vivo*, but *in vitro* studies provide the main advantage that cell behavior can be compared, independent of hormonal influences.

Neurons were derived from Cofilin1$^{wt/wt}$ and Cofilin1$^{KTRTK/KTRTK}$ total brains at the embryonic stage E18.5. Stainings with neuronal markers (NeuN and bIIItub; Golgi staining, data not shown) verified the presence neurons in Cofilin1$^{KTRTK/KTRTK}$ brain. But it should be noted that the properties of the starting tissue were not identical. Morphology of the mutant brain did not allow definite identification of brain areas. Therefore neurons were isolated from the entity of the brain. The morphology of cells was analyzed via beta-III-tubulin staining at different points of time after seeding. This

also allowed comparisons between wildtype and mutant (Figure 50), regarding the development behavior *in vitro*.

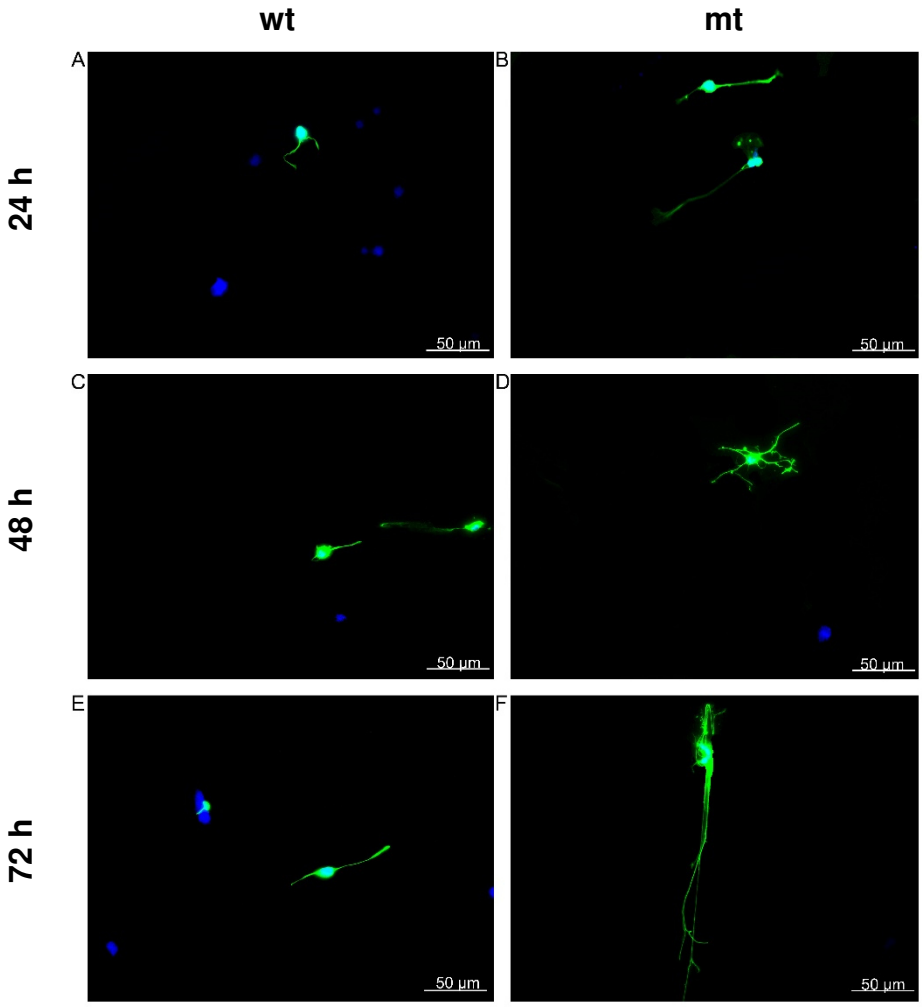

Fig. 50: Morphological development of Cofilin1$^{wt/wt}$ (wt) and Cofilin1$^{KTRTK/KTRTK}$ (mt) neurons (E18.5) in the course of 72 hours. Neurons were fixed after 24h, 48h and 72h in culture and stained with beta-III tubulin (bIIItub, green), which is specific for neurons, staining soma, axons and dendrites. For nuclear staining DAPI (blue) was used. Mutant neurons were bigger and were characterized by multiple processes. Images were obtained at 40x magnification. wt: Cofilin1$^{wt/wt}$; mt: Cofilin1$^{KTRTK/KTRTK}$

Isolated neurons adhered to the provided laminin coated coverslips within two to three hours. The impression was given, that Cofilin1$^{KTRTK/KTRTK}$ neurons displayed an increased branching activity compared to wt neurons in the same time window.

Neurons seeded on glass coverslips were fixed after 24, 48 and 72 hours to track development and spreading in culture (3.2.2.2). Observing the spreading behavior of wt and mt neurons over 72 hours at three different points of time, every 24 hours, the impression of increased branching in mt neurons was noted (Figure 50). The majority of the neurons, derived from wildtype embryos demonstrated less branching at the examined time points (Figure 50). It should also be mentioned that Cofilin1$^{KTRTK/KTRTK}$ neurons displayed a high tendency to clump.

Cofilin1$^{KTRTK/KTRTK}$ neurons displayed increased branching and wider spreading areas. Neurons derives from Cofilin1$^{wt/wt}$ embryos, remained uni-or bipolar (Figure 50).

The second group of neural cells, that were analyzed, were astrocytes. Astrocytes, specialized glia cells, excess neurons by five-fold in the brain. It is known that Cofilin1 is expressed in astrocyte and involved in their migration (Nagai et al., 2011). Therefore this groups of neural cells was also of interest.

4.6.1 KTRTK-Cofilin1 astrocytes showed a multinucleate morphology

Astrocytes, were isolated from neural tissue of Cofilin1$^{wt/wt}$ and Cofilin1$^{KTRTK/KTRTK}$ embryos at the gestational stage E17.5. Glial fibrillary acidic protein (GFAP), Vimentin and Nestin are intermediate filaments (IFs) and constitute a family of cytoskeletal components in astrocytes. Their expression level change in the progress of astrocyte maturation from Nestin to Vimentin to GFAP. Nestin is only present in immature cells, Vimentin is present in all immature astrocytes and some mature subtypes. In mature differentiated astrocytes Vimentin is replaced by GFAP during maturation. The expression of GFAP is tightly regulated during astrocyte maturation. GFAP has been associated with cell communication and mitosis (Galou et al., 1996; Colucci-Guyon et al., 1999; Menet et al., 2000).

Isolated astrocytes adhered to the provided coverslips within one to two hours. Within two to three days after seeding, cells were fixed and stained for GFAP (3.2.2.6).

In the next step ratio of GFAP- positive cells was analyzed (Figure 51+52).

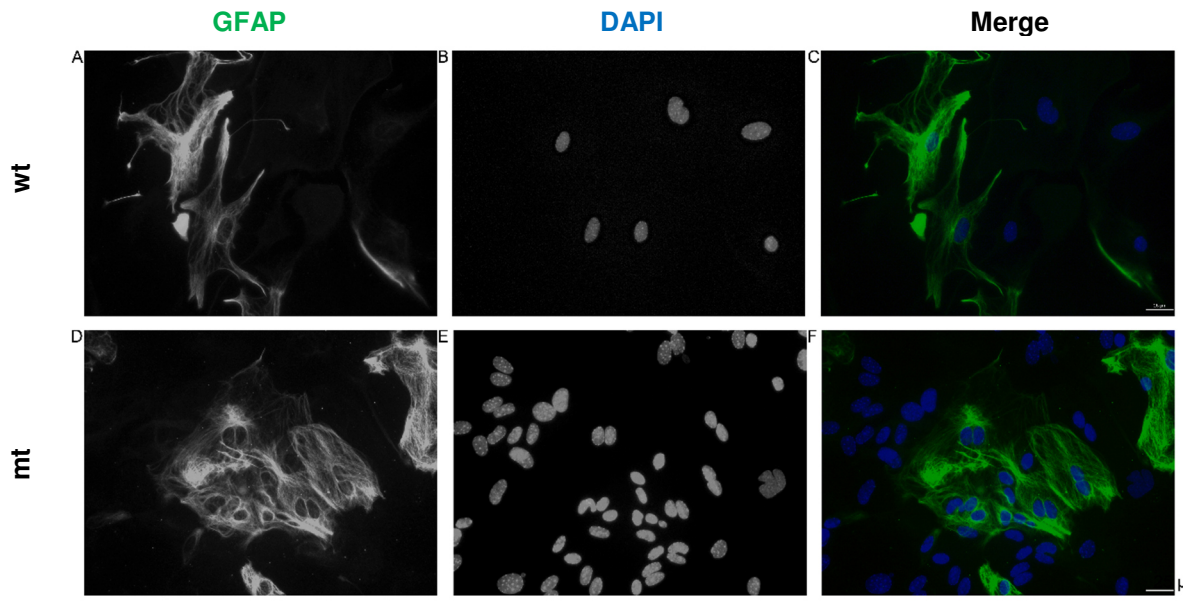

Fig 51: GFAP positive astrocytes derived from Cofilin1$^{wt/wt}$ and Cofilin1$^{KTRTK/KTRTK}$ brains (E17.5). Astrocytes were fixed and stained with GFAP (GFAP, green). More wt astrocytes were GFAP- positive. Images were obtained at 40x magnification. Scale bar: 25µm; wt: Cofilin1 $^{wt/wt}$; mt: Cofilin1$^{KTRTK/KTRTK}$

Interestingly, astrocytes isolated from Cofilin1$^{KTRTK/KTRTK}$ embryos (Figure 86), appeared to show the same morphological characteristics of increased cell size and multinuclearity as the mutant Mefs (Figure 29). This should be studied further in the future.

Previous studies showed that approximately 20% neural culture astrocytes are GFAP-positive. A total number of approximately 180 cells for each genotype derived from three wt and three mt embryos at E17.5 were counted and used for analysis of GFAP-positive cells.

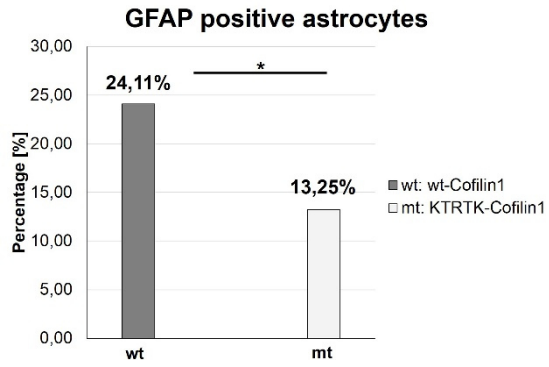

Fig. 52: Statistical analysis of GFAP-positive E17.5 wt and mt astrocytes. A total number of 180 cells was analyzed for each genotype. Significantly less mt astrocytes were GFAP-positive The number of GFAP- positive cells was decreased by 11% compared to wt. Wt: Cofilin1$^{wt/wt}$; mt: Cofilin1$^{KTRTK/KTRTK}$; Levels of significance: 0.05 >p≥ 0.01 (*); 0.01>p≥0.001 (**); p>0.001 (***).

The number of astrocytes positive for GFAP was decreased by a factor of 1.8-times in the mutant compared to wildtype (Figure 52)

Significantly less GFAP- positive KTRTK-Cofilin1 astrocytes were detected. The importance of this characteristic of KTRTK-Cofilin1 astrocytes for the morphology of the mutant brain needs to be investigated further (5.9).

4.7 The NTS mutation of Cofilin1 affected gene expression profiles of extracellular matrix proteins and actin isoforms in brain and Mefs

Microarrays provide the possibility to monitor of gene expression on a transcriptional base. They allow the quantification of expression levels of a large number of genes simultaneously. The acquired expression profiles allow the identification of genes, whose expression is changed as a direct or indirect consequence of the mutation.
In this thesis *in vivo* and *ex vivo* samples in the form of brains and Mefs were analyzed with the goal to identify significantly altered genes.

In order to identify, due to the mutation, critically altered genes in *in vivo* settings, three Cofilin1$^{wt/wt}$ and three Cofilin1$^{KTRTK/KTRTK}$ samples were compared individually. According to histology the Cofilin1$^{KTRTK/KTRTK}$ brain is differently organized and connective tissue is predominant (Figure 42), which could indicate differential

expression of genes involved in brain pattering for example in the mutant. Gestational stage E16.5 was chosen, a point in development, in which decreased mutant protein level were observed (4.3.1.1).

Whereas the analysis of brain samples allowed an *in vivo* approach the study of Mefs provided the opportunity to observe a homologous cell population *in vitro*. A factor that was not given in the analysis of brain samples. Further the analysis of Mefs at this developmental stage also represented a state in development, in which KTRTK-Cofilin1 was still present. Morphological analyses of astrocytes showed the same multinuclear and enlarged phenotype as in Mefs. Indicating a disruption of cellular activities in different Cofilin1$^{KTRTK/KTRTK}$ cell types. Mefs were isolated from E14.5 embryos. Three Cofillin1$^{wt/wt}$ (wt) and three Cofilin1$^{KTRTK/KTRTK}$ (mt) Mef lines were prepared. Cells of passages 1 and 3 were analyzed. One passage is defined as the trypsinization of confluent cells and the subsequent seeding of a portion of the acquired single cell suspension. The analysis of different passages allowed to track possible changes in gene expression in the progress of the culture. For further analyses, main focus was put on the combination of mt Pass1 vs. wt Pass1 to avoid the detection of possible expression alterations as cultural artefacts.

The Illumina® bead chip system was used for the microarray analyses. The mathematical calculation were performed with Partek® Genomic suite software.
The wildtype always acted as reference, meaning up- and down regulation were calculated according to the Cofilin1$^{wt/wt}$ sample.

In order to understand more regarding the function of the protein of interest, it was important to know in which cellular processes Cofilin1 is involved.
Table 6 presents the Go-Terms involving Cofilin1 in *mus musculus* that have been identified so far. Go-Terms are a group of genes which either have a similar function or are involved in the same cellular mechanisms.

Actin binding	GO:0003779
Actin cytoskeleton	GO:0015629
Actin filament depolymerization	GO:0030042
Actin filament organization	GO:0007015
Cell leading edge	GO:0031252
Cell projection	GO:0042995
Cell projection organization	GO:0030030
Cellular component movement	GO:0006928
Cortical actin cytoskeleton	GO:0030864
Cytokinesis	GO:0000910
Cytoplasm	GO:0005737
Cytoskeleton	GO:0005856
Cytoskeleton organization	GO:0007010
Establishment of cell polarity	GO:0030010
Intracellular	GO:0005622
Lamellipodium	GO:0030027
Membrane	GO:0016020
Negative regulation of cell size	GO:0045792
Neural cell crest migration	GO:0001755
Neural fold formation	GO:0001842
Nucleus	GO:0005634
Plasma membrane	GO:0005886
Positive regulation of actin filament depolymerization	GO:0030836
Protein import into nucleus	GO:0006606
Protein phosphorylation	GO:0006468
Regulation of cell morphogenesis	GO:0022604
Response to amino acid stimulus	GO:0043200

Table 6: Go-Terms involving Cofilin1 in *mus musculus*. A Go-Term describes a group of genes with similar function or a group of genes involved in the same cellular process. Each Go-Term can be accessed with the respective identification number via the Amigo: Gene ontology database.

In total approximately 24.000 genes were tested, which were segmented into 45.282 gene fragments, for both brain and Mefs. This increased the likelihood to also detect a number of alternative splice forms. Expression alterations in the form of fold- changes (up- or down- regulation) were mathematically calculated.

4.7.1 Gene expression profiling *in vivo* (brain) and *in vitro* (Mefs) tissue

Initially, principle component analysis (PCA, Figure 53) was used to visualize the distribution of all data of each sample. Principle component analysis is a statistical tool to convert a number of correlated variables to a smaller or equal number of uncorrelated variables that are called principle components. This method is used to reduce and discover the dimensionality of the data set as well as identify novel underlying variables (Ulas, unpublished).

PCA mapping showed that the two group of genotypes were clearly distinguishable in brain and in Mefs (Figure 53). It also provided information regarding the relationship between individual samples.

For the brain the wildtype (wt/wt: Cofilin1$^{wt/wt}$) samples were depicted in blue, the mutant samples (Nuc/Nuc: Cofilin1$^{KTRTK/KTRTK}$) in red (Figure 53, A). Two of the wildtype samples and two of mutant samples lay within closer vicinity of each other than the third sample. This reflected that the overall gene expression differed from the other two gene samples.

For the Mefs the wildtype passage 3 (wildtype: Cofilin1$^{wt/wt}$) samples (depicted in violet) and the mutant passage 3 (Nuc/Nuc: Cofilin1$^{KTRTK/KTRTK}$) samples (illustrated in blue), showed the same distance from sample to sample within the same genotype (Figure 53, B). The formation representing samples of passage 1 for wildtype (green) and mutant (red) showed two samples in closer vicinity of each other and the third sample more distant, the same pattern that was observed in the brain.

Retracing of the data to the analyzed samples determined, that the two samples which lay in closer proximity to each other originated from littermates. Regardless of same gestational age and genotype, samples were still clearly distinguishable based on parental origin. In the Mefs the effect was lost during culture.

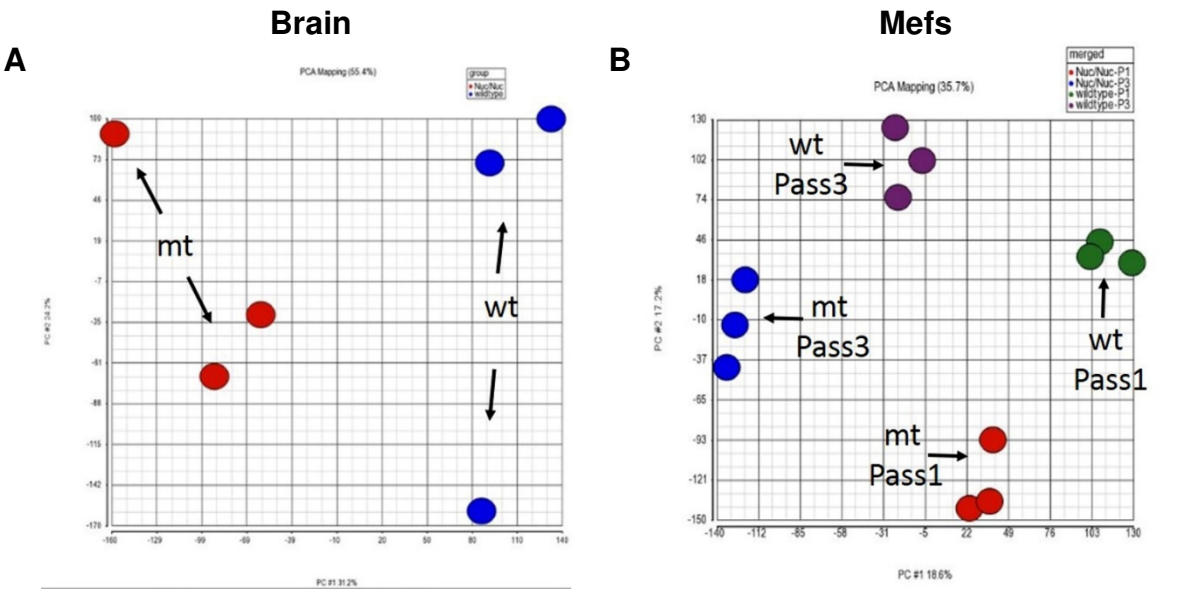

Fig. 53: PCA mapping of Cofilin1$^{wt/wt}$ (wt) and Cofilin1$^{KTRTK/KTRTK}$ (mt) samples. Graph shows relationship between individual samples. **(A)** PCA mapping of wt and mt E16.5 brains. The groups of genotypes (Cofilin1$^{wt/wt}$ is depicted in blue, while Cofilin1$^{KTRTK/KTRTK}$ is depicted in red) could be clearly distinguished. Wt/wt: Cofilin1$^{wt/wt}$ (blue)**;** Nuc/Nuc: Cofilin1$^{KTRTK/KTRTK}$ (red). **(B) PCA mapping of E14.5 wt and mt Mefs (P1+P3).** The groups of passages and genotypes could be clearly identified. The several groups can be divided into separate groups. P1: Passage 1; P3: Passage 3; Wildtype: Cofilin1$^{wt/wt}$; Nuc/Nuc: Cofilin1$^{KTRTK/KTRTK}$; wt/ wt-P1 (green); wt/ wt-P3 (violet); Nuc/ Nuc-P1 (red); Nuc/ Nuc-P3 (blue).

This should be kept in mind for future experiments. For the following steps of analysis it was possible to mathematically add a biological error variable for the parentage.

The ANOVA (analysis of variance) test is used to analyze the difference between group means. Simplified, it provides a statistical test whether or not means of different groups are equal along with statistical significance (Anderson et al., 1996). For all further steps of analyses only genes, which fluorescence signal was altered with a significance lower than $p<0.05$ were included. The data acquired in the microarray is based on the mathematical processing and conversion of fluorescent signals. In total approximately 24.000 genes were tested, which were segmented in 45.282 gene fragments. This increases the likelihood to also detect a number of alternative splice forms. In the ANOVA calculations samples were grouped by genotype and compared, the wildtype was used as reference. Negative fold-changes indicate a down-regulation (blue) in the

mutant, whereas positive fold-changes represent an up-regulation (red) in the mutant tissue (Table 7 and S8-S24).

4.7.1.1 Cofilin1$^{KTRTK/KTRTK}$ brains show massive up-regulation of extracellular matrix genes

In the brain 4566 gene fragments of significant value could be determined in the microarray analysis, which represents 10.08 % of all gene fragments tested. For analysis purposes a cut off for up-regulation at +2.5 fold and for down-regulation at -1.7 fold was set. Furthermore only genes, whose function have been annotated so far, are listed. Tables S8-S14 (supplementary data) depict the significant genes with highest fold changes. The last lane in the tables specifies in which GO-Terms the particular gene is plays a role.
Interestingly only two down-regulated genes, which fulfilled the given criteria, could be identified. Nkx2-1 (-1.82), a neural transcription factor, is important for pattern specification and cerebral cortex cell migration. It is one of the neural transcription factors expressed early in embryonic development and can be detected as early as E10.5.

Considering the phenotype of the analyzed tissue and its neural character, genes encoding GFAP, Nestin and Reelin were analyzed. Immunofluorescence stainings (Figure 48+Figure 52) showed the absence of Reelin in the mutant, whereas it could be detected in the wt. Astrocytes taken in culture showed a significant difference in the number of GFAP positive cells in the mutant. Neither Nestin nor Reelin and GFAP analyzed genes in the microarray were significantly changed and therefore not included in the analyses.

The members of the ADF/Cofilin family were also studied. A decrease on protein level of KTRTK-Cofilin1 at E16.5 and the subsequent up-regulation of Cofilin2 and ADF have been observed s in the mutant brain samples in western blot analysis. The fold-changes ranged from -1.04 to +1.20 for *cfl1* (Cofilin1), *cfl2* (Cofilin2) and *Dstn* (ADF) but were not significant. That aside for *cfl1* this result would correlate with the observations made in qPCR (Figure 25).

The genes presented in Figure 54 showed the most striking differences in expression levels in Cofilin1$^{KTRTK/KTRTK}$ brain compared to Cofillin1$^{wt/wt}$ brain. The expression of matrilin 1 was increased by a factor of 19. Matrilin 1 is a cartilage matrix protein, involved in chondrocyte differentiation and formation of extracellular matrix in various tissues. Aggrecan, up-regulated by a factor of 3, is involved in chondrocyte development, cell adhesion and collagen organization. Previous studies showed that an up-regulation of aggrecan results in the development of hypertrophic chondrocytes. Chondrocytes are found in cartilage and maintain and produce cartilaginous matrix, which consists of collagen and proteoglycans. This type of cells originate from mesenchymal stem cells, which can also differentiate into osteoblasts. Hypertrophic chondrocytes are large in size, produce collagen and are often associated with a shift in cartilage to bone ratio. Collagen 2, an isoform typical for osteoblasts and mesenchyme, was increased by 13.5-fold. The large number of genes associated with collagen, extracellular matrix and cartilage supports that the observed loose tissue is mesenchymal connective tissue. It should also be noted that the expression level of all of the genes depicted in Figure 54 was up-regulated.

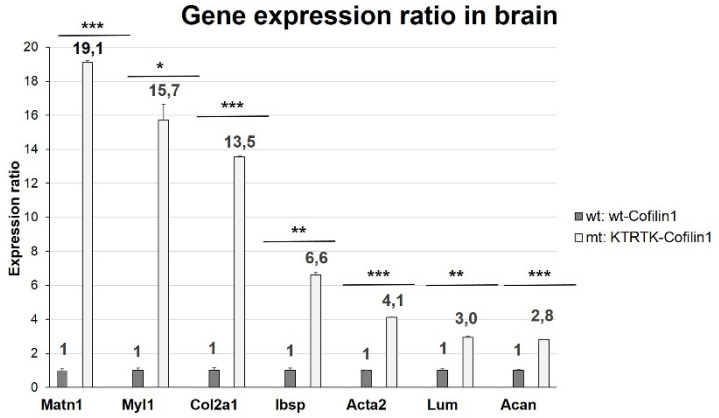

Fig. 54: Selection of Gene expression ratios in Cofillin1$^{KTRTK/KTRTK}$ compared to Cofilin1$^{wt/wt}$ brain. Expression of wt was normalized to 1. Expression ratio of mt was calculated in reference to wt. Extracellular matrix proteins are significantly up-regulated. Matn1: matrilin 1; Myl1: myosin light polypeptide 1; Col2a1: collage 2; Ibsp: integrin binding sialoprotein; Acta2: α-actin 2, smooth muscle; lum: lumican; Acan: aggrecan.

Alpha actin 2 (smooth muscle) was also up-regulated by a factor of 4. This isoform of actin is associated with muscle rather than brain. Myosins, (up-regulated by factor 15.7 and 7.9), were also detected. These myosins on the other hand are associated with skeletal contractions.

It has been shown in previous studies that the spatially and timely restricted expression pattern of transcription factors during development is crucial for the anatomical

organization of the brain. At E13.5 approximately 349 transcriptions factors are expressed in a spatially restricted manner (Gray et al., 2004). Considering the specific expression patterning of transcription factors for embryonic brain arealization, disruptions of expression patterns could form massive disorganization of the brain. Therefore the microarray data were screened for neural transcription factors (Table 7).

10 neural transcription factors that were significantly altered could be detected. Though all of them can be found in the brain they are expressed at different levels with different functions. Egr1, for example, is mainly expressed in the pallium at this age. Nkx2-1 and Six1, which was increased by a factor of 2, is mainly expressed in the rostral secondary prosencephalon. Histological analyses, showed that the Cofilin1$^{KTRTK/KTRTK}$ brains show severe malformations in the secondary prosencephalon. Though the change in expression level was not very high, it remains to be elucidated whether the sum of differently regulated TFs impacts on the morphological alterations observed in the Cofilin1$^{KTRTK/KTRTK}$ brain (Figure41).

Gene	Fold change (mt vs wt)	Function	Localization
Six1	2.09862	embryonic cranial skeleton morphogenesis, generation of neurons, negative regulation of neuron apoptotic process	Rostral secondary prosencephalon
Rbbp7	1.63971	chromatin modification, chromatin remodeling , DNA replication, negative regulation of cell growth	Pallium, midbrain, hindbrain
Egr1	1.62081	positive regulation of neuron apoptotic process, regulation of long-term neuronal synaptic plasticity,	Pallium
Sp7	1.57856	osteoblast differentiation, positive regulation of transcription from RNA polymerase II promoter	Olfactory bulb
Esrrb	1.56853	in utero embryonic development, trophectodermal cell proliferation , regulation of transcription	Diencephalon
Twist1	1.51499	cranial suture morphogenesis, embryonic skeletal system morphogenesis, neural tube closure, neuron migration	Midbrain
Nfatc4	1.50105	cell differentiation, patterning of blood vessels,	Telencephalic vesicle
Neurod2	-1.52616	nervous system development, cerebellar cortex development, positive regulation of synaptic plasticity, positive regulation of neuron differentiation, neuron development, regulation of synapse maturation	Pallium
Pbx1	-1.61873	embryonic skeletal system development, negative regulation of neuron differentiation,	Diencephalon
Nkx2-1	-1.82799	axon guidance, brain development, cerebral cortex cell migration, forebrain patterning, hippocampus development, globus pallidus development, neuron fate commitment, neuron migration, oligodendrocyte differentiation	Rostral secondary prosencephalon

Table 7: Expression levels of neural transcription factors in Cofilin1$^{wt/wt}$ brain versus Cofilin1$^{KTRTK/KTRTK}$ brain (E16.5). Cofilin1$^{wt/wt}$ was used as reference, red color indicates up-regulation in Cofilin1$^{KTRTK/KTRTK}$, down-regulation is shown in blue. Expression profiles were acquired from the Allen brain atlas, based on E15.5 embryos. Wt: Cofilin1$^{wt/wt}$; mt: Cofillin1$^{KTRTK/KTRTK}$

In order to simplify the analysis, in the next step affected genes were illustrated in Go-Term enrichment maps (4.7.1.3).

4.7.1.2 Gene expression profiling in vitro (Mef)

The data acquired in the microarray of the Mefs, derived from three Cofilin1$^{wt/wt}$ and three Cofilin1$^{KTRTK/KTRTK}$, was mathematically processed in the same way as the samples of the brain (4.7.1.1). The tested samples were abbreviated by: wildtype passage 1: wt Pass1; mutant passage 1: mt Pass1

ANOVA tables were calculated for mt Pass1 versus wt Pass1. Up- and down-regulations of gene expression levels were calculated in reference to wildtype.

In total 4472 gene fragments of significant value could be determined in the microarray, which equates 9.88 % of all gene fragments tested. Only genes with a calculated significance of $p<0.05$ were considered for analysis. Tables S15 to S24 (supplementary data) represent the significant genes with highest fold changes, detected in Mefs (mt Pass1 vs wt Pass1). In the last lane in the tables the GO-Terms are specified in which the particular gene is involved. For analysis purposes a cut off at +2.5 for up- regulation (red) and for down regulation (blue) at -2.5 was set. Only genes, whose function have been annotated so far, have been listed.

Via western blot analysis up-regulation of ADF and Cofilin2 was detected. In the microarray the expression levels for cfl1 (Cofilin1) was detected at +1.42 but with no significance, *cfl2* (Cofilin2) and *dstn* (ADF) were featured p-values below 0.05. *Clf2* was detected at an increased expression level of +1.16, *dstn* was detected at +1.48. It has to be considered at all times that the change of expression on RNA level allows no direct conclusion regarding protein expression level. Therefore, it was not uncommon that the RNA expression level, did not coincide with detected protein levels (Figure 28).

In vitro several down-regulated and up-regulated genes, which fulfilled the set criteria, could be identified. Most of the identified genes can be classified into the distinct groups: cell growth, skeletal morphogenesis, ossification and cartilage formation (collagen) and regulation of metabolic/ cellular processes.

In this experiment a fibroblast cultures after one splitting event were analyzed, therefore the identified processes ossification and skeletal morphogenesis were not expected. Discussing every gene, fulfilling the cut-off criteria would be too extensive. Therefore a selection of genes will be analyzed in this chapter. For completion all genes fulfilling the cut-off criteria are listed in the tables 16 to 25.

A number of detected genes, such as *Pdgfra* (platelet derived growth factor receptor, alpha polypeptide, for growth factors of mesenchymal origin) and *Actb* (beta actin) are involved in gene expression. *Pdgfra* were down- regulated by fold-change of -2.73. *Actb* was up-regulated by +2.6-fold (Figure 55).

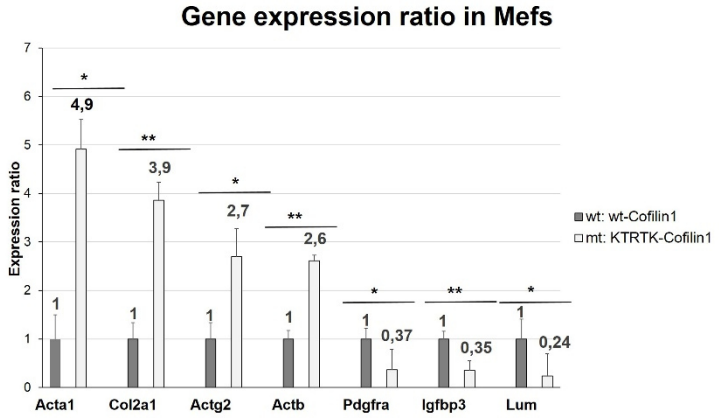

Fig. 55: Selection of Gene expression ratios in Cofillin1$^{KTRTK/KTRTK}$ compared to Cofilin1$^{wt/wt}$ Mefs. Gene expression levels of wt were normalized to 1. Expression ratio of mt was calculated in reference to wt. Actin isoform were significantly up-regulated in mutant. The other groups of genes affected were collagen- related. Acta1:α-actin, skeletal muscle; Col2a1: collage 2; Actg2: γ-actin, smooth muscle; Actb: β-actin; Pdgfra: platelet derived growth factor receptor ; Igfbp3: insulin-like growth factor binding protein 3 gene ; lum: lumican

Along with *Actb* other actin isoforms were detected to be expressed at an increased level. *Actg2* (gamma actin, smooth muscle, enteric) was expressed at a level of +2.7. The third isoform that was detected was Acta1 (alpha actin, skeletal muscle), whose expression was increased to +4.9. Interestingly, the predominant isoforms of actin in Mefs, *Acta2* and *Actg1*, did not fulfil the cut-off criteria. Increases of F-actin but constant levels of G-actin in mutant Mefs compared to wt Mefs had been observed (Figure 36), coinciding with increased actin mRNA levels.

Considering the significantly enlarged phenotype of the analyzed cells, genes involved in induction of EMT (epithelial- mesenchymal- transition) along with EMT markers were analyzed. Just one the known involved genes (*Tgfbr3*) were significant or regulated

above a level of ±1.3. Tgfbr3 was down-regulated by -2.59-fold. For further information see Table S20. The list of involved genes was derived from literature and Go-Terms. Regarding the embryonic origin of the cells, developmental factors were checked next. All detected developmental factors (*Olfml1*, *Osr2* and *Pdgfra*) were down- regulated by -3.0, -2.82 and -2.1-times, respectively. Two of the most striking morphological characteristics of Cofilin1$^{KTRTK/KTRTK}$ Mefs are the cell size and multinuclearity. It was shown that mutant Mefs display a cytokinesis defect (4.4.2.2).To further analyze possible reasons for multinuclearity, genes involved in chromosome segregation and chromatin remodeling were observed closer. Of 216 identified genes involved in the above mentioned processes, 18 genes were significant, but not a single one was detected at a level higher than +1.5. This did not allow any conclusions regarding involved genes in the multinuclear phenotype. Interestingly multinuclearity was proposed as marker for osteoclasts (Hattersley and Chambers, 1989). A number of genes involved in skeletal morphogenesis and ossification were identified with altered expression levels in the mutant compared to wildtype (see supplementary data).
For cells size analysis, genes involved in cell growth were examined. Regulation in cell growth could either be positive or negative. *Inhba* (inhibin beta A) was detected at an up-regulated RNA level of +4.59-fold, Igfbp3 (insulin-like growth factor binding protein 3) was detected at an expression level reduced to 0.35 compared to the wt (Figure 55). This disruption of at least two genes involved in cell growth control, may be part of the explanation of the phenotype of the mutant Mefs.
Lum and Col2a were identified in both Mefs and brain as differently regulated genes. Col2a was up-regulated by +3.9-fold (brain: +13.5-fold). In mutant Mefs Lum was reduced by -4.24-fold (brain: +3.0-fold). Lum is also involved in transcriptional regulation. Col2a is one of the factors involved in skeletal development.

To simplify the analysis and better visualization, affected genes were illustrated in Go-Term enrichment maps, in the next step.

4.7.1.3 In vivo KTRTK-Cofilin1 impacts on specific groups of function

A Go-Term is defined as a group of genes which either have a similar function or are involved in the same cellular processes. Go-Term enrichment visualizes the connectivity (intersection of genes) of different Go-Terms. Further it allows the grouping of different Go-Terms of similar functions (Figure 56).

For the process of Go-Term enrichment the all genes analyzed of the ANOVA are used. The link of the data to AmiGo-gene ontology database facilitates the identification of altered Go-Term on single gene level.

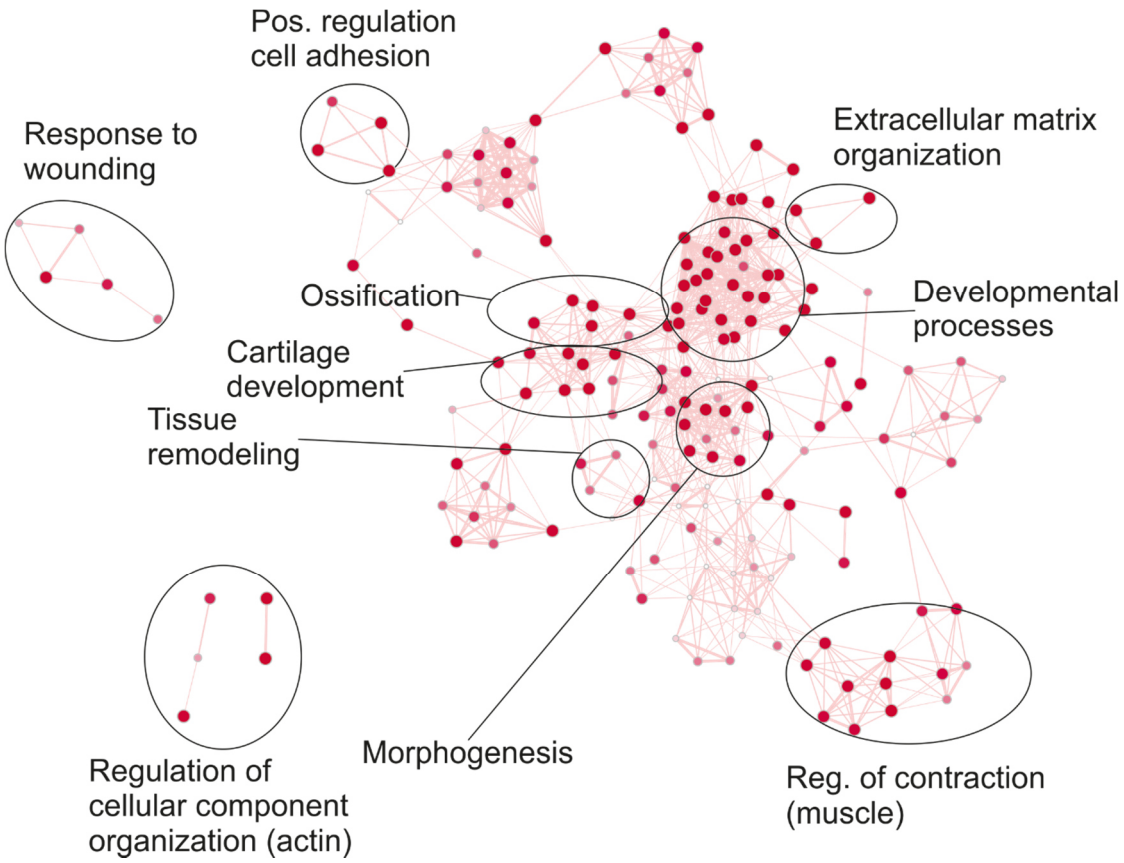

Fig. 56: Go-Term enrichment of Cofilin1$^{wt/wt}$ brain vs. Cofilin1$^{KTRTK/KTRTK}$ brain (E16.5). Cofilin1$^{wt/wt}$ was used as reference, red color indicates up-regulation in Cofilin1$^{KTRTK/KTRTK}$. Single Go-Terms are presented as dots, connections between terms signify intersection of genes. Thickness of connection correlates with number of common genes. Size and color intensity of Go-Term correlates with fold-change. Circles indicate grouping of Go-Terms of similar function.

A dot represents a Go-Term. The bigger and darker the circle the bigger the fold-change compared to the wildtype. The thickness of the connection between two Go-Terms correlates with the amount of genes, involved in both Go-Terms. The circles illustrate the grouping of Go-Terms of similar function. Fold-changes were calculated in reference to Cofilin1$^{wt/wt}$. Up-regulation of genes in Cofilin1$^{KTRTK/KTRTK}$ is depicted in red.

A large number of Go-Terms in brain involved developmental processes (e.g. chondrocyte development; central nervous system development) were affected by the mutation of the nuclear translocation sequence of Cofilin1. Further a number of Go-Terms responsible for cartilage development were also influenced (see 4.5). The mutant protein KTRTK-Cofilin1 also had an impact on a number of Go-terms involved in morphogenesis. Considering the phenotype of the brain, disturbances in morphological processes (e.g. growth plate cartilage chondrocyte morphogenesis, see supplementary).

Though brain tissue was analyzed, a number of Go-Terms associated with regulation of muscle contraction were affected, partly due to striking increases of expression levels of myosins and muscle associated actin (see supplementary).

Also a group of Go-Terms responsible for regulation of actin as a cellular component was affected. Since it was observed, that KTRTK-Cofilin1 does not depolymerize F-actin with the same capacity as wt-Cofilin1, it would make sense that other proteins had to be up-regulated to compensate this. Analysis of gene expression levels showed that ADF (Dstn) and Cofilin2 (Cfl2) were not up-regulated, though. .

After the Go-Term enrichment visualized, which Go-Terms were affected the strongest by the mutation, pathways on a single gene level were analyzed in the following step.

4.7.1.4 *In vitro* KTRTK-Cofilin1 impacts other specific groups of function than *in vivo*

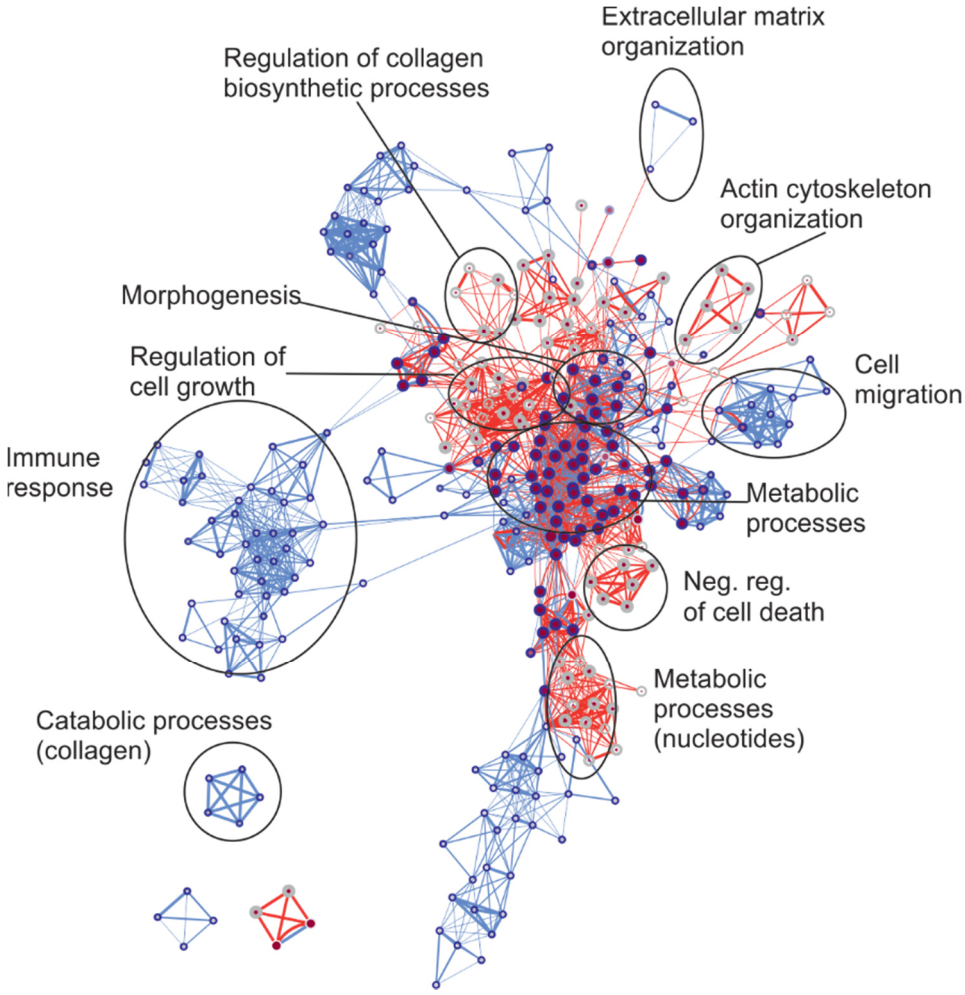

Fig. 57: Go-Term enrichment of Cofilin1$^{wt/wt}$ (Pass1) vs. Cofilin1$^{KTRTK/KTRTK}$ (Pass1) Mefs (E14.5). Cofilin1$^{wt/wt}$ Pass1 was used as reference, red color indicates up-regulation in Cofilin1$^{KTRTK/KTRTK}$, blue color indicates down-regulation in mutant Mefs. Single Go-Terms are presented as dots, connections between terms signify shared of genes. Thickness of connection correlates with number of collective genes between two Go-terms. Size and color intensity of Go-Term correlates with fold-change (grey; size correlates with number and fold-change of up-regulated genes; red dots with blue circle: Go-Term contains up- and down-regulated genes). Blank circles indicate grouping of Go-Terms of similar function. Pass1: passage 1; wt: Cofilin1$^{wt/wt}$; mt: Cofilin1$^{KTRTK/KTRTK}$

Every dot represents a Go-Term. Cofilin1$^{wt/wt}$ represents the reference. The bigger and darker the circle the bigger the fold-change compared to the wildtype. Amount of genes involved in two adjacent Go-Terms is represented by the connection between two Go-

Terms. The circle illustrates the grouping of Go- Terms of similar function. Up-regulation of genes in Cofilin1$^{KTRTK/KTRTK}$ is depicted in red, down-regulation is illustrated in blue.

Two other groups that are affected are metabolic processes in general, where up- and down-regulation could be detected (Figure 57). This group comprises a vast number of metabolic processes, the regulation of glucose metabolic process, for example. In passage 1 mutant Mefs still show a rather high proliferation rate, in order for cells to proliferate the metabolism of the cell needs to be active. Therefore it was not surprising that up- regulated as well as down- regulated genes were detected in this group. In senescent and quiescent cells metabolic processes are down-regulated in general. Also at this stage where proliferation takes place at rather high rate nucleotides are of importance for synthesis of nucleic acids (metabolic processes (nucleotides)). Genes involved in negative regulation cell proliferation were down-regulated (e.g. Igfbp3: -2.61; Tgfbr3: -2.59). The majority of the GO-Terms in the group metabolic processes (nucleotides) are up-regulated in the mutant compared to the wt. Whether this somehow correlates to the multinuclearity of the mutant Mefs needs to be investigated further. Groups of GO-Terms involved in morphogenesis and regulation of cell growth are also affected, since the altered morphology is one of the most striking features of mutant Mefs. The mutant protein KTRTK-Cofilin1 also had an impact on a number of Go-Term involved in collagen biosynthesis, this could already be observed in the brains analyzed in microarrays. Another group of Go-Terms affected by KTRTK-Cofilin1, is the group of “cell migration”. Most Go-Terms within this group are down-regulated. Changes of Cofilin1 level was shown to impair migration in several different cell types (Ghosh et al., 2004; Sidani et al., 2007; Popow-Wozniak et al., 2012). Further, a number of Go-Terms responsible for actin cytoskeleton organization were also up-regulated. This up-regulation was also observed in the brains (4.7.2.3). Since it was observed, that KTRTK-Cofilin1 does not depolymerize F-actin with the same capacity as wt-Cofilin1. Cofilin1$^{KTRTK/KTRTK}$ Mefs are bigger and comprise more F-actin compared to wildtype, therefore it would make sense that other proteins had to be up-regulated organize the cytoskeleton like profilin (4.7.1.6) to compensate this, but Mefs did not display significant up-regulation of ADF (*Dstn*) and Cofilin2 (*Cfl2*). A large number of Go-Terms involved in immune responses were down- regulated in Mefs

carrying the mutation. In how far KTRTK-Cofilin1 affects immune responses needs to be elucidated in the future.

After the visualization, of the by the mutation strongest Go-Terms, pathways on a single gene level were analyzed in the following step.

4.7.1.5 KTRTK-Cofilin1 affects a number of genes in different pathways in vivo

For the identification of altered pathways based on single cells all analyzed gene fragments of the ANOVA were used. A link of the ANOVA to the KEGG (KEGG: Kyoto Encyclopedia of Genes and Genomes) database allows the detection of affected pathways on single gene level. A significance value is assigned to the respective pathway, depending on the percentage of genes altered within the pathway. This process is called pathway enrichment. The wildtype was used as reference. Down-regulation in the mutant brain was depicted in blue, whereas up- regulation in the mutant brain tissue was presented in red. Degree of up-/down-regulation correlates to the intensity of the color.

Two of the strongest affected pathways were “Regulation of actin cytoskeleton” (Figure 58) and “ECM receptor interaction” (data not shown).

Figure 58, shows a number of differently regulated genes. The strongest affected gene in this pathway based on fold-change was *FN1*, fibronectin 1, an extracellular matrix glycoprotein, that binds collagen and is involved in cell adhesion, cell growth, differentiation and migration (Pankov and Yamada, 2002). It is known that fibronectin is crucial for embryonic and neural development (George et al., 1993; Tate et al., 2007). Another gene that was up-regulated in expression was moesin (*ERM*). Moesin is part of the ERM protein family, involved in cross linking of actin filaments (Jankovics et al., 2002).

It should be noted that most of the genes presented in this pathway were not listed in the tables of genes with highest fold change. Pathway enrichment is based on the

number of altered genes and not on the fold-change. Therefor most of the genes depicted in this pathway showed a fold-change of less the ±1.6.

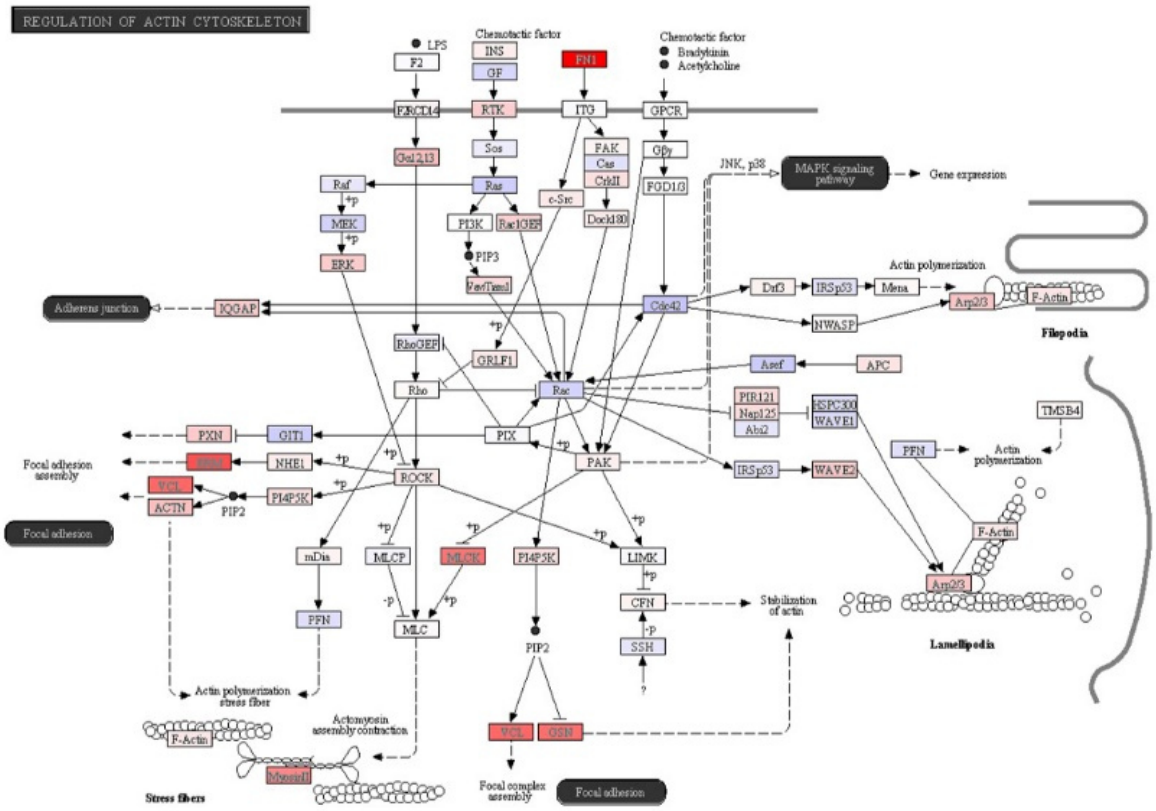

Fig. 58: Regulation of actin cytoskeleton in Cofilin1$^{wt/wt}$ vs. Cofilin1$^{KTRTK/KTRTK}$ brains (E16.5). Cofilin1$^{wt/wt}$ was used as reference, red color indicates up-regulation in Cofilin1$^{KTRTK/KTRTK}$, brain, down-regulation is shown in blue. Color intensity correlates with fold-change.

F-actin in this pathway codes beta actin (*Actb*), which is expressed brain, was up-regulated in the mutant by a factor of approximately +1.3.

From this pathway analysis it could be concluded that a large number of genes directly or indirectly involved in actin cytoskeleton regulation is altered concerning their expression level.

The pathway “ECM receptor interactions” presented a large number of strongly affected genes (data not shown). Extracellular matrix (ECM), consisting of a mixture structural and functional macromolecules, serves an important role in tissue and organ morphogenesis, amongst others in the brain (Bonneh-Barkay and Wiley, 2009).

Further, it is crucial for the maintenance of cell and tissue structure and function. Specific interactions between cells and the ECM, mediated by transmembrane molecules, lead to direct or indirect control of cellular activities such as adhesion, migration, differentiation, proliferation, and apoptosis.
The genes mainly affected in this pathway are fibronectin (see above), *OPN* (secreted phosphoprotein 1), *Perlecan*, *BSP* (integrin binding sialoprotein) and *VWF* (Von Willebrand factor homolog).

VWF encodes for a glycoprotein involved in platelet activation, cell adhesion and collagen binding. The integrin binding sialoprotein (BSP), a significant component of the bone extracellular matrix, is involved in cell adhesion, extracellular matrix organization and ossification. Perlecan can bind to and crosslink extracellular matrix components. It is also involved in brain development and chondrocyte differentiation (Giros et al., 2007). The protein encoded by *OPN* is primarily associated with bone and bone mineralization. In addition the protein has been linked to cell adhesion.
All these up-regulated extracellular matrix proteins interact with a number of integrins, transmembrane molecules, which mediate specific interactions between ECM and cells. Integrins also provide a link between the extracellular matrix and the cytoskeleton. So in consequence if the interaction of the ECM with integrins is disrupted, the interaction between the extracellular matrix and the cytoskeleton will be disrupted.

4.7.1.6 Mutant protein affects genes in pathways differently in vitro

In pathway enrichment, the wildtype was used as reference. Down-regulation in the mutant is depicted in blue, whereas up- regulation in the mutant tissue is presented in red. Degree of up- /down-regulation correlates to the intensity of the color.

In the analysis of Mefs one of the strongest affected pathways was “Regulation of actin cytoskeleton” (Figure 59).

Figure 59, shows a number of differently regulated genes. The strongest affected gene in this pathway is beta actin (*Actb*; F-actin), which was detected at an expression level of +2.62. PF*N*, profilin1, an actin monomer binding protein, that catalyzes the exchange

of ADP for ATP and thus replenishing ATP-actin subunits to the monomer pool ready to be used for assembly. Profilin1 expression was increased by a factor of +2.38. Levels of increased G- and F-actin were detected in the Mefs, this may also indicate the need for more profilin1 in the cells.

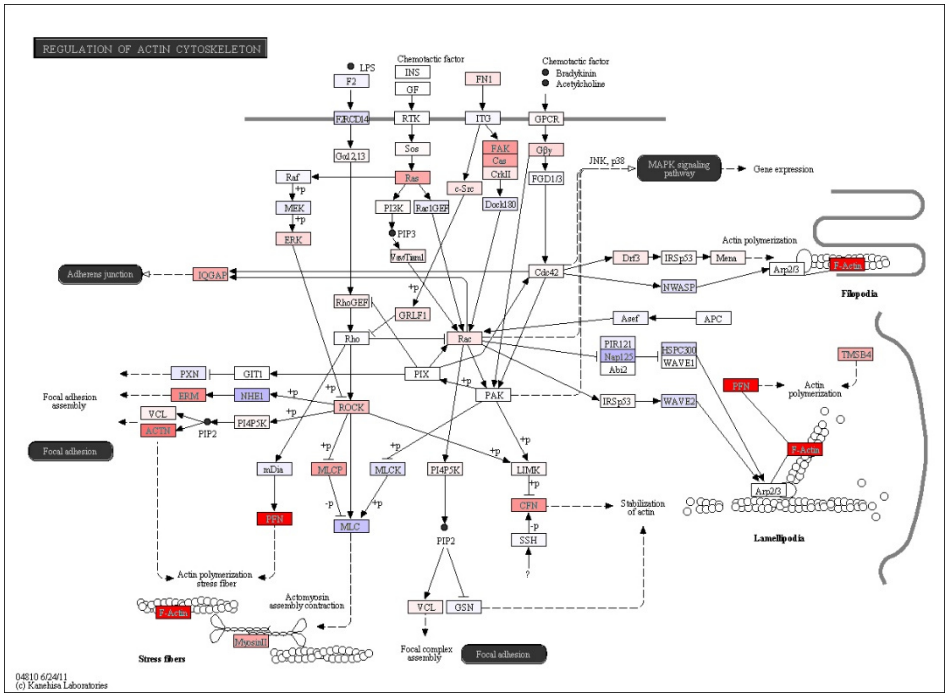

Fig. 59: Regulation of actin cytoskeleton in Cofilin1$^{wt/wt}$ vs Cofilin1$^{KTRTK/KTRTK}$ Mefs (E14.5, passage 1). Cofilin1$^{wt/wt}$ was used as reference, red color indicates up-regulation in Cofilin1$^{KTRTK/KTRTK}$, down- regulation is shown in blue. Color intensity correlates with fold-change.

Other than beta actin none of the affected genes presented in this pathway were listed in the table of genes with highest fold change. Pathway enrichment is based on the number of altered genes and not on the fold-change. Therefore most of the genes color depicted in this pathway showed a fold-change of less the ±1.3.

This concluded that a large number of genes directly or indirectly involved in actin cytoskeleton regulation is altered concerning their expression level. It should also be kept in mind, that other isoforms of actin are expressed at increased levels in Cofilin1$^{KTRTK/KTRTK}$ Mefs.

The gene expression analyses in microarrays concluded that a large number of genes are affected by the introduction of the mutation of the NTS of Cofilin1. The mutation affected genes involved in morphogenesis, extracellular matrix and actin regulation *in vivo* as well as *in vitro*.

5. Discussion

Cofilin1 plays a crucial role in the organism. It is essential for the regulation of actin dynamics, affecting locomotion, cytokinesis, migration and cell viability. Cofilin1 has an indispensable role in different physiological and developmental processes such as neural tube closure and cortical lamination (Bamburg, 1999; Dawe, 2003; Dawe et al., 2003; Gohla et al., 2005; Gurniak et al., 2005; Bellenchi et al., 2007). The members of the ADF/Cofilin family carry a conserved nuclear translocation signal (NTS), comprising the core amino acid sequence KKRKK. In analogy to the KTKTK mutation of the NTS introduced in Simian virus 40, which was shown to impair nuclear delivery of viral DNA (Nakanishi et al., 2002), the function of Cofilin1 (non-muscle Cofilin) carrying a mutated NTS with the sequence of KTRTK, named KTRTK-Cofilin1, has been analyzed in this study.

No other animal models presenting a mutation of the NTS of Cofilin1 have been published so far. The KTRTK-Cofilin1 mouse model represents the first *in vivo* model to study the repercussions of a mutated NTS. The impact of KTRTK-Cofilin1 on embryonic development and cellular processes have been focus of interest.

5.1 The KTRTK-Cofilin1 protein featured altered characteristics

Cofilin1 is primarily associated with the turnover of F-actin. For years studies strongly implied that Cofilin1 may be involved in other processes than the severing and depolymerisation of actin filaments.

Previous studies analyzed nuclear translocation and actin binding capacities of Cofilin1-NTS mutants *in vitro*. Cofilin1 and actin form bundles, so called rods, upon certain stress stimuli. Exposure to salt buffers induce cytoplasmic rods in mammalian cells, whereas DMSO and heat shock induce formation of nuclear rods (Iida and Yahara, 1986; Nishida et al., 1987). Rods are composed of ADF/Cofilin and actin in a 1:1 ratio, vary in filament length and are reversible structures. The function of rods is not clear but their frequent appearance in various tissues, suggest a physiological function (Minamide et al., 2010). Nuclear actin rods are formed from actin monomers obtained from disassembled cytoplasmic F-actin (Sanger et al., 1980).

Iida et al. analyzed KTLKK-Cofilin1 and showed the inability of the mutated to translocate to the nucleus and form nuclear rods (Iida et al., 1992). Munsie et al reported a bipartite NLS in the form of "21-RKSSTPEEVKKRKK-34" in Cofilin1. Both parts (underlined amino acids) of the bipartite NLS are evolutionary conserved between different species for both Cofilin1 and Cofilin2. Munsie and team demonstrated the inability of Cofilin1 NTS mutants, in which the sequence was mutated to AASSTPEEVKAAKK, to form nuclear and cytoplasmic rods. Additional sedimentation assays revealed a reduced F-actin binding capacity, but *in vitro* assays verified retained ability of analyzed mutants to interact with actin (Munsie et al., 2012). It was shown that HeLa cells transfected with GFP-KTRTK-Cofilin1 were unable to form nuclear actin/KTRTK-Cofilin1 rods upon DMSO treatment (Figure 17) (Roy, 2011). Upon salt buffer treatment of HeLa cells transfected with GFP-KTRTK-Cofilin1 no induction of cytoplasmic rods could be detected (Marx, 2011). These data may also indicate that the mutation of the NTS, even though it is not located near the actin binding site, may have altered the affinity of the mutant protein for actin.

Further contributing to this suggestion are actin assays that showed massively decreased severing activity and F-actin binding of KTRTK-Cofilin1 (Figurer 18+19). Altered actin binding characteristics might also affect the ability of KTRTK-Cofilin1 to shuffle actin to the nucleus. The Cofilin1 knockout is embryonic lethal around E10 (Gurniak et al., 2005), whereas homozygous Cofilin1$^{KTRTK/KTRTK}$ embryos can be found until the point of birth concluding that KTRTK-Cofilin1 maintained a level of activity. Cofilin1$^{KTRTK/KTRTK}$ embryos displayed a cranial tube closure defect in the form of exencephaly (Figure 20). Mouse embryonic fibroblasts (Mefs) derived from homozygous mutants displayed a conspicuous enlarged morphology and a significant increase in multinucleate cells. Furthermore, Cofilin1$^{KTRTK/KTRTK}$ Mefs showed a cytokinesis defect and decreased proliferation rates (4.4).

The data of Munsie coincide with our observed inability of KTRTK-Cofilin1 to form nuclear rods (Figure 17), but maintaining part of the original depolymerization activity and reduced F-actin binding capacity (Figure 18+19). In the future the binding capacity of KTRTK-Cofilin1 regarding F-actin should be analyzed in detail. It should also be studied, if the mutation caused structural changes, potentially affecting functionality and actin binding capacities of KTRTK-Cofilin1. To further understand the role of Cofilin1 it would be of interest to analyze cytoplasmic and nuclear binding partners of wildtype Cofilin1 in comparison to KTRTK-Cofilin1. Previous studies examined binding

partners for the members of the ADF/ Cofilin family in adult brain utilizing Streptag fusion proteins via Malditof (Meier, 2014). A Strep-KTRTK-Cofilin1 fusion protein should be generated and lysates from embryonic as well as adult brain should be analyzed along with Mef lysates to conclude which binding partners might be affected in the cell in general and additionally in specific cell types.

5.2 The role of Cofilin1 in the nucleus

Previous studies showed that upon stress stimuli, like heat shock or DMSO, the nuclear translocation of Cofilin1 can be induced (Iida et al., 1986; Nishida et al., 1987; Iida et al., 1992) (5.1). Cofilin1 is also present in the nucleus of normally growing cultured cells, therefore it was suggested that Cofilin1, besides its role as actin depolymerizing factor in the cytoplasm, also has a function in the nucleus (Iida et al., 1992). This assumption has been confirmed by various studies linking nuclear Cofilin1 to transcription (Obrdlik and Percipalle, 2011; Dopie et al., 2012). Tissue from Cofilin1$^{KTRTK/KTRTK}$ displayed severely changed gene expression profiles in brains and Mefs. The involvement of nuclear Cofilin1 in transcriptional regulation will be discussed in chapter 5.9

Additionally to the importance for embryonic brain development, cell cycle and proliferation, processes that were affected by the mutation of the nuclear translocation sequence of Cofilin1 (see chapter 4), nuclear Cofilin1 has been linked to DNA damage. The interaction between Cofilin1 and DNA may influence various biological responses, including DNA damage repair, a biological process essential in cancer development (Chang et al., 2015). Nuclear Cofilin1 has also been linked to neurodegenerative diseases. The accumulation of nuclear rods has been observed in Huntington's disease (HD) patients, but their role in HD still needs to be clarified. Therefore rod formation, as an early on event in the neurodegenerative cascade, is considered a target for therapeutic access (Bamburg et al., 2010). If alterations of nuclear translocation always affect depolymerizing and F-actin binding capacity, adverse defects could be profound. Further, if nuclear Cofilin1 is crucial for transcriptional regulation, targeting nuclear Cofilin1 for therapy would not be an option. Therefore, elucidating the role of Cofilin1 in the nucleus is of utter importance

5.3 Protein expression level of KTRTK-Cofilin1 decreased during embryonic development can not be compensated by the other members of the ADF/Cofilin family

An essential role of Cofilin1 has been presented in various species. The deletion of Cofilin1 results in lethality in mouse, yeast, fruit fly and the blastomere of xenopus (Bamburg, 1999; Bamburg et al., 1999; Gurniak et al., 2005). These species have different numbers of isoforms to compensate the loss of Cofilin1. In the mouse two other isoforms are known, ADF and Cofilin2. Even though ADF and Cofilin1 share a sequence identity of 73% and functional characteristics (Bamburg, 1999; Vartiainen et al., 2002), respective mouse mutants show extremely different phenotypes, indicating non-redundant roles of Cofilin1 and ADF. Further, the relative expression levels of the members of the ADF/Cofilin family are restricted in a spatial and temporal- specific manner (Gurniak et al., 2005; Van Troys et al., 2008).

The decrease of KTRTK-Cofilin1 protein level was observed during embryonic development in brain and body from heterozygous to mutant. The bodies of Cofilin1$^{KTRTK/KTRTK}$ embryos showed to phenotype, indicating that Cofilin1 is not essential for the development of the body.

The decrease of KTRTK-Cofilin1 protein level during development could not be elucidated (4.3). It was shown that the mutant protein was not lost due to change in solubility, altered stability or changed levels of total RNA. In the future the loss of KTRTK-Cofilin1 during development needs to be studied further. Two microRNAs (miRNAs), noncoding RNAs binding the 3' untranslated region (UTR) of mRNAs and mainly repressing translation were identified, specifically repressing Cofilin1 translation. Yao and team observed a comparable phenomenon. Cofilin1 mRNAs levels remained unchanged even though a distinct up-regulation of Cofilin1 on protein level could be detected in the mouse model (Yao et al., 2010). The loss of KTRTK-Cofilin1 might be caused by an increased affinity of other repressive miRNAs, usually specific to other RNA sequences, for the mutant RNA and therefore reducing the translation of the mutant protein. EWS, a proto-oncogene, represses nuclear export or translation, of its target mRNAs. EWS is known to target Cofilin1 mRNA, repressing

expression by nuclear retention of Cofilin1 mRNA (Huang et al., 2014). An increased nuclear retention of KTRTK-Cofilin1 mRNA would also lead to a repression of KTRTK-Cofilin1 translation. The bipartite NLS is connected by a unique intervening sequence, a conserved serine, serine, threonine (SST) motif, is part of this intervening sequence. The SST motif was proposed to be a target for post-translational modification and is currently the subject of further investigation (Munsie et al., 2012). It needs to be elucidated whether post-translational modification in the form of ubiquitination is altered in KTRTK-Cofilin1 for any reason.

The loss of Cofilin2 and ADF can be compensated to a certain extent. Cofilin2$^{-/-}$ mice are viable past birth and die on postnatal day 10, due to respiratory problems and diaphragm abnormity (Gurniak et al., 2014). The brain shows no obvious malformations (Gurniak and Bläsius, unpublished). ADF deficient mice display a mild hyperplasia of the cornea but show no further obvious malformations (Bellenchi et al., 2007). Protein level analyses showed no up-regulation of Cofilin1 in the ADF$^{-/-}$mutant brain, the expression level of Cofilin2 was not analyzed. In Cofilin1$^{-/-}$ E10 embryos ADF was up-regulated, whereas Cofilin2 remained unchanged (Gurniak et al., 2005; Bellenchi et al., 2007). The loss of Cofilin1 can not be compensated by ADF or Cofilin2. This assumption was also strongly implied by the data acquired in this thesis. ADF and Cofilin2 are not only unable to rescue the phenotypes in consequence to the complete loss of Cofilin1 but also the altered functions of KTRTK-Cofilin1. The mutant protein showed a reduced actin binding ability, a decreased depolymerization activity and was no longer able to translocate to the nucleus, even though all the features were unaffected in ADF and Cofilin2 the exencephalic phenotype could not be rescued. The up-regulation of ADF as well as Cofilin2, observed *in vivo* and *in vitro* (Figure 24+28), could not rescue the observed phenotype. It is not surprising that the phenotype *in vivo* was not compensated by the increased expression of ADF and Cofilin2, observed at later stages in development (Figure 23+24). At E10.5, a time point at which the exencephaly was already pronounced, no up-regulation of ADF and Cofilin2 was detected but both proteins were expressed along with KTRTK-Cofilin1 (Figure 23). The critical time point of neural tube closure occurs at E8.5–E9.5 (see 5.5), a developmental stage at which KTRTK-Cofilin1 is still present but affects cranial development and brain morphology. Even though Cofilin1$^{KTRTK/KTRTK}$ bodies also displayed decreasing KTRTK-Cofilin1 levels they had no phenotype. Mefs derived from mutants were phenotypically clearly distinguishable from wildtype control (4.4). In

passage 1 when KTRTK-Cofilin1 was still expressed Mefs already showed significant morphological and proliferation rate differences (Figure 30+33). In passages 2+3 when KTRTK-Cofilin1 was down-regulated and ADF and Cofilin2 up-regulated the phenotype of mutant Mefs remained consistent (Figure 28+30). The members of the ADF/Cofilin family are involved in cell polarization and migration, fundamental features of embryonic development. This study further showed that ADF and Cofilin2 could not countervail the reduced KTRTK-Cofilin1 with its altered biochemical properties was not sufficient for normal development, whereas heterozygous Cofilin1$^{wt/KTRTK}$ and Cofilin1$^{+/-}$ animals are completely healthy, showing that one wt-Cofilin1 is sufficient for normal development. This circumstantiates the absolute necessity of Cofilin1 in embryonic development and the inability of ADF and Cofilin2 to compensate even the mere mutant protein.

To what degree the phenotype would alter or gain in severity without the up-regulation of ADF and Cofilin2 can not be predicted at this stage. Analyzing compensatory functions of both proteins simultaneously would proof to be extremely difficult in the embryo, considering that depletion of both, ADF and Cofilin2, is most likely to be lethal. To analyze the compensatory functions *in vitro*, it would be helpful to generate Cofilin1$^{KTRTK/KTRTK}$; ADF$^{-/-}$; Cofilin2$^{-/-}$ compound Mefs with the help of a tamoxifen inducible Cre/loxP site specific recombination system, based on a chimeric Cre protein carrying a ligand binding domain of a mutated estrogen receptor (Mer), called CreMer (Littlewood et al., 1995). The generation of Cofilin1$^{wt/KTRTK}$; ADF$^{fl/fl}$; Cofilin2$^{fl/fl}$ should not be lethal. By mating these animals, embryos homozygous for KTRTK-Cofilin1 could be created. After isolation of Mefs the CreMer system could be activated facilitating the excision of the floxed ADF and Cofilin2 genes. For analyses regarding compensatory function during embryonic development, the generation of compound mutants in the form of ADF$^{-/-}$, Cofilin1$^{KTRTK/KTRTK}$ and Cofilin2$^{-/-}$, Cofilin1$^{KTRTK/KTRTK}$ would ensure a more efficient deletion of the respective protein.

These data lead to the solid conclusion that a normal activity spectrum of Cofilin1 is essential for normal brain development and in cellular processes and can not be compensated by ADF and Cofilin2. Aspects of protein structure in general and altering protein structure during development regarding KTRTK-Cofilin1 were not approached so far. Structural analysis will also provide further conclusion regarding the functionality spectrum of the mutant protein. In future it will have to be approached whether the

phenotype in Mefs and embryos results from reduced F-actin depolymerization activity, reduced actin binding, diminished protein levels or nuclear translocation or a combination of these factors. Cofilin1 is crucial for embryonic development since a knockout of Cofilin1 results in embryonic lethality around day E10 (Gurniak et al, 2005). Analysis of homozygous KTRTK-Cofilin1 embryos at different stages of embryonic development showed decreases of KTRTK-Cofilin1 protein levels with increasing age. Possibly indicating, that at some point in embryonic development Cofilin1 loses its essential status for development and potentially also altering its range of binding partners during development. The fact that Cofilin1$^{KTRTK/KTRTK}$ embryos are alive until birth leads to the conclusion that the KTRTK-Cofilin1 protein still retains at least parts of the original functional capability of Cofilin1. In addition the decrease of KTRTK-Cofilin1 protein level will have to be analyzed further. Two possible targets of future investigations could be a change in nuclear retention of KTRTK-Cofilin1 RNA and different translational regulation by miRNAs.

5.4 Cellular mechanisms are affected in Cofilin1$^{KTRTK/KTRTK}$ Mefs

In eukaryotic cells significant functions for cell viability are confined to the nucleus. Processes like proliferation, cytokinesis and gene expression are dependent on actin and Cofilin1. Cofilin1$^{KTRTK/KTRTK}$ Mefs were characterized by an enlarged cell size, multinuclearity and reduced proliferation rates. *In vitro* assays showed a reduced depolymerizing activity for the mutant protein (Figure 18). The decreased capacity of KTRTK-Cofilin1 may alter the statics of the actin filaments. The structural change may influence cell attachment. In the progress of the study the suspicion arose that cell attachment and spreading might be influenced by the mutation. Therefore in the future cell adhesion assays, comparing Cofilin1$^{wt/wt}$ and Coflin1$^{KTRTK/KTRK}$ Mefs, should be performed. Actin filaments are important for cell attachment and spreading on the substratum, a process required for cell proliferation. Further, defects in cell cycle progression were observed (Figure 31). KTRTK-Cofilin1 Mefs were observed to comprise up-regulated levels of F- and G-actin by 1.75- and 1.65-fold, respectively (Figure 36). Actin is required for cell division. The altered features of KTRTK-Cofilin1

may also explain the incorrect G1 to G2/M– phase transition (4.4.3). Several previous studies indicated a role for Cofilin1 in the cell cycle. Alteration of Cofilin1 activity resulted in the formation of multinuclear cells in different model organisms (e.g. HeLa), probably resulting from defects in cytokinesis (Gohla et al., 2005). A significantly increased incidence of multinucleated Mefs derived from Coflin1$^{KTRTK/KTRK}$ embryos was detected (Figure 30). Wt-Cofilin1 was observed to concentrate at the contractile ring in the telophase of the cell cycle, accumulating rapidly at the cleavage furrow as cleavage proceeded. Therefore it was suggested that wt-Cofilin1 disassembles F-actin in the contractile ring at the late stages of cytokinesis (Nagaoka et al., 1995), something that KTRTK-Cofilin1 can not do. Cell cycle analysis of Cofilin1 deficient embryonic cells proved the importance of Cofilin1 for G2/M-phase transition, based on the increased number of 4n cells observed (Bellenchi et al., 2007). The acquired data implicated that not only the deletion of Cofilin1 but also the mutated KTRTK-Cofilin1, with reduced activity leads to a disturbance in the transgression from the G2/M-phase (4n) to the G1-phase (2n).
Osteoclast-like cells, featuring enlarged morphology and multinuclearity have been identified it the past (Ibbotson et al., 1984). In consideration of the enlarged and multinucleate phenotype along with the altered expression of genes involved in ossification and skeletal morphogenesis that have been identified in gene expression level analysis in microarrays of Mefs, it might be of interest whether Cofilin1$^{KTRTK/KTRTK}$ Mefs adapt an osteoclast-like character.

Taking the reduced depolymerizing capacity of KTRTK-Cofilin1, the increased levels of F-actin and the possible alterations of F-actin statics into consideration, this would be an explanation for the problems in cell cycle transgression and the resulting polyploidy, acquiescing to the role of Cofilin1 in the cell cycle.

Cofilin1$^{KTRTK/KTRTK}$ Mefs displayed significantly slower proliferation rates than Cofilin1$^{wt/wt}$ Mefs in passages 0-2. In passage 1 the proliferation rate in wt Mefs was increased by 2.3-fold compared to mutant Mefs (Figure 33). Previous studies connected proliferation defects to reduced embryonic body size (Yao et al., 1998; Bi et al., 1999; Ruland et al., 2001; Tominaga et al., 2005). P300 acts as a transcriptional activator, P300 knockout embryos, exhibited pleiotropic defects in morphogenesis in the form of exencephaly, transcriptional defects along with severe deficiencies in proliferation (Yao et al., 1998). Deletion of Mrg15, a chromodomain protein, in mice

also results in proliferation defects and smaller body sizes compared to wildtype embryos. Mgr15$^{-/-}$ Mefs showed a significantly lower growth rate and were characterized by an enlarged and flattened morphology along with earlier occurrence of senescence. An earlier and increased occurrence of senescence was also observed in Cofilin1$^{KTRTK/KTRTK}$ Mefs in passage 4 (4.4.2.4). Mrg15 is potentially involved in global transcription control and essential for mitotic proliferation and regulation of growth during embryogenesis (Tominaga et al., 2005). The same characteristic features could be observed in Cofilin1$^{KTRTK/KTRTK}$ embryos and Mefs (Figure 20+30). The body size of Cofilin1$^{KTRTK/KTRTK}$ embryos was reduced compared to wildtype and heterozygous littermates (Figure 20). Proliferation assays for cells derived from Cofilin1$^{KTRTK/KTRTK}$ bodies showed decelerated proliferation rates compared to wildtype samples (Figure 33). Nuclear actin is also associated with proliferation. Early studies reported increases of nuclear actin concentration in mouse fibroblasts depending on the proliferative state of the cell, while the cytoplasmic level remained unchanged (Bertram et al., 1977). Disruption of nuclear actin levels in Cofilin1$^{KTRTK/KTRTK}$ Mefs might also affect proliferation. Dysregulation of proliferation and cell growth may cause small- sized phenotype. The phenotypically increased cell size of Cofilin1$^{KTRTK/KTRTK}$ Mefs and smaller body size Cofilin1$^{KTRTK/KTRTK}$ embryos might indicate that Cofilin1 directly or indirectly regulates negative as well as positive cell growth. Analysis of proliferative zones in Cofilin1$^{wt/wt}$ and Cofilin1$^{KTRTK/KTRTK}$ E13.5 brains showed an increase of number of proliferating cells but did not allow any conclusions regarding the proliferation rate (Figure 49).

In the past a relationship between nuclear actin and ECM has been suggested, enacting changes in transcriptional profiles (Spencer, 2011). The analyses of transcription profiles revealed significant up-regulation of extracellular matrix protein genes in Cofilin1$^{KTRTK/KTRTK}$ E16.5 brains and E14.5 Mefs (Figure 56+57).Therefore, KTRTK-Cofilin1 may affect transcription profiles indirectly by impacting nuclear actin. Cofilin1 was also linked to transcription by facilitating association of elongating Pol II and actin with active genes (Obrdlik and Percipalle, 2011). The mutation of the Cofilin1 gene in mice demonstrated its essential role in embryogenesis by cell morphology, proliferation and cytokinesis.

Morphological analysis of Cofilin1$^{KTRTK/KTRTK}$ astrocytes also revealed increased occurrence of multinucleate cells (4.6.1). In the next step proliferation and cytokinesis

of astrocytes should be studied in detail, analyzing whether the observed alterations in Mefs also extend to astrocytes. The determination of G-actin/F-actin levels of astrocytes and neurons will also be of great interest, concluding whether the reduced activity of KTRTK-Cofilin1 could impact on neural cells *in vitro*.

5.5 Cofilin1 is essential for cranial neurulation

The expression pattern of Cofilin1 changes during development. At E8.5 expression of Cofilin1 is highest in the neural fold and at E9.5 its expression continues during the development of the nervous system and the neural crest. At E10.5 Cofilin1 expression was detected in somites, neural tube and limb buds. Afterward the expression of Cofilin1 becomes more localized (Gurniak et al., 2005). The expression pattern of Cofilin1 suggests an essential role in neural tube formation. Studies showed that Cofilin1 is a genetic modifier of neural tube closure. In humans single-nucleotide polymorphisms of Cofilin1 increase the risk for spina bifida (Zhu et al., 2007). As mentioned above deletion of Cofilin1 in the mouse resulted in a complete lack of neural tube closure and misaligned somites (Gurniak et al., 2005).

Examination of the body showed no obvious malformations. Skeletal isolation showed no vertebrae misalignment (Figure 38), verifying the presence and a functionality of KTRTK- Coflin1 at that the critical stage for somite alignment. Further, the top cervical vertebrae (C1) in the mutant seemed to be affected (Figure 38, C+D). In the mutant C1 appeared to be enlarged in comparison to the top cervical vertebrae in wildtype.

Cofilin1is a key player in neurulation, preceding cranial neurulation, which is affected Cofilin1$^{KTRTK/KTRTK}$ embryos.

Examining the skeletal isolation of the embryos, the most striking feature is the failure of the formation of the calvarial dermatocranium in Cofilin1$^{KTRTK/KTRTK}$ embryos (Figure 38, B). Up to this point, not a lot is known regarding the role of Cofilin1 and bone morphogenesis. Defective skull development is a primary failure of skeletal tissue formation and does not result from a secondary degenerative process. In was shown that both neural and skeletal development are contingent upon normal cranial tube closure (Copp, 2005).

Intramembranous ossification, a process in which mesenchymal cells condense without forming a cartilage intermediate, forms a part of the craniofacial bones. Cranial neural tube closure is crucial for the initial formation of the major part of the skull. Cranial mesenchyme and cranial neural crest also contribute to the formation of the skull vault (Jiang et al., 2002). In this process the embryonic brain is used as a physical “mold” around which the skull vault is formed (Thorogood, 1994). Cranial mesenchyme is over-presented in Cofilin1$^{KTRTK/KTRTK}$ brain (Figure 42).Neural crest cells require Cofilin1 for migration, therefore KTRTK-Cofilin1 might impact migratory behavior of neural crest cells.

In exencephalic embryos, the absence of dorsal neural tissue causes the failure of the formation of dorsal skull elements (Copp, 2005) and can be observed in Cofilin1$^{KTRTK/KTRTK}$ embryos.

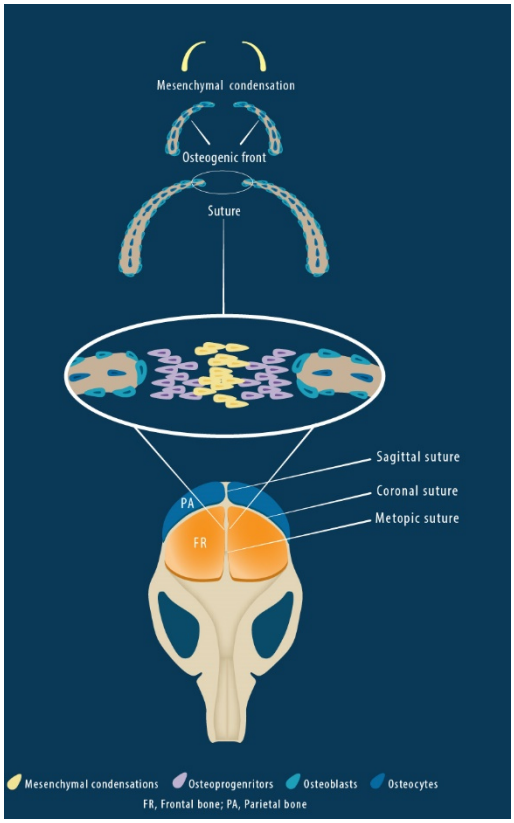

Fig. 60: Murine skull bone development. At the suture site, cells in mesenchymal condensations differentiate to form osteoprogenitor cells, which later differentiate into bone-matrix molecules-producing osteoblasts. These osteoblasts later differentiate into osteocytes, which become embedded within the bone matrix. (COMPENDIUM, 2014)

Mesenchymal condensations on the lateral side of the head start at E12.5, in murine development, to eventually yield the frontal bones. Primordia of these bones, a cellular mass bearing osteogenic activity, lie basolaterally of the brain, extending to the vertex of the skull, starting at E13.5. At E14.5, the osteoblasts in these osteogenic fronts differentiate to produce a bone matrix. Extensions of the cellular masses meet at the midline, where a suture is formed, at E15.5 (Figure 60) (Rossant and Tam, 2002; Yoshida et al., 2008). However, a different study showed a significant up-regulation of Cofilin1 in sheep in the process of bone fracture healing (Guo et al., 2015), linking the protein to bone morphogenesis for the first time. Also the elevated expression of genes (Tables S8 - S24; Brain),

expressed in many different cell types, including osteoclast, chondrocytes and mesenchymal cells are a direct reflection of the upset tissue homeostasis in the mutant tissue, confirming the importance of Cofilin1 in the patterning and homeostasis process. At this point it should be taken into consideration, that both performed microarrays (4.7) in individual tissues, demonstrated changes in a vast number of genes involved in bone morphogenesis and cartilage formation.

5.6 Is the Cofilin1$^{KTRTK/KTRTK}$ brain everted?

Disturbances of several rather different cellular mechanisms, including actin cytoskeleton regulation, neural crest migration and cell cycle progression can cause exencephaly (Wilson and Center, 1974; Wilson, 1980; Copp et al., 2003; Copp, 2005). Cofilin1 was proven to be associated with these mechanisms (Gohla et al., 2005; Gurniak et al., 2005; Bellenchi et al., 2007). Cranial neurulation, a complex morphogenetic process, is fundamental for the development of brain and head. Failure of one or more events of cranial neurulation results in exencephaly, the most abundant type of neural tube closure defect. Morphologically, exencephaly results from everted, unfused cranial neural folds, creating the appearance of excessive neural tissue, as observed in Cofilin1$^{KTRTK/KTRTK}$ brains. A congenital malformation following failed neural tube closure. Previous studies identified a functional actin cytoskeleton, emigration of neural crest cells, spatio-temporally regulated apoptosis and a balance between cell proliferation and the onset of neuronal differentiation as requirements normal dorsolateral bending (Chua et al., 2003; Copp, 2005; Rehklau et al., 2012). Altered neuronal differentiation within the neuroepithelium could render the neural plate inflexible, thus preventing dorsolateral bending. The increase of F-actin was observed in KTRTK-Cofilin1 brain, which might contribute to an inflexible neural plate. Also the release of neural crest cells could be altered or the adhesion process essential for neural fold fusion could suffer interference (Copp et al., 2005).

Taking the β-III-tubulin staining (Figure 49) and the Nissl staining (Figure 46) into consideration, the folded finger-like structures may coincide with the cortex (Figure 42). The Nissl staining showed cortical layering in coronal and sagittal sections of embryonic wt brain (Figure 46). Examining the coronal sections stained with

haematoxilin and eosin along with the Nissl staining, brain structures appear to be shifted laterally. The Nissl staining of the coronal section of the Cofilin1$^{KTRTK/KTRTK}$ brain showed layered structures, reminiscent of cortical layering, above eyes (Figure 46, D). The cortical layering in this structure within the Cofilin1$^{KTRTK/KTRTK}$ brain corresponds to a sagittal section layering of the cortex. Based on BrdU and H+E stainings hypothetical schematic models were created for the mutant brain in comparison to the wildtype (Figure 61).

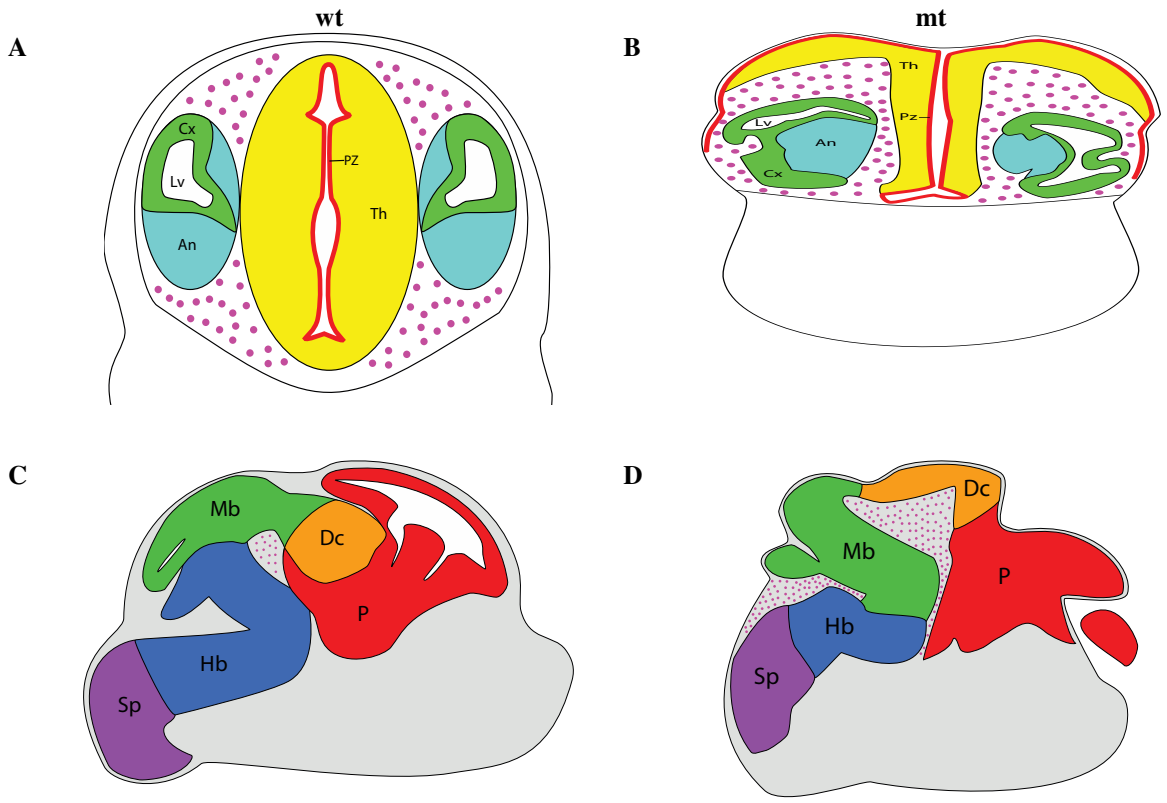

Fig. 61 Hypothetical coronal (A+B) and sagittal (C+D) schematic model of brain areas in Cofilin1$^{KTRTK/KTRTK}$ brain. Based on the BrdU staining a hypothetical schematic coronal model, showing the proliferative zone and presumed brain areas, was created. Everted expression pattern could be observed in the mutant brain (mt) (**B**) compared to Cofilin1$^{wt/wt}$ E13.5 brain (wt) (**A**). Compared to wildtype, proliferative zone and brain areas in the mutant seem to shift upward and laterally. Based on H+E staining a hypothetical sagittal schematic model of brain areas in the mutant brain, was created (**D**). In the mutant all brain areas appeared to be conserved but the prosencephalon was shifted to the anterior and less compartmentalized compared to the wt brain (**C**). Schematic models were previously shown in chapter 4.5. An: amygdaloid nucleus Cx: cortex; Ey: eye; Hp: hippocampus; LGE: lateral ganglionic eminence; Lv: lateral ventricle; MGE: medial ganglionic eminence; PZ: proliferative zone; Th: thalamus; Tv: third ventricle; Connective tissue: pink dots Dc: diencephalon; Hb: hindbrain; Mb: midbrain; P: prosencephalon; Sp: spinal cord; wt: Cofilin1 $^{wt/wt}$; mt: Cofilin1$^{KTRTK/KTRTK}$.

The BrdU proliferation staining of coronal section also indicate an upward and lateral shift of the brain structures in the Cofilin1$^{KTRTK/KTRTK}$ brain. In the wildtype a proliferative active zone was clearly detectable, surrounding the third ventricle (Figure 61, B). In Cofilin1$^{KTRTK/KTRTK}$ brain proliferating cells were detected on the margin of the “T-shaped ventricle” (Figure 42. Indicated by *I) and along the complete outer layer of the brain (Figure 61, B). Morphology in sagittal section indicated a preservation of the Cofilin1$^{KTRTK/KTRTK}$ brain areas but a spatial rearrangement (Figure 61, D).

Closer observation of the sagittal sections of Cofilin1$^{KTRTK/KTRTK}$ brains indicated that the morphology of the spinal cord and the hindbrain were conserved and not affected by KTRTK-Cofilin1 (Figure 61). It could be speculated that in Cofilin1$^{KTRTK/KTRTK}$ embryos brain structures shift to the anterior. Examining the brain structures it could be hypothesized that the midbrain in the mutant is morphologically altered and repositioned (Figure 61, Mb, green). The repositioned midbrain was connected to the structure, corresponding to the diencephalon (Figure 61, Dc, orange). In the mutant, the fusion of midbrain and diencephalon, takes place without the curved manner, which can be observed in the wildtype. Subsequently, this lead to the enlarged ventricle, filled with connective tissue (Figure 61, pink dots). Adjacent to the diencephalon the prosencephalon could be hypothesized (Figure 43, P, red). The presumed prosencephalon in the mutant appears to be enlarged and less compartmentalized. In the future the presumed identity of midbrain and diencephalon will have to be confirmed with specific markers.

Differently, irregulatory folded structures of the defectively developing telencephalon might be caused by a lateral and anterior shift of brain structures.

Across vertebrate phylogeny, morphology of different brain regions is variable. Even though the mechanisms generating brain patterning during development are much conserved (Hauptmann and Gerster, 2000; Medina et al., 2005), mechanism underlying the formation of these distinct morphologies are not understood to this day. Two major variations of the telencephalon formation have been observed across vertebrates. All vertebrates, but ray- finned fish, are characterized by an evaginated telencephalon (Folgueira et al., 2012).

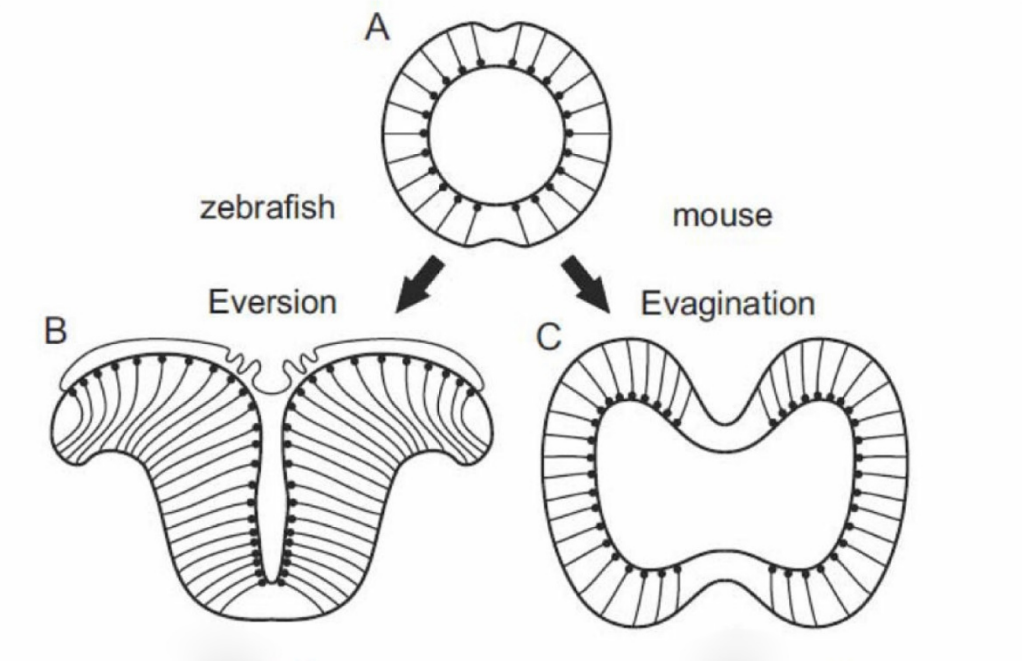

Fig. 62: Development of the telencephalon in teleosts and mammals. (A) Coronal view of the vertebrate anterior neural tube giving rise to the telencephalon. (B) The teleostean telencephalic outward folding (eversion) leads to a dorsal telencephalon (pallium). (C) The mammalian (mouse) telencephalon develops through evagination. Proliferative zones are inwardly oriented towards the ventricle. Pallial divisions in mouse simplified (Mueller et al., 2011).

The mechanisms of eversion has not been elucidated so far. There are two proposed models. First model describes the outward bending of the lateral wall of the telencephalon, resulting in a lateral out-folding of the pallium over the subpallium (Figure 62) (Nieuwenhuys, 2011). The recently proposed second model describes two key steps in telencephalon eversion. Step 1 is characterized by the generation of a ventricular sulcus at the telencephalic-diencephalic interphase, a step depending on precise cytoskeletal control. Step 2 involves the expansion of the pallial territory (Folgueira et al., 2012). Figure 40 indicates severe diencephalon malformation, concluding disturbances in early telencephalon morphogenesis. Comparing the NTS of murine Cofilin1 to ray-finned fish Cofilin1, revealed common characteristics of KTRTK-Cofilin1 and ray-finned fish Cofilin1.

The forebrain of Cofilin1$^{KTRTK/KTRTK}$ embryos, two lobes separated by a T-shaped ventricle, features morphological characteristics typical for the everted telencephalon (Figure 42, C). Cofilin1$^{wt/wt}$ brains display the expected traits of an evaginated telencephalon, two hemispheres surrounding the ventricle (Figure 61, B). Considering

the phenotype of the mutant brain this could implicate a key role for Cofilin1 in evaginated brain development. To further pursue this prospect a zebrafish Cofilin1 comprising the murine wildtype NTS mutant is currently being generated as control. Cofilin1 is crucial for zebrafish development (Ashworth et al., 2010). Following the introduction of KKRKK- Cofilin1 into the zebrafish, effects on embryonic development, particularly in regard to possible evaginated telencephalon development, will be of interest.

No literature describing an everted mouse brain phenotype could be found. Region-specific proliferation was proposed to be crucial for accurate regionalization (Zaki et al., 2003). Analysis of proliferating cells detected an increase of the proliferative zone in the mutant brain, *in vitro* analyses revealed significant decreases in proliferation rate and disturbances in G2/M cell cycle progression in KTRTK-Cofilin1 Mefs (Figure 33+31). Previous studies showed that also changes in cell cycle progression are involved in subregional patterning of the brain (Estivill-Torrus et al., 2002). Mutations leading to hypoplasia of the telencephalic tissue correlating with mitosis disturbances have been observed (Rossant and Tam, 2002). This would coincide with the observations made in Cofilin1$^{KTRTK/KTRTK}$ mutants. An inability of KTRTK-Cofilin1 to properly regulate proliferation and cell cycle progression of neuroepithelial cells could contribute to the phenotype.

A significant number of cells undergo programmed cell death at E10.5 in the forebrain (Rossant and Tam, 2002). Over the last years contrary data regarding the role of Cofilin1 in apoptosis were published. Chua et al., suggested that Cofilin1 has an essential role during the initiation phase of apoptosis (Chua et al., 2003). Whereas a more recent study indicated that Cofilin1 is generally not required for induction or progression of apoptosis (Rehklau et al., 2012). It should be taken into consideration though, that it has been postulated, that alterations of levels of Cofilin1 affects apoptosis progression in specific cell types, indicating the existence of cell-type-specific function for Cofilin1 in apoptosis signaling. Furthermore, It has been proposed that the apoptosis-inducing ability of Cofilin1, is dependent on the functional actin-binding domain (Chua et al., 2003; Klamt et al., 2009). KTRTK-Cofilin1 showed characteristics of reduced F-actin binding in quenching assays (Figure 19). Though no implication regarding altered apoptosis levels could be found in Caspase3 stainings or

on gene expression levels in E14.5 Mefs and E16.5 mutant brains (data not shown), apoptosis should be studied in vivo in early embryonic development.

Comparative analyses of Cofilin1$^{wt/wt}$ and Cofilin1$^{KTRTK/KTRTK}$ brains revealed distinct differences in morphological structures (Figure 42). Coronal sections revealed defined and symmetric structures in the mutant brain (Figure 42, D-F). Loose, low density tissue was detected in in coronal and sagittal sections, filling up cavities in the mutant (Figure 42). Further experiments identified, the tissue in question as connective tissue of expanded mesenchymal origin (Figure 45). During development of the brain, neural folds elevate in a process involving the bending of the midline neuroepethilium and the expansion of the underlying cranial mesenchyme (Copp, 2005). Microarrays showed a vast increase of collagen gene expression in the mutant brain, one of the main components of mesenchymal tissue, and other genes crucial for cartilage and extracellular matrix processes (see 5.9). This mesenchyme is morphologically characterized by loosely associated cells that lack polarity and are surrounded by large extracellular matrix containing a loose aggregate of reticular fibrils. Collagen II is one of the predominant forms of collagen in mesenchyme (Lengner et al., 2004). The detected up-regulation by a factor of 13.5-times combined with the expansion of the tissue detected histological sections showed a misregulation of a developmental process.

Mesenchymal cells are unspecialized cells, being able to develop into other cell and tissue types (e.g. connective tissues throughout the body, such as bone and cartilage). Mesenchymal cells can migrate easily. The mesenchyme forms the undifferentiated fill of the early embryo. Cells are connected by slender cell processes, which could be observed in this thesis (4.5). Connective tissue between and within the developing tissues and organs, in fetal development, is formed by mesenchyme. (Gartner et al., 2011). Mesenchymal connective tissue can be found in wildtype embryos until a certain point in development, implicating regulatory changes in the mutant prolonging and increasing the existence of the tissue throughout development. Taking a closer look at the structures in the coronal sections, identity of the labeled structures can only be speculated.

Histological data indicated nuclear Cofilin1 as a major key player in embryonic telencephalic regionalization.

Considering the role of Cofilin1 in a number of cellular mechanisms and the importance and highly delicate nature of the interaction of the different key regulators for telencephalic development, KTRTK-Cofilin1 may cause a “domino effect” by affecting different mechanisms like transcription (4.7), cytokinesis (4.4), and proliferation (4.4). The observed phenotype of Cofilin1$^{KTRTK/KTRTK}$ brains is most likely a pleiotropic effect only affecting the brain but different mechanisms. The event of brain patterning is so complex, that it is highly unlikely, that the phenotype results from one altered process. In regard to the altered brain development observed in Cofilin1$^{KTRTK/KTRTK}$ mutants it would also be of interest if the localization and cell type specific expression of Cofilin1 and KTRTK-Cofilin1 differ from one another. Structural specification using antibodies and *in situ* probes in Cofilin1$^{KTRTK/KTRTK}$ brains will be of importance to verify hypothesis of lateral and anterior shift of brain structures. The introduction of Thy1-GFP in the KTRTK-Cofilin1 might also be of interest and provide further information neuronal localization in the mutant brain.

5.7 Cortical-like layering in Cofilin1$^{KTRTK/KTRTK}$ brain

Surprisingly, in various exencephalic mouse lines, the malformed brain, shows signs of neuronal differentiation as well as formation of nerve connections, despite being anatomically abnormally positioned, exteriorized neural tissue (Matsumoto et al., 2002). Indicating that brain development still follows certain processes in the early stages even though cranial neurulation failed in these animals. Cofilin1$^{fl/fl,\ Emx1}$ and Cofilin1$^{fl/fl,\ Nex}$ mice both display cortical malformations but produce postnatal viable progenies. The Nex-Cre is under the control of a neuronal basic-helix-loop-helix transcription factor. Deletion of Cofilin1 is detectable in postmitotic neurons after E11.5 (Goebbels et al., 2006), Emx1, a homeobox gene transcription factor, is specifically expressed in cerebral cortex and hippocampus. In this case the deletion is detectable at E9.5 in principle neurons (Iwasato et al., 2000). Cofilin1 $^{fl/fl,\ Emx1}$ mice show severe disorganization of all cortical layers. In Cofilin1 $^{fl/fl,\ Nex}$ mice the cortical layers II+III are missing (Schütz, unpublished). The intermediate cortical layers (II – V) are formed between E13 and E19, showing that the absence of Cofilin1 affects cortical layering. Cortical-like lamination in Cofilin1$^{KTRTK/KTRTK}$ embryos implicated that reduced protein

levels of KTRTK-Cofilin1 (4.3.1) and reduced functionality (F-actin binding and depolymerization) were sufficient for cortical lamination (Figure 46).

The analyses of Reelin, Ctip2 and Cux1 (Figure 48), factors important for cortical patterning, revealed changes in expression patterns. It was recently proposed, that cytoplasmic Cofilin1 may influence gene expression via a nuclear actin independent pathway by ADF/Cofilin-mediated actin turnover that promotes the release of actin-bound transcription cofactors (e.g. serum response factor (SRF)) (Chang et al., 2015). IF analysis showed an expression of Cux1 in the mutant, whereas no signal could be detected in the wildtype (Figure 48). Furthermore, no Reelin expression was detected in Cofilin1$^{KTRTK/KTRTK}$ brain. This might indicate an altered temporal expression pattern of transcription factors. The differential expression of Reelin and Cux1 might explain by altered actin turnover in KTRTK-Cofilin1 mutants.

F-actin levels in neurons are crucial for cortical formation. Elevated F-actin levels were hypothesized to inhibit actin- based motor molecules (e.g. myosinIIB). So far establishment of cell migration being affected by myosin II activity in fibroblast cells was reported (Vicente-Manzanares et al., 2007). In the microarray analysis no changes in myosin II on RNA level were detected in Cofilin1$^{KTRTK/KTRTK}$ brains compared to Cofilin1$^{wt/wt}$ brains. G-actin/F-actin analysis of Cofilin1$^{wt/wt}$, Cofilin1$^{wt/KTRTK}$ and Cofilin1$^{KTRTK/KTRTK}$ brains revealed increases of F-actin levels in the heterozygous and the mutant tissue (Figure 37). Whereas the G-actin level in the wildtype and the heterozygous brain remained constant, the G-actin protein level in the mutant was decreased to approximately 71% compared to wildtype. Densitometric examination of the G-actin/ F-actin ratio revealed distinct shifts in the distribution of the total amount of actin. In the wildtype 90% of the total amount of actin consist of G-actin while the remaining 10% percent are presented by F-actin. The heterozygous brain displays a ratio of 77% G-actin/ 23% F-actin. The shift is even more explicit in the mutant with a ratio of 62% G-actin/ 38% F-actin. The total amounts of actin did change. Interestingly, even though the actin levels in the heterozygous brains are affected, Cofilin1$^{wt/KTRTK}$ mice show no phenotype, are viable and indistinguishable from wildtype littermates. Histological analysis of Cofilin1$^{wt/KTRTK}$ embryonic brain showed that the observed shift of G-actin/ F-actin ratio in heterozygous mice does not affect brain morphology (data not shown). Increases in F-actin levels were observed in Mefs isolated from

Cofilin1$^{KTRTK/KTRTK}$ embryos *in vitro,* whereas G-actin levels remained constant compared to wildtype Mefs, thereby increasing the total amount of actin (Figure 36). These data indicate that the influence of KTRTK-Cofilin1 may affect G-actin/F-actin levels differently *in vivo* compared to *in vitro* and may also be dependent on cell type. Mefs are uniform cell population whereas the brain consists of a variety of different cell types. Also, the composition of the mutant brain differs from the wildtype brain (Figure 70). Therefore, in the future F-actin and G-actin levels of Cofilin1$^{KTRTK/KTRTK}$ neurons and astrocytes compared to Cofilin1$^{wt/wt}$ should be examined, to allow conclusion regarding these specific cell types.

5.8 KTRTK-Cofilin1 alters the phenotype of neural cells

After the exencephalic phenotype in Cofilin1$^{KTRTK/KTRTK}$ embryonic brains was observed, the isolation of neural cells was of interest. Beta-III-tubulin stainings, NeuN and Golgi stainings, all specific for neurons, confirmed the presence of neurons but showed different patterning (Figure 49). Cofilin1$^{KTRTK/KTRTK}$ neurons displayed an increased branching activity and neurite growth in vitro.

The involvement of the members of the ADF/Cofilin family in neural cells has been demonstrated before. Members of the ADF/Cofilin family were associated with neurite growth and polarization (Sarmiere and Bamburg, 2004; Rust et al., 2010; Bläsius, 2012; Flynn et al., 2012).

During neurulation the entire neural plate is proliferative, cells only begin to exit the cell cycle upon completion of neurulation. Cells embark the cellular pathway towards neuronal differentiation, once they have achieved the post-mitotic state. Knockout lines, suffering from premature onset of neuronal differentiation, in the neural plate, displayed cranial neurulation failures (Copp, 2005).

Neural stem cells and their progenitor cells generate neurons and microglial cells (astrocytes and oligodendrocytes). Neurons are generated by asymmetric and symmetric cell division (Figure 63). Symmetric cell division creates two daughter cells with the same fate, whereas in asymmetric cell division two different daughter cells arise. While one cell will be identical to the mother cell, the second one will be a

different cell type. Proliferative, symmetric divisions are followed by asymmetric, generating daughter stem cells (self renewing) and a more differentiated cell such as neurons (Gotz and Huttner, 2005).

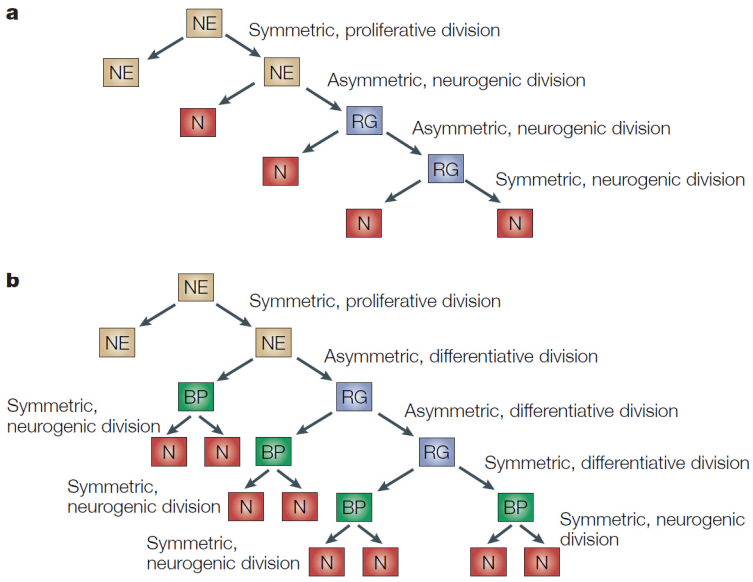

Fig. 63: Lineage trees of neurogenesis. The lineage trees shown provide a simplified view of the relationship between neuroepithelial cells (NE), radial glial cells (RG) and neurons (N), without (a) and with (b) basal progenitors (BP) as cellular intermediates in the generation of neurons. Types of cell divisions involved are shown (Gotz and Huttner, 2005).

A switch to an asymmetric cell division is induced by an elongation of the cell cycle, consequently, diminishing the progenitor pool. The mutation of Cofilin1 may impair the segregation of cell fate determinants, causing the elongation of the cell cycle inducing a switch to asymmetric cell division. Bellenchi proposed disturbances in setting of the cleavage plane in Cofilin1$^{fl/fl,\ Nes}$ cells, a critical step determination of symmetric vs. asymmetric cell division (Chenn and McConnell, 1995; Bellenchi et al., 2007) leading to a reduced number of radial glia cells, guiding postmitotic neurons from the SVZ to the plial surface during the process of radial migration (Bellenchi et al., 2007).

An increased number of 4n cells in embryonic cells lacking Cofilin1 were found, implicating an important role in the G2/M-phase transition for Cofilin1. The balance of

symmetric and asymmetric cell divisions is of utmost importance in neurons to control cell fate and neuronal development (Bellenchi et al., 2007; Flynn et al., 2012).

The analyses of neural cells derived from Cofillin1$^{KTRTK/KTRTK}$ brains is still in the early phases. It can be stated clearly, that the mutation also impacts neurons and astrocytes in culture phenotypically.

Morphological analysis of astrocytes revealed increased occurrence of multinucleate cells and a reduced number of GFAP- positive cells (Figure 51+52). Expression of GFAP is tightly regulated during astrocyte maturation. The reduced number of GFAP-positive cells in Cofilin1$^{KTRTK/KTRTK}$ astrocytes may implicate a delay in maturation. So far, the correlation of Cofilin1 and astrocyte maturation has not been studied. To this date no specific role for Cofilin1 in astrocytes other than regulation of cell membrane protrusions essential for migration has been studied (Nagai et al., 2011). The full role has not been elucidated fully so far. Absence of GFAP was associated with increased expression of extracellular matrix molecules. This would corroborate to the massively increased expression of ECM proteins found in microarray analysis in addition to the expanded connective tissue in Cofilin1$^{KTRTK/KTRTK}$ brains. Furthermore, the deletion of GFAP correlates with increased neurite growth and altered neuronal physiology (McCall et al., 1996; Menet et al., 2001). Reduced GFAP level could also contribute to the increased neurite length observed in Cofilin1$^{KTRTK/KTRTK}$ neurons (Figure 50). In future experiments the localization and expression level of GFAP in vivo will have to be analyzed.

Cortical neurons derived from BMP (bone morphogenetic protein) knockout animals show the same phenotype as neurons derived from Cofilin1$^{KTRTK/KTRTK}$ embryos. BMP is known to regulate Cofilin1 by affecting the activation state of Limk1, which phosphorylates Cofilin1 and thereby inactivates it (Phan et al., 2010).
In the case of BMP$^{-/-}$ neurons the phenotype of increased commissural axon outgrowth in chicken was a consequence of the misregulation of Cofilin1 activity state due to the lack of BMP regulating Limk1 (Yamauchi et al., 2013).In this study the phenotype of the neurons results from the dysfunction of KTRTK-Cofilin1. In both cases the altered phenotype is a consequence of Cofilin1 alteration.
Cells, expressing constitutively active LIM kinase, thereby inhibiting Cofilin1, abolish cell polarity.

Cofilin1$^{fl/fl,\ Nes}$ neurons show phenotypically alterations in the form of multiple cell protrusions, control neurons are characterized by bipolar shape. The elongated and multiple protrusions of Cofilin1$^{KTRTK/KTRTK}$ neurons is more likely to be affected by the mutation instead of decreased protein levels, since ADF$^{-/-}$, Cofilin1$^{wt/fl,\ Nes}$ mice yield a normal phenotype, even though the Cofilin1 level is reduced (Bellenchi et al., 2007).
Polarization and activity state of Cofilin1 are important during migration. Actin filament length has been linked to cortical neuron migration as a critical factor in past studies (Rivas and Hatten, 1995). Migration disturbance can be caused by two key factors: the decrease of Cofilin1 protein level or an altered activity of Cofilin1. Further, the members of the ADF/Cofilin family members are known regulators of cell polarity, to sustain already established polarity and to induce cell polarization in neuronal and non-neuronal cells (Dawe, 2003; Dawe et al., 2003; Garvalov et al., 2007; Witte and Bradke, 2008).
If the protein activity of the members of the ADF/ Cofilin family is blocked during cell polarization, proper formation of cell rear and front is inhibited. It was concluded that the members of the ADF/Cofilin family are required for the formation of oriented actin filament bundles in the cell (Mseka et al., 2007). Morphological cell polarity as well as the driving force to move the cell, necessitate correctly organized actin networks (Wittmann and Waterman-Storer, 2001; Ridley et al., 2003; Small and Resch, 2005).

Polarity can also be modulated by cell adhesion molecules and extracellular matrix proteins (Suter and Forscher, 1998). Analysis of brain tissue disclosed considerable increased RNA expression of a number of extracellular matrix proteins (e.g. *Matn1*, *Col2a1*, *Col1a1*, *Matn4*) in embryonic Cofilin1$^{KTRTK/KTRTK}$ brain along with the increase of connective tissue (4.7).

Signaling cascades that result in neurite extension lead to alterations of the phosphorylation levels of Cofilin1 and ADF. Activation of signaling pathways are often followed by elevated Ca^{2+} or the presence of cAMP. Phosphatases, involved in the dephosphorylation of ADF and Cofilin1, are activated by these second messengers. Further, growth factors (e.g. NGF) induce rapid dephosphorylation, subsequently activating ADF and Cofilin1. This strongly implicates that increases in process extension is associated with decreased phosphorylation of ADF and Cofilin1 (Meberg et al., 1998). The phosphorylation status of KTRTK-Cofilin1 might differ from the status of wt-Cofilin1.

It was shown that mammalian neurons contain about 5–10 fold more Cofilin1 than ADF (Bamburg and Bloom, 2009), overexpression of ADF causes increase in neurite length in rat cortical neurons (Meberg and Bamburg, 2000). Western Blot analyses of Cofilin1$^{KTRTK/KTRTK}$ samples showed up-regulation of ADF in Mefs at E14.5 (Figure 66) *in vitro*. In the future ADF and Cofilin1 levels in Cofilin1$^{wt/wt}$ and Cofilin1$^{KTRTK/KTRTK}$ neurons will be determined. Increased ADF levels in Cofilin1$^{KRTK/KTRTK}$ neurons might partake in observed neurite elongation. *In vitro* behavior and metabolic requirements for cells in culture differ from *in vivo* requirements. Also *in vitro* cultures represent a uniform cell population whereas brains consist of a variety of cell types and extracellular matrix proteins.
Considering this the ADF expression levels along with the phosphorylation status of KTRTK-Cofilin1 might be essential to regulate actin dynamics, neuronal outgrowth, morphology and migration in KTRTK-Cofilin1 neurons.

In Listeria tails grow very long and motility is reduced in the absence of ADF/ Cofilin, due to impaired actin recycling (Rosenblatt et al., 1997). Reduced elongation of neurites in Cofilin1$^{fl/fl, Nex}$ and Cofilin1$^{fl/fl, Emx1}$ mutant neurons was attributed to reduced recycling of the G-actin pool (Bläsius, 2012). ADF$^{-/-}$; Cofilin1$^{-/-}$ neurons exhibited shifts in G-actin/F-actin ratios, with increased F-actin levels, phenotypically resulting in the failure of neuritogenesis (Flynn et al., 2012). In future experiments the G-actin/F-actin ratios in Cofilin1$^{KTRTK/KTRTK}$ neurons compared to wildtype neurons will have to be established. G-actin/F-actin separation of brain tissue of Cofilin1$^{KTRTK/KTRTK}$ embryos also revealed increases of F-actin levels but a decrease in G-actin levels (Figure 37). These would suggest that though the depolymerization activity of KTRTK-Cofilin1 is reduced, the decreased activity was sufficient for neuritogenesis. And in combination with the presence and possible up-regulation of ADF that might explain why KTRTK-Cofilin1 neurons are characterized by elongated processes in contrast to other studied Cofilin1 mutant neurons.

Analyses of neural cells will have to be extended. The acquired data clearly indicates that the KTRTK-Cofilin1 mutation affects astrocyte and neuron morphology.
To analyze Cofilin1 $^{KTRTK/KTRTK}$ neurons in more detail polarization studies and Scholl analyses will be of great interest. Neuronal polarization is a key factor and cortical lamination and might also contribute to information to the developmental process of Cofilin1$^{KTRTK/KTRTK}$ neurons.

5.9 KTRTK-Cofilin1 affects gene expression massively

The nuclear translocation of the mutant protein KTRTK-Cofilin1 was impaired and thereby the ability to shuffle actin to the nucleus, possibly affecting transcription. Gene profiling analyses in this thesis (4.7) strongly indicated a regulatory function for Cofilin1 in transcriptional control correlating with previous studies. It was shown that Cofilin1 is in the same complex with actin and phosphorylated RNA polymerase II during the elongation phase of transcription. Active genes in Cofilin1 silenced cells were devoid of actin. This indicated the crucial role of Cofilin1 for associating actin and phosphorylated pol II with active genes. (1.3.4.3) (Obrdlik and Percipalle, 2011; Dopie et al., 2012). Many factors are involved in embryogenesis and their expression is tightly controlled in a spatio- temporal manner. Therefore, transcriptional dysregulation can impact development massively. The chosen up- and down-regulated genes should be confirmed by qPCR and in the following step by protein level analysis.

It could be noted that KTRTK-Cofilin1 affects different genes *in vivo* (brain) and *in vitro* (Mefs). Considering the different characteristics of the analyzed samples, this was not surprising. Analyzed E14.5 mouse embryonic fibroblasts represented a uniform cell population und controlled culture parameters (4.7). Transcriptional analysis revealed up- and down regulated genes. A large number of the affected genes could be assigned to distinct GO-Term groups. The next paragraph presents a small selection of genes, that should be analyzed further, in the future. *Nppa* was down- regulated in Cofilin1$^{KTRTK/KTRTK}$ Mef (-7.68), it is known to be involved in negative regulation of cell growth and biosynthesis processes. Considering the massive reduction on *Nppa* RNA in the mutant the accuracy of this value should be confirmed in qPCR. *Lum* was down-regulated by a factor of -6.37 in the mutant, should also be analyzed. It is involved collagen fibril organization and regulation of transcription. Considering alterations in a number of extracellular matrix proteins including *Col2a1*, up-regulated + 3.86 times in the mutant, proteins involved in extracellular matrix organization should be studied. *Col2a1* is also involved in regulation of gene expression and collagen fibril organization. The misregulation of a number of genes involved in the same processes might augment the phenotype of increased cell size and cytokinesis and proliferative defects. *Inhba* and *Tagln* are both up-regulated by a factor of approximately 3-fold in

Cofilin1$^{KTRTK/KTRTK}$ Mefs. Both proteins participate in cellular mechanisms, including proliferation, cell cycle progression and cytoskeletal organization. All these cellular processes were disturbed in Cofilin1$^{KTRTK/KTRTK}$ Mefs, therefore these genes might be of interest.

Analyzed E16.5 brains represented the in vivo situation, at a developmental stage at which the protein level of KTRK- Cofilin1in Cofilin1$^{KTRTK/KTRTK}$ was already decreased. Brains comprise a variety of different cellular subtypes, it should also be noted, that the composition of wildtype and mutant brain is not comparable (4.7.1). Transcriptional analysis mainly revealed up-regulated genes. A large number of the affected genes could be assigned to distinct GO-Term groups. A selection of significantly altered genes in shown Tables 8 - 15. One of the few down-regulated genes was Nkx2-1. In the mutant it was down-regulated by -1.82-times. This transcription factor, is of extreme interest, since it is one of the earliest transcription factors, essential for brain development and patterning. If the protein expression pattern of this transcription factor was already disrupted, it could corroborate with the early failure of proper prosencephalon development, observed in Cofilin1$^{KTRTK/KTRTK}$ embryos. In brain the values of up-regulation in the mutant compared to wildtype were striking. In order to verify these, further experiments in the future will be necessary.

Coronal sections of Cofilin1$^{KTRTK/KTRTK}$ embryos illustrated craniofacial malformations. *Acan* (up-regulated by 2.8 times) and *Col2a1* (up-regulated by 13.55 times) were shown to be involved in brain and craniofacial structure development (Rossant and Tam, 2002). The direction of migration can be influenced by ECM molecules, they also provide levels of cell adhesion necessary to propel cell motility (Thelen et al., 2002; Larsen et al., 2006). Analysis of brain tissue disclosed considerable increased RNA expression of a number of extracellular matrix proteins (e.g. *Matn1 (+19.1)*, *Col1a1 (+5.36)*, *Matn4* (+4.47)) in embryonic Cofilin1$^{KTRTK/KTRTK}$ samples (4.7.1). Histological analysis showed expanded connective tissue throughout development in the mutant brain. The extreme increase in a vast number of ECM proteins has to be studied further. This also leads to the question in which way Cofilin1 may directly be involved transcriptional regulation of ECM protein?

The neural crest cells have the ability to generate multiple cell lineages. Upon arrival of the cells of the neural crest at their final location they contribute to facial components such as cartilage, the cranial skeleton and connective tissue. In Cofilin1$^{-/-}$ neural crest

cells migration towards the head region was impaired and cells were randomly distributed (Gurniak et al., 2005). Microarrays of Mefs and brain showed an altered regulation of genes involved in skeletal and osteoclast development.

Neurons and glial cells of the peripheral nervous system along with mesenchyme and smooth muscle cells origin from neural crest cells. A large number of genes, which represent specific markers for the above mentioned tissues, displayed significant and distinct shifts compared to the wt. Neural crest cells are essential for skull development. KTRTK-Cofilin1 neural crest cells might also be unable to migrate to the head region, in consequence disruption the formation of the skull. Differential activation of genes contribute to the establishment of neural crest diversity (Huang and Saint-Jeannet, 2004; Kulesa et al., 2004). Four distinct signaling pathways, including the signaling molecules bone morphogenetic proteins (Bmp), Wnt proteins, fibroblast growth factor (Fgf) and Notch/Delta, have been suggested to be involved in the process of neural crest induction. In neural crest induction the role of Bmp signaling is tightly linked to the induction of the neural plate and Bmp was shown to regulate the activity state of Cofilin1 by regulating Limk1 (Huang and Saint-Jeannet, 2004; Phan et al., 2010). A conditional Wnt1-Cre mediated inactivation of the β-catenin gene, a downstream component of the WNT signaling pathway, in the mouse, displayed severe defects of craniofacial skeletal elements of neural crest origin (Brault et al., 2001). Genes in two main pathways have yielded positive findings with regard to the causation of NTDs: folate one-carbon metabolism, and non-canonical Wnt signaling (the planar cell polarity pathway) (Copp et al., 2013). In our microarray analysis of brain no significant changes in the above mentioned pathways could be detected on RNA level at this developmental stage. The induction of neural crest cells is of especially in early stages of development of importance, therefore it would be more conclusive to analyze the expression levels around E8.5-E10.

Spatially restricted expression patterns of transcription factors (TFs) are crucial for embryonic, anatomical organization. Recently, more than 2300 different TF proteins have been predicted in the murine genome (Waterston et al., 2002; Thomas et al., 2003), making up approximately more than 7% of the total genes. 27% of the TF genes are expressed in a spatially restricted pattern.

Over 100 TF genes were identified that are expressed in a spatially restricted pattern within non-neuronal tissue, such as nose, oral cavity, teeth and facial muscles (Gray et al., 2004). RNA expression analysis identified twelve differently expressed neural specific TFs at E16.5 in Cofilin1$^{KTRTK/KTRTK}$ brain. Taking the importance of correct TF expression into account, a possible disruption of the levels and patterning, may explain the malformations of the brain and the cranial facial features in the homozygous mutants.

Another crucial role is played by the specific timely and spatially coordinated expression pattern of cis-regulating enhancer elements. Corroborating the importance of enhancers is the correlating expression pattern with transcription factors important for telencephalic development (Visel et al., 2013). Cofilin1 and actin have been linked to transcription in several studies (see 5.6), it is possible that the mutant protein KTRTK-Cofilin1 regulates transcription differently than its wildtype counterpart since nuclear translocation is impaired.

Telencephalic structures can be detected as early as E8.5. Regionalization takes place during the early stages of embryonic development, mainly from E8.5 to E12.5.

The anterior ridge (ANR), lies where the most anterior neural tissue meets the non-neural ectoderm forming a junction, was suggested to mediate the earliest step of cortical VZ induction, producing Fgf8, a fibroblast growth factor. Foxg1, transcription factor selectively marks future cortical VZ progenitors, before the telencephalon is morphologically distinguishable. Foxg1 is required for cortical morphogenesis and normal telencephalic development. After telencephalic induction specification of the telencephalic dorsal (pallial) and ventral (subpallial) regions take place, regulated by transcription factors Gli3, Ngn1 and Ngn2, which are selectively expressed in dorsal telencephalic progenitors. In the following step the dorsal telencephalon must be further subdivided into dorsal midline epithelial fates and the cortical VZ. Lhx2 has a specific role in this process. Lhx2 is selectively expressed in the cortical VZ, but not in dorsal midline epithelia. After cortical VZ fate is selected, regional specification of the cortical VZ must occur.

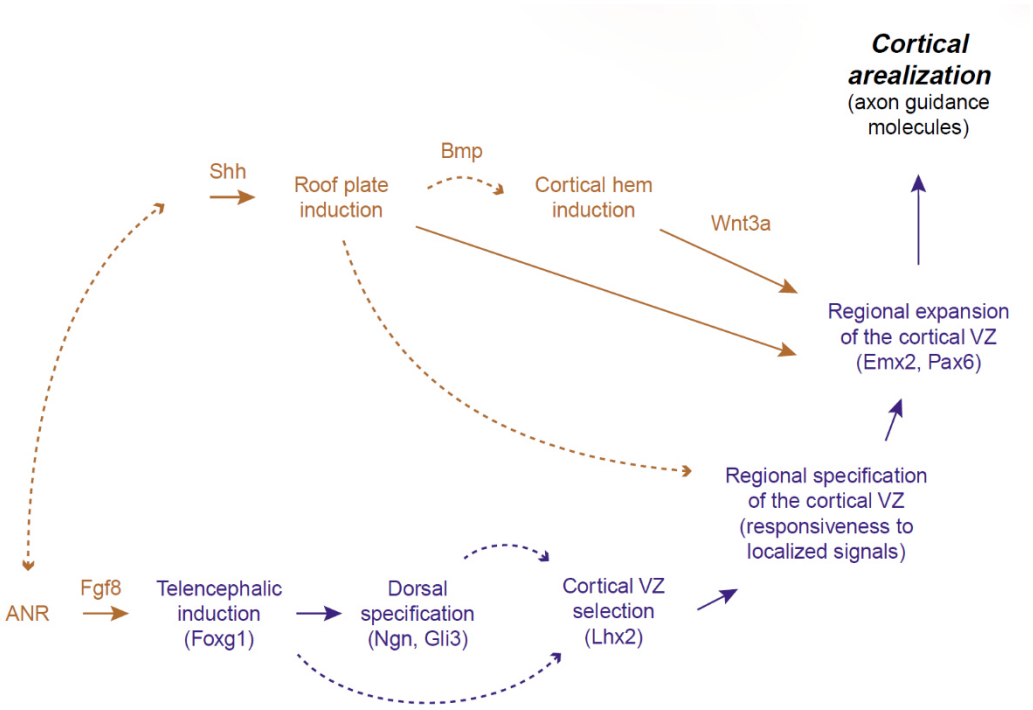

Fig. 64. Events in cortical patterning of the mouse brain. Regulatory transcription events that pattern the cortical ventricular zone (VZ) and cortical areas. Brown, extrinsic influences (organizers, signals, afferent inputs and cortical neurons generated outside the cortical VZ); blue, intrinsic events and factors in the cortical VZ. Dashed curved lines, hypothetical connections between parts of this hierarchy (Monuki and Walsh, 2001).

This critical step in cortical VZ patterning remains to be elucidated. EMX2 and Pax6, two transcriptional regulators expressed in the cortical VZ, regulate the relative sizes of cortical areas. Emx2 and Pax6 are expressed in graded and opposing fashions within the cortical VZ: the Emx2 gradient is high posterior– low anterior, whereas the Pax6 gradient is low posterior–high anterior.

Therefore it would be conclusive to screen early stages of Cofilin1$^{wt/wt}$ and Cofilin1$^{KTRTK/KTRTK}$ brain development in a microarray analysis to detect possibly altered expression levels of TFs (Nkx2.1, Emx1, Emx2, Gli3, Foxg1) during the most active part of telencephalic development. Functional studies also showed potent effects of TFs on cell proliferation in the developing telencephalon (Zaki et al., 2003). Microarray analysis would allow simultaneous screening for a vast number of transcription factors. At the same time, spatial expression was shown to be of utter importance (Figure 64) (Monuki and Walsh, 2001). Therefore, brain sections should

also be stained for transcription factors (Emx2, Pax2, Lhx2, Foxg1, and Fgf8) to verify correct spatial expression.

For several years the translocation of actin with Cofilin1 acting as a chaperone was exclusively linked to stress responses (Pendleton et al., 2003). At this point, Cofilin1 has been incriminated as an essential regulator of the continuous steady-state nuclear actin import. It was shown that accumulation of actin in the nucleus was affected upon silencing of Cofilin1, due to impaired import and not lack of monomeric actin (Dopie et al., 2012), confirming an essential role for Cofilin1 in nuclear translocation of actin. Beta-actin was shown to be essential for regulation of gene expression through control of the cellular G-actin pool (Bunnell et al., 2011). Up-regulation of different actin isoforms (Actb, Actg2 and Acta2) in brains and in Mefs was detected in microarrays (4.7). Cofilin1 depolymerization can enhance actin polymerization for cell motility and other physiological processes by replenishing the cellular actin monomer pool. In order to maintain functionality and allow cellular mechanisms to continue, the depletion of the G-actin pool would need to be compensated. This possibly implies that the in FACS analyses observed increase of in total actin in Mefs (Figure 36) and the shift of G-actin/ F-actin ratio in brain (Figure 37), could not just be a result of decreased depolymerizing activity of the mutant protein but also a consequence to the increased expression levels of actin isoforms.

In Mefs β-actin levels were increased by a factor 4 in Cofilin1$^{KTRTK/KTRTK}$ cells (4.7). Bunnell *et al*., discovered that changes of β- actin levels affects the G-actin/F-actin ratio, shifting it toward F-actin in Mefs. The same shift of F-actin has been observed in Cofilin1$^{KTRTK/KTRTK}$ Mefs. Up-regulation of actin might facilitate replenishment of the monomeric actin pool, which could allow the cells to maintain a degree of functionality. It has been discovered that actin isoforms are not fully interchangeable and possess distinct functions. β- actin is essential for embryonic development whereas the loss of γ- actin is not lethal. β- actin was also implicated to be required for cell division. Mefs, depleted of β- actin, revealed a multinucleate phenotype (Bunnell et al., 2011). This might also indicate that the Cofilin1$^{KTRTK/KTRTK}$ Mefs attempt to rescue functionality by up-regulation of β- actin. At this point the repercussion of the differential expression of the actin isoforms remains elusive and should be examined further in the future.

The analysis of genes affected by the introduction of the mutation of the NTS of Cofilin1 revealed several altered genes *in vivo* and *in vitro* involved in the regulation of the actin cytoskeleton (e.g. *Pfn1* ;*Myh3*) (4.7; S8-S24). This coincides with results of previous studies. Bravo- Cordero and team showed that the subcellular localization of Cofilin1 in combination with regulatory functions of other proteins such as Profilin 1 directly or indirectly affect the activity of Cofilin1 (Bravo-Cordero et al., 2013). The mutation of the NTS supposedly rendered KTRTK-Cofilin1 unable to enter the nucleus actively, therefore altering its subcellular localization. Further an increase of Profilin 1 expression on RNA level was detected in microarray analysis. Profilin catalyzes the exchange of ADP for ATP and thus recycling ATP-actin subunits to the monomer pool which are then ready to be used for assembly. This may further explain the increase of F-actin in Mefs. Apart from reduced depolymerizing activity of KTRTK-Cofilin1, the altered genes involved in the regulation of the actin cytoskeleton along with the altered subcellular localization, may further decrease the depolymerizing activity of KTRTK-Cofilin1, in consequence increasing the F-actin level.

Additionally, actin dynamics play a key role in the regulation of gene expression through the serum response factor (SRF) gene regulatory pathway, targeting genes including actin and actin regulators (Posern et al., 2002; Posern et al., 2004). SRF, a transcription factor, sensitive to G-actin levels interacts with the cofactor MAL. Further *Fos* and *JunB* are targeted, genes required for differentiation. MAL gets activated upon depletion of the monomeric actin pool (Pawlowski et al., 2010). G-actin binds to MAL, therefore preventing an activation of SRF, consequently, transcription is not activated. SRF also affects migration and proliferation. Analysis of the SRF regulatory pathway members in the microarray data for either brain or Mefs revealed no significant changes, even though G-actin levels in Cofilin1$^{KTRTK/KTRTK}$ brains were decreased. Actin, tagged with a NTS, failed to rescue the transcriptional alterations in Cofilin1 depleted in NIH 3T3 cells (Dopie et al., 2012) indicating that nuclear actin alone is not sufficient for normal transcriptional profiles but that nuclear Cofilin1 is also indispensable. This confirms the hypothesis that Cofilin1 comprises functions independent of actin depolymerization, indicating changed features of KTRTK-Cofilin1 that are not understood, yet.

6. Supplementary

6.1 Gene expression profiling in vivo and in vitro

The Illumina® bead chip system was used for the microarray analyses. The mathematical calculation were performed with Partek® Genomic suite software.
For all further steps of analyses only genes, which fluorescence signal was altered with a significance lower than $p<0.05$ were included. The data acquired in the microarray is based on the mathematical processing and conversion of fluorescent signals. In the ANOVA calculations samples were grouped by genotype and compared, the wildtype was used as reference. Negative fold-changes indicate a down-regulation (blue) in the mutant, whereas positive fold-changes represent an up-regulation (red) in the mutant tissue (Table S8-S24).
Go-Terms are a group of genes which either have a similar function or are involved in the same cellular mechanisms.
Each Go-Term can be accessed with the respective identification number via the Amigo: Gene ontology database.

6.1.1 Gene profiling in E16.5 embryonic brain

In order to identify, due to the mutation, critically altered genes in *in vivo* settings, three Cofilin1$^{wt/wt}$ and three Cofilin1$^{KTRTK/KTRTK}$ samples were compared individually.
Gestational stage E16.5 was chosen, a point in development, in which decreased mutant protein level were observed

Symbol	Name	p-value	Fold-Change (mt vs. wt)	Function
Nkx2-1	NK2 homeo -box 1	0.0102	-1.82	• RNA polymerase II regulatory region sequence-specific DNA binding (GO:0000977) • actor activity (GO:0003700) • RNA polymerase II distal enhancer sequence-specific DNA binding transcription • factor activity (GO:0003705) • neuron migration (GO:0001764) • pattern specification process (GO:0007389) • brain development (GO:0007420) • positive regulation of gene expression (GO:0010628) • negative regulation of epithelial to mesenchymal transition (GO:0010719) • cerebral cortex cell migration (GO:0021795)
Dync1i1	dynein cytoplasmic 1 intermediate chain 1	0.0005	-1.74	• transport (GO:0006810) • microtubule-based movement (GO:0007018)

Table S8: Highest changing genes in brain Part I. Wt samples acted as reference.
Blue numbers: down- regulation; mt: Cofilin1$^{KTRTK/KTRTK}$; wt: Cofilin1$^{wt/wt}$

	Symbol	Name	p-value	Fold-Change (mt vs. wt)	Function
BRAIN	**Myl9**	myosin, light polypeptide 9, regulatory	0.0001	2.51	• metal ion binding (GO:0046872) • platelet aggregation (GO:0070527) • stress fiber (GO:0001725)
	Col16a1	collagen, type XVI, alpha 1	0.0030	2.51	• cell adhesion (GO:0007155) • cellular response to amino acid stimulus (GO:0071230) • proteinaceous extracellular matrix (GO:0005578)
	Panx3	Pannexin 3	0.0197	2.57	• cell-cell signaling (GO:0007267)
	Hapln1	hyaluronan and proteoglycan link protein 1	0.0026	2.61	• cell adhesion (GO:0007155) • central nervous system development (GO:0007417) • extracellular matrix structural constituent (GO:0005201) • skeletal system development (GO:0001501)
	Col5a1	collagen, type V, alpha 1	<0.0001	2.63	• cell adhesion (GO:0007155) • cell migration (GO:0016477) • collagen fibril organization (GO:0030199) • collagen biosynthetic process (GO:0032964) • regulation of cellular component organization (GO:0051128) • negative regulation of endodermal cell differentiation (GO:1903225) • extracellular matrix structural constituent (GO:0005201)

Table S9: Highest changing genes in brain Part II. Wt samples acted as reference.
Red numbers: up- regulation; mt: Cofilin1$^{KTRTK/KTRTK}$; wt: Cofilin1$^{wt/wt}$

	Symbol	Name	p-value	Fold-Change (mt vs. wt)	Function
BRAIN	**Acan**	aggrecan	0.0001	2.80	• cartilage condensation (GO:0001502) • chondrocyte development (GO:0002063) • cell adhesion (GO:0007155) • central nervous system development (GO:0007417) • proteoglycan biosynthetic process (GO:0030166) • collagen fibril organization (GO:0030199) • negative regulation of cell migration (GO:0030336) • extracellular matrix structural constituent (GO:0005201)
	Col12a1	collagen, type XII, alpha 1	0.0005	2.86	• cell adhesion (GO:0007155) • extracellular matrix (GO:0031012)
	Spp1	secreted phosphoprotein 1	0.0063	2.87	• ossification (GO:0001503) • osteoblast differentiation (GO:0001649) • cell adhesion (GO:0007155) • biomineral tissue development (GO:0031214) • negative regulation of apoptotic process (GO:0043066) • positive regulation of bone resorption (GO:0045780)
	Papss2	3'phosphoadenosine 5'-phosphosulfate synthase 2	0.0023	2.88	• nucleotide binding (GO:0000166) • catalytic activity (GO:0003824)

Table S10: Highest changing genes in brain Part III. Wt samples acted as reference.
Red numbers: up- regulation; mt: Cofilin1$^{KTRTK/KTRTK}$; wt: Cofilin1$^{wt/wt}$

BRAIN

Symbol	Name	p-value	Fold-Change (mt vs. wt)	Function
Lum	lumican	0.0011	2.95	• collagen binding (GO:0005518) • collagen fibril organization (GO:0030199) • positive regulation of transcription from RNA polymerase II promoter (GO:0045944), • proteinaceous extracellular matrix (GO:0005578)
Col9a2	collagen, type IX, alpha 2	0.0012	3.26	• proteinaceous extracellular matrix (GO:0005578) • collagen trimer (GO:0005581)
Hbb-y	hemoglobin Y, beta-like embryonic chain	0.0068	3.28	• RNA polymerase II promoter (GO:0000122) • transport (GO:0006810) • metal ion binding (GO:0046872)
Capn6	calpain 6	0.0031	3.30	• microtubule bundle formation (GO:0001578) • proteolysis (GO:0006508) • regulation of cytoskeleton organization (GO:0051493)

Table S11: Highest changing genes in brain Part IV. Wt samples acted as reference.
Red numbers: up- regulation; mt: Cofilin1$^{KTRTK/KTRTK}$; wt: Cofilin1$^{wt/wt}$

BRAIN

Symbol	Name	p-value	Fold-Change (mt vs. wt)	Function
Thbs2	Thrombos-pondin 2	<0.0001	3.41	• cell adhesion (GO:0007155) • positive regulation of synapse assembly (GO:0051965) • extracellular matrix (GO:0031012)
Mgp	matrix Gla protein	0.0037	3.44	• ossification (GO:0001503) • protein complex assembly (GO:0006461) • multicellular organismal development (GO:0007275) • cell differentiation (GO:0030154) • regulation of bone mineralization (GO:0030500) • branching morphogenesis of an epithelial tube (GO:0048754) • cartilage development (GO:0051216)
Oc90	otoconin 90	0.0059	3.55	• structural molecule activity (GO:0005198) • calcium ion binding (GO:0005509) • phospholipid metabolic process (GO:0006644)
Acta2	actin, alpha 2, smooth muscle,	<0.0001	4.12	• muscle contraction (GO:0006936) • nucleotide binding (GO:0000166) • actin cytoskeleton (GO:0015629)

Table S12: Highest changing genes in brain Part V. Wt samples acted as reference.
Red numbers: up- regulation; mt: Cofilin1$^{KTRTK/KTRTK}$; wt: Cofilin1$^{wt/wt}$

BRAIN

Symbol	Name	p-value	Fold-Change (mt vs. wt)	Function
Col9a1	collagen, type IX, alpha 1	<0.0001	4.45	• tissue homeostasis (GO:0001894) • growth plate cartilage development (GO:0003417) • cartilage development (GO:0051216)
Matn4	matrilin 4	0.0017	4.74	• response to axon injury (GO:0048678)
Col1a1	collagen, type I, alpha 1	<0.0001	5.36	• positive regulation of epithelial to mesenchymal transition (GO:0010718) • negative regulation of cell-substrate adhesion (GO:0010812) • protein transport (GO:0015031) • collagen fibril organization (GO:0030199) • positive regulation of cell migration (GO:0030335) • collagen biosynthetic process (GO:0032964) • positive regulation of transcription, DNA-templated (GO:0045893) • face morphogenesis (GO:0060325)
Ibsp	integrin binding sialoprotein	0.0018	6.62	• ossification (GO:0001503) • osteoblast differentiation (GO:0001649) • cell adhesion (GO:0007155) • extracellular matrix organization (GO:0030198) • biomineral tissue development (GO:0031214) • cellular response to growth factor stimulus (GO:0071363)

Table S13: Highest changing genes in brain Part VI. Wt samples acted as reference.
Red numbers: up- regulation; mt: Cofilin1$^{KTRTK/KTRTK}$; wt: Cofilin1$^{wt/wt}$

BRAIN

Symbol	Name	p-value	Fold-Change (mt vs. wt)	Function
Myh3	myosin, heavy polypeptide 3, skeletal muscle, embryonic	0.0450	7.59	• actin binding (GO:0003779) • microfilament motor activity (GO:0000146) • nucleotide binding (GO:0000166) • actin filament binding (GO:0051015) • skeletal muscle contraction (GO:0003009)
Col2a1	collagen, type II, alpha 1	0.0003	13.55	• skeletal system development (GO:0001501) • cartilage condensation (GO:0001502) • tissue homeostasis (GO:0001894) • chondrocyte differentiation (GO:0002062) • regulation of gene expression (GO:0010468) • collagen fibril organization (GO:0030199)
Myl1	myosin, light polypeptide 1	0.0363	15.71	• muscle contraction (GO:0006936) • contractile fiber (GO:0043292) • calcium ion binding (GO:0005509)
Matn1	matrilin 1, cartilage matrix protein	0.0001	19.10	• chondrocyte differentiation (GO:0002062) • growth plate cartilage chondrocyte morphogenesis (GO:0003429) • regulation of bone mineralization (GO:0030500) • proteinaceous extracellular matrix (GO:0005578)

Table S14: Highest changing genes in brain Part VII. Wt samples acted as reference.
Red numbers: up- regulation; mt: Cofilin1$^{KTRTK/KTRTK}$; wt: Cofilin1$^{wt/wt}$

6.1.2. Gene profiling in E14.5 mouse embryonic fibroblasts

Mefs were isolated from E14.5 embryos. Three Cofillin1$^{wt/wt}$ (wt) and three Cofilin1$^{KTRTK/KTRTK}$ (mt) Mef lines were prepared. Cells of passages 1 were analyzed. One passage is defined as the trypsinization of confluent cells and the subsequent seeding of a portion of the acquired single cell suspension. For further analyses, main focus was put on the combination of mt Pass1 vs. wt Pass1.

MEF

Symbol	Name	p-value	Fold-Change (mt vs. wt)	Function
Saa3	serum amyloid A 3	0.0410	-7.99	• chemoattractant activity (GO:0042056) • cell chemotaxis (GO:0060326)
Nppa	natriuretic peptide type A,	0.0508	-7.68	• negative regulation of cell growth (GO:0030308) • receptor binding (GO:0005102) • cGMP biosynthetic process (GO:0006182) • female pregnancy (GO:0007565) • cardiac muscle hypertrophy in response to stress (GO:0014898)
Serpina3n	Serine peptidase inhibitor, clade A, member 3N	0.0149	-6.37	• negative regulation of peptidase activity (GO:0010466) • negative regulation of endopeptidase activity (GO:0010951) • response to cytokine (GO:0034097) • response to peptide hormone (GO:0043434)
Lum	lumican	0.0305	-4.23	• collagen binding (GO:0005518) • collagen fibril organization (GO:0030199) • positive regulation of transcription from RNA polymerase II promoter (GO:0045944), • proteinaceous extracellular matrix (GO:0005578)
Serping1	Serine peptidase inhibitor	0.0140	-4.11	• serine-type endopeptidase inhibitor activity (GO:0004867) • negative regulation of complement activation (GO:0045916)

Table S15: Highest changing genes in Mefs Passage 1 Part I.
WT was used as reference. Blue numbers: down- regulation; mt: Cofilin1$^{KTRTK/KTRTK}$; wt: Cofilin1$^{wt/wt}$.

MEF

Symbol	Name	p-value	Fold-Change (mt vs. wt)	Function
C3	complement component 3	0.0366	-4.09	• positive regulation of developmental growth (GO:0048639) • positive regulation of protein phosphorylation (GO:0001934) • positive regulation of apoptotic cell clearance (GO:2000427) • complement activation (GO:0006956)
Hp	haptoglobin	0.0133	-3.65	• positive regulation of cell death (GO:0010942) • catalytic activity (GO:0003824) • proteolysis (GO:0006508)
Scara5	scavenger receptor class A, member 5	0.0031	-3.44	• regulation of gene expression (GO:0010468) • protein binding (GO:0005515) • transport (GO:0006810) • cellular iron ion homeostasis (GO:0006879)
120000 9O22Rik	Component of the TLR4 signaling complex	0.0024	-3.20	• lipopolysaccharide binding (GO:0001530) • toll-like receptor 4 signaling pathway (GO:0034142) • immune system process (GO:0002376)
Reg1	regenerating islet-derived 1 Gene	0.0007	-3.14	• growth factor activity (GO:0008083) • carbohydrate binding (GO:0030246)

Table S16: Highest changing genes in Mefs Passage 1 Part II.
WT was used as reference. Blue numbers: down- regulation; mt: Cofilin1$^{KTRTK/KTRTK}$; wt: Cofilin1$^{wt/wt}$.

MEF

Symbol	Name	p-value	Fold-Change (mt vs. wt)	Function
Mfap4	microfibrillar-associated protein 4	0.0160	-3.06	• cell adhesion (GO:0007155) • regulation of collagen metabolic process (GO:0010712) • extracellular fibril organization (GO:0043206) • elastic fiber assembly (GO:0048251) • extracellular matrix (GO:0031012)
Ambp	alpha 1 microglobulin/ bikunin	0.0265	-3.05	• heme binding (GO:0020037) • protein catabolic process (GO:0030163) • protein maturation (GO:0051604)
Dpt	dermatopontin	0.0072	-2.99	• cell adhesion (GO:0007155) • negative regulation of cell proliferation (GO:0008285) • collagen fibril organization (GO:0030199) • extracellular matrix (GO:0031012)
Ifitm1	interferon induced transmembrane protein 1	0.0062	-2.93	• ossification (GO:0001503) • somitogenesis (GO:0001756) • anterior/posterior pattern specification (GO:0009952) • immune system process (GO:0002376)
Gpx3	glutathione peroxidase 3	0.0473	-2.92	• glutathione peroxidase activity (GO:0004602) • protein homotetramerization (GO:0051289) • oxidation-reduction process (GO:0055114) • glutathione metabolic process (GO:0006749)

Table S17: Highest changing genes in Mefs Passage 1 Part III.
WT was used as reference. Blue numbers: down- regulation; mt: Cofilin1$^{KTRTK/KTRTK}$; wt: Cofilin1$^{wt/wt}$.

MEF

Symbol	Name	p-value	Fold-Change (mt vs. wt)	Function
Igfbp3	insulin-like growth factor binding protein 3 Gene	0.0019	-2.89	• regulation of cell growth (GO:0001558) • negative regulation of cell proliferation (GO:0008285) • regulation of growth (GO:0040008) • positive regulation of apoptotic process (GO:0043065) • protein phosphorylation (GO:0006468) • positive regulation of insulin-like growth factor receptor signaling pathway (GO:0043568)
Sepp1	selenoprotein P, plasma, 1	0.0069	-2.85	• brain development (GO:0007420) • locomotory behavior (GO:0007626) • post-embryonic development (GO:0009791) • growth (GO:0040007)
Lpl	lipoprotein lipase	0.0032	-2.84	• receptor binding (GO:0005102) • protein binding (GO:0005515) • lipoprotein lipase activity (GO:0004465)
Adh1	alcohol dehydrogenase 1	0.0042	-2.80	• alcohol dehydrogenase (NAD) activity (GO:0004022) • protein homodimerization activity (GO:0042803) • ethanol catabolic process (GO:0006068)
Ttr	transthyretin	0.0421	-2.77	• protein heterodimerization activity (GO:0046982) • transport (GO:0006810)

Table S18: Highest changing genes in Mefs Passage 1 Part IV.
WT was used as reference. Blue numbers: down- regulation; mt: Cofilin1$^{KTRTK/KTRTK}$; wt: Cofilin1$^{wt/wt}$.

MEF

Symbol	Name	p-value	Fold-Change (mt vs. wt)	Function
Pdgfra	platelet derived growth factor receptor	0.0140	-2.73	• in utero embryonic development (GO:0001701) • multicellular organismal development (GO:0007275) • positive regulation of cell proliferation (GO:0008284) • anatomical structure morphogenesis (GO:0009653) • organ morphogenesis (GO:0009887) • cell migration (GO:0016477) • signal transduction involved in regulation of gene expression (GO:0023019) • extracellular matrix organization (GO:0030198) • positive regulation of fibroblast proliferation (GO:0048146) • embryonic cranial skeleton morphogenesis (GO:0048701)
Erdr1	erythroid differentiation regulator 1	0.0102	-2.69	• negative regulation of cell proliferation (GO:0008285) • negative regulation of cell migration (GO:0030336)
Gdf10	growth differentiation factor 10	0.0421	-2.68	• transforming growth factor beta receptor binding (GO:0005160) • growth factor activity (GO:0008083) • regulation of apoptotic process (GO:0042981) • positive regulation of osteoblast differentiation (GO:0045669) • cell development (GO:0048468) • regulation of MAPK cascade (GO:0043408)

Table S19: Highest changing genes in Mefs Passage 1 Part V.
WT was used as reference. Blue numbers: down- regulation; mt: Cofilin1$^{KTRTK/KTRTK}$; wt: Cofilin1$^{wt/wt}$.

MEF

Symbol	Name	p-value	Fold-Change (mt vs. wt)	Function
Cyp7b1	cytochrome P450, family 7, subfamily b, polypeptide 1	0.0351	-2.65	• positive regulation of epithelial cell proliferation (GO:0050679) • lipid metabolic process (GO:0006629) • bile acid biosynthetic process (GO:0006699
Figf	c-fos induced growth factor	0.0260	-2.63	• growth factor activity (GO:0008083) • multicellular organismal development (GO:0007275) • positive regulation of cell proliferation (GO:0008284) • positive regulation of cell division (GO:0051781)
Igfbp3	insulin-like growth factor binding protein 3 Gene	0.0013	-2.61	• fibronectin binding (GO:0001968) • regulation of cell growth (GO:0001558) • protein phosphorylation (GO:0006468) • negative regulation of cell proliferation (GO:0008285) • regulation of growth (GO:0040008) • positive regulation of apoptotic process (GO:0043065) • positive regulation of insulin-like growth factor receptor signaling pathway (GO:0043568)
Tgfbr3	transforming growth factor, beta receptor III	0.0174	-2.59	• fibroblast growth factor binding (GO:0017134) • epithelial to mesenchymal transition (GO:0001837) • embryo development (GO:0009790) • negative regulation of epithelial cell migration (GO:0010633) • negative regulation of epithelial cell proliferation (GO:0050680) • proteinaceous extracellular matrix (GO:0005578) • intracellular signal transduction (GO:0035556)

Table S20: Highest changing genes in Mefs Passage 1 Part VI.
WT was used as reference. Blue numbers: down- regulation; mt: Cofilin1$^{KTRTK/KTRTK}$; wt: Cofilin1$^{wt/wt}$.

MEF

Symbol	Name	p-value	Fold-Change (mt vs. wt)	Function
Sdpr	serum deprivation response	0.0066	2.51	• positive regulation of transcription from RNA polymerase II promoter (GO:0045944) • lipid binding (GO:0008289)
Eno3	enolase 3, beta muscle	0.0374	2.57	• magnesium ion binding (GO:0000287) • phosphopyruvate hydratase activity (GO:0004634)
Actb	beta actin	0.0020	2.62	• RNA polymerase II core promoter proximal region sequence-specific DNA binding (GO:0000978) • RNA polymerase II distal enhancer sequence-specific DNA binding (GO:0000980) • cytoskeleton (GO:0005856) • focal adhesion (GO:0005925) • cortical cytoskeleton (GO:0030863)
Actg2	actin, gamma 2, smooth muscle	0.0458	2.70	• nucleotide binding (GO:0000166) • ATP binding (GO:0005524) • cytoskeleton (GO:0005856)

Table S21: Highest changing genes in Mefs Passage 1 Part VII.
WT was used as reference. Red numbers: up- regulation; mt: Cofilin1$^{KTRTK/KTRTK}$; wt: Cofilin1$^{wt/wt}$.

MEF

Symbol	Name	p-value	Fold-Change (mt vs. wt)	Function
2810003C17Rik	allograft inflammatory factor 1-like	0.0253	2.87	• actin binding (GO:0003779) • actin filament binding (GO:0051015) • cell projection (GO:0042995) • protein complex (GO:0043234)
Igf2r	insulin-like growth factor 2 receptor	0.0387	2.93	• phosphoprotein binding (GO:0051219) • regulation of apoptotic process (GO:0042981)
Il1rl1	interleukin 1 receptor-like 1 Gene	0.0017	3.00	• negative regulation of cell proliferation (GO:0008285) • positive regulation of macrophage activation (GO:0043032) • interleukin-33 receptor activity (GO:0002114)
Hnrpl	heterogeneous nuclear ribonucleoprotein L	0.0220	3.05	• transcription regulatory region DNA binding (GO:0044212) • RNA binding (GO:0003723) • nucleotide binding (GO:0000166) • mRNA processing (GO:0006397)

Table S22: Highest changing genes in Mefs Passage 1 Part VIII.
WT was used as reference. Red numbers: up- regulation; mt: Cofilin1$^{KTRTK/KTRTK}$; wt: Cofilin1$^{wt/wt}$.

MEF

Symbol	Name	p-value	Fold-Change (mt vs. wt)	Function
Klk8	kallikrein related-peptidase 8	0.0015	3.06	• cell death (GO:0008219) • proteolysis (GO:0006508) • negative regulation of myelination (GO:0031642) • negative regulation of axon regeneration (GO:0048681) • neuron projection morphogenesis (GO:0048812) • regulation of synapse organization (GO:0050807)
Tagln	transgelin	0.0133	3.06	• cytoskeleton organization (GO:0007010) • epithelial cell differentiation (GO:0030855)
Inhba	inhibin beta-A	0.0260	3.08	• growth factor activity (GO:0008083) • regulation of transcription from RNA polymerase II promoter (GO:0006357) • cell cycle arrest (GO:0007050) • negative regulation of cell proliferation (GO:0008285) • G1/S transition of mitotic cell cycle (GO:0000082) • negative regulation of cell growth (GO:0030308) • DNA-templated (GO:0045893) • positive regulation of transcription from RNA polymerase II promoter (GO:0045944) • cell development (GO:0048468)

Table S23: Highest changing genes in Mefs Passage 1 Part IX.
WT was used as reference. Red numbers: up- regulation; mt: Cofilin1$^{KTRTK/KTRTK}$; wt: Cofilin1$^{wt/wt}$.

MEF

Symbol	Name	p-value	Fold-Change (mt vs. wt)	Function
Ankrd1	ankyrin repeat domain 1	0.0121	3.67	• RNA polymerase II transcription factor binding (GO:0001085) • regulation of transcription from RNA polymerase II promoter (GO:0006357) • positive regulation of apoptotic process (GO:0043065) • skeletal muscle cell differentiation (GO:0035914) • negative regulation of DNA biosynthetic process (GO:2000279)
Col2a1	collagen type II, alpha 1	0.0029	3.86	• extracellular matrix structural constituent (GO:0005201) • skeletal system development (GO:0001501) • cartilage condensation (GO:0001502) • tissue homeostasis (GO:0001894) • endochondral ossification (GO:0001958) • chondrocyte differentiation (GO:0002062) • regulation of gene expression (GO:0010468) • collagen fibril organization (GO:0030199)
Acta1	alpha actin, skeleton muscle f	0.0158	4.91	• skeletal muscle fiber development (GO:0048741) • nucleotide binding (GO:0000166) • actin cytoskeleton (GO:0015629)

Table S24: Highest changing genes in Mefs Passage 1 Part X.
WT was used as reference. Red numbers: up- regulation; mt: Cofilin1$^{KTRTK/KTRTK}$; wt: Cofilin1$^{wt/wt}$.

7. References

Agrawal, P. B., R. S. Greenleaf, K. K. Tomczak, V. L. Lehtokari, et al. (2007). "Nemaline myopathy with minicores caused by mutation of the CFL2 gene encoding the skeletal muscle actin-binding protein, cofilin-2." American journal of human genetics **80**(1): 162-167.

Aldrich, S.-. (2008). qPCR technical guide.

Amankwah, K. S. and U. De Boni (1994). "Ultrastructural localization of filamentous actin within neuronal interphase nuclei in situ." Experimental cell research **210**(2): 315-325.

Anderson, D. R., D. J. Sweeney and T. A. Williams (1996). Statistics for business and economics. Minneapolis/St. Paul, West Pub. Co.

Arber, S., F. A. Barbayannis, H. Hanser, C. Schneider, et al. (1998). "Regulation of actin dynamics through phosphorylation of cofilin by LIM-kinase." Nature **393**(6687): 805-809.

Arnold, S. J., G. J. Huang, A. F. Cheung, T. Era, et al. (2008). "The T-box transcription factor Eomes/Tbr2 regulates neurogenesis in the cortical subventricular zone." Genes & development **22**(18): 2479-2484.

Ashworth, S., B. Teng, J. Kaufeld, E. Miller, et al. (2010). "Cofilin-1 inactivation leads to proteinuria--studies in zebrafish, mice and humans." PloS one **5**(9): e12626.

Bamburg, J. R. (1999). "Proteins of the ADF/cofilin family: essential regulators of actin dynamics." Annual review of cell and developmental biology **15**: 185-230.

Bamburg, J. R., B. W. Bernstein, R. C. Davis, K. C. Flynn, et al. (2010). "ADF/Cofilin-actin rods in neurodegenerative diseases." Current Alzheimer research **7**(3): 241-250.

Bamburg, J. R. and G. S. Bloom (2009). "Cytoskeletal pathologies of Alzheimer disease." Cell motility and the cytoskeleton **66**(8): 635-649.

Bamburg, J. R., A. McGough and S. Ono (1999). "Putting a new twist on actin: ADF/cofilins modulate actin dynamics." Trends in cell biology **9**(9): 364-370.

Bamburg, J. R. and O. P. Wiggan (2002). "ADF/cofilin and actin dynamics in disease." Trends Cell Biol **12**(12): 598-605.

Bellenchi, G. C., C. B. Gurniak, E. Perlas, S. Middei, et al. (2007). "N-cofilin is associated with neuronal migration disorders and cell cycle control in the cerebral cortex." Genes & development **21**(18): 2347-2357.

Bender, M., A. Eckly, J. H. Hartwig, M. Elvers, et al. (2010). "ADF/n-cofilin-dependent actin turnover determines platelet formation and sizing." Blood **116**(10): 1767-1775.

Bertram, J. S., P. R. Libby and W. M. LeStourgeon (1977). "Changes in nuclear actin levels with change in growth state of C3H/10T1/2 cells and the lack of response in malignantly transformed cells." Cancer research **37**(11): 4104-4111.

Bi, L., I. Okabe, D. J. Bernard, A. Wynshaw-Boris, et al. (1999). "Proliferative defect and embryonic lethality in mice homozygous for a deletion in the p110alpha subunit of phosphoinositide 3-kinase." The Journal of biological chemistry **274**(16): 10963-10968.

Blanchoin, L., R. C. Robinson, S. Choe and T. D. Pollard (2000). "Phosphorylation of Acanthamoeba actophorin (ADF/cofilin) blocks interaction with actin without a change in atomic structure." J Mol Biol **295**(2): 203-211.

Bläsius, K. (2012). Neuronal migration in Cofilin 1 mutant mice. Institute of genetics. Bonn, Bonn. **Diploma**.

Bonneh-Barkay, D. and C. A. Wiley (2009). "Brain extracellular matrix in neurodegeneration." Brain pathology **19**(4): 573-585.

Bowman, G. D., I. M. Nodelman, Y. Hong, N. H. Chua, et al. (2000). "A comparative structural analysis of the ADF/cofilin family." Proteins **41**(3): 374-384.

Brault, V., R. Moore, S. Kutsch, M. Ishibashi, et al. (2001). "Inactivation of the beta-catenin gene by Wnt1-Cre-mediated deletion results in dramatic brain malformation and failure of craniofacial development." Development **128**(8): 1253-1264.

Bravo-Cordero, J. J., M. A. Magalhaes, R. J. Eddy, L. Hodgson, et al. (2013). "Functions of cofilin in cell locomotion and invasion." Nature reviews. Molecular cell biology **14**(7): 405-415.

Brouns, M. R., S. F. Matheson, K. Q. Hu, I. Delalle, et al. (2000). "The adhesion signaling molecule p190 RhoGAP is required for morphogenetic processes in neural development." Development **127**(22): 4891-4903.

Brunel, C. and M. N. Lelay (1979). "Two-dimensional analysis of proteins associated with heterogenous nuclear RNA in various animal cell lines." European journal of biochemistry / FEBS **99**(2): 273-283.

Bu, P., Y. A. Evrard, G. Lozano and S. Y. Dent (2007). "Loss of Gcn5 acetyltransferase activity leads to neural tube closure defects and exencephaly in mouse embryos." Mol Cell Biol **27**(9): 3405-3416.

Bullock, W. O., J. M. Fernandez and J. M. Short (1987). "XL1-Blue: a high efficiency plasmid transforming recA Escherichia coli\/ strain with beta-galactosidase selection." Biotechniques **5**(4): 376-379.

Bunnell, T. M., B. J. Burbach, Y. Shimizu and J. M. Ervasti (2011). "beta-Actin specifically controls cell growth, migration, and the G-actin pool." Molecular biology of the cell **22**(21): 4047-4058.

Cairns, B. R., H. Erdjument-Bromage, P. Tempst, F. Winston, et al. (1998). "Two actin-related proteins are shared functional components of the chromatin-remodeling complexes RSC and SWI/SNF." Mol Cell **2**(5): 639-651.

Campbell, C. S. and R. D. Mullins (2007). "In vivo visualization of type II plasmid segregation: bacterial actin filaments pushing plasmids." J Cell Biol **179**(5): 1059-1066.

Carlier, M. F., V. Laurent, J. Santolini, R. Melki, et al. (1997). "Actin depolymerizing factor (ADF/cofilin) enhances the rate of filament turnover: implication in actin-based motility." J Cell Biol **136**(6): 1307-1322.

Chai, X., E. Forster, S. Zhao, H. H. Bock, et al. (2009). "Reelin acts as a stop signal for radially migrating neurons by inducing phosphorylation of n-cofilin at the leading edge." Communicative & integrative biology **2**(4): 375-377.

Chai, X., E. Forster, S. Zhao, H. H. Bock, et al. (2009). "Reelin stabilizes the actin cytoskeleton of neuronal processes by inducing n-cofilin phosphorylation at serine3." The Journal of neuroscience : the official journal of the Society for Neuroscience **29**(1): 288-299.

Chang, C. Y., J. Leu and Y. J. Lee (2015). "The Actin Depolymerizing Factor (ADF)/Cofilin Signaling Pathway and DNA Damage Responses in Cancer." International journal of molecular sciences **16**(2): 4095-4120.

Chenn, A. and S. K. McConnell (1995). "Cleavage orientation and the asymmetric inheritance of Notch1 immunoreactivity in mammalian neurogenesis." Cell **82**(4): 631-641.

Chhabra, D. and C. G. dos Remedios (2005). "Cofilin, actin and their complex observed in vivo using fluorescence resonance energy transfer." Biophysical journal **89**(3): 1902-1908.

Chua, B. T., C. Volbracht, K. O. Tan, R. Li, et al. (2003). "Mitochondrial translocation of cofilin is an early step in apoptosis induction." Nature cell biology **5**(12): 1083-1089.

Chuang, C. H., A. E. Carpenter, B. Fuchsova, T. Johnson, et al. (2006). "Long-range directional movement of an interphase chromosome site." Current biology : CB **16**(8): 825-831.

Clark, Ed. (2006). Molecular Biology, Spektrum Akademischer Verlag.

Clubb, B. H. and M. Locke (1998). "Peripheral nuclear matrix actin forms perinuclear shells." Journal of cellular biochemistry **70**(2): 240-251.

Colucci-Guyon, E., Y. R. M. Gimenez, T. Maurice, C. Babinet, et al. (1999). "Cerebellar defect and impaired motor coordination in mice lacking vimentin." Glia **25**(1): 33-43.

COMPENDIUM, L. M. D.-E. D. S. C. (2014). Skull bone development.

Copp, A. J. (2005). "Neurulation in the cranial region--normal and abnormal." Journal of anatomy **207**(5): 623-635.

Copp, A. J., F. A. Brook, J. P. Estibeiro, A. S. Shum, et al. (1990). "The embryonic development of mammalian neural tube defects." Progress in neurobiology **35**(5): 363-403.

Copp, A. J. and N. D. Greene (2010). "Genetics and development of neural tube defects." J Pathol **220**(2): 217-230.

Copp, A. J., N. D. Greene and J. N. Murdoch (2003). "The genetic basis of mammalian neurulation." Nature reviews. Genetics **4**(10): 784-793.

Copp, A. J., P. Stanier and N. D. Greene (2013). "Neural tube defects: recent advances, unsolved questions, and controversies." The Lancet. Neurology **12**(8): 799-810.

Crowley, K. S. and K. Brasch (1987). "Does the interchromatin compartment contain actin?" Cell biology international reports **11**(7): 537-546.

Cruz, J. R., C. de la Torre and S. Moreno Diaz de la Espina (2008). "Nuclear actin in plants." Cell biology international **32**(5): 584-587.

Dawe, H. R. (2003). The role of ADF/cofilin family proteins in the acquisition and maintenance of cell polarity during fibroblast migration. London, University College London. **PhD**.

Dawe, H. R., L. S. Minamide, J. R. Bamburg and L. P. Cramer (2003). "ADF/cofilin controls cell polarity during fibroblast migration." Current biology : CB **13**(3): 252-257.

de Lanerolle, P., T. Johnson and W. A. Hofmann (2005). "Actin and myosin I in the nucleus: what next?" Nat Struct Mol Biol **12**(9): 742-746.

de Taxis du Poet, P., Y. Arcand, R. Bernier, Jr., J. N. Barbotin, et al. (1987). "Plasmid stability in immobilized and free recombinant Escherichia coli JM105(pKK223-200): importance of oxygen diffusion, growth rate, and plasmid copy number." Appl Environ Microbiol **53**(7): 1548-1555.

Detrait, E. R., T. M. George, H. C. Etchevers, J. R. Gilbert, et al. (2005). "Human neural tube defects: developmental biology, epidemiology, and genetics." Neurotoxicology and teratology **27**(3): 515-524.

Dimri, G. P., X. Lee, G. Basile, M. Acosta, et al. (1995). "A biomarker that identifies senescent human cells in culture and in aging skin in vivo." Proceedings of the National Academy of Sciences of the United States of America **92**(20): 9363-9367.

Dingwall, C. and R. A. Laskey (1986). "Protein import into the cell nucleus." Annual review of cell biology **2**: 367-390.

Dolk, H., M. Loane and E. Garne (2010). "The prevalence of congenital anomalies in Europe." Advances in experimental medicine and biology **686**: 349-364.

Dopie, J., K. P. Skarp, E. K. Rajakyla, K. Tanhuanpaa, et al. (2012). "Active maintenance of nuclear actin by importin 9 supports transcription." Proceedings of the National Academy of Sciences of the United States of America **109**(9): E544-552.

dos Remedios, C. G., D. Chhabra, M. Kekic, I. V. Dedova, et al. (2003). "Actin binding proteins: regulation of cytoskeletal microfilaments." Physiol Rev **83**(2): 433-473.

Douvas, A. S., C. A. Harrington and J. Bonner (1975). "Major nonhistone proteins of rat liver chromatin: preliminary identification of myosin, actin, tubulin, and

tropomyosin." Proceedings of the National Academy of Sciences of the United States of America **72**(10): 3902-3906.

Du, J. and C. Frieden (1998). "Kinetic studies on the effect of yeast cofilin on yeast actin polymerization." Biochemistry **37**(38): 13276-13284.

Estivill-Torrus, G., H. Pearson, V. van Heyningen, D. J. Price, et al. (2002). "Pax6 is required to regulate the cell cycle and the rate of progression from symmetrical to asymmetrical division in mammalian cortical progenitors." Development **129**(2): 455-466.

Evans, L. L. and P. C. Bridgman (1995). "Particles move along actin filament bundles in nerve growth cones." Proc Natl Acad Sci U S A **92**(24): 10954-10958.

Fairbridge, N. A., C. E. Dawe, F. H. Niri, M. K. Kooistra, et al. (2010). "Cecr2 mutations causing exencephaly trigger misregulation of mesenchymal/ectodermal transcription factors." Birth defects research. Part A, Clinical and molecular teratology **88**(8): 619-625.

Fairley, E. A., J. Kendrick-Jones and J. A. Ellis (1999). "The Emery-Dreifuss muscular dystrophy phenotype arises from aberrant targeting and binding of emerin at the inner nuclear membrane." Journal of cell science **112 (Pt 15)**: 2571-2582.

Falck, S. (2004). Regulation of the actin cytoskleleton by Twinfilin. Department of Biological and Environmental Sciences. Helsinki, Viikkii Graduate School in Biosciences. **PhD**.

Field, C. M. and B. M. Alberts (1995). "Anillin, a contractile ring protein that cycles from the nucleus to the cell cortex." The Journal of cell biology **131**(1): 165-178.

Flynn, K. C., F. Hellal, D. Neukirchen, S. Jacob, et al. (2012). "ADF/cofilin-mediated actin retrograde flow directs neurite formation in the developing brain." Neuron **76**(6): 1091-1107.

Folgueira, M., P. Bayley, P. Navratilova, T. S. Becker, et al. (2012). "Morphogenesis underlying the development of the everted teleost telencephalon." Neural development **7**: 32.

Fradelizi, J., V. Noireaux, J. Plastino, B. Menichi, et al. (2001). "ActA and human zyxin harbour Arp2/3-independent actin-polymerization activity." Nature cell biology **3**(8): 699-707.

Frangiskakis, J. M., A. K. Ewart, C. A. Morris, C. B. Mervis, et al. (1996). "LIM-kinase1 hemizygosity implicated in impaired visuospatial constructive cognition." Cell **86**(1): 59-69.

Fu, H., R. R. Subramanian and S. C. Masters (2000). "14-3-3 proteins: structure, function, and regulation." Annu Rev Pharmacol Toxicol **40**: 617-647.

Fukui, Y. and H. Katsumaru (1979). "Nuclear actin bundles in Amoeba, Dictyostelium and human HeLa cells induced by dimethyl sulfoxide." Experimental cell research **120**(2): 451-455.

Funaki, K., T. Katsumoto and A. Iino (1995). "Immunocytochemical localization of actin in the nucleolus of rat oocytes." Biology of the cell / under the auspices of the European Cell Biology Organization **84**(3): 139-146.

Galkin, V. E., A. Orlova, N. Lukoyanova, W. Wriggers, et al. (2001). "Actin depolymerizing factor stabilizes an existing state of F-actin and can change the tilt of F-actin subunits." The Journal of cell biology **153**(1): 75-86.

Galou, M., E. Colucci-Guyon, D. Ensergueix, J. L. Ridet, et al. (1996). "Disrupted glial fibrillary acidic protein network in astrocytes from vimentin knockout mice." The Journal of cell biology **133**(4): 853-863.

Garg, P., R. Verma, L. Cook, A. Soofi, et al. (2010). "Actin-depolymerizing factor cofilin-1 is necessary in maintaining mature podocyte architecture." J Biol Chem **285**(29): 22676-22688.

Gartner, L. P., J. L. Hiatt and J. M. Strum (2011). Cell biology and histology. Philadelphia, Wolters Kluwer Health/Lippincott Williams & Wilkins.

Garvalov, B. K., K. C. Flynn, D. Neukirchen, L. Meyn, et al. (2007). "Cdc42 regulates cofilin during the establishment of neuronal polarity." J Neurosci **27**(48): 13117-13129.

Gaspard, N., T. Bouschet, R. Hourez, J. Dimidschstein, et al. (2008). "An intrinsic mechanism of corticogenesis from embryonic stem cells." Nature **455**(7211): 351-357.

George, E. L., E. N. Georges-Labouesse, R. S. Patel-King, H. Rayburn, et al. (1993). "Defects in mesoderm, neural tube and vascular development in mouse embryos lacking fibronectin." Development **119**(4): 1079-1091.

Ghosh, M., X. Song, G. Mouneimne, M. Sidani, et al. (2004). "Cofilin promotes actin polymerization and defines the direction of cell motility." Science **304**(5671): 743-746.

Giansanti, M. G., S. Bonaccorsi and M. Gatti (1999). "The role of anillin in meiotic cytokinesis of Drosophila males." Journal of cell science **112 (Pt 14)**: 2323-2334.

Giros, A., J. Morante, C. Gil-Sanz, A. Fairen, et al. (2007). "Perlecan controls neurogenesis in the developing telencephalon." BMC developmental biology **7**: 29.

Goebbels, S., I. Bormuth, U. Bode, O. Hermanson, et al. (2006). "Genetic targeting of principal neurons in neocortex and hippocampus of NEX-Cre mice." Genesis **44**(12): 611-621.

Gohla, A., J. Birkenfeld and G. M. Bokoch (2005). "Chronophin, a novel HAD-type serine protein phosphatase, regulates cofilin-dependent actin dynamics." Nature cell biology **7**(1): 21-29.

Gonsior, S. M., S. Platz, S. Buchmeier, U. Scheer, et al. (1999). "Conformational difference between nuclear and cytoplasmic actin as detected by a monoclonal antibody." Journal of cell science **112 (Pt 6)**: 797-809.

Gotz, M. and W. B. Huttner (2005). "The cell biology of neurogenesis." Nature reviews. Molecular cell biology **6**(10): 777-788.

Gray, P. A., H. Fu, P. Luo, Q. Zhao, et al. (2004). "Mouse brain organization revealed through direct genome-scale TF expression analysis." Science **306**(5705): 2255-2257.

Grossin, L., S. Etienne, N. Gaborit, A. Pinzano, et al. (2004). "Induction of heat shock protein 70 (Hsp70) by proteasome inhibitor MG 132 protects articular chondrocytes from cellular death in vitro and in vivo." Biorheology **41**(3-4): 521-534.

Guo, Y., S. Guo, N. Lu, Y. Chai, et al. (2015). "Identification of biomarkers for bone union promoted by mechanical stimulation." Frontiers in Bioscience.

Gupta, A., L. H. Tsai and A. Wynshaw-Boris (2002). "Life is a journey: a genetic look at neocortical development." Nature reviews. Genetics **3**(5): 342-355.

Gurniak, C. B., F. Chevessier, M. Jokwitz, F. Jonsson, et al. (2014). "Severe protein aggregate myopathy in a knockout mouse model points to an essential role of cofilin2 in sarcomeric actin exchange and muscle maintenance." European journal of cell biology **93**(5-6): 252-266.

Gurniak, C. B., E. Perlas and W. Witke (2005). "The actin depolymerizing factor n-cofilin is essential for neural tube morphogenesis and neural crest cell migration." Developmental biology **278**(1): 231-241.

Hall, J. G. (1986). "Neural tube defects, sex ratios, and X inactivation." Lancet **2**(8519): 1334-1335.

Harata, M., Y. Oma, S. Mizuno, Y. W. Jiang, et al. (1999). "The nuclear actin-related protein of Saccharomyces cerevisiae, Act3p/Arp4, interacts with core histones." Mol Biol Cell **10**(8): 2595-2605.

Harata, M., Y. Oma, T. Tabuchi, Y. Zhang, et al. (2000). "Multiple actin-related proteins of Saccharomyces cerevisiae are present in the nucleus." J Biochem **128**(4): 665-671.

Harata, M., Y. Zhang, D. J. Stillman, D. Matsui, et al. (2002). "Correlation between chromatin association and transcriptional regulation for the Act3p/Arp4 nuclear actin-related protein of Saccharomyces cerevisiae." Nucleic Acids Res **30**(8): 1743-1750.

Harris, M. J. and D. M. Juriloff (1997). "Genetic landmarks for defects in mouse neural tube closure." Teratology **56**(3): 177-187.

Harris, M. J. and D. M. Juriloff (1999). "Mini-review: toward understanding mechanisms of genetic neural tube defects in mice." Teratology **60**(5): 292-305.

Harris, M. J. and D. M. Juriloff (2010). "An update to the list of mouse mutants with neural tube closure defects and advances toward a complete genetic perspective of neural tube closure." Birth defects research. Part A, Clinical and molecular teratology **88**(8): 653-669.

Hattersley, G. and T. J. Chambers (1989). "Generation of osteoclastic function in mouse bone marrow cultures: multinuclearity and tartrate-resistant acid phosphatase are unreliable markers for osteoclastic differentiation." Endocrinology **124**(4): 1689-1696.

Hauptmann, G. and T. Gerster (2000). "Regulatory gene expression patterns reveal transverse and longitudinal subdivisions of the embryonic zebrafish forebrain." Mechanisms of development **91**(1-2): 105-118.

Hildebrand, J. D. and P. Soriano (1999). "Shroom, a PDZ domain-containing actin-binding protein, is required for neural tube morphogenesis in mice." Cell **99**(5): 485-497.

Hofmann, W. A. (2009). "Cell and molecular biology of nuclear actin." International review of cell and molecular biology **273**: 219-263.

Hofmann, W. A. and P. de Lanerolle (2006). "Nuclear actin: to polymerize or not to polymerize." J Cell Biol **172**(4): 495-496.

Hofmann, W. A., L. Stojiljkovic, B. Fuchsova, G. M. Vargas, et al. (2004). "Actin is part of pre-initiation complexes and is necessary for transcription by RNA polymerase II." Nature cell biology **6**(11): 1094-1101.

Holaska, J. M., A. K. Kowalski and K. L. Wilson (2004). "Emerin caps the pointed end of actin filaments: evidence for an actin cortical network at the nuclear inner membrane." PLoS biology **2**(9): E231.

Holaska, J. M. and K. L. Wilson (2007). "An emerin "proteome": purification of distinct emerin-containing complexes from HeLa cells suggests molecular basis for diverse roles including gene regulation, mRNA splicing, signaling, mechanosensing, and nuclear architecture." Biochemistry **46**(30): 8897-8908.

Hsu, S. H., B. Z. Schacter, N. L. Delaney, T. B. Miller, et al. (1976). "Genetic characteristics of the HeLa cell." Science **191**(4225): 392-394.

Hu, P., S. Wu and N. Hernandez (2004). "A role for beta-actin in RNA polymerase III transcription." Genes & development **18**(24): 3010-3015.

Huang, L., I. Kuwahara and K. Matsumoto (2014). "EWS represses cofilin 1 expression by inducing nuclear retention of cofilin 1 mRNA." Oncogene **33**(23): 2995-3003.

Huang, T. Y., C. DerMardirossian and G. M. Bokoch (2006). "Cofilin phosphatases and regulation of actin dynamics." Curr Opin Cell Biol **18**(1): 26-31.

Huang, X. and J. P. Saint-Jeannet (2004). "Induction of the neural crest and the opportunities of life on the edge." Developmental biology **275**(1): 1-11.

Hussey, P. J., E. G. Allwood and A. P. Smertenko (2002). "Actin-binding proteins in the Arabidopsis genome database: properties of functionally distinct plant actin-depolymerizing factors/cofilins." Philos Trans R Soc Lond B Biol Sci **357**(1422): 791-798.

Ibbotson, K. J., G. D. Roodman, L. M. McManus and G. R. Mundy (1984). "Identification and characterization of osteoclast-like cells and their progenitors in

cultures of feline marrow mononuclear cells." The Journal of cell biology **99**(2): 471-480.

Iida, K., H. Iida and I. Yahara (1986). "Heat shock induction of intranuclear actin rods in cultured mammalian cells." Experimental cell research **165**(1): 207-215.

Iida, K., S. Matsumoto and I. Yahara (1992). "The KKRKK sequence is involved in heat shock-induced nuclear translocation of the 18-kDa actin-binding protein, cofilin." Cell structure and function **17**(1): 39-46.

Iida, K. and I. Yahara (1986). "Reversible induction of actin rods in mouse C3H-2K cells by incubation in salt buffers and by treatment with non-ionic detergents." Experimental cell research **164**(2): 492-506.

Itahana, K., J. Campisi and G. P. Dimri (2007). "Methods to detect biomarkers of cellular senescence: the senescence-associated beta-galactosidase assay." Methods in molecular biology **371**: 21-31.

Iwasato, T., A. Datwani, A. M. Wolf, H. Nishiyama, et al. (2000). "Cortex-restricted disruption of NMDAR1 impairs neuronal patterns in the barrel cortex." Nature **406**(6797): 726-731.

Jaffe, A. B. and A. Hall (2005). "Rho GTPases: biochemistry and biology." Annual review of cell and developmental biology **21**: 247-269.

Jankovics, F., R. Sinka, T. Lukacsovich and M. Erdelyi (2002). "MOESIN crosslinks actin and cell membrane in Drosophila oocytes and is required for OSKAR anchoring." Current biology : CB **12**(23): 2060-2065.

Jansen, S., A. Collins, C. Yang, G. Rebowski, et al. (2011). "Mechanism of actin filament bundling by fascin." The Journal of biological chemistry **286**(34): 30087-30096.

Jiang, X., S. Iseki, R. E. Maxson, H. M. Sucov, et al. (2002). "Tissue origins and interactions in the mammalian skull vault." Developmental biology **241**(1): 106-116.

Jordan, M. A. and L. Wilson (1998). "Microtubules and actin filaments: dynamic targets for cancer chemotherapy." Curr Opin Cell Biol **10**(1): 123-130.

Kabsch, W., H. G. Mannherz, D. Suck, E. F. Pai, et al. (1990). "Atomic structure of the actin:DNase I complex." Nature **347**(6288): 37-44.

Kamal, J. K., S. A. Benchaar, K. Takamoto, E. Reisler, et al. (2007). "Three-dimensional structure of cofilin bound to monomeric actin derived by structural mass spectrometry data." Proceedings of the National Academy of Sciences of the United States of America **104**(19): 7910-7915.

Kang, K. W., S. J. Lee, J. W. Park and S. G. Kim (2002). "Phosphatidylinositol 3-kinase regulates nuclear translocation of NF-E2-related factor 2 through actin rearrangement in response to oxidative stress." Molecular pharmacology **62**(5): 1001-1010.

Kelman, Z. (1997). "PCNA: structure, functions and interactions." Oncogene **14**(6): 629-640.

Khaitlina, S. Y. (2001). "Functional specificity of actin isoforms." Int Rev Cytol **202**: 35-98.

Klamt, F., S. Zdanov, R. L. Levine, A. Pariser, et al. (2009). "Oxidant-induced apoptosis is mediated by oxidation of the actin-regulatory protein cofilin." Nature cell biology **11**(10): 1241-1246.

Koleske, A. J., A. M. Gifford, M. L. Scott, M. Nee, et al. (1998). "Essential roles for the Abl and Arg tyrosine kinases in neurulation." Neuron **21**(6): 1259-1272.

Kriegstein, A. and J. G. Parnavelas (2006). "Progress in corticogenesis." Cerebral cortex **16 Suppl 1**: i1-2.

Kuhn, J. R. and T. D. Pollard (2005). "Real-time measurements of actin filament polymerization by total internal reflection fluorescence microscopy." Biophys J **88**(2): 1387-1402.

Kulesa, P., D. L. Ellies and P. A. Trainor (2004). "Comparative analysis of neural crest cell death, migration, and function during vertebrate embryogenesis." Developmental dynamics : an official publication of the American Association of Anatomists **229**(1): 14-29.

Kusano, K., H. Abe and T. Obinata (1999). "Detection of a sequence involved in actin-binding and phosphoinositide-binding in the N-terminal side of cofilin." Mol Cell Biochem **190**(1-2): 133-141.

Lanier, L. M., M. A. Gates, W. Witke, A. S. Menzies, et al. (1999). "Mena is required for neurulation and commissure formation." Neuron **22**(2): 313-325.

Larsen, M., V. V. Artym, J. A. Green and K. M. Yamada (2006). "The matrix reorganized: extracellular matrix remodeling and integrin signaling." Current opinion in cell biology **18**(5): 463-471.

Lattanzi, G., V. Cenni, S. Marmiroli, C. Capanni, et al. (2003). "Association of emerin with nuclear and cytoplasmic actin is regulated in differentiating myoblasts." Biochemical and biophysical research communications **303**(3): 764-770.

Lenart, P., C. P. Bacher, N. Daigle, A. R. Hand, et al. (2005). "A contractile nuclear actin network drives chromosome congression in oocytes." Nature **436**(7052): 812-818.

Lengner, C. J., C. Lepper, A. J. van Wijnen, J. L. Stein, et al. (2004). "Primary mouse embryonic fibroblasts: a model of mesenchymal cartilage formation." Journal of cellular physiology **200**(3): 327-333.

Lestourgeon, W. M., A. Forer, Y. Z. Yang, J. S. Bertram, et al. (1975). "Contractile proteins. Major components of nuclear and chromosome non-histone proteins." Biochimica et biophysica acta **379**(2): 529-552.

Lewin, B., L. Cassimeris, V. Lingappa and G. Plopper, Eds. (2007). Cells. Sudbury, Massachusetts, Jones and Bartlett Publishers.

Lin, C. W., S. T. Yen, H. T. Chang, S. J. Chen, et al. (2010). "Loss of cofilin 1 disturbs actin dynamics, adhesion between enveloping and deep cell layers and cell movements during gastrulation in zebrafish." PloS one **5**(12): e15331.

Littlewood, T. D., D. C. Hancock, P. S. Danielian, M. G. Parker, et al. (1995). "A modified oestrogen receptor ligand-binding domain as an improved switch for the regulation of heterologous proteins." Nucleic acids research **23**(10): 1686-1690.

Lomaga, M. A., J. T. Henderson, A. J. Elia, J. Robertson, et al. (2000). "Tumor necrosis factor receptor-associated factor 6 (TRAF6) deficiency results in exencephaly and is required for apoptosis within the developing CNS." J Neurosci **20**(19): 7384-7393.

Lopez, I., R. G. Anthony, S. K. Maciver, C. J. Jiang, et al. (1996). "Pollen specific expression of maize genes encoding actin depolymerizing factor-like proteins." Proc Natl Acad Sci U S A **93**(14): 7415-7420.

Luo, H., X. Liu, F. Wang, Q. Huang, et al. (2005). "Disruption of palladin results in neural tube closure defects in mice." Mol Cell Neurosci **29**(4): 507-515.

Ma, M., L. Zhou, X. Guo, Z. Lv, et al. (2009). "Decreased cofilin1 expression is important for compaction during early mouse embryo development." Biochimica et biophysica acta **1793**(12): 1804-1810.

Marx, C. (2011). Cell culture studies on the localization of cofilin 1 under different stimulatory conditions Institute of Genetics. Bonn, Bonn. **BSc**.

Matsumoto, A., T. Hatta, K. Moriyama and H. Otani (2002). "Sequential observations of exencephaly and subsequent morphological changes by mouse exo utero development system: analysis of the mechanism of transformation from exencephaly to anencephaly." Anatomy and embryology **205**(1): 7-18.

Maundrell, K. and K. Scherrer (1979). "Characterization of pre-messenger-RNA-containing nuclear ribonucleoprotein particles from avian erythroblasts." European journal of biochemistry / FEBS **99**(2): 225-238.

McCall, M. A., R. G. Gregg, R. R. Behringer, M. Brenner, et al. (1996). "Targeted deletion in astrocyte intermediate filament (Gfap) alters neuronal physiology." Proceedings of the National Academy of Sciences of the United States of America **93**(13): 6361-6366.

McGough, A. and W. Chiu (1999). "ADF/cofilin weakens lateral contacts in the actin filament." J Mol Biol **291**(3): 513-519.

McKim, K. S., C. Matheson, M. A. Marra, M. F. Wakarchuk, et al. (1994). "The Caenorhabditis elegans unc-60 gene encodes proteins homologous to a family of actin-binding proteins." Mol Gen Genet **242**(3): 346-357.

Meberg, P. J. and J. R. Bamburg (2000). "Increase in neurite outgrowth mediated by overexpression of actin depolymerizing factor." The Journal of neuroscience : the official journal of the Society for Neuroscience **20**(7): 2459-2469.

Meberg, P. J., S. Ono, L. S. Minamide, M. Takahashi, et al. (1998). "Actin depolymerizing factor and cofilin phosphorylation dynamics: response to signals that regulate neurite extension." Cell motility and the cytoskeleton **39**(2): 172-190.

Medina, L., A. Brox, I. Legaz, M. Garcia-Lopez, et al. (2005). "Expression patterns of developmental regulatory genes show comparable divisions in the telencephalon of Xenopus and mouse: insights into the evolution of the forebrain." Brain research bulletin **66**(4-6): 297-302.

Meier, S. (2014). Interaction partners of the ADF/cofilin family. Institute for genetics. Bonn, Bonn. **BSc**.

Menet, V., M. Gimenez y Ribotta, N. Chauvet, M. J. Drian, et al. (2001). "Inactivation of the glial fibrillary acidic protein gene, but not that of vimentin, improves neuronal survival and neurite growth by modifying adhesion molecule expression." The Journal of neuroscience : the official journal of the Society for Neuroscience **21**(16): 6147-6158.

Menet, V., Y. R. M. Gimenez, F. Sandillon and A. Privat (2000). "GFAP null astrocytes are a favorable substrate for neuronal survival and neurite growth." Glia **31**(3): 267-272.

Menzies, A. S., A. Aszodi, S. E. Williams, A. Pfeifer, et al. (2004). "Mena and vasodilator-stimulated phosphoprotein are required for multiple actin-dependent processes that shape the vertebrate nervous system." J Neurosci **24**(37): 8029-8038.

Merriam, R. W. and R. J. Hill (1976). "The germinal vesicle nucleus of Xenopus laevis oocytes as a selective storage receptacle for proteins." The Journal of cell biology **69**(3): 659-668.

Milankov, K. and U. De Boni (1993). "Cytochemical localization of actin and myosin aggregates in interphase nuclei in situ." Experimental cell research **209**(2): 189-199.

Milunsky, A., H. Jick, S. S. Jick, C. L. Bruell, et al. (1989). "Multivitamin/folic acid supplementation in early pregnancy reduces the prevalence of neural tube defects." JAMA : the journal of the American Medical Association **262**(20): 2847-2852.

Minamide, L. S., S. Maiti, J. A. Boyle, R. C. Davis, et al. (2010). "Isolation and characterization of cytoplasmic cofilin-actin rods." The Journal of biological chemistry **285**(8): 5450-5460.

Miralles, F. and N. Visa (2006). "Actin in transcription and transcription regulation." Current opinion in cell biology **18**(3): 261-266.

Mitchell, L. E. (2005). "Epidemiology of neural tube defects." American journal of medical genetics. Part C, Seminars in medical genetics **135C**(1): 88-94.

Monuki, E. S. and C. A. Walsh (2001). "Mechanisms of cerebral cortical patterning in mice and humans." Nature neuroscience **4 Suppl**: 1199-1206.

Moretti, M. E., B. Bar-Oz, S. Fried and G. Koren (2005). "Maternal hyperthermia and the risk for neural tube defects in offspring: systematic review and meta-analysis." Epidemiology **16**(2): 216-219.

Moriyama, K., K. Iida and I. Yahara (1996). "Phosphorylation of Ser-3 of cofilin regulates its essential function on actin." Genes Cells **1**(1): 73-86.

Moriyama, K., S. Matsumoto, E. Nishida, H. Sakai, et al. (1990). "Nucleotide sequence of mouse cofilin cDNA." Nucleic Acids Res **18**(10): 3053.

Moriyama, K. and I. Yahara (2002). "Human CAP1 is a key factor in the recycling of cofilin and actin for rapid actin turnover." J Cell Sci **115**(Pt 8): 1591-1601.

Mseka, T., J. R. Bamburg and L. P. Cramer (2007). "ADF/cofilin family proteins control formation of oriented actin-filament bundles in the cell body to trigger fibroblast polarization." Journal of cell science **120**(Pt 24): 4332-4344.

Mueller, T., Z. Dong, M. A. Berberoglu and S. Guo (2011). "The dorsal pallium in zebrafish, Danio rerio (Cyprinidae, Teleostei)." Brain research **1381**: 95-105.

Mullis, K. B. and F. A. Faloona (1987). "Specific synthesis of DNA in vitro via a polymerase-catalyzed chain reaction." Methods Enzymol **155**: 335-350.

Munsie, L. N., C. R. Desmond and R. Truant (2012). "Cofilin nuclear-cytoplasmic shuttling affects cofilin-actin rod formation during stress." Journal of cell science **125**(Pt 17): 3977-3988.

Mustonen, P., J. A. Virtanen, P. J. Somerharju and P. K. Kinnunen (1987). "Binding of cytochrome c to liposomes as revealed by the quenching of fluorescence from pyrene-labeled phospholipids." Biochemistry **26**(11): 2991-2997.

Nadarajah, B. and J. G. Parnavelas (2002). "Modes of neuronal migration in the developing cerebral cortex." Nature reviews. Neuroscience **3**(6): 423-432.

Nagai, S., O. Moreno, C. A. Smith, S. Ivanchuk, et al. (2011). "Role of the cofilin activity cycle in astrocytoma migration and invasion." Genes & cancer **2**(9): 859-869.

Nagaoka, R., H. Abe, K. Kusano and T. Obinata (1995). "Concentration of cofilin, a small actin-binding protein, at the cleavage furrow during cytokinesis." Cell motility and the cytoskeleton **30**(1): 1-7.

Nakanishi, A., D. Shum, H. Morioka, E. Otsuka, et al. (2002). "Interaction of the Vp3 nuclear localization signal with the importin alpha 2/beta heterodimer directs nuclear entry of infecting simian virus 40." Journal of virology **76**(18): 9368-9377.

Nakayasu, H. and K. Ueda (1983). "Association of actin with the nuclear matrix from bovine lymphocytes." Experimental cell research **143**(1): 55-62.

Nebl, G., S. C. Meuer and Y. Samstag (1996). "Dephosphorylation of serine 3 regulates nuclear translocation of cofilin." The Journal of biological chemistry **271**(42): 26276-26280.

Nieto, M., E. S. Monuki, H. Tang, J. Imitola, et al. (2004). "Expression of Cux-1 and Cux-2 in the subventricular zone and upper layers II-IV of the cerebral cortex." The Journal of comparative neurology **479**(2): 168-180.

Nieuwenhuys, R. (2011). "The development and general morphology of the telencephalon of actinopterygian fishes: synopsis, documentation and commentary." Brain structure & function **215**(3-4): 141-157.

Nishida, E. (1985). "Opposite effects of cofilin and profilin from porcine brain on rate of exchange of actin-bound adenosine 5'-triphosphate." Biochemistry **24**(5): 1160-1164.

Nishida, E., K. Iida, N. Yonezawa, S. Koyasu, et al. (1987). "Cofilin is a component of intranuclear and cytoplasmic actin rods induced in cultured cells." Proceedings of the National Academy of Sciences of the United States of America **84**(15): 5262-5266.

Nix, D. A. and M. C. Beckerle (1997). "Nuclear-cytoplasmic shuttling of the focal contact protein, zyxin: a potential mechanism for communication between sites of cell adhesion and the nucleus." The Journal of cell biology **138**(5): 1139-1147.

Obrdlik, A. and P. Percipalle (2011). "The F-actin severing protein cofilin-1 is required for RNA polymerase II transcription elongation." Nucleus **2**(1): 72-79.

Ohnishi, T., H. Kawamura and Y. Tanaka (1964). "[Actin and Myosin-Like Proteins in the Calf Thymus Cell Nucleus]." Journal of biochemistry **56**: 6-15.

Ohnishi, T., H. Kawamura and T. Yamamoto (1963). "[Extraction of a Protein Resembling Actin from the Cell Nucleus of the Calf Thymus]." Journal of biochemistry **54**: 298-300.

Ohta, Y., E. Nishida, H. Sakai and E. Miyamoto (1989). "Dephosphorylation of cofilin accompanies heat shock-induced nuclear accumulation of cofilin." The Journal of biological chemistry **264**(27): 16143-16148.

Olave, I. A., S. L. Reck-Peterson and G. R. Crabtree (2002). "Nuclear actin and actin-related proteins in chromatin remodeling." Annual review of biochemistry **71**: 755-781.

Ono, S. (2003). "Regulation of actin filament dynamics by actin depolymerizing factor/cofilin and actin-interacting protein 1: new blades for twisted filaments." Biochemistry **42**(46): 13363-13370.

Ono, S., D. L. Baillie and G. M. Benian (1999). "UNC-60B, an ADF/cofilin family protein, is required for proper assembly of actin into myofibrils in Caenorhabditis elegans body wall muscle." J Cell Biol **145**(3): 491-502.

Onoda, K., F. X. Yu and H. L. Yin (1993). "gCap39 is a nuclear and cytoplasmic protein." Cell motility and the cytoskeleton **26**(3): 227-238.

Orlova, A., E. C. Garner, V. E. Galkin, J. Heuser, et al. (2007). "The structure of bacterial ParM filaments." Nat Struct Mol Biol **14**(10): 921-926.

Otterbein, L. R., P. Graceffa and R. Dominguez (2001). "The crystal structure of uncomplexed actin in the ADP state." Science **293**(5530): 708-711.

Padrick, S. B., L. K. Doolittle, C. A. Brautigam, D. S. King, et al. (2011). "Arp2/3 complex is bound and activated by two WASP proteins." Proceedings of the National Academy of Sciences of the United States of America **108**(33): E472-479.

Pagoulatos, G. N. and M. Yaniv (1978). "Proteins bound to heterogeneous nuclear RNA of simian-virus-40-infected cells." European journal of biochemistry / FEBS **91**(1): 1-10.

Pankov, R. and K. M. Yamada (2002). "Fibronectin at a glance." Journal of cell science **115**(Pt 20): 3861-3863.

Paulin, D., J. F. Nicolas, M. Jacquet, H. Jakob, et al. (1976). "Comparative protein patterns in chromatins from mouse teratocarcinoma cells." Experimental cell research **102**(1): 169-178.

Pawlowski, R., E. K. Rajakyla, M. K. Vartiainen and R. Treisman (2010). "An actin-regulated importin alpha/beta-dependent extended bipartite NLS directs nuclear import of MRTF-A." The EMBO journal **29**(20): 3448-3458.

Pederson, T. and U. Aebi (2002). "Actin in the nucleus: what form and what for?" Journal of structural biology **140**(1-3): 3-9.

Pendleton, A., B. Pope, A. Weeds and A. Koffer (2003). "Latrunculin B or ATP depletion induces cofilin-dependent translocation of actin into nuclei of mast cells." The Journal of biological chemistry **278**(16): 14394-14400.

Percipalle, P., N. Fomproix, K. Kylberg, F. Miralles, et al. (2003). "An actin-ribonucleoprotein interaction is involved in transcription by RNA polymerase II." Proceedings of the National Academy of Sciences of the United States of America **100**(11): 6475-6480.

Percipalle, P., A. Jonsson, D. Nashchekin, C. Karlsson, et al. (2002). "Nuclear actin is associated with a specific subset of hnRNP A/B-type proteins." Nucleic acids research **30**(8): 1725-1734.

Percipalle, P. and N. Visa (2006). "Molecular functions of nuclear actin in transcription." The Journal of cell biology **172**(7): 967-971.

Percipalle, P., J. Zhao, B. Pope, A. Weeds, et al. (2001). "Actin bound to the heterogeneous nuclear ribonucleoprotein hrp36 is associated with Balbiani ring mRNA from the gene to polysomes." The Journal of cell biology **153**(1): 229-236.

Peters, J. M., W. W. Franke and J. A. Kleinschmidt (1994). "Distinct 19 S and 20 S subcomplexes of the 26 S proteasome and their distribution in the nucleus and the cytoplasm." The Journal of biological chemistry **269**(10): 7709-7718.

Phan, K. D., V. M. Hazen, M. Frendo, Z. Jia, et al. (2010). "The bone morphogenetic protein roof plate chemorepellent regulates the rate of commissural axonal growth." The Journal of neuroscience : the official journal of the Society for Neuroscience **30**(46): 15430-15440.

Philimonenko, V. V., J. Zhao, S. Iben, H. Dingova, et al. (2004). "Nuclear actin and myosin I are required for RNA polymerase I transcription." Nature cell biology **6**(12): 1165-1172.

Pollard, T. D., S. Almo, S. Quirk, V. Vinson, et al. (1994). "Structure of actin binding proteins: insights about function at atomic resolution." Annu Rev Cell Biol **10**: 207-249.

Pollard, T. D. and G. G. Borisy (2003). "Cellular motility driven by assembly and disassembly of actin filaments." Cell **112**(4): 453-465.

Pollard, T. D. and J. A. Cooper (1982). "Methods to characterize actin filament networks." Methods in enzymology **85 Pt B**: 211-233.

Pollard, T. D. and J. A. Cooper (1986). "Actin and actin-binding proteins. A critical evaluation of mechanisms and functions." Annu Rev Biochem **55**: 987-1035.

Pollard, T. D. and J. A. Cooper (2009). "Actin, a central player in cell shape and movement." Science **326**(5957): 1208-1212.

Pollard, T. D. and W. C. Earnshaw, Eds. (2008). Cell Biology. Heidelberg, Springer.

Popow-Wozniak, A., A. J. Mazur, H. G. Mannherz, M. Malicka-Blaszkiewicz, et al. (2012). "Cofilin overexpression affects actin cytoskeleton organization and migration of human colon adenocarcinoma cells." Histochemistry and cell biology **138**(5): 725-736.

Posern, G., F. Miralles, S. Guettler and R. Treisman (2004). "Mutant actins that stabilise F-actin use distinct mechanisms to activate the SRF coactivator MAL." The EMBO journal **23**(20): 3973-3983.

Posern, G., A. Sotiropoulos and R. Treisman (2002). "Mutant actins demonstrate a role for unpolymerized actin in control of transcription by serum response factor." Molecular biology of the cell **13**(12): 4167-4178.

Purves, D., J.W. Lichtman (1985). Principles of Neural Development. Sunderlande, Sinauer Assocs.

Rando, O. J., K. Zhao and G. R. Crabtree (2000). "Searching for a function for nuclear actin." Trends in cell biology **10**(3): 92-97.

Rasmussen, S. A., S. Y. Chu, S. Y. Kim, C. H. Schmid, et al. (2008). "Maternal obesity and risk of neural tube defects: a metaanalysis." American journal of obstetrics and gynecology **198**(6): 611-619.

Rehklau, K., C. B. Gurniak, M. Conrad, E. Friauf, et al. (2012). "ADF/cofilin proteins translocate to mitochondria during apoptosis but are not generally required for cell death signaling." Cell death and differentiation **19**(6): 958-967.

Rice, D. S. and T. Curran (2001). "Role of the reelin signaling pathway in central nervous system development." Annual review of neuroscience **24**: 1005-1039.

Ridley, A. J., M. A. Schwartz, K. Burridge, R. A. Firtel, et al. (2003). "Cell migration: integrating signals from front to back." Science **302**(5651): 1704-1709.

Rivas, R. J. and M. E. Hatten (1995). "Motility and cytoskeletal organization of migrating cerebellar granule neurons." The Journal of neuroscience : the official journal of the Society for Neuroscience **15**(2): 981-989.

Rogner, U. C., D. D. Spyropoulos, N. Le Novere, J. P. Changeux, et al. (2000). "Control of neurulation by the nucleosome assembly protein-1-like 2." Nat Genet **25**(4): 431-435.

Rosenblatt, J., B. J. Agnew, H. Abe, J. R. Bamburg, et al. (1997). "Xenopus actin depolymerizing factor/cofilin (XAC) is responsible for the turnover of actin filaments in Listeria monocytogenes tails." The Journal of cell biology **136**(6): 1323-1332.

Roskams, A. J., X. Cai and G. V. Ronnett (1998). "Expression of neuron-specific beta-III tubulin during olfactory neurogenesis in the embryonic and adult rat." Neuroscience **83**(1): 191-200.

Rossant, J. and P. P. L. Tam (2002). Mouse development : patterning, morphogenesis, and organogenesis. San Diego, Academic Press.

Roy, N. (2011). Study on the nuclear translocation of the actin binding protein n-cofilin. Institute of Genetics. Bonn, University of Bonn. **Diploma thesis:** 157.

Rugh, R., Ed. (1990). The mouse its reproduction an development, OXFORD SCIENCE PUBLICATIONS.

Ruland, J., C. Sirard, A. Elia, D. MacPherson, et al. (2001). "p53 accumulation, defective cell proliferation, and early embryonic lethality in mice lacking tsg101." Proceedings of the National Academy of Sciences of the United States of America **98**(4): 1859-1864.

Rust, M. B., C. B. Gurniak, M. Renner, H. Vara, et al. (2010). "Learning, AMPA receptor mobility and synaptic plasticity depend on n-cofilin-mediated actin dynamics." The EMBO journal **29**(11): 1889-1902.

Sabapathy, K., W. Jochum, K. Hochedlinger, L. Chang, et al. (1999). "Defective neural tube morphogenesis and altered apoptosis in the absence of both JNK1 and JNK2." Mech Dev **89**(1-2): 115-124.

Sahlas, D. J., K. Milankov, P. C. Park and U. De Boni (1993). "Distribution of snRNPs, splicing factor SC-35 and actin in interphase nuclei: immunocytochemical evidence for differential distribution during changes in functional states." Journal of cell science **105 (Pt 2)**: 347-357.

Sanger, J. W., J. M. Sanger, T. E. Kreis and B. M. Jockusch (1980). "Reversible translocation of cytoplasmic actin into the nucleus caused by dimethyl sulfoxide." Proceedings of the National Academy of Sciences of the United States of America **77**(9): 5268-5272.

Sanger, J. W., J. M. Sanger, T. E. Kreis and B. M. Jockusch (1980). "Reversible translocation of cytoplasmic actin into the nucleus caused by dimethyl sulfoxide." Proc Natl Acad Sci U S A **77**(9): 5268-5272.

Sarmiere, P. D. and J. R. Bamburg (2004). "Regulation of the neuronal actin cytoskeleton by ADF/cofilin." Journal of neurobiology **58**(1): 103-117.

Sasseville, A. M. and Y. Langelier (1998). "In vitro interaction of the carboxy-terminal domain of lamin A with actin." FEBS letters **425**(3): 485-489.

Sauman, I. and S. J. Berry (1994). "An actin infrastructure is associated with eukaryotic chromosomes: structural and functional significance." European journal of cell biology **64**(2): 348-356.

Schambra, Ed. (2008). Atlas of the Prenatal Mouse Brain: Color images and annotated diagrams of: Gestational Days 12,14,16 and 18 Sagittal, coronal and horizontal section Berlin.

Schwenk, F., U. Baron and K. Rajewsky (1995). "A cre-transgenic mouse strain for the ubiquitous deletion of loxP-flanked gene segments including deletion in germ cells." Nucleic Acids Res **23**(24): 5080-5081.

Scott, J. E., G. Quintarelli and M. C. Dellovo (1964). "The chemical and histochemical properties of Alcian Blue. I. The mechanism of Alcian Blue staining." Histochemie. Histochemistry. Histochimie **4**(2): 73-85.

Scott, J. M., D. G. Weir, A. Molloy, J. McPartlin, et al. (1994). "Folic acid metabolism and mechanisms of neural tube defects." Ciba Foundation symposium **181**: 180-187; discussion 187-191.

Shapland, C., J. J. Hsuan, N. F. Totty and D. Lawson (1993). "Purification and properties of transgelin: a transformation and shape change sensitive actin-gelling protein." The Journal of cell biology **121**(5): 1065-1073.

Sheterline, P., J. Clayton and J. Sparrow (1998). Protein Profile: Actin. G.-A. a. F.-A. Sheterline, Oxford University Press.

Shumaker, D. K., E. R. Kuczmarski and R. D. Goldman (2003). "The nucleoskeleton: lamins and actin are major players in essential nuclear functions." Current opinion in cell biology **15**(3): 358-366.

Sidani, M., D. Wessels, G. Mouneimne, M. Ghosh, et al. (2007). "Cofilin determines the migration behavior and turning frequency of metastatic cancer cells." The Journal of cell biology **179**(4): 777-791.

Skare, P., J. P. Kreivi, A. Bergstrom and R. Karlsson (2003). "Profilin I colocalizes with speckles and Cajal bodies: a possible role in pre-mRNA splicing." Experimental cell research **286**(1): 12-21.

Small, J. V. and G. P. Resch (2005). "The comings and goings of actin: coupling protrusion and retraction in cell motility." Current opinion in cell biology **17**(5): 517-523.

Soler, N. G., C. H. Walsh and J. M. Malins (1976). "Congenital malformations in infants of diabetic mothers." The Quarterly journal of medicine **45**(178): 303-313.

Spencer, V. A. (2011). "Nuclear actin: A key player in extracellular matrix-nucleus communication." Communicative & integrative biology **4**(5): 511-512.

Stiefel, D., T. Shibata, M. Meuli, P. G. Duffy, et al. (2003). "Tethering of the spinal cord in mouse fetuses and neonates with spina bifida." Journal of neurosurgery **99**(2 Suppl): 206-213.

Stumpo, D. J., C. B. Bock, J. S. Tuttle and P. J. Blackshear (1995). "MARCKS deficiency in mice leads to abnormal brain development and perinatal death." Proc Natl Acad Sci U S A **92**(4): 944-948.

Stuven, T., E. Hartmann and D. Gorlich (2003). "Exportin 6: a novel nuclear export receptor that is specific for profilin.actin complexes." The EMBO journal **22**(21): 5928-5940.

Sun, H. Q., M. Yamamoto, M. Mejillano and H. L. Yin (1999). "Gelsolin, a multifunctional actin regulatory protein." The Journal of biological chemistry **274**(47): 33179-33182.

Suter, D. M. and P. Forscher (1998). "An emerging link between cytoskeletal dynamics and cell adhesion molecules in growth cone guidance." Current opinion in neurobiology **8**(1): 106-116.

Tabb, J. S., B. J. Molyneaux, D. L. Cohen, S. A. Kuznetsov, et al. (1998). "Transport of ER vesicles on actin filaments in neurons by myosin V." J Cell Sci **111 (Pt 21)**: 3221-3234.

Tanaka, K., Y. Okubo and H. Abe (2005). "Involvement of slingshot in the Rho-mediated dephosphorylation of ADF/cofilin during Xenopus cleavage." Zoological science **22**(9): 971-984.

Tate, C. C., M. C. Tate and M. C. LaPlaca (2007). "Fibronectin and laminin increase in the mouse brain after controlled cortical impact injury." Journal of neurotrauma **24**(1): 226-230.

Thelen, K., V. Kedar, A. K. Panicker, R. S. Schmid, et al. (2002). "The neural cell adhesion molecule L1 potentiates integrin-dependent cell migration to extracellular matrix proteins." The Journal of neuroscience : the official journal of the Society for Neuroscience **22**(12): 4918-4931.

Thiery, J. P. (2003). "Epithelial-mesenchymal transitions in development and pathologies." Current opinion in cell biology **15**(6): 740-746.

Thomas, P. D., M. J. Campbell, A. Kejariwal, H. Mi, et al. (2003). "PANTHER: a library of protein families and subfamilies indexed by function." Genome research **13**(9): 2129-2141.

Thorogood, P. (1994). Differentiation and morphogenesis of cranial skeletal tissue. The skull. J. Hanken. Chicago: University of Chicago Press**:** pp. 113-152.

Tominaga, K., B. Kirtane, J. G. Jackson, Y. Ikeno, et al. (2005). "MRG15 regulates embryonic development and cell proliferation." Molecular and cellular biology **25**(8): 2924-2937.

Tronche, F., C. Kellendonk, O. Kretz, P. Gass, et al. (1999). "Disruption of the glucocorticoid receptor gene in the nervous system results in reduced anxiety." Nature genetics **23**(1): 99-103.

Van Troys, M., L. Huyck, S. Leyman, S. Dhaese, et al. (2008). "Ins and outs of ADF/cofilin activity and regulation." European journal of cell biology **87**(8-9): 649-667.

Vartiainen, M. K. (2008). "Nuclear actin dynamics--from form to function." FEBS letters **582**(14): 2033-2040.

Vartiainen, M. K., T. Mustonen, P. K. Mattila, P. J. Ojala, et al. (2002). "The three mouse actin-depolymerizing factor/cofilins evolved to fulfill cell-type-specific requirements for actin dynamics." Molecular biology of the cell **13**(1): 183-194.

Vicente-Manzanares, M., J. Zareno, L. Whitmore, C. K. Choi, et al. (2007). "Regulation of protrusion, adhesion dynamics, and polarity by myosins IIA and IIB in migrating cells." The Journal of cell biology **176**(5): 573-580.

Visa, N. (2005). "Actin in transcription. Actin is required for transcription by all three RNA polymerases in the eukaryotic cell nucleus." EMBO reports **6**(3): 218-219.

Visegrady, B., D. Lorinczy, G. Hild, B. Somogyi, et al. (2005). "A simple model for the cooperative stabilisation of actin filaments by phalloidin and jasplakinolide." FEBS Lett **579**(1): 6-10.

Visel, A., L. Taher, H. Girgis, D. May, et al. (2013). "A high-resolution enhancer atlas of the developing telencephalon." Cell **152**(4): 895-908.

Waterston, R. H., K. Lindblad-Toh, E. Birney, J. Rogers, et al. (2002). "Initial sequencing and comparative analysis of the mouse genome." Nature **420**(6915): 520-562.

Webster, W. S. and M. J. Edwards (1984). "Hyperthermia and the induction of neural tube defects in mice." Teratology **29**(3): 417-425.

Weins, A., K. Schwarz, C. Faul, L. Barisoni, et al. (2001). "Differentiation- and stress-dependent nuclear cytoplasmic redistribution of myopodin, a novel actin-bundling protein." The Journal of cell biology **155**(3): 393-404.

Wiggan, O., B. W. Bernstein and J. R. Bamburg (2005). "A phosphatase for cofilin to be HAD." Nat Cell Biol **7**(1): 8-9.

Wilson, D. B. (1980). "Cellular proliferation in the exencephalic brain of the mouse embryo." Brain research **195**(1): 139-148.

Wilson, D. B. and E. M. Center (1974). "The neural cell cycle in the looptail (Lp) mutant mouse." Journal of embryology and experimental morphology **32**(3): 698-705.

Winder, S. J. and K. R. Ayscough (2005). "Actin-binding proteins." J Cell Sci **118**(Pt 4): 651-654.

Witke, W., W. Li, D. J. Kwiatkowski and F. S. Southwick (2001). "Comparisons of CapG and gelsolin-null macrophages: demonstration of a unique role for CapG in receptor-mediated ruffling, phagocytosis, and vesicle rocketing." The Journal of cell biology **154**(4): 775-784.

Witte, H. and F. Bradke (2008). "The role of the cytoskeleton during neuronal polarization." Current opinion in neurobiology **18**(5): 479-487.

Wittmann, T. and C. M. Waterman-Storer (2001). "Cell motility: can Rho GTPases and microtubules point the way?" Journal of cell science **114**(Pt 21): 3795-3803.

Wolf, M., A. M. Zimmermann, A. Gorlich, C. B. Gurniak, et al. (2014). "ADF/Cofilin Controls Synaptic Actin Dynamics and Regulates Synaptic Vesicle Mobilization and Exocytosis." Cerebral cortex.

Wu, M., D. F. Chen, T. Sasaoka and S. Tonegawa (1996). "Neural tube defects and abnormal brain development in F52-deficient mice." Proc Natl Acad Sci U S A **93**(5): 2110-2115.

Xu, W., H. Baribault and E. D. Adamson (1998). "Vinculin knockout results in heart and brain defects during embryonic development." Development **125**(2): 327-337.

Yamauchi, K., S. G. Varadarajan, J. E. Li and S. J. Butler (2013). "Type Ib BMP receptors mediate the rate of commissural axon extension through inhibition of cofilin activity." Development **140**(2): 333-342.

Yao, J., T. Hennessey, A. Flynt, E. Lai, et al. (2010). "MicroRNA-related cofilin abnormality in Alzheimer's disease." PloS one **5**(12): e15546.

Yao, T. P., S. P. Oh, M. Fuchs, N. D. Zhou, et al. (1998). "Gene dosage-dependent embryonic development and proliferation defects in mice lacking the transcriptional integrator p300." Cell **93**(3): 361-372.

Yonezawa, N., E. Nishida, K. Iida, I. Yahara, et al. (1990). "Inhibition of the interactions of cofilin, destrin, and deoxyribonuclease I with actin by phosphoinositides." J Biol Chem **265**(15): 8382-8386.

Yoshida, T., P. Vivatbutsiri, G. Morriss-Kay, Y. Saga, et al. (2008). "Cell lineage in mammalian craniofacial mesenchyme." Mechanisms of development **125**(9-10): 797-808.

Zaki, P. A., J. C. Quinn and D. J. Price (2003). "Mouse models of telencephalic development." Current opinion in genetics & development **13**(4): 423-437.

Zhang, S., K. Buder, C. Burkhardt, B. Schlott, et al. (2002). "Nuclear DNA helicase II/RNA helicase A binds to filamentous actin." The Journal of biological chemistry **277**(1): 843-853.

Zhu, H., J. O. Enaw, C. Ma, G. M. Shaw, et al. (2007). "Association between CFL1 gene polymorphisms and spina bifida risk in a California population." BMC Med Genet **8**: 12.